THE UNIVERSITY
of EDINBURGH

Functional Characterisation of Spontaneously Active $GABA_A$ Receptors in Rat Dentate Gyrus Granule Cells

Nathanael O'Neill B.Medsc. (Hons)

Doctor of Philosophy
The University of Edinburgh
2020

Declaration

I declare that this thesis was composed solely by myself and has not been submitted for any other degree or processional qualification. Except where states otherwise by reference or acknowledgment, the work presented is entirely my own.

Parts of this work have been published:

Experimental:

O'Neill N, Sylantyev S. Spontaneously opening $GABA_A$ receptors play a significant role in neuronal signal filtering and integration. Cell Death Dis. 2018;9(8).

O'Neill N, Sylantyev S. Selective modulation of tonically active $GABA_A$ receptor functional subgroups by G-proteins and protein kinase C. Exp Biol Med. 2018;243(13):1046–55.

Mini-Review:

O'Neill N, Sylantyev S. The Functional Role of Spontaneously Opening $GABA_A$ Receptors in Neural Transmission. 2019;12:1–7.

Signed: Date: 24/03/2020

.

Abstract

$GABA_A$ receptors ($GABA_ARs$) are the principal inhibitory neurotransmitter receptors in the adult mammalian central nervous system. $GABA_ARs$ mediate two forms of inhibition: fast, phasic conductance; and slow, tonic conductance. Tonic conductance arises due to the persistent activation of $GABA_ARs$. This persistent activation can occur by GABA-dependent or GABA-independent mechanisms. Low concentrations of ambient GABA activate high affinity $GABA_ARs$ located outside the synapse – at peri-/extra-synaptic sites – to generate GABA-dependent tonic conductance. In contrast, GABA-independent tonic conductance is generated by $GABA_ARs$ that activate spontaneously, in the absence of GABA, due to constitutive receptor gating. Because spontaneously active $GABA_ARs$ (s-$GABA_ARs$) do not require GABA to activate, they are resistant competitive antagonists, e.g. SR-95531, but can be inhibited by the channel-blockers, e.g. picrotoxin.

s-$GABA_ARs$ have been shown to produce GABA-independent tonic conductances in the hippocampus and the amygdala. However, despite the good evidence for the *presence* of s-$GABA_ARs$, their *function* and *pharmacology* remain largely unknown.

Here we show, for the first time, using both current- and voltage-clamp recording techniques, that the s-$GABA_AR$-mediated tonic conductance exerts a powerful inhibitory effect in rat dentate gyrus granule cells. We find that at resting membrane potential, s-$GABA_ARs$ generate a shunting conductance that decreases both the membrane resistance and the membrane time constant of the neuron. When the membrane potential is depolarised, s-$GABA_ARs$ conduct hyperpolarising currents that exhibit outward-rectification; this means that their net inhibitory effect is greater when the neuron is close to firing threshold than when it is at rest. Consistent with this, we find that block of s-$GABA_ARs$ shifts the neuron into a more excitable state, as evidenced by the increase in the gain of the input-output relationship and the decrease in the rheobase current and the hyperpolarisation of the action potential threshold. At the network level, s-$GABA_ARs$ regulate the precision of signal transmission in the dentate gyrus: blocking s-$GABA_ARs$ widens the temporal window over which multiple excitatory inputs can be successfully summated to generate an action potential. Finally, we report that s-$GABA_AR$ tonic currents are resistant to pharmacological compounds that target extrasynaptic $GABA_ARs$ (L-655,708 and DS2), but are augmented by the clinically used benzodiazepine site modulators, zolpidem and midazolam, and partially inhibited by the inverse agonist, DMCM. The sensitivity of s-$GABA_ARs$ to these compounds suggests the involvement of the γ2-subunit.

Lay Summary

Neurons communicate with each other using a group of proteins called receptors. Receptors are found on the surface of neurons and when they are activated (switched ON) they cause either excitation or inhibition. The appropriate balance between excitation and inhibition is critical for proper brain function. When this balance is upset, brain dysfunction quickly follows; as happens in a variety of diseases such as epilepsy. The main inhibitory receptor in the brain – and the topic of my PhD – is called the $GABA_A$ receptor.

$GABA_A$ receptors can be thought of as switches. A simple view states that $GABA_A$ receptors are normally switched OFF, and are only switched ON in the presence of their neurotransmitter, which is called GABA (γ-aminobutyric acid). According to this view, all $GABA_A$ receptor effects therefore require GABA. However, is this an oversimplification? Are we seeing these receptors and, in turn, the brain, for what it really is?

Prior to my PhD it was shown that, contrary to the simplistic view expressed above, $GABA_A$ receptors can actually switch ON in the absence of GABA. However, at this point in time, nobody knew if these GABA-independent $GABA_A$ receptors did anything important in the brain.

During my PhD I recorded the electrical activity from thin slices of rat brains in order to examine the role of GABA-independent $GABA_A$ receptors. I was able to show, for the first time, that these receptors play an important role in maintaining the proper balance between excitation and inhibition in the brain. When I blocked these receptors from turning ON, neurons and their networks became hyper-excitable and were no longer able to filter incoming signals as effectively. This meant neurons that had previously been silent were now active. The hyper-excitability that I observed in the brain was similar to what has been found in some cases of epilepsy. This led me to test if anti-convulsants could modulate GABA-independent $GABA_A$ receptors. I was able to show that midazolam, a clinically used anti-convulsant, makes these receptors turn ON more. And, as a result, increases the inhibitory signal that they provide.

In a narrow sense, my PhD shows that GABA-independent $GABA_A$ receptors play an important role in maintaining proper brain function. It also shows that these receptors can be modulated by anti-epileptic drugs, and thus can potentially be considered as new drug targets. But more broadly, it forces us to wonder: How many other receptors, in other brain regions, mediate some of their effects in the absence of their neurotransmitter? And what might this tell us about the brain?

Acknowledgements

I would first like to thank Dr Sergiy Sylantyev for his supervision throughout my PhD. Without Sergiy, I would not have been able to enjoy three excellent years in the wonderful city of Edinburgh. I am thankful for the trust he put in me: I was able to take the project in the direction that I wanted to and was given the freedom to make mistakes (and hopefully learn from them) without judgement. This was especially generous of him, given that most of the equipment was brand new (and expensive!). I am also indebted to him for his inclusiveness on projects outside of my PhD. The Sylantyev Lab became a much less lonely place when Molly Hickey, a gifted undergraduate student, arrived to undertake a summer project with us. Molly generated some of the data in Chapter 4 and adapted to life in the lab exceedingly well. She was able to learn new and difficult skills quickly and had a knack for asking interesting questions. None of the lab work would have been possible without the lovely Sprague Dawley rats. And thanks to Will and Ami for taking such good care of them.

I would also like to thank Professor Seth Grant, who co-supervised this project. It was a privilege to attend the Grant Lab's weekly meetings. Seth broadened my scientific horizons and was a constant source of good, solid advice – especially on presentations. I am also thankful to Seth, as it was through in his lab that I met some of my closest friends in Edinburgh. Vlad Anton, forever a legend: discretion never was your middle name, but this, coupled with the daily compost-coffee, livened up Little France tremendously. And the regular dose of absurdist humour (and fluorescent PSD-95) that you provided got me through some of the toughest bits of my PhD. Thanks also to George, for being such a passionate advocate of the good life: good friends, good food, good drink, and, of course, Greece. And to Sarah, for lovely chats, good humour and thoughtful advice; and to Cathy for always keeping cheerful and for help with the cell culture. And to Malik, Max, Jamie, Dimitra, Edita, Noboru, Erik, Ann and Colin.

I also want to express my deepest gratitude to Dr Matt Livesey. Matt helped tremendously with putting this PhD together and was a constant source of support in the last few months of writing. I cannot express how much I appreciate the time that Matt gave up, and the fact he went so out of his way to help me out. Throughout the PhD, Matt also instilled in me a greater sense of confidence in my work and was always on hand to provide expert experimental advice. He is also incredibly kind and will make an excellent Lab PI. I would also like to thank my previous supervisors, Dr Jonathan Wolf Mueller, Dr Andrew Powell, Dr Gillian Grafton, Professor Nick Barnes, and Professor Richard Barrett-Jolley.

And, finally, to thank the people, without whom, I could not have got through the PhD: Phoebe, Mum, Dad, and Lillie.

To Phoebe, thank you for all the love and support. The best times in Edinburgh were spent with you, be it at the Fringe, dog-spotting on the meadows, or eating ice-cream at Mary's. Words don't do justice to how amazing you have been.

And to my family, whose selflessness and kindness never ceases to amaze me. Thank you for always being there to support me.

Contents

List of Figures

Abbreviations

Abbreviation	Definition
[_]	Concentration
µM	Micromolar
5-HT_3R	Serotonin 3 receptor
Å	Angstrom
ACh	Acetylcholine
ACSF	Artificial cerebrospinal fluid
AHP	After-hyperpolarisation
AIS	Axon initial segment
AP	Action potential
ATP	Adenosine triphosphate
BCs	Basket cells
BDZ	Benzodiazepine
BGT-1	Betain/GABA transporter type 1
Ca^{2+}	Calcium
CCK	Cholecystokinin
Cl^-	Chloride
CNS	Central nervous system
CO_2	Carbon dioxide
CTRL	Control
DG	Dentate gyrus
DGGCs	Dentate gyrus granule cells
EC	Entorhinal cortex
EC_{50}	Half maximal effective concentration
E_{Cl^-}	Chloride reversal potential
E_{GABA}	Reversal potential for $GABA_AR$ responses
E_{HCO3^-}	Bicarbonate reversal potential
E-I	Excitatory-inhibitory
ELIC	*Erwinia* ligand-gated ion channel
EPSCs	Excitatory postsynaptic currents
EPSPs	Excitatory postsynaptic potentials
F	Frequency
F-I	Firing rate-to-injected current
G	Conductance
GABA	γ-aminobutyric acid
$GABA_AR$	GABA type A receptor
$GABA_BR$	GABA type B receptor
GAD65+67	Glutamate decarboxylase 65+67
GAT1-4	GABA transporters 1-4
GLIC	*Gloebacter* ligand-gated ion channel
GlyR	Glycine receptor
GPCR	G-protein coupled receptors
HCO_3^-	Bicarbonate
HIPP	Hilar perforant path
I	Current
I_{hold}	Holding current
IC_{50}	Half maximal inhibitory concentration
IPSCs	Inhibitory postsynaptic currents
IPSPs	Inhibitory postsynaptic potentials
ISI	Interstimulus interval
K^+	Potassium
KCC2	Chloride-extruding potassium–chloride co-transporter
kD	Kilodalton
Ki	Inhibitory constant
LPP	Lateral perforant pathway
LTD	Long-term depression

LTP	Long-term potentiation
MA	Membrane associated
MC-4R	Melanocortin-4 receptor
mIPSCs	Mini inhibitory postsynaptic potentials
mM	Millimolar
MPP	Medial perforant pathway
ms	Milliseconds
mV	Millivolts
MWC	Monod wyman changeux
Na^+	Sodium
nAChR	Nicotinic acetylcholine receptor
nM	Nanomolar
O_2	Oxygen
PERT	Pertussis toxin
PKA	Protein kinase A
PKC	Protein kinase C
pLGICs	Pentameric ligand-gated ion-channels
PTX	Picrotoxin
PV	Parvalbumin
$Q_{AV.IPSC}$	average charge transferred by an IPSC
Q_{phasic}	Phasic charge transfer
Q_{tonic}	Tonic charge transfer
R	Resistance
RMP	Resting membrane potential
s-$GABA_AR$	Spontaneously activating $GABA_A$ receptor
SOM	Somatostatin
SR	SR-95531 (gabazine)
T	Time
TBS	Theta-burst stimulation
THDOC	Tetrahydrodeoxycorticosterone
TTX	Tetrodotoxin
vGAT	Vesicular GABA transporters
Vm	Membrane potential
V	Voltage
α5-$GABA_ARs$	$GABA_ARs$ containing the α5-subunit
Δ	Change
δ-$GABA_ARs$	$GABA_ARs$ containing the δ-subunit
μs	Microsecond
τ_m	Membrane time constant

Chapter 1

Introduction

Background

The mammalian brain is extraordinarily complex. Even the brain of one of the smallest mammals, the Etruscan shrew, has over two million neurons (1); the adult rat has around 100 times more (2,3); whereas an estimated 86 billion neurons are found in the adult human brain (4). But the number of neurons alone does not do justice to brain complexity. Neurons are connected by synapses and arranged into intricate, highly organised, interconnected circuits (5–8). Within these circuits, neurons integrate and process synaptic inputs and transform them into specific action potential firing patterns (9–11). The circuit architecture of the brain is a product of evolution and, as such, is patterned by the genome, whilst also being shaped by the process of development, which introduces a degree of stochasticity (12–16). The innate brain circuitry allows mammals to perceive and interact with their environment and bestows upon them a repertoire of inherited instinctive behaviours (14,15,17–19). However, neuronal circuits are not static – they exhibit a degree of plasticity – and are routinely modified and updated throughout life as the animal learns, adapts, and forms new memories (20–24).

The remarkable complexity of the structure and activity patterns in the mammalian brain, and the cognitive functions that it performs, is mirrored and – in all likelihood – underpinned by the high diversity of its constituent neurons. Indeed, the total neuronal repertoire of the mammalian brain can be divided and subdivided into many hundreds of distinct classes and sub-classes (25–29).

And yet, amidst the aforementioned complexity, two distinct neuronal families are absolutely dominant, underpinning many aspects of brain function: 1) the **excitatory principal neurons** that release glutamate as their primary neurotransmitter and 2) the **inhibitory interneurons** that release γ-aminobutyric acid (GABA). It is primarily by way of these two neuron families, using their respective neurotransmitter, that the phenomena of excitation and inhibition are delivered and regulated in the brain. An appropriate ‘excitatory-inhibitory’ (E-I) balance between

glutamatergic-excitation and GABAergic-inhibition is crucial for proper brain function (30). However, the role of GABA-ergic inhibition in the brain cannot be reduced simply to homeostatic regulation of circuit excitability – wherein inhibition acts solely to restrain rampant excitatory cell firing (akin to turning a thermostat to maintain an optimum temperature). Instead, excitation and inhibition are of equal importance for proper brain function, with the GABAergic inhibitory system taking an active – often central – role in the integration, processing and output of information in neural circuits. It is a system that is both ubiquitous and highly heterogeneous; 20-30% of neurons release GABA as their primary neurotransmitter (interneurons) (34), but virtually all neurons can (and do) respond to GABA. Understanding the GABA-ergic inhibitory system is, henceforth, a major goal of neuroscience; and a prerequisite for discerning how computations take place in the brain – at virtually every level of circuit complexity. In the present thesis, we will characterise one component of the GABAergic neurotransmitter system: the tonic conductance that is generated by spontaneously active $GABA_A$ receptors.

1.1 GABA

GABA is the principal inhibitory neurotransmitter in the adult mammalian central nervous system (CNS). GABA was shown to be present in the brain in 1950 (31–33), and the first report of its inhibitory effect on neurons was in 1956-57 by Bazemore, Elliott, and Florey (34,35). They identified GABA to be the extracted brain substance – known as 'Factor I' – that inhibited the rhythmic action potential (AP) firing of the crayfish stretch receptor (34–36). At the time they posited that GABA "is possibly a transmitter substance of inhibitory impulse" (35). This early idea turned out to be prescient.

In a series of experiments during the 1960s, GABA was shown to be released from inhibitory terminals in response to stimulation (37), and when GABA was applied by iontophoresis to cortical neurons in cats, it was shown to mimic native inhibitory postsynaptic potentials (IPSPs) in these neurons (38,39). Specifically, GABA caused membrane hyperpolarisation and decreased the membrane resistance, with inhibitory synaptic and GABA responses reversing similar potentials (38,39). In 1970, Curtis *et al* showed that the convulsant, bicuculline, could antagonise GABA-evoked responses *and* synaptic inhibition in cortical and cerebellar neurons (40,41). It was in this study that GABA was considered to be "the actual transmitter at inhibitory synapses" (40). The detection of the GABA receptors being widespread in the brain (42–44) and the subsequent purification, cloning and functional expression of these receptors ultimately confirmed the view of GABA as the most important inhibitory neurotransmitter in the CNS (45–47).

1.2 GABA synthesis, metabolism, sequestration, release and uptake

GABA is synthesised by the pyridoxal 5′-phosphate-dependent enzyme glutamate decarboxylase (GAD). There are two GAD isoforms in mammals and they are denoted according to their respective molecular weights in kDa (GAD65 + GAD67). Both of these isoforms catalyse the decarboxylation of glutamate to produce GABA and carbon dioxide – but do so under different conditions and for different purposes (48,49). GAD67 is distributed evenly throughout the cytoplasm of neurons (50); despite making up only ~20% of total GAD expression, it is constitutively active and mediates basal GABA synthesis, producing > 90% of

total GABA (51,52). In contrast, GAD65 is membrane-associated, with expression restricted to GABA-ergic presynaptic terminals (50); here, GAD65 oscillates – in an activity-dependent manner – between active and inactive states (53). This reflects the importance of GAD65-mediated GABA synthesis during periods of elevated synaptic transmission when basal – GAD67 mediated – GABA synthesis does not meet demand (54–56).

GABA is metabolised by GABA-transaminase, which is expressed in neurons, astrocytes, and in the periphery (57,58). GABA-transaminase converts GABA to succinic semialdehyde, which is, in turn, oxidised to succinate by succinic semialdehyde dehydrogenase. Succinate is an intermediate of the tricarboxylic acid (TCA) cycle and is converted to α-ketoglutarate, a precursor of glutamate, which is itself a precursor for GABA. This metabolic route is termed "GABA shunt" (59).

Once synthesised, cytosolic GABA is loaded into synaptic vesicles by vesicular GABA transporters (vGAT), which utilise the proton electrochemical gradient that is generated by vacuolar-type H^+ ATPase (60). Each loaded synaptic vesicle contains several thousand molecules of GABA (61). Vesicle exocytosis is triggered by a rise in presynaptic Ca^{2+} concentration (but can also occur spontaneously) and results in the release of a quanta of GABA into the synaptic cleft (61). The concentration of GABA in the cleft rapidly increases to approximately 1-3 mM (62,63), which causes the concerted – but incomplete in terms of occupancy – activation of GABA receptors on the postsynaptic terminal (61,64). However, GABA does not remain in the synaptic cleft for long: the rate of diffusion is fast, meaning that GABA clears from the synapse in ~100 μs. Diffusion of GABA away from the synapse can cause short-term, 'spill-over', and long-term, 'tonic', activation of GABA receptors situated on the presynaptic (65) and peri- and extrasynaptic membranes (66–72). GABA diffusion and the kinetics of GABA receptors primarily determine the profile of inhibitory synaptic responses (61).

The level of extrasynaptic or 'ambient' GABA is tightly regulated but does vary across different brain regions (Reviewed in (59)). In the hippocampus, for instance, [extracellular GABA] is lower than in the substantia nigra pars compacta and the hypothalamus (73). *In vivo* microdialysis experiments show that hippocampal [extracellular GABA] is kept very low (sub-μM), reported to be between 3 nM - 0.3 μM (74–78). This level of ambient GABA is influenced by the amount of

synaptic GABA transmission (70,79,80) but is also regulated by GABA transporters (GATs) (71,81–83) and is affected by non-vesicular mechanisms of GABA release (59,70,81,84,85).

Four GATs isoforms have been described in rat brain so far: GAT-1,2,3 and the Betain/GABA transporter type 1 (BGT-1) (82). Transport of GABA through GATs is dependent on the gradient of Na^+ and Cl^- across the membrane (GATs are Na^+/Cl^- coupled transporters) (82). For each molecule of GABA that is removed from the extracellular space and transported across the membrane into the cytoplasm, two Na^+ and one Cl^- ion also enters the cytoplasm (82). Although GATs are not coupled directly to ATP hydrolysis, the transport of GABA is an active process because the Na^+/K^+ ATPase is required to create and maintain the necessary Na^+ gradient. GATs differ in their regional, cellular, and subcellular localisation and this is thought to reflect their function (82,86). In the hippocampus, the two main GATs are GAT-1+3. GAT-1 is the principal neuronal GAT and is primarily expressed on the axon terminals of symmetrical synapses, although it is also present on glial cells. GAT-3, by contrast, is localised on astrocytic processes, close to GABA-ergic synapses on the dendrites and cell body (82,86). Both GAT-1 and GAT-3 affect extracellular levels of GABA (81–83). GAT-1 curtails the movement of GABA from the synaptic cleft to the extracellular space to limit 'spill-over', whereas GAT-3 controls the actual levels of extracellular GABA (70,71,81–83,87). In the dentate gyrus GAT-1 and GAT-3 work synergistically, but GAT-1 appears to have a greater role (88,89).

GABA can also be released into the extracellular space by non-vesicular mechanisms (59,81,84). One such mechanism is the reversal of GATs (85) that can occur due to changes in the electrochemical gradients of Na^+, Cl^- and GABA (e.g Na^+ influx and intracellular Cl^- accumulation during depolarisation) (85,90). The role GAT-1 reversal in neurons is controversial, with a recent study showing that synaptic GABA release prevents sustained efflux of GABA through GAT-1 (90). In line with this, GAT reversal does not appear to be a feature in the dentate gyrus in basal normotopic conditions (59,71,83). Glia have been shown release GABA (91) due to GAT-3 reversal (92,93) and through Bestrophin 1 anion channel (94).

1.3 GABA receptors

GABA mediates its effects via two types of GABA receptors (GABA_Rs): 1) ionotropic $GABA_A$Rs and 2) metabotropic $GABA_B$Rs receptors, both of which – via direct and indirect mechanisms, respectively – use ionic fluxes to affect the activity of mature neurons. $GABA_A$Rs are the principal mediator of GABAergic neurotransmission in the CNS and are the topic of the present PhD – the structure and function of these receptors will be discussed extensively throughout this section. Briefly on $GABA_B$Rs: they are G-protein coupled receptors (GPCRs) that are expressed both on the pre- and postsynaptic membrane; they are formed by the heterodimerisation of $GABA_{B1}$ and $GABA_{B2}$ subunits and are the site of action of baclofen, a $GABA_B$R agonist, which is used clinically as a muscle relaxant (95). Activation of $GABA_B$Rs causes inhibition via activation of inwardly rectifying K^+ channels and inhibition of voltage-gated Ca^{2+} channels and adenylyl cyclase (95). $GABA_B$Rs have an important role in modulating neuron firing and regulating neural plasticity (96); however, they are overshadowed by $GABA_A$Rs, which absolutely dominate the landscape of inhibitory neurotransmission.

1.4 $GABA_A$Rs

$GABA_A$Rs are pentameric ligand-gated ion channels (pLGICs) that are permeable to the anions chloride (Cl^-) and, to a lesser degree, bicarbonate (HCO_3^-) (97–99). $GABA_A$Rs belong to the "Cys-loop" receptor superfamily; other members include nicotinic acetylcholine receptors (nAChR), zinc activated ion channel (ZAC), serotonin 3 receptor ($5\text{-}HT_3R$), and strychnine sensitive glycine receptors (GlyR) (100). Cys-loop receptors function as allosteric signal transducers: they have been refined by evolution to rapidly and efficiently convert a chemical signal into an ion flux across a plasma membrane (101,102).

1.4.1 $GABA_A$R subunits

$GABA_A$Rs – as with all Cys-loop receptors – are formed by the assembly of five receptor subunits around a central ion-permeable pore (98,103,104). There are 20 vertebrate $GABA_A$R subunit encoding genes (*Gabr_*), grouped into eight subclasses according to sequence homology (α1-6, β1-4, γ1-3, δ, ε, θ, π, ρ1-3) (104–107). The number of subunits is often given as 19, omitting the β_4 subunit, but this subunit should be included as expression has been confirmed in both chickens (108) and humans (109), but not in rats or mice. The repertoire of

$GABA_AR$ subunits is expanded further due to alternative splicing of certain subunit mRNAs, e.g. α6, β2, β3 and γ2 (110).

Different subunits are incorporated into different $GABA_AR$ isoforms (104,106,107), and these isoforms have different functional properties and show heterologous expression across the brain (111–113). Although the theoretical maxima for the *possible* number of $GABA_AR$ isoforms is vast (>150,000), the *actual* number of isoforms that *are* expressed is in the brain is far less, probably ~50 (107). The number of $GABA_AR$ isoforms is constrained, first, by regional differences in subunit mRNA expression, with specific neuron types only expressing a subset of $GABA_AR$ genes (111,114–116). And, second, by various rules of $GABA_AR$ assembly that cause the preferential assembly of certain subunits (117). Not all of these rules are currently known, but various residues in α- (118–120), β-(121), and γ2 (119,122) subunits have been shown to be involved (for review see (117)). The majority of $GABA_AR$ isoforms are heteromeric assemblies (consisting of more than one subunit subclass). The few homomeric isoforms that been shown to exist typically exhibit unusual properties. For example, the β3 homomer is largely insensitive to GABA (123–125) and bicuculline (125), but can by activated by histamine (124) and pentobarbital (125). Another example is the ρ1 homomer (formerly $GABA_CR$); these receptors are expressed in retina and are insensitive to bicuculline, benzodiazepines and barbiturates (126). In heteromeric $GABA_AR$ isoforms, two α and two β subunits are necessary to confer GABA sensitivity; di-heteromeric isoforms composed of just α and β subunits do exist (127), but most receptors are tri-heteromers, wherein the two identical α and two β subunit pairs combine with and an axillary subunit (e.g. γ2, δ, ε) (98,128–130). Some $GABA_AR$ isoforms have also been shown to incorporate two non-identical α and β subunit pairs e.g. α1+α6 (131,132)

The number of $GABA_AR$ isoforms that have been denoted as “existing with a certain probability” in the brain was posited to be 26 by Olsen and Sieghart in 2008, with only 11 of these isoforms conclusively identified (105). Although there have been no substantial revisions this list of $GABA_AR$ isoforms, Smart and Stephenson recently outlined a slightly amended version, which is presented in **Table.1.1** (107).

The identified subunit composition of native $GABA_AR$ isoforms

Tentatively identified	Probable	Possible
α1β2γ2	α1β3γ2	αβγ1
α2βγ2	α1βδ	αβγ3
α3βγ2	α5β3γ2	αβθ
α4βγ2	αβ1γ	αβε
α4β2δ	αβ1δ	αβπ
α4β3δ	αβ	α_β_γ2
α5β2γ2	α1α6βγ	
α6β2γ2	α1α6βδ	
α6β2δ		
α6β3δ		
ρ1-3		

Table adapted from: Smart and Stephenson*, 2019* (107)*.* The most abundant $GABA_AR$ isoform is the brain is the α1β2γ2 heteromer (2:2:1 stoichiometry), which makes up 40-60% of all $GABA_ARs$ in the brain, followed by the α2β3γ2 and α3β3γ2 (126). These isoforms have a clockwise arrangement of α−β−γ−α−β subunits when viewed from the extracellular space (98,128,129). Expression of α1, β1-3, and γ2 subunits is virtually ubiquitous throughout the brain (111–113,116); α1β2γ2, α2β3γ2 and α3β3γ2 isoforms are the principal synaptic $GABA_ARs$ and mediate phasic (synaptic) inhibition. However, owing to their significant motility in the membrane (133–135) and the large extrasynaptic surface area, these isoforms are also found outside of the synapse, at peri- and extrasynaptic sites (136) and are able to produce tonic conductance (137). Indeed, Kasugai *et al* demonstrated using freeze-fracture replica immunolabelling that 60% of α1, α2, and β3 subunits are in extrasynaptic receptors (136).

The prototypical 'extrasynaptic' $GABA_AR$ isoforms that are primarily responsible for tonic inhibition are α4βδ, α6βδ, α5βγ2 and α1βδ (138); isoforms containing αβ (127,139) αβε (140) appear to contribute, and possibly α4βγ2 (141,142), α6βγ2 (143). Although these receptor isoforms are far less abundant than α1β2γ2, α2β3γ2 and α3β3γ2 receptors, they, nevertheless,

play an important function in the brain by generating GABA-dependent tonic conductance. Interestingly, the assembly of α4β2δ receptor isoforms appears to be less strict than αβγ2 receptors (144). The subunit composition of $GABA_AR$ isoforms thus has a major impact on their localisation within the cell; it also influences many of the functional and kinetic properties of the receptor, including GABA potency, maximal response, desensitisation, pharmacology, and constitutive activity. Whilst different $GABA_AR$ subtypes have different properties, they share a pentagonal shape that is common to all Cys-loop receptors. The gross topology of Cys-loop receptors has been known for some time thanks to the pioneering work of Nigel Unwin and colleagues.

1.4.2 $GABA_AR$ structure

Unwin's approach, which began in the mid-1980s (145–149), was to use cryoelectron microscopy to image the nAChR from the *Torpedo marmorata* electroplax. The technique was gradually refined to over the next 20 years (150–155), increasing the resolution from 25 Å down to 4Å, and culminated in a high-resolution atomic structure of the nAChR (156) – a truly seminal achievement. In the 1990s, relatively low resolution (~70 Å) electron microscopy images of native porcine $GABA_ARs$ confirmed that they adopt a matching pentagonal shape (157); however, for a considerable amount of time, there were no $GABA_AR$ structures on a par with Unwin's nAChR. This meant that the high-resolution structure of the $GABA_AR$ (and other Cys-loop receptors) had to be extrapolated from Unwin's prototypical nAChR, and other analogous proteins (158–160). These structural analogies include the molluscan acetylcholine-binding proteins, which are soluble homopentamers that exhibit a high similarity to the extracellular domain of the nACHR (161). As well as the glutamate-gated chloride channel, which is a Cys-loop receptor expressed in *Caenorhabditis elegans* (162); and the prokaryote receptor homologs: *Erwinia* ligand-gated ion channel (ELIC) and *Gloebacter* ligand-gated ion channel (GLIC), which both have an analogous structure to Cys-loop receptors (they are pLGICs), but lack the eponymous Cys-loop motif (163).

It was not until 2014 that the first high-resolution (3 Å), three-dimensional structure of a $GABA_AR$ – the β3 homopentamer – was obtained by Aricescu and colleagues (99). Several other $GABA_AR$ structures have since been resolved (164–168), with a notable high point occurring in

2019, again by Aricscu and colleagues, with the publication of the long sought after full-length, high-resolution (3.2 Å) structure of the α1β3γ2L tri-heteromer (103) bound to a variety of ligands (98). This receptor isoform is one of the most prevalent in the brain. And resolving its structure gives a much clearer view of the topology of $GABA_AR$ subunits and their assembly into a receptor. This study also made important steps forward in understanding how the architecture of the receptor changes in the conducting vs. non-conducting states.

1.4.3 $GABA_AR$ subunit topology

Each $GABA_AR$ subunit is comprised of three topographically distinct domains (see **Fig.1.1A**). The N-terminal *extracellular domain,* which consists mainly of β-sheets and contains the eponymous disulphide-linked Cys-loop (a pair of disulphide-linked cysteine residues that are separated 13 highly conserved amino acids); the *transmembrane domain,* which consists of four hydrophobic membrane-spanning alpha helices; and the *intracellular domain,* which is formed by the linker between the third and fourth transmembrane helices. The C-terminus is short and protrudes extracellularly. In a functional receptor, five $GABA_AR$ subunits are arranged quasi-symmetrically around a central channel that is selectively permeable to the anions Cl^- and, to a lesser degree, HCO_3^- (97). Proper assembly gives rise to a large (molecular mass of ~300 kD), bullet-shaped receptor that has three domains – corresponding to the respective subunit domains (**Fig.1.1B**).

1.4.4 $GABA_AR$ quaternary structure

The extracellular domain of the $GABA_AR$ is the largest of the three domains and exhibits a round, donut-like, shape when viewed from the extracellular space (perpendicular to the plasma membrane) (98,103). It contains the two agonist binding sites for orthosteric ligands (e.g. GABA) that are located on the domain's outer surface, at the interfaces between adjacent β and α subunits (98,103). Each of the orthosteric binding sites is a pocket-like structure formed from the principal (+) side of the β subunit, which contributes loops A-C, and complementary (-) side of the α subunit, which contribute loops D–F. GABA binds underneath loop-C, inside an "aromatic-box", where extensive hydrophilic interactions stabilise it; GABA is orientated so that its amino group is closer to the β subunit and its carboxyl group faces the α subunit (98,103). In αβγ2 receptor isoforms there is an analogous binding site, between adjacent α+ and γ2- subunits, for benzodiazepine(BDZ)-site ligands, such as diazepam, and BDZ-like compounds,

such as zolpidem (98,103). The inner surface of the extracellular domain is a water-filled vestibule that marks the entrance of the channel; its surface is enriched with a ring of positively charged residues that act as an anion selectivity filter (169,170). Another anion selectivity filter is present at the cytoplasmic end of the transmembrane domain (171–173).

The membrane-spanning ion channel is situated at the centre transmembrane receptor domain, which is formed by the assembly of five lots (one for each subunit) of four membrane-spanning alpha-helices (M1-4). In each subunit, the helices are ordered in such a manner that M1, M3, and M4 form an outer ring to shield M2 from the lipid environment (98,103). Residues protruding from the five M2 helical domains line the hydrophobic channel and dictate the maximal size of permeant ions (98,103). The diameter of the channel is not uniform along its length: there are multiple constrictions that act to preclude the flow of ions when the receptor occupies a non-conducting state (98,103). One constriction, at the centre of the channel (residue leucine 9'), is purported to be the activation gate; and another, the tightest constriction, is located at the cytoplasmic end (residue Proline/Alanine -2') and acts as the desensitisation gate (99,174).

The intracellular domain of the $GABA_AR$ sits directly beneath the cytoplasmic end of the ion channel. It has proven to be the most challenging domain to resolve, likely due to the absence of interacting postsynaptic proteins in structural analyses. However, it is thought to adopt a hanging-basket like structure, formed by five large loops – one from each subunit – that protrude into the cytoplasm to link M3 and M4 transmembrane helices. Located within the intracellular loops is the membrane-associated (MA) helix. The intracellular domain is the least well studied of the three receptor domains but has been shown to affect ion permeation (175), receptor trafficking and targeting (176,177), and is a site of receptor phosphorylation (178).

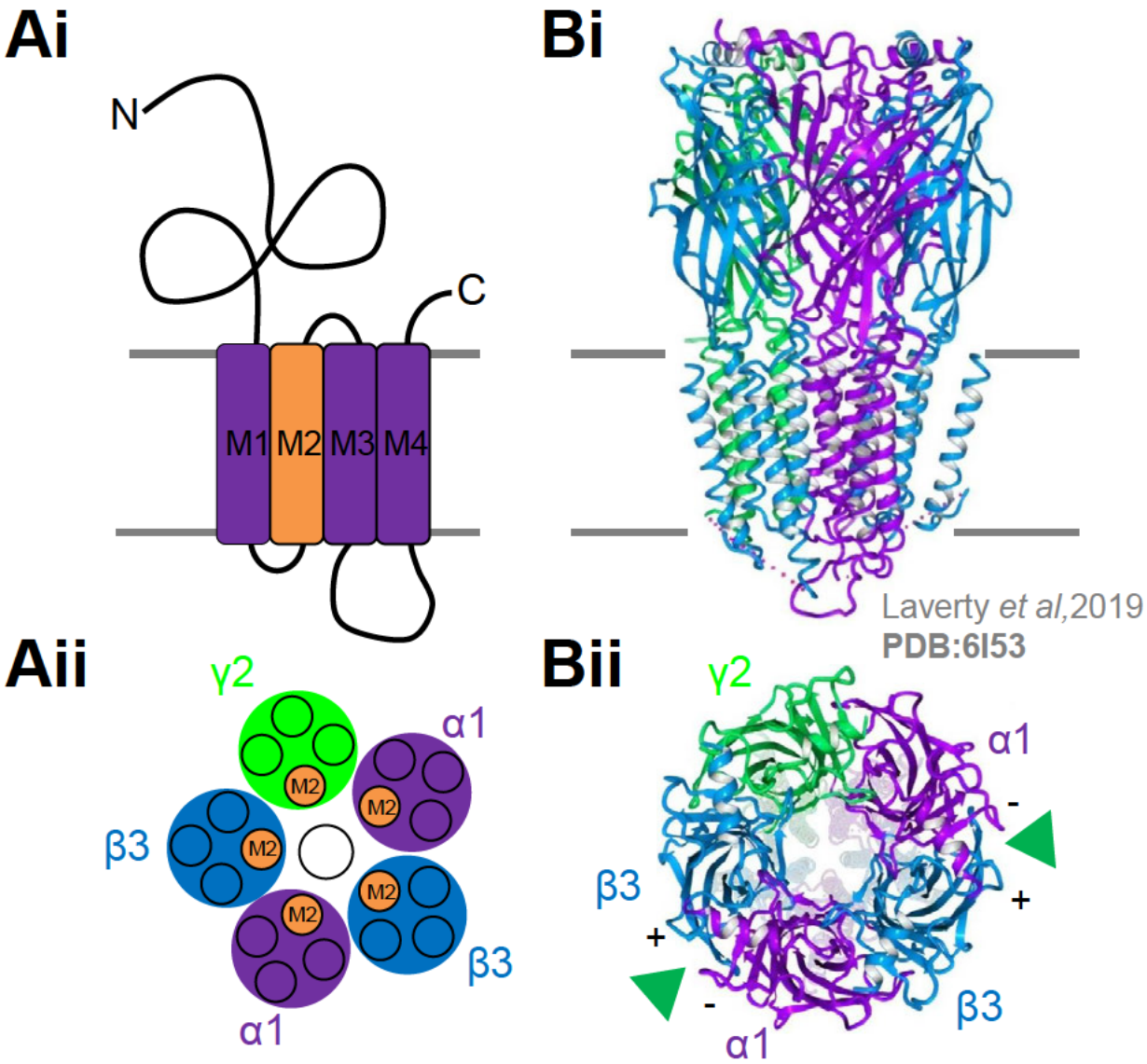

Fig.1.1. $GABA_AR$ subunit and receptor structure.
Ai) A cartoon depiction of an individual $GABA_AR$ subunit: long extracellular N-terminus, short extracellular C-terminus and four transmembrane domains (M1-M4). M2 (orange) lines the pore as shown in **Aii). Bi)** α1β3γ2 receptor showing the extracellular domain and transmembrane domain; the intracellular domain is not fully resolved. **Bii)** Top down view of the α1β3γ2 receptor shows the pentameric structure and the two GABA (green triangles) binding sites (β+/α- subunit interface). Structure from *Laverty et al, 2019 PDB:6I53*

1.5 $GABA_AR$ signalling

The orthosteric sites of the $GABA_AR$ can bind a variety of ligands. Ligands are typically characterised by their *affinity*: the strength of binding to the receptor. And their *efficacy*: the effectiveness with which a ligand can affect gating (i.e. activate or inhibit receptor opening). Reflecting both the affinity of a ligand and its gating efficacy is the *potency*: the concentration of the ligand needed to produce an effect of given intensity (e.g. half maximal effective concentration; EC_{50}). Potency is a measure of the sensitivity of $GABA_ARs$ to a ligand. The potency of GABA (and other ligands) is influenced by the subunit composition of $GABA_AR$ isoforms (179), and differences in GABA potency underpins important aspects of $GABA_AR$ signalling (e.g. tonic inhibition) (61), as will be discussed later.

From the perspective of affinity and efficacy, full agonists have affinity and efficacy: they bind to the orthosteric sites and once bound cause maximal opening (gating activation) at saturating concentrations (e.g. an efficacy of 1). Partial agonists have affinity but lower efficacy: they also bind to the orthosteric sites and activate the receptor, but their effect on channel opening at saturating concentrations is submaximal in relation to full agonists (e.g. efficacy of <1, but >0). Partial agonists can thus antagonise the effect of a full agonist. Antagonists have affinity but no efficacy: they bind to the orthosteric sites but do not affect the opening of the receptor; they cause neither activation nor inhibition but prevent the binding of other orthosteric ligands (e.g. affinity for the receptor but efficacy of 0). Unliganded receptors – including $GABA_ARs$ – can spontaneously open due to constitutive receptor activity. Inverse agonists have affinity and negative efficacy: they bind to the orthosteric sites and decrease (fully or partially) spontaneous receptor openings (e.g efficacy <1). Another family of ligands that are able to inhibit spontaneous receptor activity and agonist activated openings are non-competitive antagonists. These compounds inhibit the receptor at allosteric (non-orthosteric) sites (e.g. channel blockers) (**Fig.1.2**).

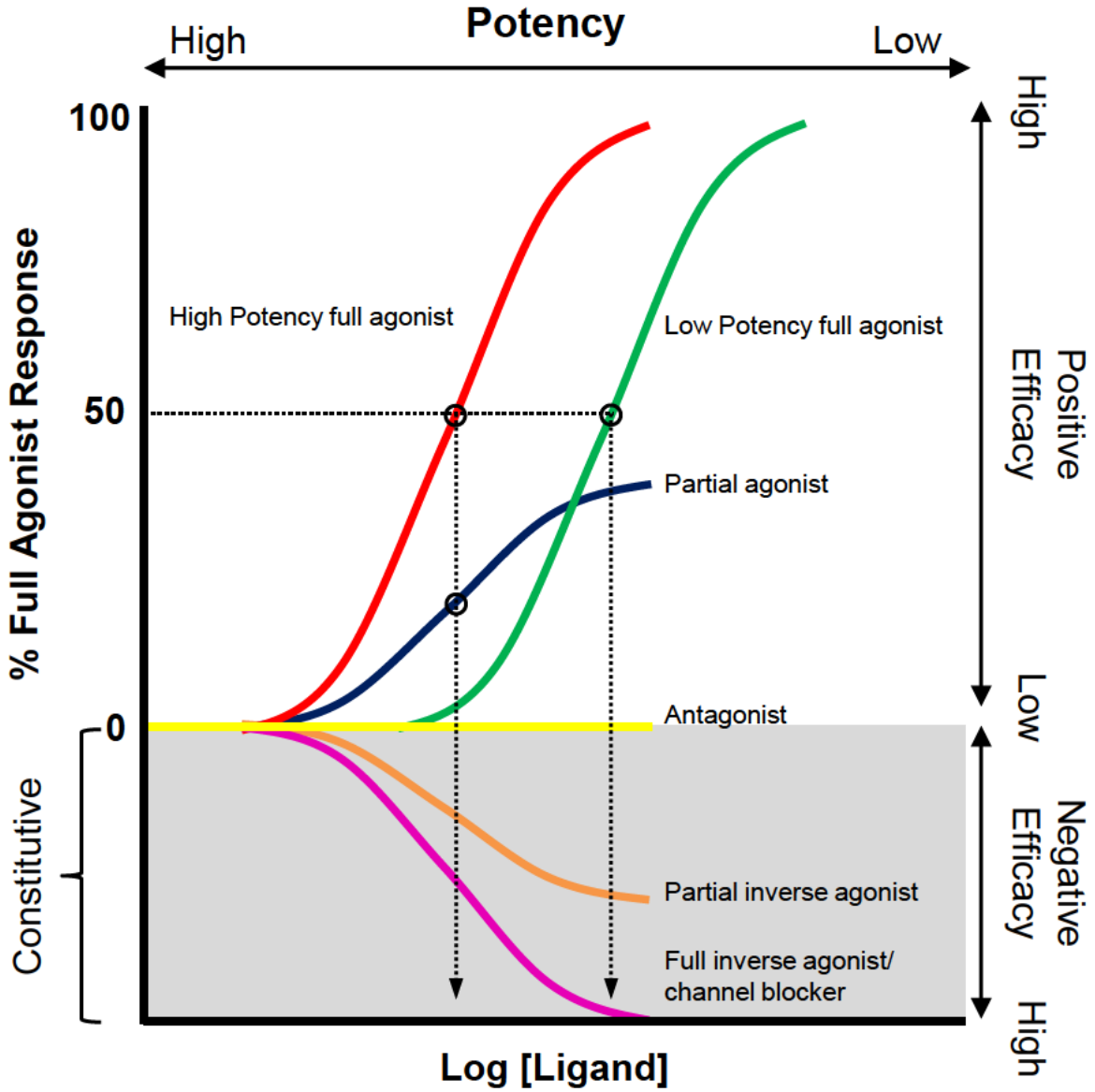

Fig.1.2.Mock Concentration–response curves.
Red: High potency full agonist produces maximum response at saturating concentrations. **Blue:** An equally highly potent partial-agonist has an identical EC_{50} to the full agonist, but has a lower gating efficacy and so at saturating concentrations produces a submaximal response. **Green:** Low potency full agonist is able to produce a maximal response, but the lower potency means that a greater concentration is required for a given response (higher EC_{50}). **Yellow:** Competitive neutral antagonist has affinity but no efficacy. **Orange:** High potency partial inverse agonist and **Pink**: High potency full inverse agonist (or channel blocker) is able to decrease constitutive activity (inhibit spontaneous openings).

The scheme on the previous page is based on that in Weir, 2010 (180). Although still common in the lexicon, it is important to note that affinity and efficacy are not easily separated (181,182). Fundamentally, the problem is that binding and gating are reciprocal: binding affects gating, and so gating will affect binding (181,182). Thus, experimental measures of the binding of an agonist (e.g. in a radioligand binding assay), reflects not only binding but also its ability to open the channel once it is bound (gating efficacy). Despite this important caveat, affinity and efficacy are still useful when discussing drug action at $GABA_A$Rs and other pLGICs (181).

There are various kinetic models that have examined – and have been proposed to explain – how the $GABA_A$R activates. Such models propose that the receptor can exist in a number of discrete states that are connected by reversible chemical reaction steps, and that the rate constants of these reactions determine the frequency of state changes (e.g. from open to closed). Any model of the $GABA_A$R has to be able to explain various fundamental properties of $GABA_A$R gating, including: 1) The difference in gating efficacy of full and partial agonists, 2) that unliganded $GABA_A$Rs can open spontaneously, and 3) that there are agonist-bound $GABA_A$R desensitised state(s) (183). Desensitisation occurs in the sustained presence of an agonist, which causes receptors to transition from agonist-bound open states to agonist bound shut (desensitised) states. Desensitised states are refractory to any further activation, requiring agonist dissociation to return to an agonist sensitive, resting state (184).

Linear Receptor Models

A very early and important model was proposed by Castillo–Katz mechanism in an attempt to explain the partial agonism of choline vs. the full agonism of ACh at frog endplate nAChRs (185),

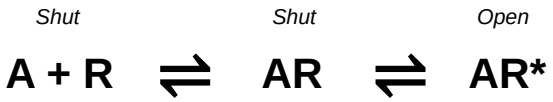

Reaction scheme from: Colquhoun and Lape, 2012 (186). The model proposes that an agonist (A) binds to a resting (shut) receptor (R) to form an intermediate shut agonist-receptor complex (AR) that can transition into an open receptor (AR*). This two-step model has separate

equilibrium constants that govern binding affinity (A + R → AR) and gating efficacy (AR → AR*). And can explain the difference between full agonists and partial agonists and antagonists. Each of these compounds have affinity for the receptor (A + R → AR) but differ in their ability to shift the gating equilibrium constant (AR→AR*). Agonists act to shift the gating equilibrium in favour of AR* to a greater extent than partial agonists. Conversely, antagonists do bind but do not affect this equilibrium. Crucially, in this model, agonists are *inducing* conformational changes in the receptor to affect gating. However, the model is too simple to describe the activation of the $GABA_AR$ and other LGICs. It does not account for spontaneous openings or additional agonist bound desensitised states.

The simple linear model can be modified, as in the below example from Mortensen *et al* (187), to incorporate a desensitised state (A_2D) and separate states for mono and di-liganded $GABA_AR$ activation. This is important because although $GABA_AR$s require the binding of two molecules of GABA to fully activate, they can also activate (submaximally) when bound to a single molecule of GABA (188,189).

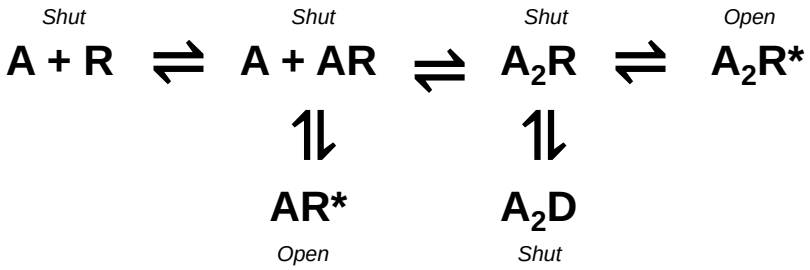

Reaction scheme from: Mortensen et al, 2004 (187). This relatively simple kinetic model can account for many aspects of $GABA_AR$ activation (187) and can – along with other models like it – be used to distinguish between different synaptic and extrasynaptic $GABA_AR$ isoforms (190,191). However, as indicated by Chang and Weiss, it struggles to account for spontaneous openings of the $GABA_AR$ (192). Specifically, when the authors incorporated an unbound closed state (R) to an unbound open state (R*) transition (R→R*) into a linear model, it required that agonist binding affinity was also increased (192). However, in the spontaneously opening mutant receptor that they studied, the mutation in the TMD is not thought to affect binding but instead destabilise the closed state (192). Cyclic models of receptor activation can circumvent this problem.

Cyclic MWC Receptor Model

The Monod Wyman Changeux (MWC), or “two-state”, model was originally proposed for the binding to oxygen to haemoglobin (193,194) and has since been applied widely to $GABA_A$Rs (e.g. (102,195–199)), other LGICs and other proteins (102,194,200). The MWC model has two simple rules: 1) that receptors can adopt two global conformational states, closed (_R) and open (_R*), and 2) that these two conformations have a different affinity for a ligand.

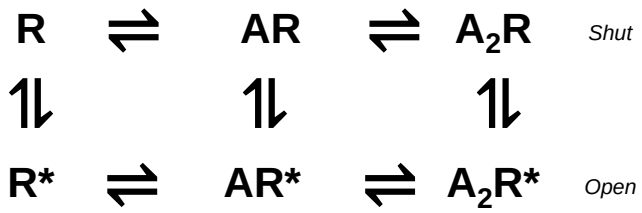

Reaction scheme from: Colquhoun and Lape, 2012 (186). An attractive aspect of the MWC model is how simply it accounts for spontaneous openings: in the absence of an agonist, open and closed states spontaneously establish an intrinsic equilibrium (R⇌R*), which mean that spontaneous openings occur with a certain probability. The probability that a receptor occupies the open state is determined by the equilibrium constant (energy barrier) between the two states. In this model, the action of an agonist is explained by 1) them having a higher affinity for the open (R*) state and 2) when they bind to this state (AR* or A_2R*) they stabilise (select) the open conformation so that the equilibrium between two states shifts in favour of the open state (AR→AR*). Antagonists bind with similar affinity to the open and closed state (i.e. they do not select one state over another) and so do not affect the equilibrium between AR⇌AR*. Conversely, inverse agonists preferentially bind and stabilise the receptor closed state, thereby shifting the equilibrium in favour of AR (selecting the closed state) to reduce spontaneous activity AR←AR*. Thus, unlike the linear models, the MWC mechanism is not one of conformational *induction.* Instead, it is based on conformational *selection*: agonists are not inducing conformational changes that open the channel, they are preferentially stabilising the open conformation that already exists in thermal equilibrium at rest.

Flip Receptor Model

However, one problem with the two-state MWC model is that it is apparent from single-channel recordings of $GABA_A$Rs, and other LGICs, that channel gating results from transitions among more than two discrete states (201,202). Both native and recombinant $GABA_A$Rs exhibit complex bursting patterns, which indicates that in the absence of an agonist they have more than one shut state from which they can open, and more than one open state in the presence of saturating concentrations of an agonist (203–209). An early model incorporating additional states was proposed by Jones and Westbrook to explain $GABA_A$R deactivation and desensitisation (188). In this model, there are two agonist bound shut states, from which the receptor can either enter an open *or* desensitised state (e.g AD ⇌ AR ⇌ AR*) i.e. the open state and desensitised (shut) state lie either side of the resting agonist bound state (also shut). More recently, an alternative, partially cyclic, model has been applied to $GABA_A$Rs (203,210,211) and other LGICs (212,213): the, so-called, 'flip' model. This model incorporates 'flip' (F) states, which are between resting (R) and open states (F*). The flip state is preactivated: it is non-conducting but immediately precedes channel opening (i.e. it might correspond to the conformational change in the receptor that occurs before opening).

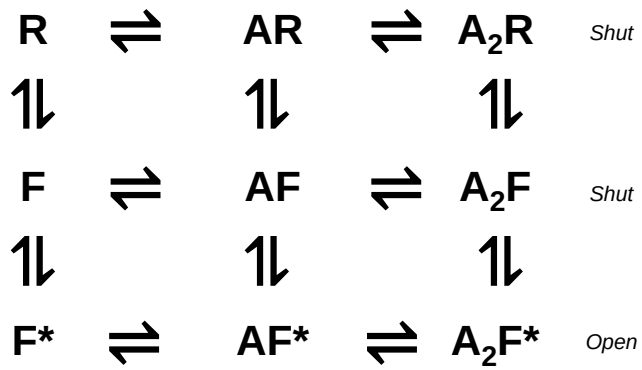

Reaction scheme from: Colquhoun and Lape, 2012 (186). The flip model was originally developed to explain the behaviour of heteromeric GlyRs (213) and was later extended to explain partial agonism at nACHRs (212). Analogous to the MWC model, the flip model proposes that the receptor is in equilibrium between states, and agonists bind with different affinities to particular states to preferentially stabilise them. However, in the flip model, this equilibrium is between resting and flipped states – not resting and open – and agonists have a

higher affinity for the flipped state compared to the resting state. The action of partial agonists is explained by them being less able to 'flip' the receptor (AR→AF) than full agonists, but both partial and full agonists are just as effective at opening the receptor once flipped (AF→AF*). The flip model has since been applied to spontaneous activation of $GABA_AR$s (210,211) and to explain the action of BDZ-site ligands at $GABA_AR$s (203).

At the structural level, agonist-mediated activation of the $GABA_AR$ is associated with the closing, or 'capping', of extracellular domain loop-C, which constricts the orthosteric site around the agonist (98,100,214,215). Conversely, antagonists cause expansion of this site. The constriction of the orthosteric site results in a concerted rotation of the five subunit extracellular domains (98,100,214). As the entire extracellular domain of the receptor rotates, it triggers conformational changes in the transmembrane domain to cause tilting of the M2 helices away from the channel pore to cause gating (98,100,214).

1.6 The $GABA_AR$ signal

Although some of the kinetics and structural underpinnings of $GABA_AR$ signalling are yet to be fully resolved, what is clear is that receptor activation – by an agonist or due to constitutive activity – causes the channel to open. The $GABA_AR$ channel is permeable to Cl^- and, to a lesser degree HCO_3^-, and so the effect of channel opening on a neuron is two-fold. First, activation of $GABA_AR$s causes an increase in membrane conductance. Second, if there is a net driving force on the permeant anions, there will be a net flow of charge (a current) across the membrane and, in turn, a change in the membrane potential.

The ionic driving force is determined by the position of the reversal potential for $GABA_AR$ responses (E_{GABA}) relative to the resting membrane potential (RMP) of the neuron (216,217). When E_{GABA}<RMP, activation of $GABA_AR$s results in the net influx of Cl^- and membrane *hyperpolarisation*. Conversely, when E_{GABA}>RMP, activation of $GABA_AR$s results in the net efflux of Cl^- and membrane *depolarisation*. Or, to put it another way, activation of $GABA_AR$s shifts membrane potential (Vm) toward E_{GABA}. E_{GABA} itself depends on the relative concentration of ions Cl^- and HCO_3^- across the membrane (i.e. the Nernst equation) (216,217). Because Cl^- is the major permeant ion, it means that E_{GABA} is predominantly determined by E_{Cl^-}, which in most mature adult neurons, is -85 mV to −70 mV (216,217). However, the E_{HCO3^-} is more depolarised,

typically −40 mV to −20 mV, which means that E_{GABA} is often more depolarised than E_{Cl^-} (216,217). Thus, in most mature neurons, E_{GABA} is only slightly more hyperpolarised than the RMP (-75 to -65 mV), and so $GABA_AR$ signalling is usually only weakly hyperpolarising (and sometimes non-polarising/depolarising) (216,217). It is important to note, however, that $GABA_ARs$ can affect a neuron even in the absence of significant membrane polarisation by increasing membrane conductance (decreasing input resistance), which is termed “shunting”.

The E_{Cl^-} is hyperpolarised in most mature adult neurons because intracellular [Cl^-] is kept low, typically in the range of 5-15 mM (218–221), relative to extracellular [Cl^-] (~120 mM). Adult neurons primarily use the neuron-specific chloride-extruding potassium–chloride co-transporter (KCC2) to maintain this low [Cl^-] (216,217). KCC2 is localised to inhibitory and excitatory synapses, as well as the dendrites and cell body (222). It is a secondary active transporter, in that it uses the electrochemical gradient of K^+ to efflux Cl^- against its gradient (although changes to the K^+ gradient can result in Cl^- import). In contrast to the adult brain, during development KCC2 expression is low, whereas the Cl^- accumulator NKCC1 is high. Intracellular [Cl^-] is thus elevated during development and $GABA_AR$-mediated responses are depolarising (216,217,223).

1.7 Modes of $GABA_AR$ inhibition

There are two principal modes of $GABA_A$Rs-mediated signalling: *phasic* and *tonic* inhibition. There is also a third signalling mode, which overlaps phasic and tonic, termed 'spillover' inhibition. Spillover inhibition is caused by GABA released during phasic inhibition activating the $GABA_A$Rs that typically produce tonic inhibition (66–72). Note that, for the sake of readability in the following section, we will use the term 'inhibition' when describing the modes of $GABA_A$R signalling. This is in line with much of the literature on $GABA_A$R physiology (61,224). Nevertheless, it is important to note that $GABA_A$R activation can also produce excitation. One of the main factors in determining if activation of $GABA_A$Rs causes excitation or inhibition is their effect on membrane potential (depolarisation or hyperpolarisation). But it is an oversimplification to think that depolarisation = excitation: because $GABA_A$R activation causes a concomitant increase in membrane conductance, even with depolarisation the net effect can be inhibitory (225,226). Nor is it the case that hyperpolarisation = inhibition: it can trigger hyperpolarisation-activated excitatory currents that drive a neuron to rebound fire (227).

1.7.1 Phasic inhibition

Phasic inhibition is a fast, point-to-point form of neurotransmission that is mediated by α1β2γ2, α2β3γ2 and α3β3γ2 receptor isoforms that are clustered on the post-synaptic membrane. These post-synaptic $GABA_A$Rs are transiently activated by high concentrations of GABA released from the presynaptic terminal (1-3 mM; 100 µs duration) (62,63). The inhibitory postsynaptic currents (IPSCs) that are generated are fast activating (<1 ms) and rapidly decaying (tens to hundreds of milliseconds) (188,191,208). IPSC properties vary across brain regions and can be both action-potential independent, due to spontaneous vesicle fusion (minis, mIPSCs), and action-potential dependent (spontaneous, sIPSCs or experimentally evoked). Because synaptic $GABA_A$Rs have to respond to a high concentration of GABA, they have a relatively low potency for GABA (EC_{50}): α1β2γ2 (6.6 µM) α2β3γ2 (13.4 µM) and α3β3γ2 (12.5 µM) compared to receptors that are excluded from the synapse (179). The clustering of these isoforms at the synapse is primarily driven by the scaffolding protein, Gephyrin, which anchors $GABA_A$R subunits to the cytoskeletal proteins (228,229).

1.7.2 Tonic inhibition

Tonic inhibition, or more specifically, the tonic *conductance* that is generated by persistently active $GABA_A$Rs, is a slow form of neurotransmission and is expressed widely across many different neuron types (61,224,230–232). The persistent activation of $GABA_A$Rs can occur via two mechanisms: GABA-*dependent* and GABA-*independent* (74,224,233,234).

To briefly summarise:

GABA-dependent tonic inhibition is mediated by peri-/extra-synaptic $GABA_A$Rs that have a high-potency for GABA (61,224,230–232). Because of their high potency, extrasynaptic receptors can be persistently activated by low concentrations of ambient GABA (179,235). GABA-dependent tonic currents can be blocked by saturating concentrations of competitive antagonists, inverse agonists, and channel-blockers.

GABA-independent tonic inhibition is mediated by $GABA_A$Rs that activate spontaneously, in the absence of GABA, because they exhibit constitutive receptor gating (74,233,234,236,237). Because spontaneously activating $GABA_A$Rs do not require GABA to activate, they are resistant to competitive antagonists but can be inhibited by inverse agonists and channel-blockers (sometimes termed non-competitive antagonists) (74,233,234,236,237).

1.7.3 Measuring tonic inhibition

Tonic inhibition is revealed and, in turn, can be measured by applying saturating concentrations of $GABA_AR$ antagonists. The most commonly used are SR-95531 (gabazine), bicuculline, and picrotoxin (230). $GABA_AR$ responses are often recorded with a symmetrical concentration of Cl^- on either side of the membrane (E_{Cl^-} ~ 0 mV). In this recording configuration, when the holding potential is -70 mV, GABA-ergic currents are inward. This means that phasic currents, IPSCs, are seen as transient negative-going defections, whereas the block of the tonic conductance causes an outward current (230).

SR-95531: (SR) is a specific, competitive, and potent antagonist of $GABA_ARs$ (74,238–242). The apparent inhibitory constant (Ki) value for the displacement of GABA binding by SR is 140 - 150 nM (239,243), and for the displacement of muscimol is 74 nM (244). SR has a <1 µM relative IC_{50} for antagonising $GABA_AR$ responses evoked by concentrations of GABA at, or close to, EC_{50} in recombinant expression systems (245–255) and in cultured neurons (256). It also has a <1 µM relative IC_{50} against $GABA_AR$ responses evoked by 20 µM isoguvacine, another $GABA_AR$ agonist (244). SR has a very limited negative intrinsic efficacy against constitutively active receptors and receptors activated by allosteric ligands; for this reason, it is generally used as a neutral competitive antagonist (192,199,246,257–260). This means that it is only effective against GABA-dependent tonic inhibition and phasic inhibition; it is ineffective against the GABA-independent form of tonic inhibition (because competitive antagonists do not affect constitutive receptor activity). From the perspective of the MWC model, SR binds with similar affinity to the closed state (R) and the active receptor state (R*), and thus does not affect the equilibrium that dictates the level of spontaneous activity ($R \rightleftharpoons R^*$). SR is considered saturating when used at 10 - 100 µM (261–268). For the study of GABA-dependent tonic inhibition, <1 µM SR can be insufficient to fully displace GABA from the receptor and block the GABA-activated conductance (269). However, when the concentration of SR is increased to ~10 µM it is able to fully displace GABA from the receptor and block GABA-activated tonic conductance (267,269).

Bicuculline: is a $GABA_AR$ inverse agonist: it blocks GABA binding to the orthosteric site *and* partially inhibits receptor gating arising from allosteric activation or constitutive activity (74,192,233,246,256,260,270–274). The apparent Ki for bicuculline is 5.2 μM (239,243) and its recorded IC_{50} for antagonising $GABA_AR$ responses evoked by EC_{50} GABA is 7.2 μM at recombinant receptors (247), and is 2.7 μM at native receptors (275). From the perspective of the MWC model, bicuculline preferentially binds and stabilises the R conformation vs. R*, shifting the equilibrium in favour of R to partially decrease spontaneous activity (R←R*). Because of its negative efficacy, bicuculline can inhibit GABA-dependent tonic conductance *and* partially inhibit GABA-independent tonic conductance (74,233).

Picrotoxin: (PTX) is a channel-blocker that binds within the open-channel pore and acts allosterically, not via simple hindrance of ion flow, to stabilise the $GABA_AR$ in a closed/resting, non-conductive state (98). Similar to bicuculline, PTX shifts the open/shut equilibrium in favour of R to reduce spontaneous activity (R←R*); however, because PTX is more efficacious than bicuculline, it can virtually eliminate spontaneous activity. Henceforth, PTX is able to fully block both GABA-dependent and GABA-independent conductance (74,233). Furthermore, because PTX binds within the channel, it can inhibit $GABA_ARs$ even when the orthosteric site is occupied by a neutral antagonist (SR). This allows for the specific block of GABA-independent conductance, without a confounding effect of GABA-mediated receptor activation. The recorded IC_{50} of PTX inhibiting $GABA_AR$ responses evoked by EC_{50} GABA is 1.1 μM at recombinant receptors (276), and 5.1 μM at native receptors (275).

Modes of $GABA_AR$ inhibition

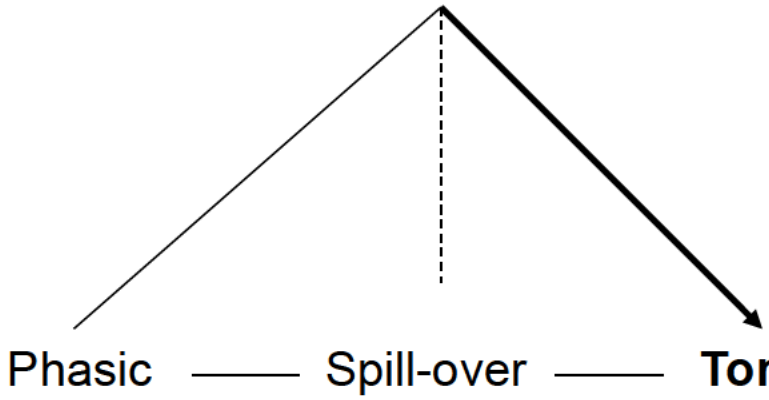

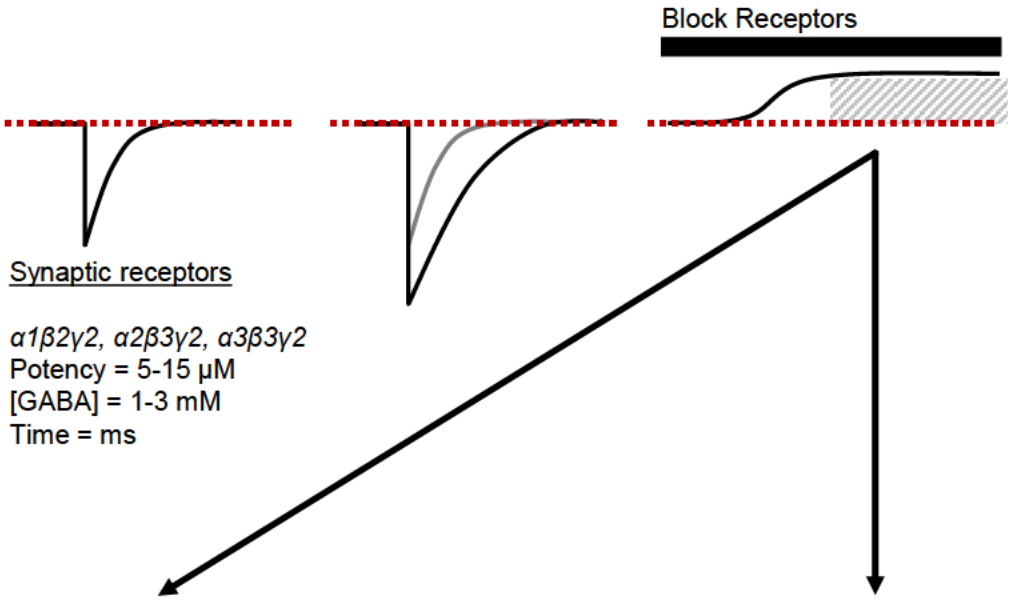

Synaptic receptors

α1β2γ2, α2β3γ2, α3β3γ2
Potency = 5-15 μM
[GABA] = 1-3 mM
Time = ms

GABA-dependent

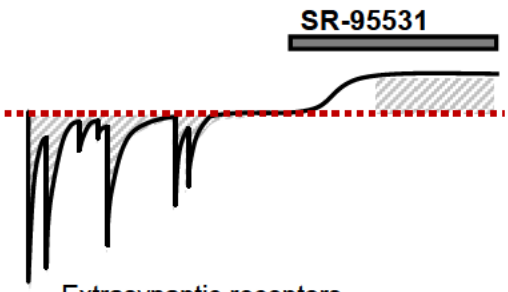

Extrasynaptic receptors

α4βδ, α6βδ, α5βγ2, α1βδ
Potency = 0.2-2 μM
[GABA] = 3 nM - 0.3 μM
Time = seconds, minutes

Blocked by:
- Competitive antagonists (SR-95531)
- Inverse agonists (bicuculline)
- Channel blockers (PTX)

GABA-independent

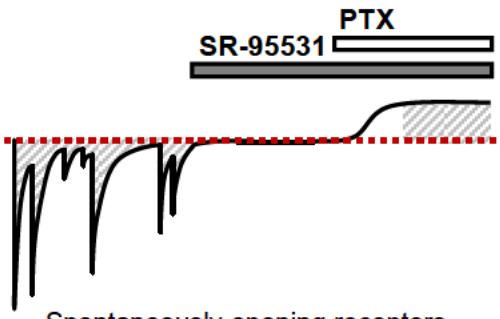

Spontaneously-opening receptors

Maybe: α4βδ, α5βγ2, α1β1γ2, α1β3γ2
Potency = n/a
[GABA] = 0
Time = seconds, minutes

Blocked by:
- Inverse agonists (bicuculline)
- Channel blockers (PTX)

Resistant to:
- Competitive antagonists (SR-95531)

1.8 GABA-dependent tonic inhibition

High-potency, peri-/extra-synaptic $GABA_A$Rs are activated by low concentrations of ambient GABA to generate a persistent GABA-dependent, tonic conductance (61,224,230–232). A tonic conductance that is exclusively GABA-dependent should be completely blocked by saturating concentrations of SR, bicuculline, or PTX. The concentration of GABA in the extracellular space varies across brain regions (between 1 nM to 2.5 µM) (70,73), but in the hippocampus is very low: 3 nM - 0.3 µM (74–78). The level of extracellular GABA depends on the release and reuptake mechanisms outlined in **1.2**; it is also influenced by temperature (72,277), redox reagents (278), and can be altered substantially by a variety of pharmacological compounds that affect GABA metabolism, vesicle loading and reuptake (61).

The idea that extrasynaptic $GABA_A$Rs respond to extracellular 'ambient' GABA has its roots in studies of the peripheral nervous system by Bowery and Brown in the 1970s (279,280). However, it was not until 1991 that tonic $GABA_A$R conductance was first observed in the CNS. Specifically, Otis *et al* demonstrated that the application of bicuculline to hippocampal granule cells blocked spontaneous (TTX-resistant) IPSCs *and* caused a block of tonic conductance (as indicated an outward current) (281). Similar bicuculline-mediated outward currents were recorded from embryonic hippocampal neurons by Valeyev *et al* (282) and in early postnatal hippocampal neurons by Ben-Ari *et al* in 1994 (283). In 1996, the presence of tonic conductance outside of the hippocampus was reported by Salin and Prince in somatosensory cortex neurons (284). The authors posited that the tonic conductance "results from ongoing activation of synaptic or extrasynaptic GABA receptors located so remotely on dendrites" (284). Cerebellar granule cells were also shown to exhibit a tonic $GABA_A$R conductance that could be blocked by SR and bicuculline (79,285,286), and it was in these cells that the first comprehensive analysis of tonic $GABA_A$R conductance was performed by Brickley *et al* in 1996 (80). They made several important findings that would shape much of the subsequent work on tonic $GABA_A$R conductance. First, they showed that development (P7 to P21) is associated with a substantial increase in the tonic $GABA_A$R conductance to the degree that, in mature neurons, tonically active $GABA_A$Rs net contribute 99% of the total inhibitory charge (80). Second, they showed that blocking tonic $GABA_A$R conductance increases the excitability of cerebellar granule cells, as indicated by the decrease in the minimum current required for fire an action potential

(rheobase) and the additive (leftward) offset in the input-output (AP frequency-current, F-I) relationship (80). This study, in particular, demonstrated that tonic $GABA_AR$ conductance is not just *present* but is *sufficient* to affect neuron function and paved the way for many further investigations.

Over the last two and a half decades, it has been realised that GABA-dependent tonic $GABA_AR$ conductance is widely expressed in the brain, across a litany of neuron types, and is a critical regulator for proper brain function (224,230). The ubiquity of this signal is well summarised by Lee and Maguire in 2014 (224), which details over 60 neuron types that express a tonic $GABA_AR$ conductance. At the level of the single neuron, GABA-dependent tonic conductance has been shown to regulate cell excitability (80,287,288), input-output gain (289–295), firing characteristics (225,296), signal integration (297,298), and synaptic plasticity (299,300). At the network level, GABA-dependent tonic inhibition affects network oscillations (301–303), synchronisation (225), and the propagation of seizure activity (304–306). These effects of tonic inhibition manifest at the behavioural level, with tonic inhibition involved in learning and memory (307,308), anxiety (306,309), and sleep (310,311), to name but a few. Furthermore, disruptions to tonic inhibition are associated with various pathological conditions, including temporal lobe epilepsy (312,313), fragile-X syndrome (314), Alzheimer's disease (299), and stroke (315).

1.8.1 The GABA-dependent tonic signal

The aforementioned functional consequences of GABA-dependent tonic inhibition are governed by 1) the nature of the tonic signal inputted to the neuron, and 2) how this signal is integrated and interpreted by the neuron. The tonic signal that is inputted to a neuron by GABA-dependent tonic conductance has two components: 1) a persistent increase in membrane conductance (shunting), and 2) if there is a driving force on the permeant anions, a persistent membrane polarisation (depolarisation or hyperpolarisation).

An increase in membrane conductance always accompanies the activation of $GABA_ARs$ and many of the functional effects of GABA-dependent tonic inhibition are a consequence of this membrane shunt. As a result, a great deal of energy has been directed at trying to dissect how membrane shunting affects neuronal function.

The functional consequences of tonic membrane shunting differs when the neuron is above vs. below AP threshold. Below threshold, shunting inhibition reduces excitability by exerting a divisive effect on sub-threshold voltages in accordance with Ohm's law (V=I/G): the amplitude of a voltage transient (V) elicited by a given excitatory current (I) is reduced proportionately to the increase in membrane conductance (G). This means that more current is required for the neuron to cross the AP threshold voltage and initiate an action potential (the rheobase current). Furthermore, shunting also decreases the membrane time constant, meaning that voltage transients are not just smaller, but decay faster (316–318). This means that to cross threshold, excitatory inputs need to coincide within a narrower temporal window, thereby enhancing the precision of neural signalling (297,298,319).

The divisive effect of shunting was originally thought to persist above AP threshold and lead to a decrease in the gain of the firing rate-to-injected current (F-I) relationship (316,318,320,321). This was based on the assumption that AP firing rate was essentially a function of – and could, therefore, be calculated from – the membrane potential that the neuron would reach were spiking to be disabled (this is sometimes referred to as the generator potential) (320,322–324). Because shunting conductance would have a divisive effect on the generator potential, it was inferred that AP firing rate would follow suit: that the slope of the F-I curve would be divisively scaled by shunting inhibition (322–325).

However, when theoretical and experimental studies tested this hypothesis with constant, step-wise current injections, they provided evidence to the contrary: F-I curves were offset in a subtractive, *not* divisive, manner by shunting inhibition – the slope was unchanged, but the entire curve was shifted to the right (80,322). The reason for shunting-induced subtraction, not division, was explained in a seminal study by Koch and Holt, entitled *"Shunting Inhibition Does Not Have a Divisive Effect on Firing Rates"* (322). What the original "divisive hypothesis" failed to take into account was the extent to which the spiking mechanism affects the biophysical membrane properties (322,325). Indeed, during sustained excitation, the APs do not simply ride atop the generator potential once the threshold is crossed. Instead, the spiking mechanism, specifically the large K^+ conductance responsible for repolarisation and the after-hyperpolarisation (AHP) (326), clamps the steady-state potential at (or close to) threshold – and

keep it there for the duration of the input current step, irrespective of the input amplitude and the number of spikes it elicits (322,325). This means that above AP threshold, the inhibitory effect of a shunting conductance does not scale proportionately with the excitatory input (322,325). It is the uncoupling of excitation and inhibition that prevents a shunting conductance from acting divisively (322,325). Instead, by clamping the steady-state potential approximately at AP threshold, an inward driving force on Cl^- is established (E_{GABA}<Vm); and so the conductance that was shunting at RMP is now converted into a source for a hyperpolarising 'leak' current (322,325). The amplitude of this current is uniform across different input strengths (so long as they are suprathreshold), which is why it causes a subtractive offset to the F-I curve.

The aforementioned schema holds up well, across numerous neuron types, as an accurate description of the effect tonic shunting inhibition has on F-I curves that are generated with square-wave depolarising current injections. However, there are (at least) three major factors when the 'subtractive hypothesis' breaks down. These are 1) stochastic noise (292,293), 2) active dendritic conductances (295), and 3) spike-frequency adaptation (294,317). A detailed description of each of these mechanisms can be found in the appendix. In short, each of these mechanisms allow a tonic shunting conductance to control neuronal gain (the slope of the F-I curve). Thus, a GABA-dependent tonic shunt can act in an additive/subtractive *or* multiplicative/divisive manner, depending on various intrinsic and extrinsic neuron properties.

If there is a driving force on the permeant anions, the tonic conductance will also be accompanied by a persistent membrane polarisation. When E_{GABA}<RMP, GABA-dependent tonic inhibition results in a persistent membrane hyperpolarisation. Although there are exceptions, in general, by shifting the RMP further from the AP threshold, hyperpolarisation works synergistically with the membrane shunt to decrease excitability. Neurons not only require larger depolarising currents to overcome the increased conductance, but also to traverse the larger voltage difference between RMP and threshold. This is the case, for instance, with GABA-dependent tonic conductance in thalamic relay neurons, where GABA-dependent tonic conductance promotes burst firing (327). When E_{GABA}>RMP, GABA-dependent tonic inhibition results in a persistent membrane depolarisation. The relationship between shunting and depolarisation is more complex than with hyperpolarisation. If E_{GABA} is more depolarised than

AP threshold, then tonic activation of $GABA_A$Rs can depolarise the neuron to fire an action potential. And even if E_{GABA} is less depolarised than AP threshold, tonic conductance can still trigger an action potential by activating voltage-dependent channels (226). That said, membrane shunting and depolarisation generally work antagonistically, which can lead to a complex interplay between the two signalling mechanisms. A good example of this can be found in Song *et al* in 2011 (226). The authors reported that hippocampal interneurons respond in a biphasic manner to GABA-dependent tonic inhibition. Underlying this biphasic response is that, in these neurons, E_{GABA}>RMP and tonic inhibition is depolarising. As a result, low levels of tonic conductance generate a membrane depolarisation that activates voltage-gated Na^+ channels to increase action potential firing rate (excitatory). However, at higher levels of tonic conductance, the membrane shunt overwhelms the depolarisation leading to a decrease in firing rate (inhibition) (226).

1.8.2 Receptor isoforms responsible for GABA-dependent tonic conductance

The prototypical extrasynaptic $GABA_A$Rs that mediate GABA-dependent tonic conductance are: α4βδ, α6βδ, α5βγ2 and α1βδ receptors (138,224,328). They exhibit a higher potency for GABA than synaptic receptors (see below). The potency of $GABA_A$Rs for GABA is influenced by the α-subunit: high potency α6; intermediate potency α1, α4, and α5; low potency α2 and α3 (179). Potency is also influenced by the β-subunit: β3 > β2 > β1(179). As well as the auxiliary subunits: δ > γ (248).

Potency of GABA at synaptic and extrasynaptic $GABA_A$Rs

Synaptic	**Extrasynaptic**	**Neuron type**
α1β2γ2 (6.6 μM)	α4β2δ (0.91 μM)	dentate gyrus granule cells, thalamic relay cells
α2β3γ2 (13.4 μM)	α4β3δ (1.7 μM)	thalamic relay cells
α3β3γ2 (12.5 μM)	α6β3δ (0.17 μM)	cerebellar granule cells
	α5β3γ2 (1.4 μM)	hippocampal pyramidal + granule cells
	α1β2δ (3.7 μM)	hippocampal interneurons

1.9 GABA-independent tonic inhibition

GABA-independent tonic conductance is mediated by $GABA_A$Rs that activate spontaneously, in the absence of GABA, because they exhibit constitutive receptor gating (74,233,234,236,237). Because spontaneously activating $GABA_A$Rs do not require GABA to activate, they are resistant to competitive antagonists (SR) but can be inhibited by inverse agonists (bicuculline) and channel-blockers (PTX) (74,233,234,236,237).

Note: *'s-$GABA_A$Rs'* will be used from hereon in to denote 'spontaneously activating $GABA_A$Rs'

One of the first indications that tonic conductance could arise from constitutively active s-$GABA_A$Rs was the study Bai *et al,* in 2001 (270). The authors recorded from hippocampal pyramidal neurons and showed that phasic and tonic inhibition were differentially sensitive to the competitive antagonist, SR (270). Whereas SR could effectively block phasic inhibition, no block of tonic inhibition was observed, even with saturating concentrations of SR (20 μM). This did not simply reflect tonic inhibition being absent in these neurons, because tonic inhibition was blocked by bicuculline and PTX (270). On its own, there are multiple explanations for these observations (270).

One possibility is that SR simply has a low affinity for the $GABA_A$Rs that are producing tonic inhibition in these neurons, and so is unable to displace GABA from its binding sites. To test this, Bai *et al* applied SR, and then, in its continued presence, bicuculline (270). They found that, in the presence of SR, bicuculline was no longer able to block tonic inhibition. This demonstrated that SR competes with, and effectively blocks, bicuculline from binding at the orthosteric site. Thus, both antagonists are binding to the same receptor population, at the same site. And, therefore, the lack of effect of SR on tonic inhibition does *not* simply reflect a lack of binding to the $GABA_A$Rs that are responsible for this conductance. This raised the possibility that 1) s-$GABA_A$Rs are generating a GABA-independent tonic conductance. And 2) that the different effects of SR vs. bicuculline could be explained by differences in the amount of negative efficacy. Specifically, it suggests that SR lacks significant negative efficacy and functions as a neutral competitive antagonist, whereas bicuculline has a significant degree of negative efficacy and functions as an inverse agonist, thereby inhibiting some of the spontaneous openings.

At the time of Bai *et al's* publication, the proposed negative efficacy of bicuculline (i.e. inverse agonist) and lack of efficacy of SR (i.e. neutral competitive antagonist) was supported by four key studies by Uchida *et al* (256), Ueno *et al* (246), Thompson *et al* (260), and Chang and Weiss (192).

Uchida *et al* (256) and Ueno *et al* (246) showed that $GABA_AR$ currents induced by pentobarbital, etomidate or alphaxalone were differentially affected by bicuculline and SR. Pentobarbital, etomidate and alphaxalone act via allosteric sites, but at high concentrations can activate native (256) and recombinant $GABA_ARs$ (246). Both studies demonstrated that bicuculline was far more efficacious than SR at inhibiting allosterically activated $GABA_ARs$ (246,256). At the time, bicuculline's allosteric inhibitory action had been well documented (271–274); what was novel was that SR was far less effective at inhibiting allosteric receptor activation. This contrasts with GABA-activated currents, which could be blocked by both bicuculline and SR (and SR was the more potent) (246,256).

The above findings are mirrored by the studies of Thompson *et al* (260) and Chang and Weiss (192). They showed that mutant α1β2ΔL259Sγ2 receptor isoforms spontaneously open in the absence of GABA to produce leak currents that are fully blocked by PTX (192,260). Thompson *et al* showed that, relative to PTX, SR caused only a marginal (13%) inhibition of 'spontaneous' current, which is far less than that caused by bicuculline (85%) (260). Chang and Weiss reported similar effects: bicuculline was ~four times more effective at blocking spontaneous currents than SR (192). Interestingly, Thompson *et al* also showed that BDZ-site ligands could bi-directionally modulate spontaneous current (260). Thus, bicuculline is far more effective than SR at inhibiting allosteric or spontaneously activated $GABA_ARs$; this infers that bicuculline has significant negative efficacy, whereas SR does not (246,256).

The proposition that $GABA_ARs$ can spontaneously open to produce GABA-independent currents was supported by early electrophysiological studies. Spontaneous-channel openings from native (329–334) and recombinant (335,336) $GABA_ARs$ were detected not long after the creation (337–339) and refinement of the giga-seal recording technique (340–343). Spontaneous $GABA_AR$ openings are typically brief, unitary, and infrequent (sometimes described as having a 'spikey' appearance); however, they have the same conductance

amplitude as GABA-activated openings from the same patches (329–336). Spontaneous activity can also be detected in the whole-cell recording mode as GABA-independent leak currents that can be blocked by PTX. Prior to Bai *et al's* study, it was shown that recombinant α4β1 (344), α1β1(345), β1 (345–347), β3 (123), α6β2γ2 (348) and α1β3ε (336) receptor isoforms all produced GABA-independent PTX-sensitive leak currents. In the case of the β1 and β3 homomers, these currents can be potentiated by pentobarbital and propofol, blocked by Zn^{2+} (and PTX) but not by bicuculline (123,345–347)

The earliest recordings of *native* spontaneous $GABA_AR$ openings were obtained from cultured chick cerebral neurons (330), and cultured mouse cerebellar (329) and spinal neurons (331–334). As such, it was not clear if native, intact rodent hippocampal neurons – in which Bai *et al* reported the SR-resistant tonic currents – had s-$GABA_ARs$. Two important studies by Bryndis Birnir and colleagues addressed this ambiguity (236,349). They demonstrated that s-$GABA_AR$ activity could be recorded in the absence of GABA from rat CA1 pyramidal neurons in slices (236,349) and in culture (236), and that spontaneous openings could be modulated by a variety of different ligands (236,349). Spontaneous openings were present in both cell-attached and inside-out recording configurations and exhibited outward rectification at depolarised voltages (increased conductance and open probability) (236,349). Importantly, these s-$GABA_AR$ openings could be blocked by bicuculline, which again indicates that it can decrease channel open probability (236,349). Furthermore, the conductance of s-$GABA_AR$ openings could be increased by diazepam, which suggests that the $GABA_ARs$ that are spontaneously opening contain the γ2 subunit (236,349). Spontaneous openings were also potentiated by pentobarbital (236). The authors posited that "spontaneously opening receptors may have a role in providing a nonsynaptic background tonic inhibition of neurons" (349). This proved to be prescient.

1.9.1 Neurons that express s-$GABA_A$R-mediated tonic conductance

GABA-independent tonic s-$GABA_A$R conductance in hippocampal pyramidal neurons

The first formal investigation into s-$GABA_A$R-mediated tonic conductance was by McCartney *et al* in 2007 (233). They used cultured hippocampal pyramidal neurons – the same neuron types that Birnir *et al* had recorded s-$GABA_A$R single-channel openings – and set out to better understand the nature of the SR-resistance of tonic conductance that had been previously reported by Bai *et al* (270). In doing so, they resolved the apparent paradox: how is it that the $GABA_A$Rs mediating tonic conductance in these neurons are SR-resistant but all GABA-evoked responses are inhibited by SR? They confirmed that the spontaneous activity of s-$GABA_A$Rs is sufficient to generate a GABA-independent tonic conductance (tonic inhibition) in hippocampal pyramidal neurons (233).

McCartney *et al* demonstrated that phasic conductance could be effectively blocked by PTX, bicuculline or SR; whereas only PTX could fully block tonic conductance. Tonic conductance was partially blocked by bicuculline and but was completely resistant to SR (no outward currents were observed) (233). This did not reflect an inability of SR to bind to the receptor, as it was able to block GABA-dependent tonic conductance elicited by 5 μM GABA, and was also able to block bicuculline-mediated inhibition (233). The GABA-independent s-$GABA_A$R tonic conductance was partially inhibited by Zn^{2+} and was resistant to strychnine, indicating that it was not mediated by GlyRs. Propofol could potentiate s-$GABA_A$R tonic conductance in a manner that was resistant to SR but sensitive to bicuculline, which further supports the difference in efficacy of these two compounds. Furthermore, s-$GABA_A$R single-channel openings could be detected in the absence of GABA using the outside-out recording configuration. These spontaneous openings were resistant to SR but blocked by PTX (233).

Next, McCartney *et al* set out to better understand the pharmacology of GABA-independent tonic conductance in order to infer what subunits might make up s-$GABA_A$Rs. They showed that the tonic conductance was resistant to furosemide, indicating that they do not arise from isoforms containing the ε subunit, which had been previously shown to spontaneously open (336,350). But, interestingly, tonic conductance could be potentiated by flunitrazepam (a BDZ-

site agonist) and loreclezole. These potentiating effects suggest the involvement of γ2 and β2/3 subunits, respectively. They pursued this line of inquiry further and demonstrated that recombinant α1β1γ2 and α1β3γ2 receptor isoforms expressed in human embryonic kidney (HEK) cells show spontaneous GABA-independent leak currents and a virtually identical pharmacological profile to the native pyramidal cell tonic conductance.

McCartney *et al's* study thus demonstrated that in cultured hippocampal pyramidal neurons, GABA-independent s-$GABA_A$Rs deliver a tonic conductance. It also confirmed the different efficacy of $GABA_A$R antagonists against s-$GABA_A$Rs: PTX can block fully, bicuculline can block partially, whereas they are resistant to SR.

GABA-independent tonic s-$GABA_A$R conductance in Dentate Gyrus Granule cells

The obvious question that flows from McCartney *et al's* study is whether the GABA-independent s-$GABA_A$R tonic conductance is also present in adult, *ex vivo* neurons, not just cultured neurons. The first study to formally address this was Wlodarczyk *et al* in 2013. They demonstrated that in mature dentate gyrus granules (DGGCs), under baseline conditions, or when the perfusate contained the same concentration of GABA that is found *in vivo*, the major contributors to the tonic conductance were s-$GABA_A$Rs.

Wlodarczyk *et al* recorded the tonic conductance from DGGCs and found that it was resistant to SR (0.5–125 μM), partially blocked by bicuculline, and fully blocked by PTX. As with previous studies, they showed that the lack of effect of SR was not due to a lack of binding: SR could displace bicuculline and reverse its inhibitory effect on tonic conductance. Thus, under baseline conditions, only negligible ambient GABA can be detected by DGGCs – i.e. virtually all of the tonic conductance is GABA-independent. In further support of this, they found that depleting vesicular GABA by using concanamycin did not affect the PTX-sensitive tonic conductance. Furthermore, it was shown using 'sniffer patches' and zero-net-flux microdialysis that the concentration of extracellular GABA *ex vivo* and *in vivo*, respectively, was ~100 nM. This is in line with the values obtained from other microdiaylsis studies (74–78) and the predicted equilibrium of the GAT-1 transporter (85). This makes it abundantly clear that supplementing the perfusate with 1-to-5 μM GABA, as is common across the field, is wildly un-physiological.

Wlodarczyk *et al* observed that when the perfusate was supplemented with 200 nM GABA (double that recorded *in vivo*) the tonic conductance is still almost exclusively mediated by s-$GABA_A$Rs (SR-resistant and GABA-independent). Thus, in conditions comparable to those *in vivo*, s-$GABA_A$Rs are still the principal mediators of tonic conductance.

Wlodarczyk *et al* also confirmed the presence of s-$GABA_A$Rs in DGGCs by recording GABA-independent single-channel openings in nucleated patches. Spontaneous openings persisted in the presence of SR, and their conductance was virtually identical to GABA-dependent openings; however, their open time and frequency was lower.

One of the significant advances made by Wlodarczyk *et al* was to develop an approach to specifically isolate, block, and then measure the s-$GABA_A$R conductance. First, SR is added to block GABA-dependent signalling, thereby isolating s-$GABA_A$Rs. And then, second, in the continued presence of SR, PTX is added to block the GABA-independent signalling of s-$GABA_A$Rs. The difference in conductance in SR vs in SR+PTX corresponds to that which is mediated by s-$GABA_A$Rs. This s-$GABA_A$R conductance could be blocked by pentylenetetrazole, another noncompetitive antagonist, but was not affected by strychnine and so it is not mediated by GlyRs. It was also not affected by TPMPA, an antagonist at homomeric ρ-subunit $GABA_A$Rs.

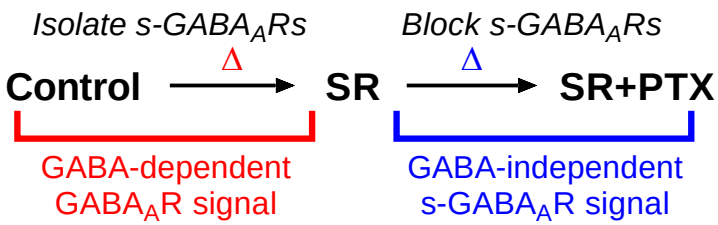

Finally, Wlodarczyk *et al* investigated which subunits are required for s-$GABA_A$R tonic conductance. In DGGCs, δ-subunits (351) primarily assemble with α4-subunits (254) and β2-subunits (352) to form α4β2δ receptors. These receptors are the principal extrasynaptic $GABA_A$R in DGGCs and produce ~70% of a GABA-dependent tonic current that can be evoked by adding GABA into the perfusate or blocking its reuptake (351). Wlodarczyk *et al* examined if δ-subunit-containing $GABA_A$Rs can also generate GABA-independent tonic currents under conditions of no-to-low GABA. They used δ-subunit knockout mice (*Gabrd−/−*) and showed that in the absence of the δ-subunit the SR-resistant, PTX sensitive s-$GABA_A$R tonic current was

reduced by ~60% compared to wild-type mice. This indicated that a portion of the s-$GABA_A$Rs in DGGCs contain the δ-subunit (74).

GABA-independent tonic s-$GABA_A$R conductance in the central amygdala

s-$GABA_A$R-mediated tonic conductance is not restricted to hippocampal neurons; in 2015, Botta *et al* reported their presence in central amygdala neurons that express PKCδ (234). They showed that tonic conductance was blocked by PTX but largely insensitive to SR, and that SR partially antagonized the inverse agonist effect of bicuculline. They reported that α5-subunit containing receptor isoforms likely contribute to the s-$GABA_A$R tonic current: the amplitude of the PTX sensitive tonic conductance was reduced using two different inverse agonists of α5-$GABA_A$Rs, L-655,708 and PWZ-029, or by knocking out the α5-subunit gene (*Gabra5−/−*). In contrast, zolpidem and tetrahydrodeoxycorticosterone (THDOC) had no impact on the conductance amplitude.

Botta *et al's* study was the first, and is currently the only, study to have investigated the functional impact of GABA-independent s-$GABA_A$R signalling. To selectively block s-$GABA_A$Rs, they exposed the neuron to SR and then, in its continued presence, to PTX. Block of s-$GABA_A$Rs increased the input resistance, caused a small depolarising shift in the RMP, and increased the excitability of the neurons as indicated by the input-output function and the spontaneous firing rate.

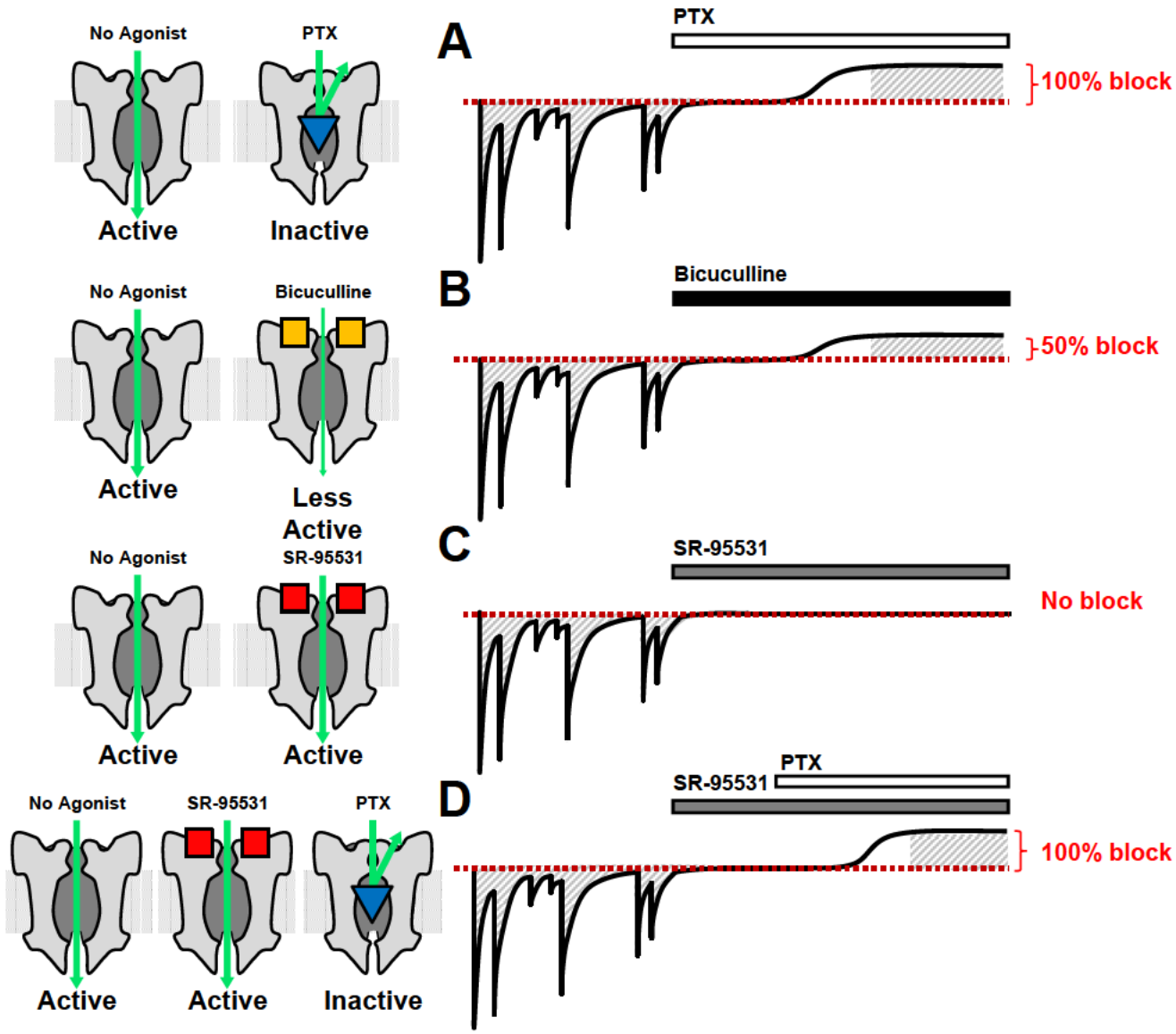

Fig.1.3. Pharmacology of the GABA-independent s-GABA$_A$R tonic conductance.
A Simple pictorial representation of the sensitivity of IPSCs and s-GABA$_A$R-mediated tonic currents to various GABA$_A$R antagonists (values from Wlodarczyk *et al*). **A)** Picrotoxin (PTX) binds within the channel and blocks GABA$_A$Rs irrespective of if they are activated by GABA or spontaneously: PTX blocks IPSCs and s-GABA$_A$R tonic conductance. **B)** Bicuculline is a partial inverse agonist; it displaces GABA from the binding site and inhibits receptor gating: IPSCs are blocked and s-GABA$_A$R tonic conductance is partially blocked. **C)** SR-95531 is a neutral antagonist; it displaces GABA from the binding site but does not affect receptor gating: IPSCs are blocked but s-GABA$_A$R tonic conductance is not. **D)** Pharmacological workflow used to *isolate* and then *block* (and in so doing quantify) the s-GABA$_A$R signal. **Control→SR** GABA-dependent IPSCs are blocked by SR, but tonic currents are not (because they are GABA-independent). **SR→SR+PTX** allows for the subsequent quantification of the GABA-independent s-GABA$_A$R signal: PTX blocks the tonic s-GABA$_A$R current as revealed by the outward shift in the holding current.

1.9.2 How prevalent is s-GABA$_A$R-mediated tonic conductance in the brain?

Although s-GABA$_A$R-mediated tonic conductance has received notably less attention than its GABA-dependent counterpart and has only been conclusively identified in three neuron types, there is good evidence that its prevalence in the CNS has been underestimated. The strongest evidence supporting this notion is the relatively large group of studies that – although often not acknowledged as such – have recorded tonic conductances with a pharmacological profile indicative of s-GABA$_A$Rs. Namely, a conductance that is sensitive to PTX/bicuculline, but is fully or partially resistant to SR (353–363). In some of these studies, SR was not applied at saturating concentrations, and so it is possible that SR was simply unable to out-compete GABA at the orthosteric site. This could easily explain the tonic conductance in hippocampal interneurons that is resistant to 0.5 µM SR, but sensitive to PTX (353). Indeed, other studies have reported a tonic conductance that was resistant to SR applied at 0.5 µM, only for it to be fully blocked when SR concentration was increased to 10 µM (269). There are, however, a number of studies in which SR *was* applied at saturating concentrations (10-100 µM) and tonic conductance was still not blocked (but was by bicuculline or PTX). This is the case for tonic conductances in: hypothalamic supraoptic nuclei neurons (357), hypothalamic paraventricular nucleus to rostral ventrolateral medulla neurons (358), solitary tract nucleus neurons (359), sympathetic preganglionic neurons (360), dorsal motor nucleus of the vagus neurons (361), midbrain periaqueductal grey neurons (363), cardiac vagal neurons in the nucleus ambiguus (355), gonadotropin-releasing hormone neurons (364) and central amygdala neurons (365). The presence of GABA-independent s-GABA$_A$R openings can explain these findings. However, in many cases, it is not possible to make this definitive post-hoc pronouncement because some of the necessary control experiments have not been performed. For example, SR-insensitive, PTX-sensitive tonic currents that are recorded in the absence of strychnine may be mediated by GlyRs, not s-GABA$_A$Rs. Nevertheless, it strongly suggests that some of these neurons express a GABA-independent, s-GABA$_A$R-mediated tonic conductance. Interestingly, a recent study by Yelhekar *et al* reported that in neurons of the medial preoptic nucleus, SR-resistant, PTX-sensitive GABA$_A$R conductance facilitates the recovery of intracellular [Cl^-] following Cl^--loading. This was not mediated by GlyRs because it was resistant to strychnine. The authors suggested that GABA-independent s-GABA$_A$R openings contribute to recovery from Cl^- loading (366)

It is also worth noting that a large proportion of the studies that purport to investigate GABA-dependent tonic inhibition do so using only one antagonist. In studies using *either* SR *or* PTX, it is impossible to determine if s-$GABA_A$Rs make a contribution to the overall tonic conductance. In Lee and Maguire's review of the literature on tonic inhibition (2014), 20% of the neuron-type tonic conductances were obtained using only PTX (224). In these studies, it is possible that because PTX blocks GABA-dependent and -independent currents indiscriminately, some, or indeed all, of the tonic current could be mediated by s-$GABA_A$Rs. The reverse is true for studies that use only SR to measure tonic currents. In these studies, which represent 25% of the neurons tabled in Lee and Maguire, 2014 (224), if there is a partial contribution by s-$GABA_A$Rs to tonic currents it will not be detected by SR. The *measured* tonic current (GABA-dependent $GABA_A$Rs) will be smaller than the *actual* tonic current (GABA-dependent $GABA_A$Rs and s-$GABA_A$Rs). Complicating matters further, many measurements of tonic conductance are obtained in the presence of a supraphysiological concentration of ambient GABA. This is achieved by supplementing the perfusate with 1-5 μM GABA (at least an order of magnitude greater than the *in vivo* concentration) or blocking GABA reuptake (224). In these studies, the non-physiological GABA-dependent tonic conductance may be masking an underlying smaller s-$GABA_A$R conductance (74).

Finally, it is worth considering that many of the $GABA_A$R isoforms expressed in the brain have been shown to spontaneously open in recombinant systems. This includes the principal synaptic receptor isoforms: **α1β1γ2** (233,367), **α1β2γ2** (198,205,259,368), **α1β3γ2** (233,369). And the principal extrasynaptic receptor isoforms: **α6β2δ** (259,370), **a4β1δ** (371,372), **a4β2δ** (259,372–375), **a4β3δ** (371,372,376,377), **α1β2δ** (259). As well as other isoforms: **α1β1ε** (336,350), **α1β3ε** (257,336). **α1β1** (345,367), **α4β1** (344), **α6β2γ2** (259,348), **α4β3γ2** (376), **β1** (345–347), **β3** (123). Thus, virtually all neurons will express $GABA_A$Rs that have been shown to exhibit constitutive activity, albeit in recombinant systems and inconsistently across different studies. Furthermore, the three studies investigating s-$GABA_A$Rs in neurons have concluded that a different receptor isoform was responsible for producing the GABA-independent tonic conductance: **α1β1γ2** and **α1β3γ2** (233), **δ-**$GABA_A$Rs (74), and **α5-**$GABA_A$Rs (234). These receptor isoforms are expressed in many neuron types, and so s-$GABA_A$R-mediated tonic

conductance could be a widespread signal in the brain. This possibility alone justifies further investigation into s-$GABA_A$Rs.

1.9.3 A significant unknown: What is the function of s-$GABA_A$R-mediated tonic conductance in the brain?

To summarise, although there is evidence that s-$GABA_A$R-mediated tonic conductance could be widespread in the brain, it has, so far, only been formally identified and investigated in three neuron types: hippocampal pyramidal neurons (233), dentate gyrus granule neurons (74), and a subpopulation of central amygdala neurons that express PKCδ (234). However, it is not just the *presence* of s-$GABA_A$Rs in the nervous system that needs to be considered, but also whether the conductance they provide is *sufficient* to affect neuronal function (e.g. excitability). So far, the function of the tonic s-$GABA_A$R conductance has only been investigated in one neuron type: the PKCδ positive neurons of the central amygdala – it is not currently known if the same is true in other neuron types (234). Thus, s-$GABA_A$R-mediated tonic conductance is a relatively understudied signalling mechanism, with many significant **unknowns**.

It is not currently known whether s-$GABA_A$R mediated tonic conductance is of any functional importance to hippocampal neurons (**unknown 1**). Moreover, none of the aforementioned studies have assessed if s-$GABA_A$Rs affect more complex signalling dynamics, such as temporal summation and synaptic plasticity (**unknown 2**). Various ligands have been shown to inhibit s-$GABA_A$Rs (PTX, bicuculline, pentylenetetrazole, Zn^{2+}, L-655,708 and PWZ-029); however, fewer compounds have been shown to potentiate s-$GABA_A$Rs (propofol, flunitrazepam and loreclezole). It is not known how consistent the pharmacological profile of s-$GABA_A$Rs is across different neuron types, or what other compounds can modulate s-$GABA_A$Rs (**unknown 3**). This reflects a more fundamental ambiguity surrounding s-$GABA_A$Rs: which $GABA_A$R isoforms responsible for the GABA-independent conductance? (**unknown 4**).

The lack of information on the functional role of constitutively active $GABA_A$Rs reflects that of the pLGIC family more broadly. Constitutive activity in pLGICs has been important for developing kinetic models that describe channel gating (e.g. MWC) (102,195–199). However, the physiological and pathological role of spontaneously opening pLGICs has received relatively little attention. That said, there are some examples within the literature. For instance, mutations

in the nAChR that are associated with elevated constitutive activity have been identified as causing congenital myasthenia and frontal lobe epilepsy (378). Furthermore, knock-in mice with a mutation in the 5-HT3$_A$R, which enhances constitutive activity, leads to severe obstructive uropathy (379).

In comparison to pLGICs, much more attention has been directed at agonist-independent constitutive signalling by GPCRs (380). GPCRs are seven-pass-transmembrane domain receptors that signal via tri-heteromeric G-proteins to downstream effectors. Constitutive activity of GPCRs was first observed in the 1980s, at recombinant β2-adrenergic receptors (381). Soon after, the ability of inverse agonists to inhibit constitutive activity was observed at δ opioid receptors in membranes of NG108-15 neuroblastoma cells (382). Since then, it has become clear that agonist-independent constitutive activity of certain GPCRs is an important signalling mechanism (381). And that there are a variety of disease-causing mutations that disrupt proper GPCR signalling by affecting constitutive activity (381). For instance, the melanocortin-4 receptor (MC-4R), a regulator of energy homeostasis and metabolism, exhibits strong basal constitutive activity in the absence of its endogenous ligands. MC-4Rs are expressed in the paraventricular nucleus of the hypothalamus and activation of the receptor, via constitutive activity or by its endogenous peptide agonist, α-melanocyte stimulating hormone, decreases food intake and increases metabolic rate (383,384). Conversely, MC-4R constitutive activity is inhibited by the endogenous inverse agonists, agouti and agouti-related peptide (385). Mutations in MC-4R are the most common genetic cause of obesity and some of these mutations are associated with decreased levels of constitutive activity (386). From this, it has been posited that constitutive MC-4R activity is required for the prevention of obesity (386). Cleary then, constitutive signalling by receptors can be of functional importance. However, it is currently not known if this is also applicable to s-GABA$_A$Rs.

Probably the strongest evidence supporting the functional importance of s-GABA$_A$R-mediated tonic conductance is the well characterised role of GABA-dependent tonic conductance. As outlined **1.8**, the signal that is inputted by GABA-dependent tonic conductance (membrane shunting and membrane polarisation) impacts many aspects of neuronal function. s-GABA$_A$Rs have the *ability* to deliver an analogous signal, but whether this signal is large enough to

produce a meaningful effect in neurons outside of the central amygdala is unknown. Moreover, there are variations in the properties of GABA-dependent tonic conductance that affect its function across the brain. A key example of one such property is outward rectification. GABA-dependent tonic conductances are frequently outwardly rectifying (225,288,353,387,388), meaning that a greater inhibitory effect can be delivered close to or above threshold voltage than at RMP. This can affect whether tonic inhibition causes a subtractive or divisive effect on the neuronal input-output relationship (387). Single-channel s-$GABA_AR$ openings in hippocampal pyramidal cells are not outwardly rectifying (233), but it is not known whether this is the case in any other neuron types. Thus various aspects of the s-$GABA_AR$ tonic signal are unresolved.

1.10 Statement of purpose

The purpose of this PhD is to characterise the hitherto unknown function of s-$GABA_AR$-mediated, GABA-independent tonic conductance in DGGCs. Because s-$GABA_ARs$ do not require GABA to activate, they are resistant to the competitive antagonist, SR, but can be inhibited by the channel-blocker, PTX. The s-$GABA_AR$ 'signal' can be isolated and then measured by sequentially exposing a neuron to SR and then, in its continued presence, to PTX (**CTRL→SR→SR+PTX**). Whole-cell voltage-clamp and current-clamp recordings were used to characterise the nature of the s-$GABA_AR$ signal and assess whether it is sufficient to affect DGGC function. As explored in Chapter 3, the dentate gyrus is a key brain region and is thought to act as both a gate to aberrant excitation and as a pattern separator. Both of these functions are thought to rely heavily on the sparse activity across the DGGC population. The tonic conductance that is generated by s-$GABA_ARs$ might be one mechanism through which DGGC activity is restrained. This study is thus of importance to understanding dentate gyrus function. Another purpose of this PhD is to characterise how s-$GABA_AR$-mediated tonic conductance can be modulated. Henceforth, this study is also important for understanding which $GABA_AR$ subunits are involved in generating GABA-independent tonic conductance. This may also be of clinical significance, facilitating a better understanding of existing drugs and, potentially, the development of novel compounds that modulate s-$GABA_ARs$ activity.

1.11 Overall thesis aims

Aim 1: It has been previously shown that constitutively active s-$GABA_A$Rs generate a GABA-independent tonic conductance in DGGCs (74). However, the functional impact of this conductance upon cellular excitability is currently unknown. The experiments performed for this thesis aimed to characterise the function of s-$GABA_A$R signalling in DGGCs. Specifically, we aimed to characterise both 1) the nature of the s-$GABA_A$R signal delivered to DGGCs and 2) how it is interpreted by these neurons.

To achieve this aim, we measured the effect of s-$GABA_A$R-mediated conductance on passive membrane properties (input resistance, membrane time constant, RMP), active membrane properties (excitability, rheobase, AP threshold voltage) and the input-output (I-O) function of DGGCs (as expressed in F-I curves). We also explored the impact of s-$GABA_A$Rs on the temporal precision of signal integration (coincidence detection) and on neural plasticity (LTP), both of which are important for proper DGGC function in the brain. The findings of these experiments are presented in Chapter 3 (Results 1).

Aim 2: It has been previously shown that the s-$GABA_A$R-mediated tonic conductance in DGGCs is resistant to SR, partially blocked by bicuculline, and fully blocked by PTX (74). Beyond this, the pharmacological profile of s-$GABA_A$Rs in DGGCs is not well characterised. The experiments performed for this thesis aimed to characterise the effect of a variety of ligands on the amplitude of the s-$GABA_A$R-mediated tonic conductance.

To achieve this aim, we first assessed the impact of compounds that target δ-$GABA_A$Rs. This is informed by the reduction in the s-$GABA_A$R tonic conductance in mice lacking the δ-subunit. Second, we assessed if inhibiting α5-$GABA_A$Rs decreased the s-$GABA_A$R-mediated conductance amplitude. This is informed by previous findings in the central amygdala, showing that α5-subunit $GABA_A$Rs can spontaneously open. Third, we assessed if, as with hippocampal pyramidal cells, BDZ-site ligandss could affect the s-$GABA_A$R tonic conductance. Finally, we assessed if inhibitors and activators of PKA/PKC could modulate the s-$GABA_A$R tonic conductance. Modulating serine/threonine kinases has been previously shown to affect GABA-dependent tonic conductance and spontaneous openings of recombinant $GABA_A$Rs. The findings of these experiments are presented in Chapter 4 (Results 2).

Chapter 2

Materials and Methods

2.1 Animals and Procedures

All procedures were performed in accordance with the amended *(2013) UK Home Office legislation**,** The Animals (Scientific Procedures) Act 1986* and under the authority of The University of Edinburgh internal ethics committee (Project license number:70/7870). Three-to-six week old, wild-type female Sprague Dawley rats were used for all experiments in this PhD thesis. Rats were bred in Charles River Laboratories (UK) and delivered in litters of between three and seven rats to Little France Biomedical Research Resources Unit 2 where they were then housed under standard institution protocols (12:12 hour light/dark cycle; received food and water *ad libitum*). Rats were culled by cervical dislocation (a Schedule 1 Method). In order to minimise animal and experimenter stress, rats were handled on a weekly basis in their housing unit and for a further ten minutes prior to being culled. Such handling meant that rats were calm and did not resist being restrained.

2.2 Preparation of acute brain slices

Brain slice electrophysiology is a routine, virtually ubiquitous procedure in neuroscience laboratories (389–400). The following procedure yielded excellent quality sagittal brain slices that permitted stable and long (>40 minutes) patch-clamp recordings from DGGCs.

Rats were decapitated immediately after culling. The head was placed on a flat surface and held between the thumb and forefinger of one hand. The skin and underlying musculature were removed using large surgical scissors to expose, but not cut through, the skull. Small, sharp-tipped dissecting scissors were inserted in the foramen occipitale magnum and used to cut along the length of the sagittal suture, past bregma, and into the frontal bone; following which, coarse tweezers were used to uncover both sides of the skull plate and carefully remove the underlying dura matter. The open skull, together with the exposed brain, was then immersed into a ‘slush’ of semi-frozen sucrose-artificial cerebrospinal fluid (ACSF) (see recipe below) for ~5 seconds to chill the brain *in situ*. This cooling ‘firmed up’ the tissue and prevented excessive

twisting when liberating the brain from the skull. The brain was removed in one smooth motion: a small spatula was inserted underneath the brain at the level of the olfactory bulbs and moved caudally to sever the cranial nerves. The spatula was then used to gently scoop out the brain into the beaker of semi-frozen sucrose-ACSF that had been pre-bubbled with carbogen gas (95% O_2/5% CO_2). In order to produce brain slices of optimum health, the aforementioned procedure had to be completed in less than 40 seconds.

The brain was allowed to uniformly cool in the beaker of semi frozen, carbogenated sucrose-ACSF for 2-3 minutes and then placed on filter paper (Whattman) in a plastic petri-dish, surrounded by the 'slush' of sucrose-ACSF that was undergoing constant carbogenation. The brain was blocked using a single edge razor blade: the cerebellum and the rostal third of the frontal cortices were removed, and then the hemispheres were separated by cutting along the longitudinal fissure (**Fig.2.1A**). One hemisphere was chosen and placed on the flat of the razor blade, dried using filter paper and mounted medial-side down on a vibratome stage (Leica VT1200S, Leica Microsystems) that was coated with a shallow strip (~4 cm x 2 cm) of cyanoacrylate glue (**Fig.2.1B+C**). Proper brain-glue adherence was achieved by lightly shaking the stage and by squirting ~5 ml of sucrose-ACSF on top of the hemisphere. This both accelerated the curing of the glue and, crucially, prevented the glue from creeping up the side of the brain. The stage was then placed into the slicing chamber, submerged in semi-frozen sucrose-ACSF and oriented so that the dorsal extent of the brain faces the vibratome blade (**Fig.2.1D**).

Parasagittal brain slices containing the hippocampus and surrounding structures were cut using the vibratome at an angle of ~18° relative to horizontal, using high-quality, double-edged stainless-steel razor blades (Personna Super or Feather blades; cleaned with ethanol and d.H_20 before use). For whole-cell patch-clamp recordings, a slice thickness of 350 µm was chosen; however, for field recordings, thickness was increased to 400 µm. The blade was advanced through the hippocampus at a horizontal oscillation amplitude of 1.75 mm and slow forward velocity of 0.05 mm.s^{-1} (the forward velocity was increased to 0.14 mm.s^{-1} when cutting through other brain regions to decrease overall slicing time). Cut slices were transferred individually using a wide mouth Pasteur pipette into a submerged brain slice holding chamber containing

sucrose-ACSF that had previously been sterile filtered (0.22 µm), warmed to 35.5 °C and continuously bubbled with carbogen (**Fig.2.1E**; and see **Fig.2.2** for details of how to construct the slice chamber). Slice orientation was the same in the holding chamber as it was during slicing (e.g. the blade-facing side of the slice rested on the nylon-mesh platform of the holding chamber). One of the primary factors in determining good slice health was accurate timing of the recovery period: after transferring the *fourth* slice into the holding chamber, the temperature was maintained at 35.5 °C for 9 minutes. After this recovery period the chamber was removed from the water bath and allowed to equilibrate at room temperature for a minimum of 30 minutes prior to starting electrophysiology experiments. From a 3-6-week-old rat, approximately 6 slices can be cut from one brain hemisphere.

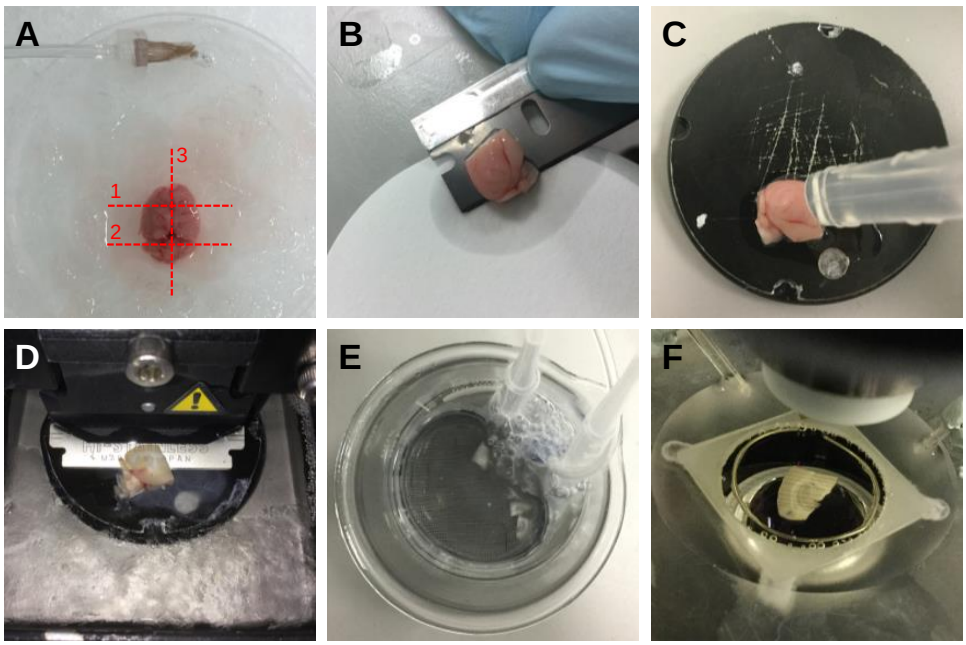

Fig.2.1. Preparation of acute hippocampal slices.
A) A freshly excised rat brain surrounded by sucrose-ACSF slush bubbled with carbogen; blocking cuts (**1-3**) shown in red. **B)** A single hemisphere is selected, dried on filter paper and mounted on the vibratome stage with a thin strip of fresh cyanoacrylate glue **C)**. A small amount of sucrose-ACSF is applied to set the glue and prevent creepage. **D)** Cutting of 350 µm para-sagittal brain slice using a Leica VT1200S in the sucrose-ACSF slush; the hemisphere is positioned so that the cortex is cut first. **E)** Freshly cut slices are transferred to the slice holder which contains sucrose-ACSF undergoing constant carbogenation; the chamber should was maintained at 35.5 °C for 9 mins and then allowed to sit for 30 mins at room temperature. **F)** Individual slices were transferred to the recording chamber and held in place with the 'harp'. Chamber contains recording ACSF, bubbled with carbogen at 33°C.

Following the incubation period, individual slices were transferred into a submerged recording chamber and constantly perfused, at flow rate of 8 – 10 ml.min^{-1}, with recording ACSF that was continually bubbled with carbogen and heated to 33°C using an in-line heater (HPC-G; ALA Scientific Instruments) driven by a TC-10 temperature control unit. Slices were held in place with a 'harp' constructed of an O-shaped platinum wire strung with parallel nylon threads and were visualised with infrared differential interference contrast microscopy using an upright microscope (BX51WI, Olympus) equipped with a 10x Plan N objective and a ×40 water-immersion objective. A 'healthy' dentate gyrus was identified by a large number of round, moderately contrasted granule cells with smooth, shiny membranes. After confirming good slice health and allowing the slices to equilibrate for 10 minutes, electrophysiological recordings were performed in either the whole-cell patch-clamp or extracellular field configuration.

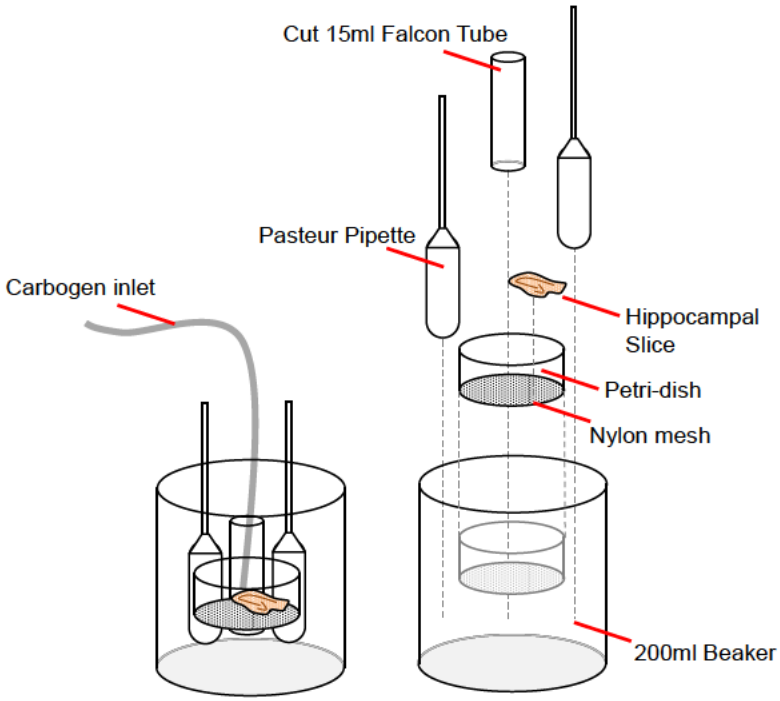

Fig.2.2. Fabrication of an acute brain slice holding chamber.
The holding chamber consists of a 200 ml glass beaker with a petri-dish and cut-off falcon tube wedged inside. The base of the petri dish was removed and replaced with a nylon mesh; this mesh provides a platform which the slices can sit on. The beaker was filled with sucrose-ACSF so that the level of the solution just covers the top of the falcon tube. We attached an air diffuser stone to the carbogen inlet and placed it inside the falcon tube to properly oxygenate the slices. The up-turned Pasteur pipettes which flank the falcon tube acted to direct the carbogen bubbles over the slice. The slice holder was properly cleaned after every use: we washed it with dilute NaOH, 70% ethanol and then rinsed with d.H_20. The holding chamber was replaced holder every few months.

2.3 Solutions

All reagents for the preparation of dissection and electrophysiological recording solutions were purchased from Sigma-Aldrich (St Louis, MO, US) or Tocris (Bristol, UK) apart from QX-314.Br, which was purchased from Alomone Labs (Jerusalem, Israel) and DPP-4-PIOL, which was very kindly provided by Professor Bente Frølund (University of Copenhagen).

2.3.1 Extracellular solutions

	Sucrose-ACSF (mM)	**Recording ACSF (mM)**
NaCl	85	125
KCl	2.5	2.5
NaH_2PO_4	1.25	1.25
$NaHCO_3$	20	20
HEPES	10	10
Glucose	25	25
Sucrose	75	0
$CaCl_2$	0.5	2
$MgCl_2$	4	1
Osmolarity	*340-350 mOsM*	*315 - 320 mOsM*
pH (adj. NaOH)	*7.32-34 at RT*	*7.35-37 at 33℃*

N.B. Because both slicing and recording solutions contained HEPES, it was imperative that the pH was only measured and adjusted *after* the solution had first been saturated with carbogen (95% O_2/5% CO_2). ACSF solutions were carbogenated using air diffuser stones for at least 40 minutes at the indicated temperature, and only then was the pH adjusted.

2.3.2 Cesium chloride-based intracellular solution

(High $[Cl^-]$ = 128.4 mM; E_{Cl^-} at 33°C = -1.03 mV)

	Concentration (mM)
CsCl	120
HEPES	10
CsOH-EGTA	2
NaCl	8
$MgCl_2$	0.2
Mg-ATP	2
Na_3-GTP	0.3
QX-314.Br	5
Osmolarity (adj. sucrose)	*290 - 295 mOsM*
pH (adj. CsOH)	*7.25 - 7.30*

2.3.3 Potassium gluconate-based intracellular solution

(Physiological $[Cl^-]$ = 8 mM; E_{Cl^-} at 33°C = -74.3 mV)

	Concentration (mM)
K-Gluconate	140
HEPES	10
KOH-EGTA	0.2
NaCl	8
Mg-ATP	2
Na_3-GTP	0.3
Osmolarity (adj. sucrose)	*290 - 295 mOsM*
pH (adj. KOH)	*7.25 - 7.30*

2.3.4 Cesium methanesulfonate-based intracellular solution

(Physiological $[Cl^-]$ = 8 mM; E_{Cl^-} at 33°C = -74.3 mV)

	Concentration (mM)
$CsMeSO_4$	135
HEPES	10
CsOH-EGTA	0.2
NaCl	8
Mg-ATP	2
Na_3-GTP	0.3
QX-314.Br	5
Osmolarity (adj. sucrose)	*290 - 295 mOsM*
pH (adj. CsOH)	*7.25 - 7.30*

2.4 Whole-cell patch-clamp recordings

Visualized whole-cell patch-clamp recordings from mature dentate granule cells (DGGCs) were made using patch-pipettes with an open tip resistance of 3-5 MΩ. Pipettes were fabricated from thick-walled, filamented boroscillate glass capillaries (1.5 mm outer diameter, 0.86 mm inner diameter; Harvard apparatus, UK) using a P-87 Flaming Brown Micropipette Puller (Sutter Instruments, US) and back-filled with 0.22 µm filtered 'intracellular' pipette solution. For voltage-clamp experiments we used cesium-based intracellular solutions, containing either high (CsCl; 128.4 mM), or physiological (Cs-methanesulfonate; 8 mM) concentrations of Cl^-. For current-clamp experiments we used a K-gluconate-based internal solution that had a physiological concentration of Cl^- (8 mM). Note here that 'physiological' corresponds to the concentration of Cl^- found in adult, mature neurons (which is usually in the range of 5-15 mM) (218–221). This concentration of Cl^- gives rise to an E_{GABA} at 33℃ of -74.3 mV, which, again, matches that typically found in adult mature DGGCs (typically -70 mV to -80 mV) (307,401–403). A pipette containing the required intracellular solution was secured into a G23 micropipette holder, on a CV-7B head-stage that was mounted on a PatchStar micromanipulator (Scientifica). Whole-cell patch-clamp recordings were obtained in the standard manner. Briefly, the tip of the patch-pipette was submerged in the recording chamber and junction potential was corrected for in voltage-clamp mode; the pipette was then lowered onto the cell body of a selected neuron. Contact between the pipette and the cell membrane was signified by a bright 'dimple' on the membrane surface and a slight increase in tip resistance – measured with a +3 mV, 30 ms, 33.3 Hz square-wave seal-test. Sealing of the pipette to the membrane was triggered by releasing positive pressure and applying a -20 mV holding voltage. A high resistance seal (>2 GΩ: gigaseal) was formed by applying a light suction to the pipette and decreasing the holding voltage to -70 mV; fast and slow pipette capacitance transients were neutralised. The patch of membrane encircled by the pipette was ruptured by several sharp pulses of suction: successful breakthrough into 'whole-cell' mode was evidenced by the emergence of large, relatively slowly decaying capacitive transients.

Patch-clamp signals were amplified and filtered at 8 kHz (–3 dB cutoff; 4-pole Bessel filter) using a Multiclamp 700B, and digitized at 10 kHz (Digidata 1550, Molecular Devices). 50/60 Hz line noise was largely eliminated using a Humbug. Data were recorded using Clampex (pClamp

10.7, Molecular Devices) program installed on a Lenovo PC running Windows 7; offline analysis was performed using Clampfit (pClamp 10.7, Molecular Devices), Microsoft Excel and Graphpad Prism software package (GraphPad, CA, USA). For the purposes of illustration only, representative traces were filtered offline at 0.8 kHz; this reduces the signal-to-noise ratio of the trace and renders changes in tonic inhibition more easily visible.

Whole-cell capacitance was compensated using the Multiclamp 700B with the amplifier-default (8 x tau) duration. Only cells that had a stable series resistance of ≤ 25 MΩ (monitored throughout/after recordings) were included for analysis. In voltage-clamp experiments, unless otherwise stated, granule cells were clamped at -70 mV; this approximates the RMP of DGGCs recorded both *ex vivo* (404–412) and *in vivo* (413,414) (typically between -68 mV and -80 mV). When clamped at -70 mV, using the CsCl intracellular solution, DGGCs required a holding current of between -40 and -70 pA; any neuron that that needed a holding current more negative than -120 pA was rejected. Similarly, current-clamp experiments were only performed on DGGCs that had a RMP < -65 mV when measured immediately after break-in. Another important pre-requisite before commencing experiments was to ensure that the cell had a stable holding current: recordings were monitored for a minimum of 7 minutes after break-in to permit complete dialysis of the intracellular milieu with the solution in the pipette. No experiments were performed on neurons that exhibited sudden changes in holding current or erratic levels of noise – these are almost always indicative of seal degradation, which renders the measurement of changes to holding current and basic membrane properties impossible.

2.5 Quantification of the spontaneously active $GABA_AR$ signal

In the present thesis we used a previously published pharmacological approach to *isolate* and then *block* (and in so doing *quantify*) the signal that is provided by spontaneously opening $GABA_ARs$ (s-$GABA_ARs$) (74,233,234,415–417). The full workflow in pictorial form can be found in **Fig.2.3.** The first step in this methodology, the *isolation* of s-$GABA_AR_S$, required the antagonism of two distinct pools of neurotransmitter receptors: 1) the non-$GABA_AR$ neurotransmitter receptors and 2) the GABA-activated $GABA_ARs$.

2.5.1 Antagonising non-$GABA_AR$ neurotransmission

The vast majority of whole-cell patch-clamp recordings in this thesis were performed in the presence of six antagonists that together block non-$GABA_AR$-mediated neurotransmission. This block-cocktail provides a 'baseline' state for assaying total $GABA_AR$ activity because, crucially, both GABA-activated and spontaneously opening $GABA_ARs$ remain active. The only exceptions to this are experiments that utilised evoked synaptic excitatory synaptic activity. This collection of antagonists, from hereon in referred to as the 'block-cocktail', contains:

2.5.1.1 Block-cocktail Composition:

	Final Conc	Solvent	Pharmacology
DL-AP5	50 µM	1 eq.NaOH	NMDAR antagonist
NBQX	10 µM	dH_20	AMPAR antagonist
MCPG	250 µM	1 eq.NaOH	mGluR(group I) antagonist
NPS 2390	10 µM	DMSO	mGluR(group I) antagonist
CPPG	5 µM	1 eq.NaOH	mGluR(group II+III) antagonist
Strychnine	1 µM	dH_20	GlyR antagonist
CGP55845	1 µM	DMSO	$GABA_BR$ antagonist

N.B.1 Chemical Names:
DL-AP5: DL-2-Amino-5-phosphonopentanoic acid
NBQX: 2,3-Dioxo-6-nitro-1,2,3,4-tetrahydrobenzo[f]quinoxaline-7-sulfonamide
MCPG: (S)-α-methyl-4-carboxyphenylglycine
NPS 2390: N-tricyclo-[3.3.1.13,7]-dec-1-yl-2-quinoxalinecarboxamide
CPPG: (RS)-α-Cyclopropyl-4-phosphonophenylglycine
Strychnine: Strychnidin-10-one hydrochloride
CGP55845: (2S)-3-[[(1S)-1-(3,4-dichlorophenyl)ethyl]amino-2 hydroxypropyl] (phenylmethyl) phosphinic acid

N.B.2 The vast majority of experiments used NPS 2390 to block group 1 mGluRs. However, in a few of the early experiments reported in Chapter 3 MCPG was used instead.

2.5.2 Antagonising GABA-activated $GABA_ARs$

GABA-activated $GABA_AR$ responses were blocked – thereby completing the isolation of s-$GABA_ARs$ – using the potent, selective competitive $GABA_AR$ antagonist, SR-95531 (SR; gabazine)(74,238–242). Two features of SR make it a powerful pharmacological tool to isolate s-$GABA_ARs$: 1) its ability to potently block the binding of GABA to $GABA_ARs$ to prevent agonist-dependent receptor activation, and 2) its very limited negative intrinsic efficacy, with previous studies showing that SR can only inhibit a small fraction of spontaneous receptor activity (192,199,246,257–260). SR has a <1 μM relative IC_{50} for antagonising $GABA_AR$ responses evoked by concentrations of GABA at, or close to, EC_{50} in recombinant expression systems (245,246,248–255) and cultured neurons (256). It also has a <1 μM relative IC_{50} against $GABA_AR$ responses evoked by 20 μM isoguvacine, another $GABA_AR$ agonist (244). The potency of SR, as with other $GABA_AR$ antagonists (418), but unlike agonists (179,235), is largely independent of the subunit composition of the receptor (104,248,252,254,419,420). And when used at 10 - 100 μM SR is considered saturating (261–268). Both McCartney and Wlodarczyk *et al* demonstrated that SR – at 20 and 25 μM, respectively – *completely* blocked both synaptic $GABA_AR$ currents and, crucially, tonic $GABA_AR$ currents activated by 5 μM of' 'ambient' GABA (74,233). This concentration of ambient GABA is an order of magnitude greater than hippocampal [GABA] recorded *in vivo* and, henceforth, under basal conditions ([extracellular GABA] = 0.03-0.3 μM (74–77)), 25 μM SR will block all GABA-dependent $GABA_AR$ openings, whilst preserving virtually all of the s-$GABA_AR$ constitutive activity. Importantly, both McCartney *et al* and Wlodarczyk *et al* have shown using a 'bicuculine control' that the preservation of s-$GABA_AR$ signalling is *not* simply due to a failure of SR to bind to these receptors. Bicuculline is a competitive $GABA_AR$ inverse agonist: it blocks GABA binding to the orthosteric site *and* it also partially inhibits constitutive (s-$GABA_AR$) receptor activity (because its negative efficacy is much higher than SR) (74,233,246,270). In the two aforementioned studies, application of SR completely reversed bicuculline-mediated inhibition. This competing interaction of SR and bicuculline – the ability of an antagonist to reverse the effects of an inverse agonist – confirms that both bicuculline *and* SR bind to s-$GABA_ARs$. And, furthermore, that the preservation of s-$GABA_AR$ activity in the presence of SR is due to a lack of significant negative efficacy – not a lack of binding. As a result, application of 25 μM SR produces an

experimental setting were any detectable $GABA_AR$ conductance can be attributed to constitutively active s-$GABA_A$Rs.

2.5.3 The pharmacological block of s-$GABA_A$Rs

The final step in this experimental paradigm is to quantify s-$GABA_A$R conductance by completely *blocking* their activity using picrotoxin (PTX), a potent mixed $GABA_AR$ blocker. PTX inhibits the $GABA_AR$ via unconventional channel block, initially binding within the open-channel pore but then acting allosterically, not via simple hindrance of ion flow, to stabilise the $GABA_AR$ in a closed/resting, non-conductive state (98). Crucially, whilst PTX block is use-dependent because it requires an open-channel to access its binding site, it blocks *both* GABA-activated *and* spontaneously opening s-$GABA_A$Rs. The great utility of PTX is its ability to completely inhibit s-$GABA_A$Rs even when the orthosteric site is occupied by the neutral antagonist, SR, and, therefore, allows for precise quantification without confounding effects of GABA.

In summary, in the present PhD both forms of tonic $GABA_AR$ activation – GABA-dependent and independent – can be independently quantified by exploiting the different the mechanism of action of SR and PTX (Summarised in **Fig.2.3**). In brief, SR is a competitive neutral antagonist that competes with GABA and, at saturating concentrations, eliminates GABA-dependent $GABA_AR$ activity; conversely, PTX binds to the inside the channel pore to block all active $GABA_A$Rs, irrespective of if they were activated by GABA or open spontaneously. In a paired experimental paradigm, the input of GABA-dependent $GABA_A$Rs was measured as the change in response (e.g. input resistance, firing rate, holding current, etc.) obtained under control conditions vs. after application of SR; whereas s-$GABA_AR$ activity was measured as the change in the response obtained in the presence of SR vs. after subsequent application of SR + PTX. In an unpaired experimental approach (e.g. for LTP), the measured response will be binary: s-$GABA_A$Rs will either be intact in the presence of SR, or blocked entirely with SR+PTX.

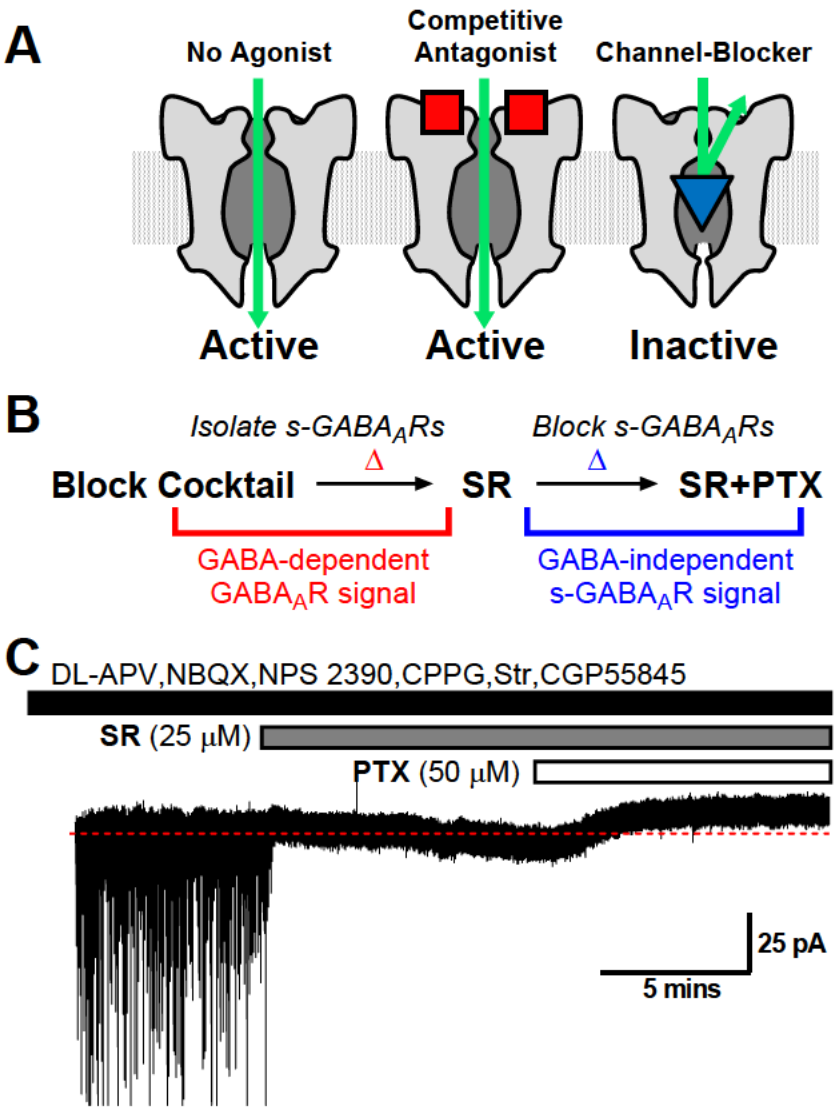

Fig.2.3. Understanding the workflow for isolating and quantifying the s-GABA$_A$R signal.
A) A simple pictorial representation of s-GABA$_A$Rs showing they are active in the absence of GABA, and remain active in the presence of a silent competitive antagonist (e.g. SR; red squares), but are inhibited by channel blockers (e.g. PTX; blue triangle). **B)** The pharmacological workflow used to *isolate* and then *block* (and in so doing quantify) the s-GABA$_A$R signal. Isolating s-GABA$_A$Rs requires 1) the blocking cocktail to inhibit non-GABA$_A$R-mediated neurotransmission, and then 2) SR to inhibit GABA-dependent GABA$_A$R activity. 3) Blocking s-GABA$_A$Rs requires the addition of PTX in the continuous presence of SR. **C)** A representative voltage-clamp trace (CsCl; -70 mV) showing the application of this pharmacological workflow to DGGCs. **Blocking cocktail→SR** allows for the quantification of the GABA-dependent signal GABA$_A$R signal: IPSCs are blocked by SR, but tonic currents are not (because they are GABA-independent). **SR→SR+PTX** allows for the subsequent quantification of the GABA-independent s-GABA$_A$R signal: PTX blocks the tonic s-GABA$_A$R current as revealed by the outward shift in the holding current.

2.6 Measuring GABA-dependent and GABA-independent inhibition

Whole-cell voltage-clamp recordings were made using the high [Cl^-] (CsCl) 'intracellular' in order to quantify record $GABA_AR$-mediated currents tonic and phasic currents at -70 mV.

2.6.1 Tonic inhibition

Tonic $GABA_AR$-mediated currents were measured in a similar manner to that outlined in "Methods for recording and measuring tonic $GABA_A$ receptor-mediated inhibition" Bright and Smart, 2013 (230) (**Fig.2.4**). GABA-*dependent* tonic inhibition was measured as the difference between the mean holding current measured in the control blocking cocktail (DL-AP5, NBQX, CPPG, NPS2390, CGP55845 and strychnine) vs in the presence of SR. GABA-*independent* tonic inhibition was quantified as the holding current change of SR vs. SR+PTX. Mean holding current was recorded within a region where the drug(s) response had reached a stable maxima, and was calculated by averaging over 5 ms epochs that are free of IPSCs, taken every 250 ms, during a 30 second period (120-point average) (**Fig.2.4**). All drugs were bath applied. Typically, the maximal SR effect was observed 2 minutes after the drug entered the recording chamber; PTX took longer, typically 8 minutes, to exert maximal block due to its activity-dependent mechanism of action.

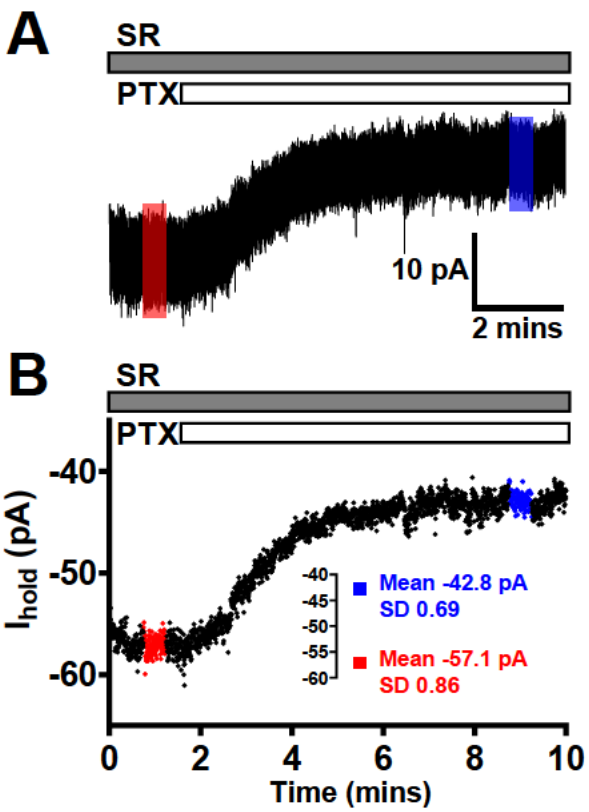

Fig.2.4. Method for measuring tonic inhibition.
A) A portion of the representative voltage-clamp trace depicted in Fig.2.3 (DGGC, CsCl; -70 mV), showing the block of s-$GABA_AR$ mediated tonic-currents by applying PTX in the continued presence of SR (**SR→SR+PTX**). The red highlighted area in **A)** and **B)** corresponds to the 30 second portion over which the average holding current in SR was calculated; the blue area corresponds to the same measure in SR+PTX. **B)** Shows how the tonic current amplitude is calculated: each point on the holding current vs time graph corresponds to the 5 ms average holding current sampled every 250 ms (at 4Hz); 120 of these points are to calculate the 30 second mean holding current in SR (red) and SR+PTX (blue) – values are shown in the inset. In this example s-$GABA_AR$ tonic current was calculated to be 14.3 pA.

2.6.2 Pharmacological modulation of tonic inhibition

In experiments examining the modulation s-$GABA_AR$ tonic currents, all compounds, apart from those used to directly target the intracellular second-messenger signalling pathways, were bath applied and allowed to perfuse the whole slice. At the flow rate used (8-10 $ml.min^{-1}$), the exchange time in the recording chamber was ~40 seconds. Compounds targeting the intracellular second messenger signalling pathways (Gαi, PKC, PKA) were dissolved into the intracellular solution prior to loading into the patch-pipettes. All compounds were prepared as concentrated stocks in their respective solvents and then added to the ACSF or intracellular solution to yield the appropriate final concentration.

Bath-applied compounds were added either 1) prior to SR, when GABA-dependent $GABA_AR$ signalling was still intact – and so any change in holding current may be due to modulation of GABA-dependent $GABA_ARs$ and/or s-$GABA_ARs$; or 2) after SR, when GABA-dependent $GABA_AR$ signalling was blocked – and so any change in holding current will not be due to modulation GABA-dependent $GABA_A$ signalling. The impact of any bath-applied compound was assessed first, by measuring the change in holding current before and after the drug, and, second – and most importantly – by measuring the amplitude of the outward current caused by PTX in the presence of the drug and SR and comparing it to with SR. (e.g. **SR→SR+PTX** vs**. DRUG+SR→DRUG+SR+PTX**).

The compounds tested in this thesis are as follows:

	Final Conc	**Solvent**	**Pharmacology**
Zinc	100 µM	dH_20	Non-competitive $GABA_AR$ antagonist
L-655,708	20 µM	DMSO	α5-subunit $GABA_AR$ inverse agonist
DS2	3 + 10 µM	DMSO	δ-subunit $GABA_AR$ PAM
DPP-4-PIOL	1,3,10 +30 nM	DMSO	δ-subunit antagonist
Diazepam	1 µM	dH_20	BDZ-site agonist
Zolpidem	500 nM	dH_20	BDZ-site agonist
Flumazenil	10 µM	dH_20	BDZ-site antagonist
DMCM	1 + 2 µM	DMSO	BDZ-site inverse agonist
Midazolam	40 + 120 nM	DMSO	BDZ-site agonist
Pertussis Toxin	$1\mu g.ml^{-1}$	dH_20	Gαi blocker
Bisindolylmale-imide ii	50 nM	DMSO	PKC inhibitor
PKI	10 µM	dH_20	PKA inhibitor
Br-cAMP	1 mM	dH_20	PKA activator

2.7 GABA-independent vs phasic charge transfer

The relative contribution of s-$GABA_A$Rs to total inhibitory tone in DGGCs was assessed by comparing the total charge delivered in 1 minute by s-$GABA_A$Rs (GABA-independent tonic currents) to that provided by phasic currents (IPSCs). The net charge transferred by tonic s-$GABA_A$Rs (Q_{tonic}) was calculated according to the equation: $Q_{tonic} = \Delta I_{hold} \times t$. Here, ΔI_{hold} is the amplitude of the tonic current measured at state between SR vs. SR+PTX, and t is the duration (60 s). IPSCs were detected over a 3 minute period using the inbuilt template search function in Clampfit; charge transfer for each of the detected IPSCs was measured as the area under the curve. The total charge transferred in one minute by IPSCs (Q_{phasic}) was calculated using: $Q_{phasic} = F \times Q_{AV.IPSC} \times t$; where F is the frequency (Hz) of IPSCs, $Q_{AV.IPSC}$ is the average charge transferred by an IPSC during the 3 minute period, and t is the duration (60 s).

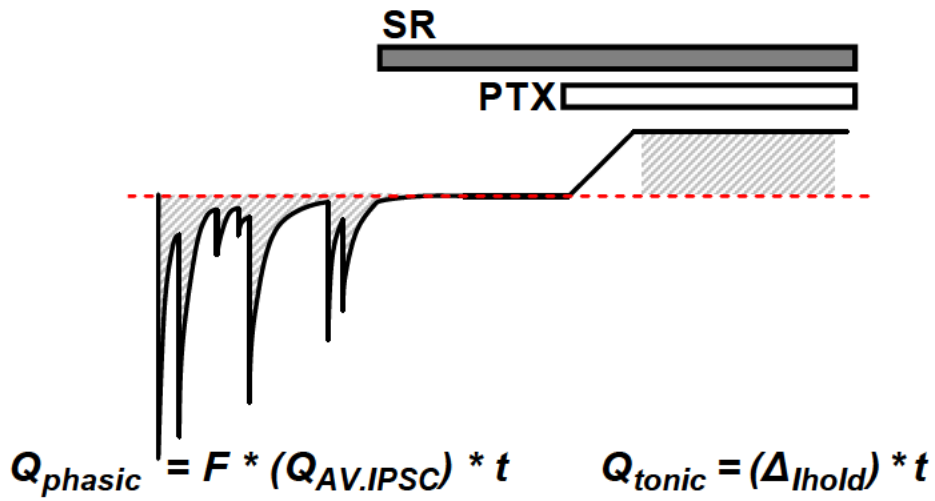

Fig.2.5. Method comparing tonic and phasic charge transfer.
A simplified, cartoon depiction of a voltage-clamp trace similar to that shown in Fig.2.3: **SR→SR+PTX** (DGGC, CsCl; -70 mV). The grey striped area indicates how inhibitory charge transfer per unit time is calculated by using the area under curve of phasic and tonic currents. Phasic charge transfer (Q_{phasic}) is calculated in each cell by multiplying the average IPSC frequency (F; Hz) by 60 seconds (t), by the average charge transfer of an IPSC ($Q_{Av.phasic}$). Tonic s-$GABA_A$R charge transfer (Q_{tonic}) is calculated by multiplying the steady state **SR→PTX** outward current (ΔI_{hold}) by 60 seconds (t).

2.8 I–V relationship of s-$GABA_A$Rs and $GABA_A$R reversal potential

The I–V relationship of s-$GABA_A$R-mediated currents was recorded using a Cs-methanesulfonate-based intracellular solution conferring adult, mature physiological levels of Cl^- (8 mM); the extracellular ACSF contained the standard 'block-cocktail' supplemented with 1 µM TTX and 1 µM Nifedipine in order to block voltage-gated sodium and calcium channels, respectively. Cadmium, the broad-spectrum voltage-gated calcium channel blocker, was not used because it has been reported to block $GABA_A$R currents (421,422).

The I-V profile of the recorded neuron was obtained by stepping the membrane from a resting potential of -90 mV to holding potentials between -105 and +15 mV, using +15 mV, 5s steps. The current delivered by s-$GABA_A$Rs at a given holding potential was calculated by deducting the steady-state current (last 50ms of the voltage step) obtained in the presence of SR+PTX from that obtained with just SR.

The reversal potential and rectification properties of s-$GABA_A$R-mediated tonic currents were compared to evoked $GABA_A$R IPSCs using a similar voltage step paradigm. IPSCs were evoked from the MPP and peak IPSC was recorded at holding potentials between -120 and +30 mV (+30 mv, 2.5 second steps; resting potential = -90 mV). The same Cs-methanesulfonate intracellular solution was used as in s-$GABA_A$R I-V experiments; however, TTX and Nifedipine were omitted from the ACSF-blocking cocktail solution in order to permit neurotransmitter release. The I-V relationships were fit with Boltzmann functions, as in Pavlov *et al,* 2009 (387), and rectification was assessed by comparing the slope of the curve at -70 mV to that at 0 mV. The slope was obtained from the first-order derivative of the Boltzmann function (dI/dV). Below is the Boltzmann functions, where V50 is the potential at which current is halfway between Top and Bottom; and the slope describes the steepness of the curve.

$$y = Bottom + \frac{Top - Bottom}{1 + \exp(\frac{V50 - x}{slope})}$$

2.9 Recording of passive and active membrane properties

The effect of s-$GABA_AR$ conductance on passive and active membrane properties was assessed using K-gluconate intracellular solution containing physiological (8 mM) Cl^-; all recordings were made in current-clamp mode were performed from RMP (I_{hold} = 0). In each of these experiments, apart from firing frequency vs. current (f–I) relationship, the input of s-$GABA_ARs$ was measured using the paired recording protocol: in the majority of experiments the same measurement was made in ACSF containing (1) the blocking cocktail only (GABA-activated and s-$GABA_ARs$ intact); (2) then with SR added (only s-$GABA_ARs$ active); and (3) finally, SR+ PTX (s-$GABA_ARs$ blocked). In the minority of these "paired" experiments, measurements were only taken in condition (2) and (3), with condition (1) was omitted. For F-I curves, experiments were performed on separate neurons in condition (1) *or* (2) *or* (3). This unpaired approach was conducted in order to prevent near-maximal levels of neuron firing modifying subsequent membrane excitability, thereby complicating analysis.

2.9.1 Input resistance

DGGC input resistance was measured by recording the anti-peak voltage in response to 9 hyperpolarising, -50 pA 500 ms, square-wave current injections from -50 to −450 pA. Input resistance was calculated according to Ohm's Law, as the gradient of the straight line fitted to the voltage change against the injected current.

2.9.2 Membrane time constant

Membrane time constant (τ_m) was obtained by applying 30x -5 pA, 500 ms hyperpolarising current steps (from I_{hold} = 0); τ_m was calculated by the fitting the fall of the average membrane voltage with a mono-exponential decay.

2.9.3 Resting membrane potential

The input of s-$GABA_ARs$ into RMP was assessed in a similar manner to changes in holding current: mean RMP values over 30 second recording periods, and the contribution of s-$GABA_ARs$ to RMP was determined as the difference in average RMP in the presence of SR, compared with SR + PTX.

2.9.4 Rheobase

Rheobase was determined by incrementally depolarising the neuron using +5 pA, 0.7 s current injections and recording the minimum current necessary to trigger an action potential. The action potential evoked at rheobase was analysed for AP threshold voltage, with threshold defined as when ΔdV/Δt exceeds 20 mV/ms.

2.9.5 F-I relationship

The F–I relationship of a neuron was obtained by recording the number of action potentials elicited in response to a series of 25 pA, 0.5 s depolarising current injections between 0 and 250 pA. The gain of the F-I relationship, measured as the slope of the linear region of the curve (50 pA to 175 pA) and the area under the F-I curve.

2.10 Evoking postsynaptic responses by electrical stimulation

Orthodromic synaptic stimulation was delivered through a bipolar tungsten stimulating electrodes: the medial perforant pathway (MPP) was stimulated by placing electrodes in the middle one-third of the molecular layer; for the lateral perforant pathway (LPP) electrodes were placed in the outer third. Stimulation intensity was controlled using DS2A constant voltage isolator (duration = 100 μs unless otherwise stated; intensity = 0.5 – 10 V).

2.11 Measuring the temporal window for successful coincidence detection

The summation capacity of a neuron is under strong GABA-ergic control and, henceforth, may be influenced by s-$GABA_A$Rs. The temporal window within which two excitatory inputs, activated asynchronously, can be successfully summated to trigger an action potential was used as a measure of coincidence detection precision.

Coincidence detection experiments were performed in current-clamp mode (I_{hold} = 0 pA) using the K-gluconate intracellular solution in an ACSF, which – in order to be able to evoke EPSPs – *did not* contain any of the blockers of excitatory transmission and, instead, only contained CGP55845 and strychnine. Strychnine was included to prevent the results being confounded by PTX-mediated block of GlyRs; CGP55845 was included to prevent activation of $GABA_B$Rs by spill-over GABA, the amount of which could have been increased by SR. Two distinct EPSPs were evoked using two separate stimulation electrodes: one placed in the LPP, the other in the MPP. The stimulation intensity was then adjusted so that when the two pathways were activated simultaneously (t= 0 ms), the patched neuron generated an action potential 50 – 60 % of the time.

The temporal summation protocol had 4 steps. (1) A selected pathway (e.g. MPP) was stimulated so that it precedes stimulation of the other by an inter-stimulus interval (ISI) of 40 ms; (2) the ISI was then decreased, in 10 ms increments at a rate of 0.1 Hz, until the two stimulations were delivered simultaneously (ISI = 0ms). (3) This stimulation protocol was then reversed so that the pathway stimulated second was now stimulated first (4). In order to produce a firing probability, the entire protocol was repeated 3 times, meaning that for each ISI (from +40 ms to – 40 ms, in 10 ms increments) there was an accompanying firing probability of either: 0%, 33.3%, 66.6% or 100%.

In the absence of any $GABA_A$R antagonists, evoked potentials are a composite of excitatory and inhibitory signalling. GABA-dependent receptors were blocked using SR, and the experiment was repeated. In all experiments, SR caused a saturation of the response: a high percentage firing probability was observed at all ISIs. Henceforth, in order to be able to detect if the subsequent addition of PTX (blocking s-$GABA_A$Rs) had an additional effect

relative to SR alone, stimulation intensity was adjusted to, as close as possible, match the spiking probability observed under the control (50 – 60 % firing probability for an ISI of 0 ms). The cell was exposed to PTX, and the stimulation protocol was repeated in order to quantify the input of s-$GABA_A$Rs into temporal summation in DGGCs. Data were fitted with a Gaussian function, where σ is standard deviation and μ is the mean.

$$y = \frac{1}{\sigma\sqrt{2\pi}} e^{-\frac{(x-\mu)^2}{2\sigma^2}}$$

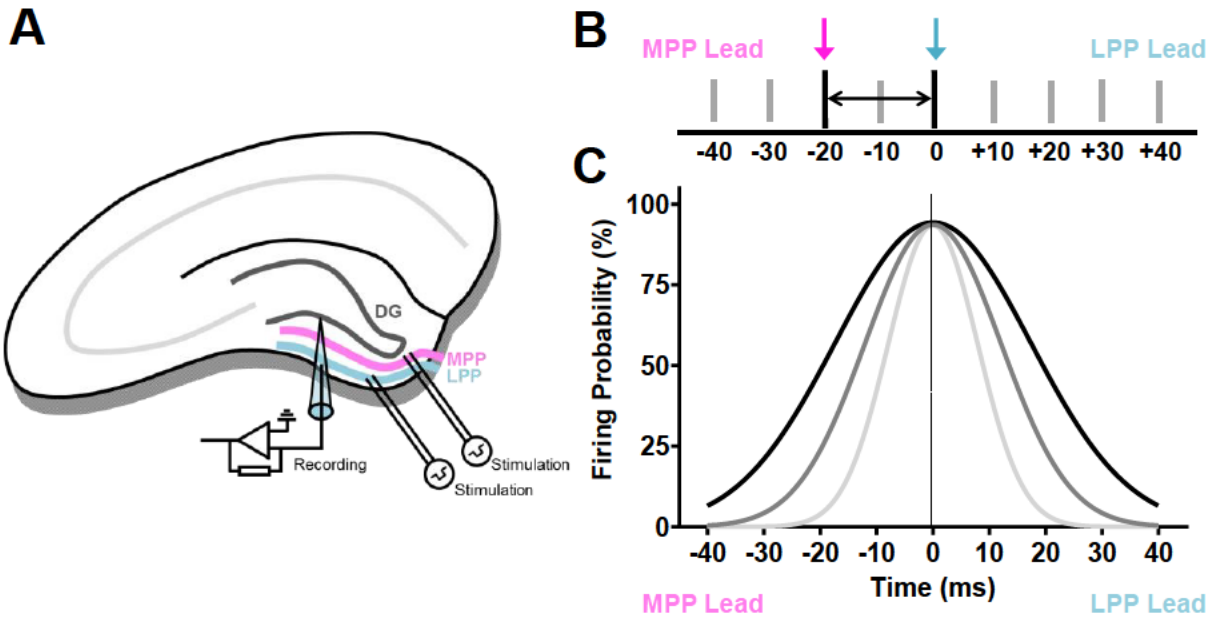

Fig.2.6. Electrode Placement and stimulus timing protocol for coincidence detection experiments.
A) A simplified, cartoon depiction of the hippocampal slice and electrodes. Recording electrode for whole-cell current-clamp recordings from DGGCs. Responses are recorded from stimulating the medial perforant pathway (MPP) and the lateral perforant pathway (LPP). **B)** Timing protocol for measuring coincidence detection showing how the onset of the MPP varies relative to that of the LPP. Negative values designate the time by which MPP stimulus leads LPP stimulus. Positive values designate the time by which MPP stimulus lags behind LPP. **C)** Example firing probability-stimulus interval curves. Increasing intensity (grey→**black**) indicates an example of a widening of the temporal window for successful coincidence detection.

2.12 LTP in the medial perforant pathway

The effect of s-$GABA_AR$ signalling on LTP amplitude was assessed in the extracellular field recording configuration. Two other modifications were made to the basic recording set-up. Firstly, the flow-rate of ACSF was reduced to ~4 $ml.min^{-1}$; this increased the stability of the field response in these long, often in excess of 90 minutes, recordings. Secondly, the low-pass filter was changed from 8 kHz to 1.4 kHz. The recording protocol used in these experiments was unpaired: meaning that there was no sequential addition of GABA antagonists; instead, the entire recording was performed in the presence of SR *or* SR+PTX – the only other drug included in the recording ACSF was strychnine, which was present in all recordings.

Field potentials were evoked in the MPP using bipolar stimulating electrodes placed in the middle one-third of the molecular layer, 50 to 100 µm below the slice surface, near the apex of the dentate gyrus. Extracellular field postsynaptic potentials (fEPSPs) were recorded in current-clamp mode (I_{hold} = 0 pA) using low resistance recording pipettes filled with ACSF (1-2 MΩ); pipettes were placed in the middle-third of the molecular layer, ~200 µm away from the stimulating electrode.

fEPSPs were evoked at 30 second intervals using a square wave, 50 µs in duration, voltage pulses, and quantified according to the slope of their linear rising phase. Stimulation intensity was set to give an fEPSP slope ~40% of maximum, as determined by the input/output relationship (1 – 8 V; 1 V increments). fEPSPs evoked at this intensity were typically stable and exhibited a visible population spike; any slices that yielded unstable responses or exhibited small population spikes were discarded. A baseline fEPSP slope was calculated from the average of the 20 responses over the 10 min prior to LTP conditioning.

LTP was induced by theta-burst stimulation (TBS), repeated 4 times at 30 second intervals. Each TBS episode was comprised of 10 bursts of five pulses at 100 Hz, with each burst separated by 200 ms. During LTP induction the pulse duration was increased from 50 to 200 µs. The LTP protocol described was chosen because it robustly induced sustained potentiation in the DG in all pilot experiments; this meant that it was a suitable protocol to address the hypothesis 'do s-$GABA_AR$s modify LTP *amplitude*?' Henceforth, the analysis of LTP was not

complicated by changes to the threshold by which LTP can be induced (which s-$GABA_A$Rs may alter).

Following the 4 episodes of TBS-LTP conditioning, the stimulation duration was returned to 50 µs and fEPSPs were recorded, once every 30 seconds, for 60 minutes. LTP amplitude was quantified by comparing the average baseline fEPSP slope (10 minutes prior to LTP) to the fEPSP slope after 1 hour (50-60 minute average).

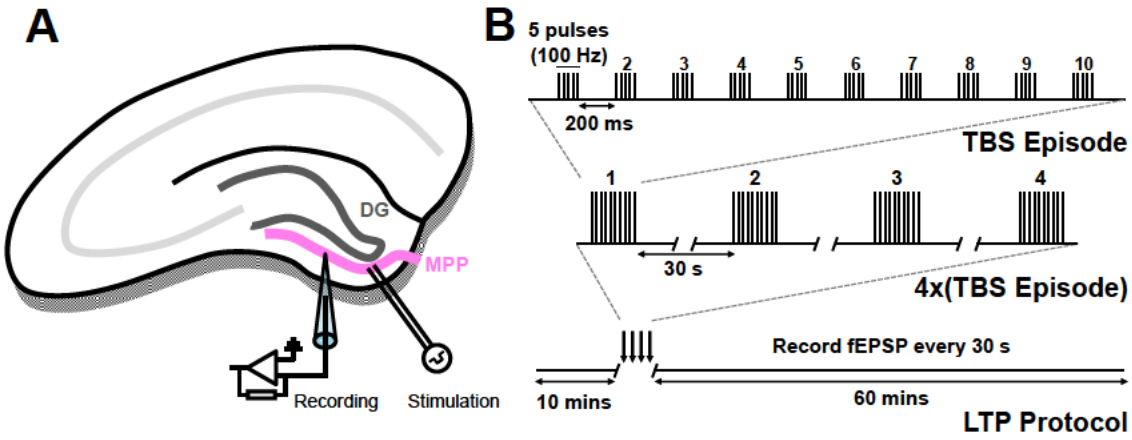

Fig.2.7. Electrode placement and stimulus protocol for LTP experiments.
A) A simplified, cartoon depiction of the hippocampal slice showing placement of the recording and stimulation electrode. The bi-polar stimulation electrode was placed in the MPP; fEPSPs were recorded using electrodes placed in the medial molecular layer. **B)** LTP was induced using 4XTBS episodes, with each episode delivered at 30 second intervals. A TBS episode consisted of 10 bursts of five pulses at 100 Hz, with each burst separated by 200 ms.

2.13 Statistical analysis

All data are expressed as the arithmetic mean value ± SEM (standard error of the mean), unless otherwise stated. In all experiments statistical significance was compared between two groups using the Student's t-test (paired or unpaired, Graphpad PRISM) and three groups using an ANOVA (followed post-hoc by Student's t-tests with Bonferroni correction; Graphpad PRISM). Data were considered significant when $p < 0.05$. Abbreviations used throughout: n.s = no significant difference, * = $p < 0.05$, ** = $p < 0.01$, *** = $p < 0.001$.

Chapter 3

The Functional Impact of s-$GABA_A$Rs in Dentate Gyrus Granule Cells

3.1 Overview

It has been previously shown that spontaneously opening $GABA_A$ receptors (s-$GABA_A$Rs) generate a GABA-independent tonic conductance in granule cells of the dentate gyrus (DGGCs) (74). However, at the time of commencing the present thesis, the functional impact of this conductance upon cellular excitability was unknown. The experiments performed for this chapter sought to address this ambiguity by characterising the function of s-$GABA_A$R signalling in DGGCs. Specifically, we aimed to characterise both 1) the nature of the s-$GABA_A$R signal delivered to DGGCs and 2) how it is interpreted by these neurons. To achieve this aim, we measured the effect of s-$GABA_A$R-mediated conductance on passive membrane properties (input resistance, membrane time constant, RMP), active membrane properties (excitability, rheobase, AP threshold voltage) and the input-output (I-O) function of DGGCs (as expressed in F-I curves). We also explored the impact of s-$GABA_A$Rs on the temporal precision of signal integration (coincidence detection) and on neural plasticity (LTP), both of which are important for proper DGGC function in the brain. Some of the findings presented in this chapter have been published (415,417).

Experimental:

> O'Neill N, Sylantyev S. Spontaneously opening $GABA_A$ receptors play a significant role in neuronal signal filtering and integration. Cell Death Dis. 2018;9(8).

Mini-Review:

> O'Neill N, Sylantyev S. The Functional Role of Spontaneously Opening $GABA_A$ Receptors in Neural Transmission. 2019;12:1–7

3.2 Introduction

Tonic inhibition, or more specifically, the tonic *conductance* that is generated by persistently active $GABA_A$Rs, is a slow form of neurotransmission that is expressed widely across many different neuron types (61,224,230). The persistent activation of $GABA_A$Rs can occur via GABA-dependent and GABA-independent mechanisms (74,224,233,234). Low concentrations of GABA activate high-affinity $GABA_A$Rs located outside the synapse – at peri-/extra-synaptic sites – to generate GABA-dependent tonic conductances (224). In contrast, GABA-independent tonic conductances are generated by $GABA_A$Rs that activate spontaneously, in the absence of GABA, because they exhibit constitutive receptor gating (74,233,234,236,237). Because spontaneously activating $GABA_A$Rs (s-$GABA_A$Rs) do not require GABA to activate, they are resistant to competitive antagonists (e.g. SR) but can be inhibited by inverse agonists (e.g. bicuculline) and channel-blockers (sometimes termed non-competitive antagonists e.g., PTX) (74,233,234,236,237).

The literature on *GABA-dependent* tonic currents is vast and sprawling: persistent currents activated by ambient GABA have been detected in most brain regions, across a litany of neuron types (224,230). The ubiquity of this signal is well summarised by Lee and Maguire in 2014, which details over 60 neuron types that express tonic $GABA_A$R currents (224).

By contrast, there is a relative paucity of studies that have formally and knowingly detected the presence of GABA-independent tonic currents. To date, s-$GABA_A$R-mediated tonic currents have been confirmed in only three neuron types: hippocampal pyramidal neurons (233) and granule neurons (74), and a subpopulation of central amygdala neurons that express PKCδ (234). As discussed in the introduction, this does necessarily reflect a dearth of s-$GABA_A$R-mediated tonic conductances in the CNS. There is evidence that s-$GABA_A$R signalling is more widespread phenomenon than has been previously anticipated; this reaffirms the importance of gaining a proper understanding of their function.

So far, however, the function of the tonic s-$GABA_A$R conductance has only been investigated in one neuron type: the PKCδ positive neurons of the central amygdala (234). In this study, Botta *et al* showed that selectively blocking s-$GABA_A$R currents caused a slight depolarizing shift in

RMP, an increase in input resistance, a higher spontaneous firing rate, and an increase in excitability (234).

At present, there are no corresponding functional data on s-$GABA_AR$ mediated tonic currents from any other brain region/neuron type. The two studies that recorded s-$GABA_AR$ tonic currents in the hippocampus – McCartney, 2007 *et al* from pyramidal cells (233) and Wlodarczyk *et al* from granule cells (74) – performed all their experiments using high-[Cl^-], Cs-based intracellular solution. This intracellular solution enables $GABA_AR$ currents to be recorded at RMP (E_{GABA} ~ 0 mV); it also has excellent space-clamp properties due to block of membrane K^+ current (423), but as a result cannot be used to measure the passive and active properties of a membrane in a physiological state (e.g. with K^+ channel conductance intact). To assess the physiological function of $GABA_AR$ currents, K^+ must be used as the major intracellular solution cation, not Cs^+.

Thus, the function of s-$GABA_AR$-mediated tonic conductances remains largely unexplored, and in the hippocampus is unknown – this is despite the fact that s-$GABA_ARs$ provide virtually of the tonic conductance in DGGCs (74). In this chapter, we sought to characterise 1) the nature of the s-$GABA_AR$ signal delivered to DGGCs and 2) how it is interpreted by these neurons. We opted to study DGGCs because, first, s-$GABA_AR$ tonic conductances have been confirmed in these neurons and, second, because the DG, located as it is at the interface between the cortex and the hippocampus (424), has an important role in the brain. The DG has been postulated to perform a variety of important functions that are necessary for proper cognitive, emotional and mnemonic processing in the brain. Notable among the proposed functions of the DG are 1) pattern separation and 2) gating (thereby curtailing) the flow of aberrant excitation into the hippocampus proper. In the following section, we will explore how the circuit organisation of the DG and particularly the intrinsic properties of DGGCs facilitate its role as both a pattern separator and a gate. At the conclusion of this section, we will hypothesise how s-$GABA_ARs$ may affect these properties, thereby setting the scene for the results section, in which we explore the function of s-$GABA_AR$-mediated tonic conductances in DGGCs.

3.2.1 The Dentate Gyrus: Gateway into the hippocampus

The dentate gyrus (DG) is one of the major hippocampal sub-regions and marks the entry of the canonical ***tri-synaptic loop*** (Entorhinal cortex (EC) Layer II → ***DG*** → ***CA3*** → ***CA1***) (424,425) (*see diagram on the following page*). The tri-synaptic loop is the main route of information flow through the hippocampus (424,425) and has been used extensively as an anatomical substrate for the study of learning and memory (426–428). The DG is a V-shaped structure that consists of three layers: the outermost, molecular layer; the middle, granule cell layer; and the innermost, hilus (polymorphic layer) (425). The granule layer surrounds the hilus on three sides and contains the principal excitatory cells of the DG: the DGGCs. There are ~1,000,000 of these small, round, bipolar cells per hemisphere in rats (and ~10 million in humans) (425,429). DGGCs send their apical, cone-shaped dendritic trees into the molecular layer and receive their main excitatory input from EC layer II stellate cells (~120,000 per hemisphere in rat) via the perforant pathway, so termed because it 'perforates' the hippocampal subiculum (425).

The perforant pathway has two divisions, named after the EC subdivision from which they emanate: the lateral perforant path (LPP), which terminates on DGGC dendrites in the outer third of the molecular layer and conveys novel object information (430,431); and the medial perforant path (MPP), which terminates on DGGC dendrites in the middle third of the molecular layer and transmits spatial information (430,431). DGGCs integrate and interpret this signal, and when they fire an action potential, they send excitatory signals via their axons, termed mossy fibres. These fibres project through the hilus and make sparse but strong excitatory connections with CA3 pyramidal cells; there are ~300,000 of these neurons per hemisphere in rat, and each of them receives only ~50 mossy fiber inputs (390,425,432). Pyramidal cells in area CA3 then send axons via the Schaffer collateral pathway to CA1 pyramidal neurons, which, in turn, project to the subiculum and back to the EC, thereby closing the loop (425).

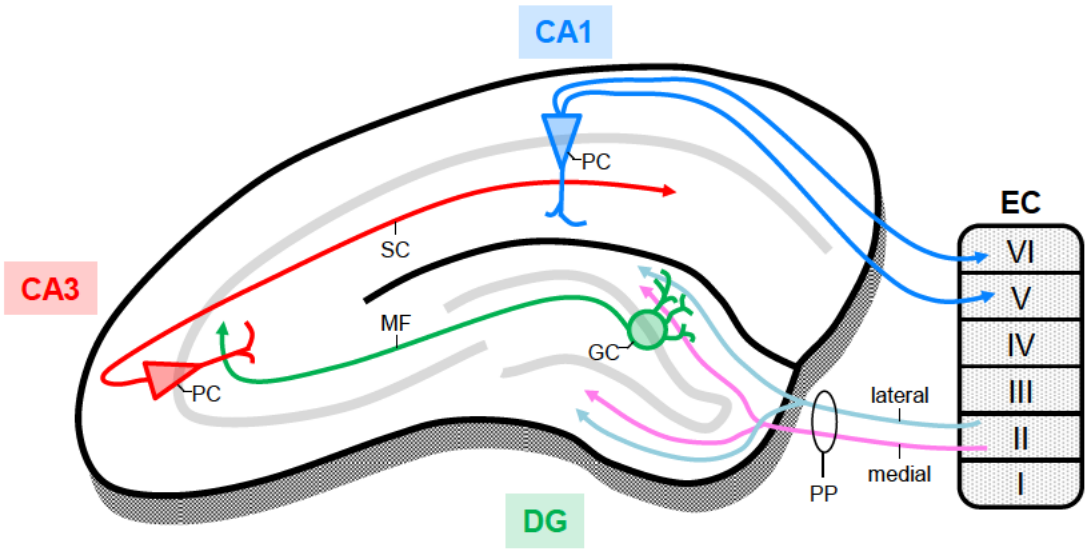

Hippocampal trisynaptic loop. A simplified, cartoon depiction of a hippocampal slice shows the canonical tri-synaptic loop circuit. Stellate cells project from layer II of the entorhinal cortex (EC) via the medial (MPP) and lateral performant path (LPP) to the molecular layer of the dentate gyrus (DG) which contains the dendrites of granule cells (GC). DGGCs project via their mossy fibers (MF) to CA3 pyramidal cells (PCs), which in turn send Schaffer collaterals (SC) to CA1 PCs. These neurons project to both the subiculum and to EC layer V+VI, thereby closing the loop.

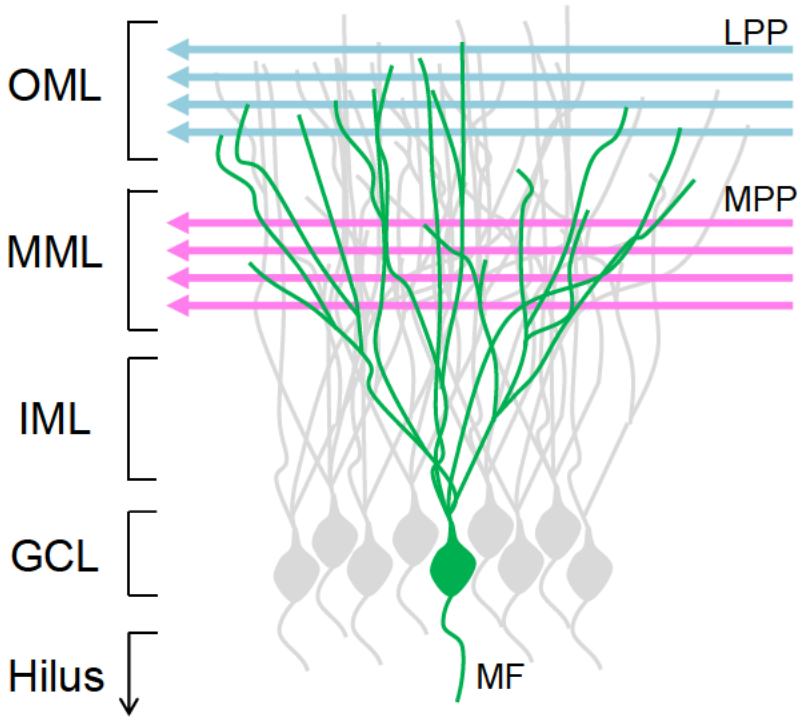

Perforant path inputs to DGGCs. A simplified, cartoon depiction of the structure of the perforant path inputs to a DGGC (green) in the DG. DGGC cell bodies are in the granule cell layer (GCL), they send their mossy fiber (MF) axons into the hilus and their dendrites into the molecular layer. Dendrites in the outer molecular layer (OML) receive EC inputs via the lateral perforant path (LPP), those in the middle molecular layer via the medial perforant path (MPP). Mossy cell axons terminate in the inner molecular layer (IML).

DGGCs also receive inhibitory inputs (both feed-forward and feed-back) from at least four families of GABAergic interneurons (433,434): 1) parvalbumin-positive (PV) basket cells (targeting the somata of DGGCs as well as other PV cells), and parvalbumin-positive fast spiking axo-axonic cells (targeting the axon initial segment (AIS) of DGGCs); 2) cholecystokinin-positive (CCK) hilar associational/commissural path-associated cells (targeting DGGC dendrites in the inner molecular layer and the somata as well as other CCK and PV cells), and cholecystokinin-positive total molecular layer cells (targeting DGGC dendrites across the entire molecular layer as well as hilar interneurons); 3) somatostatin-positive (SOM) hilar associated cells (targeting GABA-ergic interneurons in the hilus as well as the medial septum), and SOM-positive hilar perforant path cells (targeting DGGC dendrites in the outer molecular layer as well as PV and other SOM cells); 4) Molecular layer perforant path cells (targeting DGGC dendrites in the outer 2/3rds of the molecular layer and interneurons) (433,434). A neurogliaform interneuron subtype is also present in the DG.

In addition to DGGCs and GABA-ergic interneurons, the other major cell type in the DG is the mossy cell. These glutamatergic neurons are loosely distributed throughout the hilus (the polymorphic region between the granule cell layer and CA3); they receive inputs from and send excitatory commissural/associative connections to DGGCs, other mossy cells and GABA-ergic interneurons (425). Because of their connections with GABA-ergic interneurons, in normal conditions, the net effect of mossy cell excitation on DGGCs is actually inhibitory (435).

3.2.2 The Dentate Gyrus functions as a gate and pattern separator

The DG is optimised at both the network and cellular level to act as a ‘gate’, or filter, that controls both the amount and the character of the excitatory signals that flow from the cortex into the hippocampus proper (436). In the normotopic brain, the DG, by acting as a gatekeeper, helps to prevent the propagation of pathological epileptiform discharges into the downstream hippocampal circuits (436–439). However, the DG is not just a barrier aberrant excitation: it is also a critical locus for a set of computations that support proper cognitive processing in the brain. Chief among these computations is neural *pattern separation:* the orthogonalization of a set of similar input patterns into a dissimilar set of output patterns (432,440,441). At the level of

the hippocampal circuit, pattern separation describes the transformation of highly overlapping EC input signals into dispersed (orthogonalized) representations in the DG, which are then projected to area CA3 as lowly overlapping patterns of DGGC firing (432,440).

The idea that certain neural circuits can perform pattern separation – and that pattern separation at the level of cell ensembles aids proper cognitive processing – was originally proposed by David Marr, in three ground breaking computational studies on the cerebellum (442), neocortex (443) and the hippocampus (444). Marr noted that the DG might increase the "sparseness of representations" in CA3, but it was in subsequent computational studies that the DG was proposed explicitly as the pattern separator in the hippocampus (432,445–453). This was initially motivated the anatomy of the DG circuitry, specifically, the over three-fold higher cell number in the DG relative to their EC inputs and because DGGCs making few but relatively powerful contacts with CA3 pyramidal cells (390,425). It is thought that the expansion in network size from EC to DG causes similar input signals to be dispersed (pattern separated), thereby reducing the chance of the same population of DGGCs becoming active (432,445–453).

It has been posited at the behavioural level that neural pattern separation – by producing anticorrelated firing patterns for similar contexts – better enables animals to 1) discriminate similar environments and experiences (discrimination learning) and 2) encode memory traces with minimal the interference, or blending, making them more precise and less susceptible to recall errors (454,455). Multiple studies support the DG acting as a pattern separator (reviewed in (455)): animals with impaired DG function, either through selective lesion (456,457), knockout of the GluN1 subunit of the NMDAR (458), or optogenetic silencing (459–461), show deficits in tasks thought to rely on neural pattern separation e.g. spatial separation (456), context-specific fear conditioning (458,460,461), location or object discrimination (457,459,460). In addition, fMRI recordings from human subjects performing show increases in blood-oxygen-level-dependent (BOLD) signal in the DG during pattern separation tasks (462,463). Finally, *in vivo* electrophysiological recordings from the DG provide perhaps the best empirical evidence that the DG is a locus for pattern separation (464–466), notable among these is Neunuebel and Knierim, 2013+2014 (431,466). Collectively, the *in vivo* recordings show that correlated patterns of activity in the DG are highly sensitive to small alterations to the environment, with changes

(decorrelations) in DG activity observed for even very subtle modifications to the shape of the animal's environment (464–466).

Although it was the DG network anatomy that initially marked it out as a pattern separator, subsequent studies have shown that the intrinsic properties of DGGCs and their circuit connectivity also facilitate pattern separation (432,441,445–453). These same properties likewise enable the DG to perform the more straightforward role of gatekeeping aberrant excitation (436,439). Many of the intrinsic properties of DGGCs could be affected by the s-$GABA_AR$-mediated tonic conductance.

3.2.3 DGGCs are sparsely active

Perhaps the most important property of DGGCs in relation to pattern separation and gating is their sparse activity (441): recordings from awake behaving rats or mice have demonstrated that only a small portion (2-5%) of the DGGC population are active during a given cognitive task (467,468), and that the DGGCs that are active have a low overall firing rate (413,468–470); typically < 1 Hz; but can vary a range of 0.04 Hz to 2.9 Hz for individual DGGCs (469).

When DGGCs do fire, however, they typically do so in bursts of 2-6 APs over a time frame in the tens of milliseconds (413,468). AP bursts are typically separated by periods of quiescence ranging between 4 and 7 seconds (413), and the timing of the APs within a burst is phase-locked to theta (4-10 Hz)-gamma (30-90 Hz) cycles in the local field potential (LFP) (413,470). There is strong evidence that the theta LFP is largely dependent on excitatory synaptic transmission coming from the EC, whereas the gamma LFP relies on local GABA-ergic transmission (413). In terms of pattern separation, because only a tiny proportion of the DGGC population are active at a given time, it means that similar inputs can be readily encoded in the DG as non-overlapping (orthogonalized) representations (432,441,445–453).

The sparsification of neuronal activity across the DGGC population is dependent on the active/passive membrane properties of DGGCs and the circuit organisation of the DG. At the circuit level, there are two key factors at play: the first is the dearth of excitatory (recurrent) connections between DGGCs (425,471); the second is that DGGCs are subject to strong inhibition from GABA-ergic interneurons (436).

3.2.4 Circuit organisation facilitates pattern separation and gating

The lack of recurrent excitation allows for the specific activation of a small subpopulation of DGGCs without causing collateral excitation of other DGGCs throughout the network. In animal models and patients with temporal lobe epilepsy, wherein the DG gate is often compromised, there is an increase in the number of recurrent excitatory connections between DGGCs due to so-called mossy fiber 'sprouting', which describes the retrograde projection of DGGC axons (mossy fibers) into the inner molecular layer (425,471,472). These aberrant excitatory connections cause otherwise silent DGGCs to spike (472), and this has been shown to cause a breakdown in DG gate-keeping: in *ex vivo* slices, epileptiform discharges are able to propagate from the EC, through the DG and into CA3 (438). Computational models indicate that aberrant recurrent excitation also prevents the DG from acting as an effective pattern separator (473).

The GABA-ergic system of interneurons also facilitates the sparse firing of DGGCs; they do so by affecting the membrane properties of DGGCs and by precipitating temporal oscillations across the DG network (433,434,474,475). Of the interneuron sub-types mentioned previously the two most widely studied are 1) the PV basket cells (BCs), which target the soma of DGGCs as well as other PV interneurons; and 2) the SOM hilar perforant path (HIPP) cells, which target DGGC dendrites in the molecular layer (434).

PV BCs have been shown to facilitate sparse DGGC firing and pattern separation through a 'winner-takes-all' strategy, in which the most excited DGGCs recruit PV BCs to inhibit the less-excited DGGCs – or, to put it another way, PV BCs allow the most excited DGGCs to compete with the less excited ones (476,477). The key to this mechanism is that in the DG there is uniquely high proportion of lateral inhibition (unidirectional: DGGC→PV BC→other DGGCs) relative to recurrent inhibition (bi-directional: DGGC⇄ PV BC); also important is the fast-signalling characteristics of PV BCs, specifically their high firing rate, rapid dendritic processing, short AP duration and somatic targeting (434,476,477). The high level of lateral inhibition allows highly excited 'winner DGGCs' to efficiently inhibit a large population of less excited 'non-winner DGGCs' without inhibiting themselves (476,477).

DGGCs can also laterally inhibit other DGGCs by activating SOM HIPPs (476,478,479); however, because SOM HIPPs innervate the dendrites they do not affect AP firing directly (as is the case for PV BCs), but instead constrain DGGC excitability by shunting the synaptic input to DGGCs (478,479). GABA-ergic inhibition thus provides a competitive mechanism for enhancing pattern separation. A recent fMRI study in humans further supports this notion: Koolschijn *et al* showed that reducing the concentration of GABA using transcranial direct current stimulation acts to increase the amount of memory interference in proportion to the reduction in GABA (463).

3.2.5 Intrinsic properties of DGGCs facilitates pattern separation and gating

The intrinsic (active and passive) membrane properties of DGGCs also facilitate their sparse activation pattern. And it is primarily by augmenting these properties, that extrinsic inhibitory factors, such as GABA-ergic inputs – and thus perhaps s-$GABA_A$Rs – can decrease excitability. *In vivo* (413,414) and *ex vivo* recordings (404–412) demonstrate that DGGCs have a relatively hyperpolarised membrane potential, typically between -68 mV and -80 mV (404–411,413,414), which is >15 mV more hyperpolarised than CA1 and CA3 pyramidal neurons (414). This hyperpolarised resting membrane potential is coupled with a relatively depolarised AP threshold of ~ -41 mV (~10 mV more depolarised than CA1 pyramidal neurons) (414), which leads to DGGCs requiring a large amount of depolarising current to fire an action potential: *in vivo*, the AP threshold current, or rheobase, in DGGCs is six times greater than that of CA1 and CA3 pyramidal cells (414). It is chiefly because DGGCs require a high amount of depolarising current to spike that they are, as a population, extremely reluctant to activate and, thus, largely quiescent. When DGGCs do fire, however, they preferentially do so in bursts (413,468); this is owing to their high gain (over four times greater than CA1 and CA3 pyramidal cells) (414) and substantial spike-frequency adaptation/accommodation (the decrease in firing rate during prolong suprathreshold depolarisation); the latter of which is caused by depolarisation-dependent voltage-gated Na^+ channel inactivation (480). The burst firing of DGGCs is crucial because it – along with the high strength of mossy fiber synapses – allows the DGGCs that are active to reliably excite their target neurons in CA3 (481,482).

The active and passive properties of dendrites affect how synaptic inputs are integrated and processed, and in DGGCs they are optimised to facilitate sparse firing (483,484). DGGCs are relatively small cells, but their dendritic trees show profuse branching, which leads to lots of small calibre, sub-micron in diameter, branches (483). Dual somatodendritic recordings have demonstrated that DGGC dendrites are linear integrators of synaptic inputs and exhibit a strong distance-dependent attenuation for synaptic potentials and back-propagating APs (483,485). Attenuation is caused by DGGC dendrites having a relatively low density of voltage-gated Na^+ channel, but a high enrichment (relative to the soma) of A-type K^+ channels (483,485). As a result, DGGCs require a large number of synchronised synaptic inputs – posited to be approximately 400 concurrently active afferent fibers (486) – to discharge: they can thus act as highly effective coincidence detectors (483,485,487).

Another consequence of highly attenuating dendrites is that DGGCs do not support a classical mode of LTP that relies on the pairing of synaptic excitation with axosomatic APs that back-propagate into the dendritic tree (485). Instead, voltage-gated Na^+ channels in DGGC dendrites, despite their relatively low density, generate local dendritic spikes (485). It is these spikes that provide the associative postsynaptic depolarisation required for Ca^{2+} entry through NMDARs and, in turn, the induction and expression of LTP at perforant path-DGGC synapses (485,488–490). The role of LTP – and its opposite, LTD (long-term depression) – in pattern separation are not fully understood. Evidence supporting the role of an increase in synaptic efficacy in pattern separation comes from mice lacking the GluN1 subunit of the NMDAR in their DGGCs (458). In these mice, contextual fear discrimination learning, a behavioural level pattern separation task, is significantly impaired. In contrast, other behaviours that are not thought to require pattern separation, such as contextual fear conditioning and water maze spatial learning, are unaffected (458)**.** This disruption to behavioural pattern separation in GluN1 KO mice is not associated with changes to standard excitatory transmission but is connected to an impairment in LTP, indicating that pattern separation involves/requires the strengthening of synaptic connections (458). Conversely, network simulations of the DG and computational studies have shown that enhancing the level of LTP actually attenuates circuit pattern separation, whereas LTD, because it can remove redundant DGGC representations, enhances pattern separation (452,491).

Another brain function that has been posited to involve both the DG and LTP is long-term memory. Indeed, it was in the DG of rabbits that LTP was originally observed following high frequency (tetanic) stimulation of the rabbit's perforant path, first by Terje Lømo in 1966 (492) and later in 1973 by Bliss and Lomo (493), who reported "input specificity" of LTP, and by Bliss and Gardner-Medwin, who reported that LTP could persist for days in unanaesthetized rabbits (494). LTP is defined as a long-lasting enhancement in synaptic efficacy following the delivery of a brief, high-frequency stimulation. In the first full report of LTP by Bliss and Lømo, it was posited that LTP might be "potentially useful for information storage" (493). This notion – that memories are stored in the brain via modifications to synaptic efficacy – has its origins in the work of Cajal, who posited that learning leads to a change in the 'resistance' or strength of synapse (495,496); and Konorski, who was the first to apply the term 'plasticity' (497), and Hebb, whose famous postulate stated "when an axon of cell A is near enough to excite a cell B and repeatedly or persistently takes part in firing it, some growth process or metabolic change takes place in one or both cells such that A's efficiency, as one of the cells firing B, is increased" (498).

Over the past half-century following LTP's initial discovery, a heroic amount of research has been undertaken in order to try and answer the so-called "million dollar question": does memory = LTP/LTD? (499). What is clear from this body of research is:

1) LTP and LTD exhibit many of the characteristics that are necessary for cellular mechanism that underlies learning and memory: LTP is *persistent*, in that under the right conditions LTP *in vivo* can be expressed for months (500); LTP is *input specific,* in that LTP only occurs at active synapses (inputs) (493)*;* LTP is *co-operative,* in that it requires the concerted activation of a considerable number of active inputs (501); LTP is *associative,* in that weakly active inputs, which would otherwise be unable to induce LTP, can be potentiated when they occur with a concurrently active strong inputs (502). In addition, **2)** LTP is detectable in animals that are learning and forming memories (503–509). And **3)** Blocking LTP prior to its induction or reversing it once it is expressed attenuates memory (503–508).

However, what has proved particularly difficult, is the transition from showing that LTP is *associated* (or *correlated*) with memory to confirming that LTP is *responsible* for memory.

Recent technological advances, notably engram cell labelling (24,509–511) and engineering LTP/LTD with optogenetics (512) have allowed researchers to test if artificially inducing LTP can generate an apparent memory; this mimicry goes some way to showing causality and gives further credence to the view, shared by many, that LTP is a physiological process that underlies many forms of memory and learning in the brain. Nevertheless, it is important to note that the LTP model of learning and memory is still highly controversial, with no apparent consensus – see (499,510,513–515) for thoughtful discussions.

3.2.6 Studying the impact of tonically active s-$GABA_A$Rs on DGGC function

As outlined in the previous section, the DG is proposed to function as both a pattern separator and a gate to aberrant excitation. Both of these functions are thought to rely heavily on the sparse activity across the DGGC population. The circuit organisation of the DG is optimised for sparse DGGC firing through the low level of recurrent excitatory connections between DGGCs and the high level of interconnections between DGGCs and GABA-ergic interneurons. The intrinsic properties of DGGCs are also optimised sparse firing: a relatively hyperpolarised RMP, a depolarised AP threshold voltage and a high rheobase, as well as pronounced spike-frequency adaptation and strongly attenuating dendrites, all work in concert to make DGGCs a neuron type that is very resistant to firing. In order for DGGCs to fire an AP, they require a relatively large amount of concerted excitation over a narrow temporal window and are, therefore, considered effective coincidence detectors.

GABA-dependent tonic $GABA_AR$ conductances have been shown – across multiple brain regions and neuron types – to modulate many of the above mentioned intrinsic cell properties that are critical for sparse firing and proper function of DGGCs (see the overview in Chapter 1). What is not currently known is whether GABA-*independent*, s-$GABA_AR$-mediated tonic conductances can impact neural function to a similar degree or in the same manner as their GABA-*dependent* counterpart – although, as a starting point, it does seem appropriate to assume that there is reasonable parity between the two signals. Given this, and in light of s-$GABA_A$Rs provide virtually all the tonic conductance in DGGCs, we propose – and in the results section aim to test the idea – that s-$GABA_A$Rs act as a significant brake on excitability and thus can be considered to be of direct functional importance for the sparse firing of DGGCs and, in turn, the function of the DG network as a whole.

From the extensive literature on the function of *GABA-dependent* tonic conductances, it is clear that their functional impact varies substantially between different neuron types (Reviewed in Lee and Maguire 2014; (224)). Most of this variation in the functional impact tonic $GABA_AR$ signalling (i.e. whether the neuron more or less likely to fire) is accounted for by neuron-specific

differences in 1) the nature of the tonic input signal and 2) how it is integrated and interpreted by the neuron.

The input signal of tonically active $GABA_A$Rs is a composite of increased membrane conductance (shunting) and – if there is a Cl^- driving force – membrane polarization, which can be hyperpolarising (when E_{GABA}<RMP) or depolarizing (when E_{GABA}>RMP). These two facets of the input signal can be synergistic with one another (e.g. when an increase in membrane conductance is coupled with hyperpolarisation) or act antagonistically (e.g. when an increase in membrane conductance occurs alongside depolarisation) – and so modulating either one of them can change (on occasion even invert) the nature of the signal that is inputted to the neuron (226).

The integration and interpretation of the tonic $GABA_A$R signal by the neuron is what ultimately determines its function. There are a host of intrinsic neural properties that control how a neuron processes the tonic $GABA_A$R signal, such as the RMP (291), the level of stochastic noise (292,293), active dendritic conductances (289–291,295) and spike-frequency adaptation (294,406,516,517). And because different neuron families exhibit strong deviations in these properties, it means that identical tonic $GABA_A$R input signals can elicit very different output responses across different neuronal populations (291).

These two factors will be critical to understanding s-$GABA_A$R function; however, neither the nature of the input signal that s-$GABA_A$Rs provide, nor how it is integrated and interpreted by DGGCs is currently known.

In regard to the s-$GABA_A$R input signal: in DGGCs, because E_{GABA} is typically close to RMP, and well below AP threshold voltage, $GABA_A$Rs typically deliver shunting inhibition: an increase in membrane conductance without a substantial change in RMP. That said, it is important to note that activation $GABA_A$Rs has, on occasion, been reported to weakly depolarising in DGGCs (518), whereas others have shown they are weakly hyperpolarising (414). Typically, the E_{GABA} in mature, adult DGGCs is between -70 mV and -80 mV (307,401–403); and the RMP is between -68 mV and -80 mV (404–414). For the experiments pertaining to the functional impact s-$GABA_A$Rs, we will employ an ACSF and intracellular pipette solution that accurately mimics

the physiological E_{GABA} and RMP of DGGCs; under these conditions it is expected that s-$GABA_A$Rs will produce shunting inhibition. This means that s-$GABA_A$R currents should be close to zero at RMP, and thus, blocking s-$GABA_A$Rs should not significantly impact RMP.

Shunting inhibition, as explained in the introduction, typically exerts different functional effects when the neuron is below AP threshold voltage vs. when it is above threshold. Below threshold, shunting inhibition reduces excitability by exerting a divisive effect on sub-threshold voltages in accordance with Ohm's law (V=I/G): the increase in conductance caused by shunting means that a depolarising voltage change that is initiated by a given excitatory current is lower, and decays *faster* due to a decrease of the membrane time constant (316–318). This means that more excitatory current is required to cross the AP threshold voltage and initiate an action potential (the rheobase current). Thus, through its actions on subthreshold voltages, an s-$GABA_A$R-mediated shunt might be one of several shunting conductances that are present in DGGCs that facilitate sparse firing by raising the rheobase current. If this is the case, then blocking s-$GABA_A$Rs should reduce the rheobase.

Although shunting has a divisive effect at sub-threshold voltages, above threshold, it generally exerts a purely subtractive effect on the I-O function of the neuron, with no divisive/multiplicative effect on the I-O gain (322,325). In the AP firing number-current (F-I) curves, which is a common method for assessing the I-O function of a neuron, subtraction is indicated by a rightward shift (offset) of the F-I curve along the x-axis, with no effect on the slope (gain) of the curve (322,325). In accordance with this, if 1) s-$GABA_A$Rs produce a shunting conductance and 2) this conductance is large enough to affect DGGC excitability, then this change in excitability should be underpinned by a subtractive effect on the I-O function. If this is indeed the case, then blocking s-$GABA_A$R activity will cause a leftward (additive) offset in the F-I curve of DGGCs, with no effect on the slope (gain) of the curve.

That said, certain intrinsic neural properties can cause shunting inhibition to act divisively to affect the gain of the I-O function – see (289–295,517) and the appendix for more on this topic. The idea that the intrinsic properties of a neuron can affect how it processes incoming signals is linked to the second unknown we will be exploring in this results chapter: namely, how do DGGCs interpret the s-$GABA_A$R input signal? One notable intrinsic property that facilitates gain

control of I-O by shunting inhibition is spike-frequency adaptation. Specifically, shunting *enhances* spike-frequency adaptation to *decrease* steady state firing rate and, in turn, *decrease* gain (294,517). DGGCs show pronounced spike-frequency adaptation (480,516), and this might, therefore, provide a route through which s-$GABA_A$Rs can affect the F-I gain. If this is the case, then blocking s-$GABA_A$R activity should increase the slope of the F-I curve but not offset it. Another factor, this time related to the input signal, that can facilitate gain control through shunting inhibition, is whether or not the shunting conductance exhibits outward rectification (387). Henceforth, it will be important to characterise the I-V profile of s-$GABA_A$Rs, which is currently unknown, in order to understand their function in DGGCs properly.

In vivo, neurons face a constant barrage of excitatory and inhibitory synaptic inputs that induce high-amounts of stochastic fluctuations in the membrane potential (519). One of the principal actions of DGGCs is to essentially 'filter' perforant-path inputs and only deliver an output (e.g fire one or a burst of APs) to CA3 when there is a relatively large amount of convergent excitation. Underscoring the filtering function of DGGCs is the narrow temporal window over which they can summate synaptic inputs to fire an action potential i.e. DGGCs are effective coincidence detectors. In principle, and in line with findings for GABA-dependent tonic currents (297,298), s-$GABA_A$R shunt might be one mechanism by which DGGCs maintain a narrow temporal window for coincidence detection and increase precision for temporal integration. If s-$GABA_A$Rs do support a narrow temporal window for coincidence detection, then blocking their activity should increase the time interval over which two subthreshold inputs can be summated to fire an action potential with high probability.

Finally, if indeed it is the case that s-$GABA_A$Rs can modulate both excitability and the temporal precision of input signal integration, this would strongly suggest that s-$GABA_A$Rs will also be able to interact with, and perhaps modulate, the mechanisms that underlie neural plasticity. Notably, LTP, probably the most widely studied form of neural plasticity, is strongly influenced by both the excitability state of a neuron and its ability to summate synaptic potentials to fire an action potential. Reflecting this, enhancing $GABA_A$R activity typically attenuates LTP (520), whereas blocking their activity enhances LTP (521). If s-$GABA_A$Rs exert a similar attenuating effect on LTP then blocking their activity should enhance LTP amplitude.

In summary, DGGCs provide a useful model for assessing the functional role of s-$GABA_A$Rs in the brain circuits. The sparse activity across the DGGC population is one of the defining properties of the DG network, and determining what causes DGGCs to activate sparsely is critical for understanding how the DG performs its role as both a gate and pattern separator. The low intrinsic excitability of DGGCs is one of the most important factors for sparse firing. DGGCs employ numerous cellular mechanisms to retain this low level of intrinsic excitability, some of which are not yet known. We posit that s-$GABA_A$Rs might one of these mechanisms.

3.3 Aims

The overall aim of the present chapter (Chapter 3; Results 1) was to characterize the functional role of s-$GABA_A$Rs in DGGCs. We opted for an iterative approach: first assessing the impact of s-$GABA_A$Rs on basic membrane properties of DGGCs and then studying how this affects some of the more complex neural dynamics that are thought to support the role of the DG as a pattern separator and gatekeeper. Four experimental steps were pursued to achieve the aims of this chapter:

Step 1) Replicate the key observation made by Wlodarczyk *et al*: that SR-insensitive, PTX-sensitive s-$GABA_A$Rs produce virtually all of the tonic current in DGGCs (74). And as an extension to this, assess the contribution of s-$GABA_A$Rs to the total inhibitory tone that DGGCs receive (net inhibitory charge transfer).

Step 2) Characterise the nature of the signal that s-$GABA_A$Rs provide (i.e. its I-V profile and impact on RMP) and determine its impact on the passive membrane properties of DGGCs (input resistance and membrane time constant).

Step 3) Characterise the manner in which DGGCs integrate and interpret to s-$GABA_A$R signal by assessing its impact on active membrane properties (rheobase, AP threshold, F-I curve gain and spike-frequency adaptation)

Step 4) Assess if the changes to passive, active, and integrative properties of DGGCs affect 1) the temporal window over which DGGCs can respond to physiologically relevant synaptic inputs (coincidence detection) and 2) the plasticity of the DG network (LTP).

3.4 Hypothesis

The previous work on GABA-dependent tonic currents has demonstrated that small but, crucially, persistent changes to membrane conductance can transfer a relatively large amount of inhibitory charge, and that this leads to a significant decrease in excitability. For this reason, it is hypothesised that the persistent s-$GABA_AR$ openings will produce a significant amount of inhibitory charge — likely even larger than that delivered by phasic IPSCs. Because E_{GABA} is close to the RMP in mature DGGCs, we also hypothesise that s-$GABA_A$Rs will provide a shunting conductance, meaning that their I-V relationship should reverse (be equal to zero) at RMP. If this is the case, it is hypothesised that blocking s-$GABA_A$Rs will lead to an increase in input resistance and a slowing of the membrane time constant, without a significant change in RMP. Shunting inhibition has been shown to decrease excitability by offsetting in the F-I curve to the right (a subtractive, not divisive effect). Therefore, we hypothesised that the slope/gain of the F-I curve will be unchanged by blocking s-$GABA_A$Rs, but the relative position of the entire curve will be shifted to the left, reflecting an increase in excitability. If this is indeed the case, it will show that s-$GABA_A$Rs play an important role in maintaining the characteristic sparse firing of DGGCs, which is required for the DG to be able to function as a pattern separator and gatekeeper. Additional requirements for pattern separation in the DG are that DGGCs are coincidence detectors and that their synapses show plastic changes in strength. Thus it is finally hypothesised that blocking s-$GABA_A$Rs will widen the temporal window for coincidence detection and will potentiate LTP at perforant path synapses.

3.5 Results

3.5.1 SR-resistant, PTX sensitive spontaneously opening $GABA_A$Rs produce tonic inhibitory currents in DGGCs

For the first experimental step, validating findings reported by Wlodarczyk *et al* (74), membrane currents from DGGCs were recorded in whole-cell voltage-clamp mode using CsCl intracellular solution (E_{Cl} = ~0 mV); neurons required a mean baseline current (I_{hold}) of -64 ± 5 pA to maintain the voltage of the cell at -70 mV (N=26 cells). In this recording configuration, GABA-ergic currents are inward (negative), meaning that that phasic currents, IPSCs, are seen as transient negative-going defections, whereas the block of tonic currents is seen as an outward (positive) shift in the baseline I_{hold} (because a less negative current is required to clamp the membrane voltage at -70 mV). To test if Wlodarczyk *et al*'s key finding – that s-$GABA_A$Rs deliver tonic inhibitory currents (74) – could be replicated, neurons were exposed to *either* SR (25 µM) *or* PTX (50 µM).

Just as Wlodarczyk *et al*, 2013 previously reported (74), tonic and phasic currents in DGGCs differ in their sensitivity to competitive (SR) and non-competitive (PTX) antagonism (Phasic:**Fig.3.1**; Tonic:**Fig.3.2**). **Fig.3.1** demonstrates that IPSCs were effectively blocked by either SR or PTX. We wanted to compare the rate of IPSC block between antagonists and then use this to relate the degree of IPSC block with the changes in holding current (or lack thereof in the case of SR). The effect of SR on IPSCs was rapid: it took an average 43 secs (95% confidence interval (CI) = 38-47 sec) for IPSC frequency to decrease by half ($T_{IPSC:50\%}$) and an average of 81 ± 15.6 seconds for complete block ($T_{IPSC:0\%}$) (**Fig.3.1A,C,D**); no IPSCs were detected, in *any* of the neurons (N=12), 150 secs after SR was added. The effect of PTX on IPSCs was significantly slower when measured at $T_{IPSC\ 50\%}$ = 99 secs (95%CI =82-118 sec) – note the non-overlapping 95%CI with SR – and at $T_{IPSC:0\%}$ = 246 ± 36 sec (SR vs PTX, Unpaired Student's t-test, $t_{(11,4)}$= t=5.0, P = 0.0002) (**Fig.3.1B,C,D**), but produced the same end result: IPSCs were undetectable, in *all* of the neurons tested (N=5), 400 secs after PTX was added.

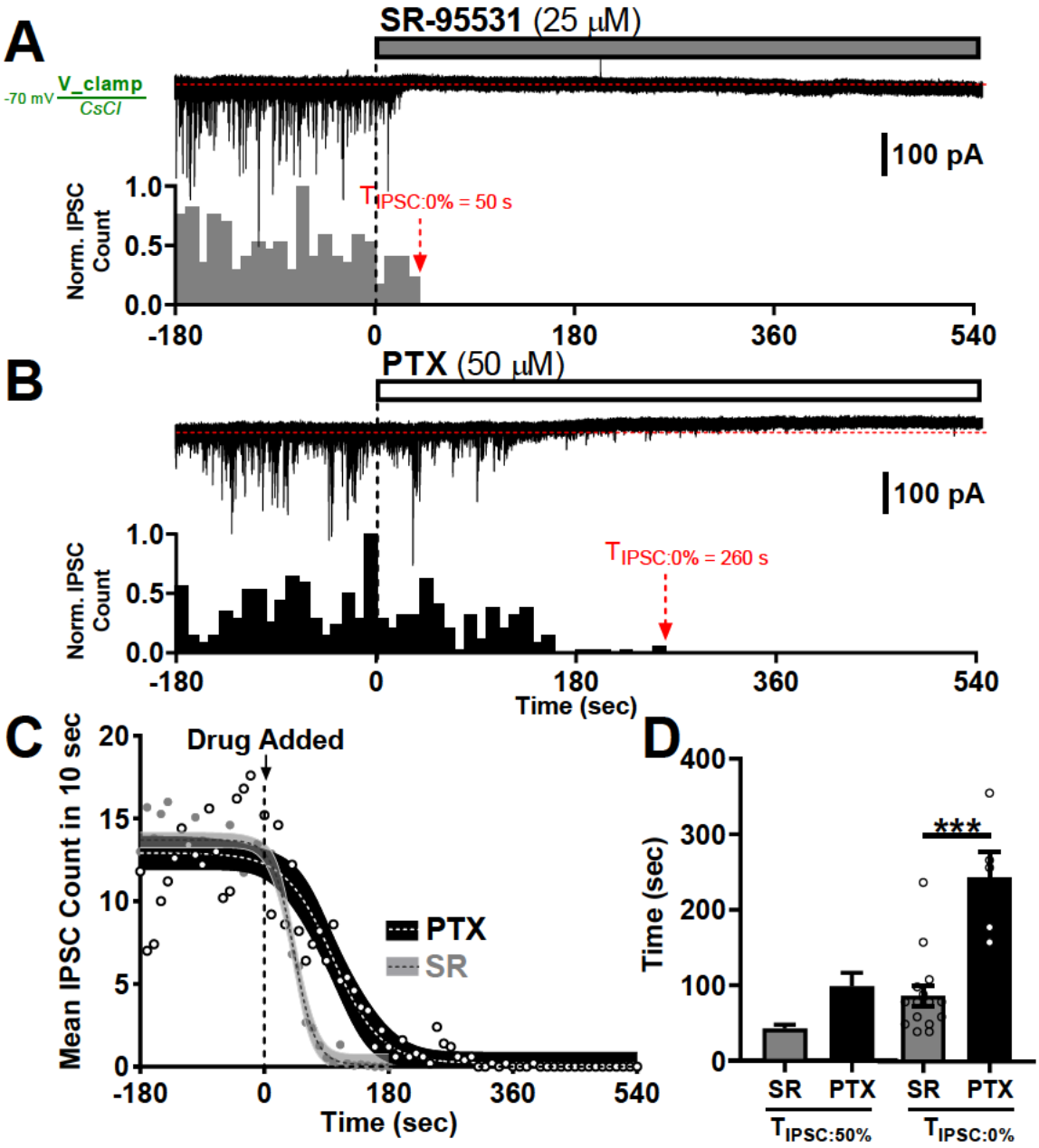

Fig.3.1. IPSCs are abolished by SR and PTX.

Example WC-voltage clamp traces from DGGCS (-70 mV; CsCl) and histograms (normalised IPSC count vs time; 10s bins) show the effect of **A)** SR-95531 (SR; 25 µM) and **B)** picrotoxin (PTX; 50 µM) on IPSCs in DGGCs. The red $T_{IPSC:0\%}$ arrow in **A)** and **B)** corresponds to the time for IPSC count to reach zero in those traces. Both SR and PTX caused a complete block of IPSCs. **C)** Shows that the rate of IPSC blockade was faster with SR than PTX. Each point corresponds to the mean IPSC count over 10 second intervals in neurons exposed to SR (grey circles) and PTX (white circles). Boltzmann sigmoidal curves were applied to these data – SR (gray line) or PTX (black line) – and used to interpolate the time taken for IPSC count to decay by half ($T_{IPSC:50\%}$); filled areas correspond to 95% confidence interval. **D)** Plot of $T_{IPSC:50\%}$ (± 95%CI) and $T_{IPSC:0\%}$ (mean±SEM) showing that block of IPSCs is faster with SR than PTX. SR N= 12; PTX N=5.

Whilst phasic currents could be effectively blocked by either SR or PTX, tonic currents, as expected, were only sensitive to PTX and were completely resistant to SR (**Fig.3.2**) As can be observed in the representative raw **Fig.3.2Ai** trace and the 30 second running average trace from 12 cells in **Fig.3.2.Aiii**, the addition of SR produced no significant outward currents. Measuring the baseline ΔI_{hold} change at time points corresponding to significant reductions in phasic currents emphasises the lack of SR efficacy on tonic currents: at $T_{IPSC:50\%}$ mean baseline ΔI_{hold} was 0.9 ± 1.0 pA (Before vs after SR at $T_{IPSC:50\%,}$ Paired Student's t-test, $t_{(11)}$= t=0.82, P= 0.429); at $T_{IPSC:0\%}$ baseline ΔI_{hold} = -0.5 ± 1.2 pA (Before vs after SR at $T_{IPSC\ 0\%,}$ Paired Student's t-test, $t_{(11)}$= 0.36, P= 0.729) (**Fig.3.1D**); at the 3-4 minute time point, which is over double the time taken for complete IPSC block ($T_{IPSC:0\%}$), there was, once again, no outward current: baseline ΔI_{hold} = -2.4 ± 0.8 pA (Before vs after SR, Paired Student's t-test, $t_{(11)}$= 3.03, P= 0.011). The small inward current reported is likely exaggerated because it is superimposed on a baseline that has a tendency to decrease, albeit slowly, over time due to increasing leak. Small inward SR-currents have been previously reported (74,140,270,522,523), and their potential origin is explored in the discussion.

The insensitivity of tonic currents to SR-mediated competitive antagonism contrasts markedly with its sensitivity to PTX, which reliably induced outward current in DGGCs. This is clear in both the raw (**Fig.3.2Bi+Bii**) and the 30 second running average traces (**Fig.3.2Biii**), and acts as an important to control, in that it demonstrates that tonic inhibitory currents are not simply absent from DGGCs – they are present, just not blocked by SR. The PTX-induced block of tonic currents is observed alongside IPSC block, with outward currents detectable at $T_{IPSC:50\%,}$ when mean baseline ΔI_{hold} was 3.6 ± 1.3 pA (Before vs after PTX at $T_{IPSC:50\%}$, Paired Student's t-test, $t_{(4)}$= 2.31, P= 0.082); at $T_{IPSC:0\%,}$ when baseline ΔI_{hold} = 7.5 ± 0.9 pA (Before vs after SR at $T_{PSC:0\%}$, Paired Student's t-test, $t_{(4)}$= 6.441, P= 0.003) (**Fig.1D**); and finally, at the 9-10 minutes time point, which corresponds to approximately double $T_{IPSC:0\%,}$ when outward current has plateaued to reveal a mean tonic current of 12.4 ± 1.1 pA (Before vs after PTX, Paired Student's t-test, $t_{(4)}$= 10.11, P< 0.0001). The difference between SR and PTX on holding current is highly significant (SR vs PTX, Unpaired Student's t-test, $t_{(11,4)}$= 10.28 P < 0.001).

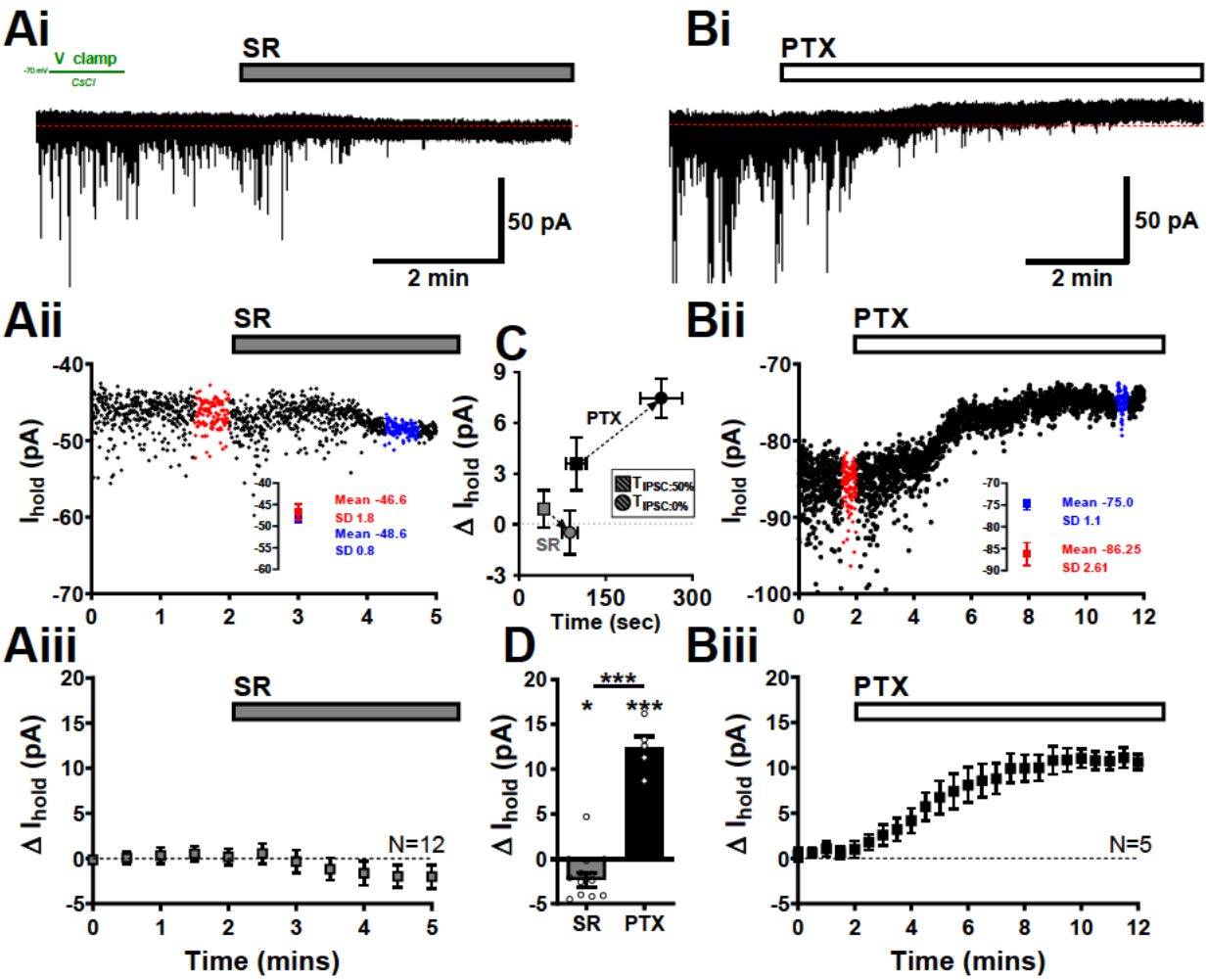

Fig.3.2. Tonic currents are blocked by PTX, but not SR.

A) Example WC-voltage clamp traces (-70 mV; CsCl) illustrate that tonic currents are resistant to SR (25 µM) **Ai)**, but are blocked by PTX (50 µM) **Bi)** – as revealed by the outward shift in holding current. Current-time plots of these traces are shown below in **Aii+Bii)**: each point represents the average IPSC-free holding current, sampled once every 250 ms (4 Hz), over 5 ms epochs. The change in holding current (ΔI_{hold}) is calculated by taking the 120-point (30 sec) average holding current before **(red)** and after **(blue)** adding SR or PTX. Average ΔI_{hold}-time plots (**Aiii+Biii**), taken at 30 seconds epochs and show that SR (N=12) causes a small inward current, whereas PTX (N=5) causes a large outward current. The ΔI_{hold} was explored in relation %IPSC block in **C)**: significant outward currents are recorded at $T_{IPSC:50\%}$ (squares) and $T_{IPSC:0\%}$ (circles) with PTX; but no such currents are observed with SR. **D)** Summarises the mean tonic current recorded with SR (-2.4 ± 0.8 pA) and PTX (12.4 ± 1.1 pA). Error bars, all S.E.M. apart from $T_{IPSC:50\%}$ (±95%CI). Stats: paired t-test control vs SR, control vs PTX; unpaired t-test SR vs PTX.

Fig.3.3 illustrates the final step in validating the SR-resistance and PTX-sensitivity of tonic currents that was previously demonstrated by Wlodarczyk *et al* (74): the sequential exposure of a neuron to SR and then, in the continued presence of SR, to PTX. The trace in **Fig.3.3A+B** demonstrates, as with **Fig.3.2**, that tonic currents were left intact in the presence of SR (despite the complete block of IPSCs), but were blocked after being exposed to PTX, which caused a clear outward current that plateaued after ~8 minutes (**Fig.3.3B**). This outward current was observed in every neuron that was assessed (n=10) and exhibited a high degree of consistency in terms of amplitude and onset, as can be seen in the small error bars in (**Fig.3.3C**)**.** The average ΔI_{hold} induced by PTX in the continued presence of SR was 12.45 ± 0.79 pA (**Fig.3.3C**); this represented a highly significant change relative to both the SR-baseline taken 30 seconds prior to PTX addition (SR(before) vs SR+PTX(after), Paired Student's t-test, $t_{(9)}$= 15.7, P < 0.0001), and the change in holding current induced by SR (Unpaired Student's t-test, $t_{(11,9)}$= 13.7, P < 0.0001); however, there was no significant difference in the amplitude of PTX induced outward current in neurons that had been exposed to SR (**SR→SR+PTX** = 12.5 ± 0.8 pA), vs those that had not (**CTRL→PTX** = 12.4 ± 1.1 pA) (PTX vs SR+PTX, Unpaired Student's t-test, $t_{(9,4)}$= 0.02, P = 0.988) **Fig.3.3Ci**.

This experiment confirms two key fundamentals: 1) SR is not blocking tonic currents in a manner that is undetectable in voltage-clamp mode (e.g. SR is not activating a non-$GABA_AR$ leak current of roughly equal amplitude to tonic currents, thus masking the tonic current blockade); and 2) the small inward current induced by SR has a negligible effect on tonic current amplitude, meaning that the tonic current that is blocked by PTX is not dependent on, or augmented by, prior exposure to SR. As explained in Methods, the pharmacological approach presented in **Fig.3.3** (**CTRL→SR→SR+PTX**) is used repeatedly throughout this thesis to record the various aspects of s-$GABA_AR$ biology – including function, pharmacology, and intracellular modulation.

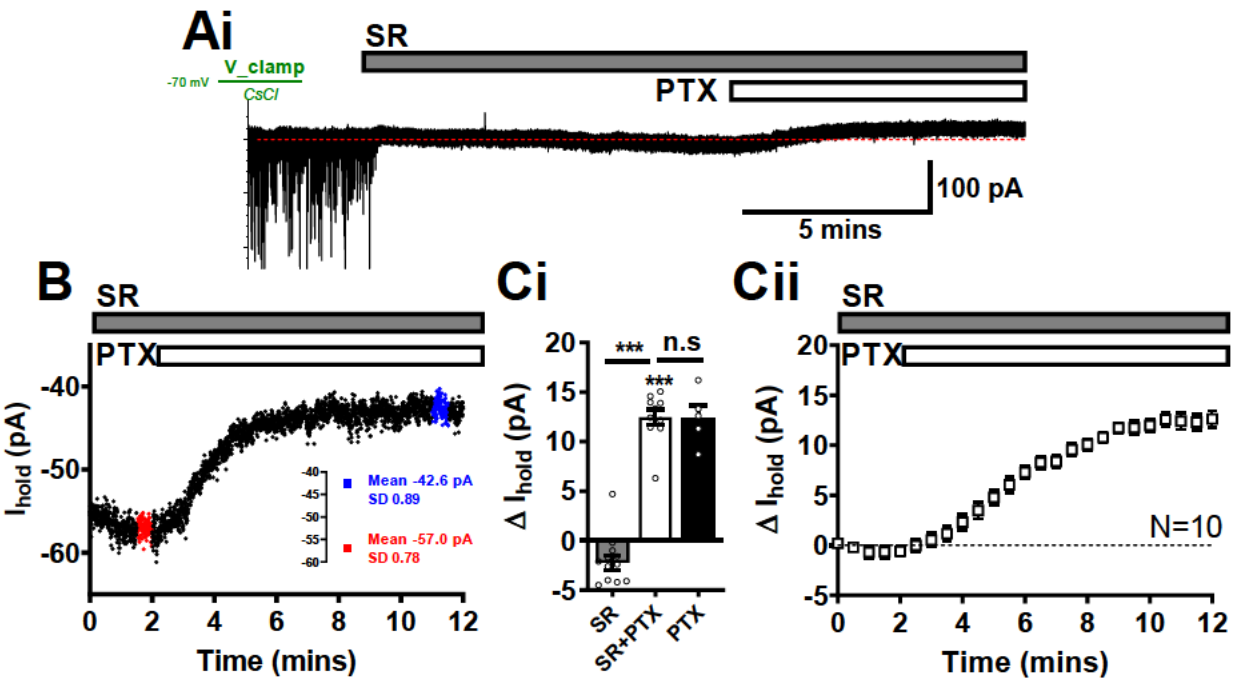

Fig.3.3. s-GABA$_A$Rs produce SR-resistant, PTX-sensitive tonic currents in DGGCs.
A) Example WC-voltage clamp trace (-70 mV; CsCl) illustrates the pharmacological approach for isolating (**CNTRL→SR**) and blocking (**SR→PTX**) the tonic current mediated by s-GABA$_A$Rs. SR abolishes IPSCs but leaves tonic currents untouched; subsequent addition of PTX, in the continuing presence of SR, causes a block of the tonic current. This PTX-induced outward current was measured as shown in the current-time plot in **B)** (sampled at 4 Hz using 5 ms epochs). **Ci)** Summarises the average outward current induced by **SR→PTX** (12.5 ± 0.8 pA; N=10). This **SR→PTX** current is significantly different from the SR-baseline before adding PTX (paired t-test), and the small SR-inward current (**CNTRL→SR**; unpaired t-test). Importantly it is indistinguishable from the outward current induced PTX alone (**CNTRL→PTX;** unpaired t-test). The time averaged **SR→ PTX** outward current, using 30 second epochs, is shown in **Cii).** All data is mean ± SEM.

3.5.2 GABA-independent tonic currents deliver the majority of inhibitory charge in DGGCs

Since IPSCs typically have an amplitude between -30 and -40 pA, and can reach amplitudes in excess of -100 pA, does this mean that s-$GABA_AR$-mediated tonic currents, which have comparably smaller amplitudes (~12 pA), make a minimal net transfer of charge compared to the phasic form? Whilst this can certainly be the case *transiently*, over the 10-100ms when an IPSC occurs, the persistent nature of tonic currents means that, over larger time scales (seconds to minutes), a relatively low amplitude tonic current can give rise to a large quantity of inhibitory tone (80,524).

The relative contribution of GABA-independent tonic currents to inhibitory tone was assessed by comparing the inhibitory charge delivered (area under the curve), over a one minute period, by IPSCs to that which is delivered by tonic currents over the same time period (see **Fig.3.4A** for schematic and area under the curve equations). We found that, as has been previously reported for GABA-dependent tonic currents (80,524), GABA-independent tonic currents deliver the (vast) majority of overall inhibitory charge (**Fig.3.4B**): on average GABA-independent tonic currents deliver 787 ± 27 $pC.min^{-1}$, which is significantly more than IPSCs (Tonic vs IPSC charge transfer, Paired Student's t-test, $t_{(9)}= 24.7$, $P < 0.0001$), which provide 45.7 ± 11 $pC.min^{-1}$ (**Fig.3.4Bi**). Comparing within the same neuron, this means that – with notable caveats that this is an *ex vivo* slice preparation, when excitatory transmission blocked and equimolar Cl^- solution is used – s-$GABA_AR$s deliver 95 ± 1% of overall inhibitory charge (**Fig.3.4Bii**).

The addition of GABA into the ACSF generates a GABA-dependent tonic current that is sensitive to competitive antagonism. We performed a simple experiment to estimate the concentration of GABA necessary to produce tonic currents equivalent in amplitude to those generated by s-$GABA_AR$s. Neurons were exposed to either 1 µM or 5 µM GABA (bath applied), which, based on previous reports, should produce tonic currents that bracket the ~ 12 pA s-$GABA_AR$ current (74). And indeed, 1 µM GABA generated an average inward current of -10.4 ± 1.9 pA (n=4), and 5 µM GABA generated an average inward current of -44.4 ± 8.5 pA (n=4) (**Fig.3.4C+D**). Thus, the amplitude (albeit with opposite polarity) of s-$GABA_AR$ susceptible to block by PTX is close to that generated by 1 µM ambient GABA: indeed, they do not differ significantly

(1 µM GABA vs SR+PTX, Unpaired Student's t-test, $t_{(9,3)}$= 1.13, P = 0.281) and interpolating the s-$GABA_AR$ tonic current from the linear fit describing the log.current/log.[GABA] predicts that 1.24 µM of GABA would be required to generate a current equal in amplitude to that generated by s-$GABA_A$Rs (**Fig.3.4D**)

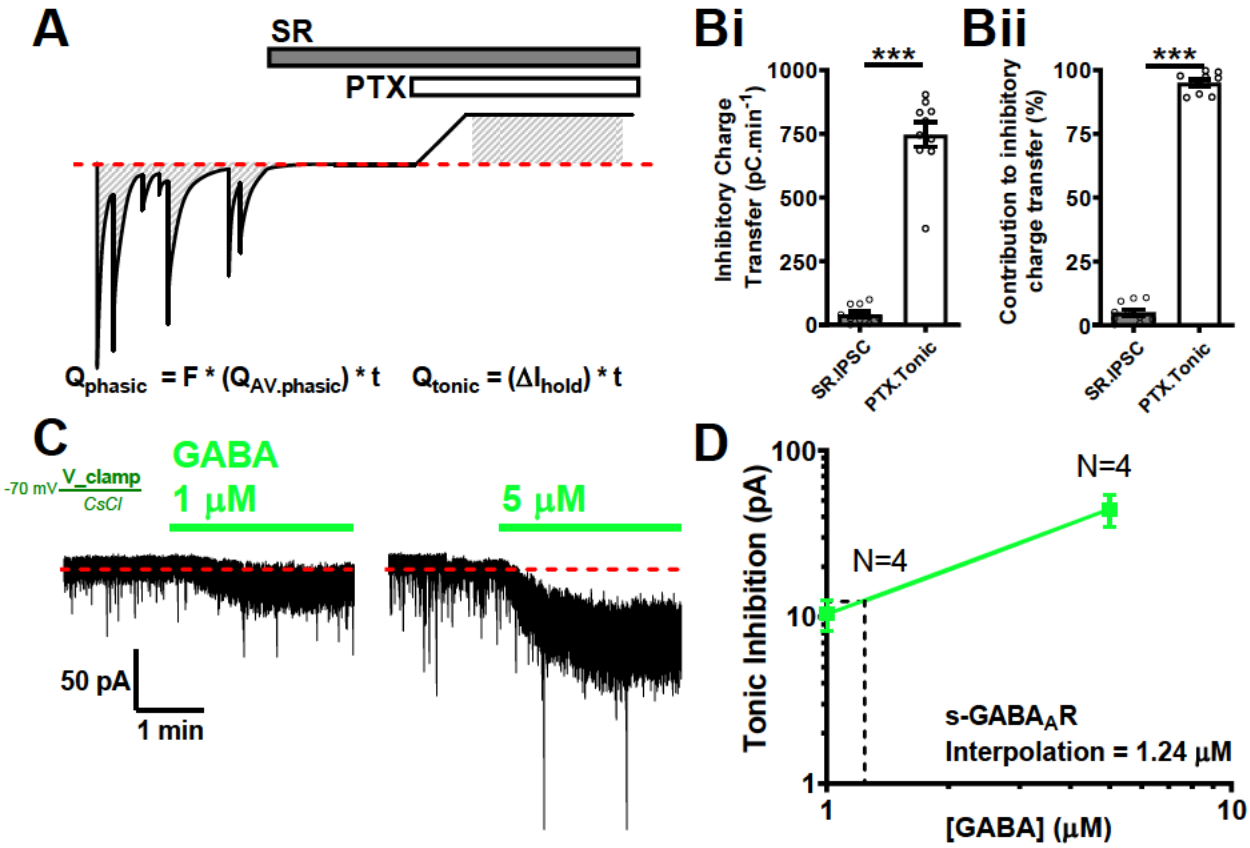

Fig.3.4. s-$GABA_A$Rs provide the vast majority of inhibitory charge in DGGCs.
A) Schematic showing the how inhibitory charge transfer per unit time is calculated by using the area under curve (grey striped area) of phasic and tonic currents. Phasic charge transfer (Q_{phasic}) is calculated in each cell by multiplying the average IPSC frequency (F; Hz) by 60 seconds (t), by the average charge transfer per IPSC ($Q_{Av.phasic}$). Tonic s-$GABA_AR$ charge transfer (Q_{tonic}) is calculated by multiplying the steady state **SR→PTX** outward current (ΔI_{hold}) by 60 seconds (t). Bar graphs show that **Bi)** on average s-$GABA_AR$ currents transfer vastly more inhibitory charge (787 ± 27 $pC.min^{-1}$) than phasic currents (45.7 ± 11 $pC.min^{-1}$)(N=10). **Bii)** shows that normalised to each cell, on average, s-$GABA_AR$ currents provide 20-times the amount of inhibitory charge (95% of total) as phasic currents (5%). **C)** Example WC-voltage clamp traces (-70 mV; CsCl) of the inward currents induced by 1 and 5 µM GABA. Average inward currents are plotted in **D)** (N=4 for both concentrations). The linear fit describing the log.current/log.[GABA] was used to interpolate the concentration of ambient GABA (1.24 µM) required to generate a current equal to that generated by s-$GABA_A$Rs. All data is mean ± SEM. Stats: paired t-test.

3.5.3 Blocking s-GABA$_A$Rs increases input resistance and slows the membrane time constant

Given that s-GABA$_A$Rs make a sizeable net contribution to the overall inhibitory tone, we next tested if blocking their conductance affected the passive and active properties of the membrane. All previous measurements of s-GABA$_A$Rs in the hippocampus, both in this thesis and in previous reports (74,233), have been performed using ~symmetrical [Cl^-], which gives rise to an E_{Cl}^- of ~ 0 mV (33˚C = -1.03 mV). However, for the following experiments, we used intracellular solutions conferring a low concentration (8 mM) of Cl^-, which approximates levels found in adult, mature neurons (218–221). This solution enabled us to record s-GABA$_A$Rs under more physiological conditions *and, importantly,* rule out spontaneous openings being an artefact of high levels of intracellular Cl^-. This is a necessary control because Cl^- ions have been previously shown to directly modulate GABA$_A$R function – for instance, high intracellular [Cl^-] concentrations slow the decay of GABA evoked currents (525).

The effect of s-GABA$_A$Rs on input resistance was measured in current-clamp mode from the linear fit of the I-V trace that was obtained using 9x -50 pA, 500 ms hyperpolarising current steps applied from RMP (I_{hold} = 0 pA), from -50 to −450 pA (**Fig.3.5A**). The intracellular solution used was K-gluconate based; TTX (1 µM) was included in the ACSF to prevent rebound action potentials. Input resistance was significantly affected by blocking GABA$_A$R activity as indicated by comparing resistance values obtained in CTRL (161 ± 6 MΩ), SR (167 ± 7 MΩ), and SR+PTX (179 ± 9 MΩ) using an ANOVA (One-way, matched ANOVA, $F_{(2,7)} = 20.0$; P= 0.002) (**Fig.3.5A-B**). Paired Student's t-test with Bonferroni correction demonstrated that SR induced a small (3.9%) but significant increase relative to CTRL (CTRL vs SR, Paired Student's t-test $t_{(7)}$= 4.716 P = 0.0065); subsequent addition of PTX to block s-GABA$_A$Rs induced an additional, larger (7.1%) increase in resistance compared to SR alone (SR vs SR+PTX, Paired Student's t-test $t_{(7)}$= 3.189 P = 0.0459), which corresponds to an 11% increase in resistance compared to CTRL (CTRL vs SR+PTX, Paired Student's t-test $t_{(7)}$= 5.927 P = 0.0017) (**Fig.3.5B**). The effect of s-GABA$_A$Rs onto membrane time constant could not be accurately determined by averaging the step responses used to obtain input resistance, so a new experiment was performed by applying 30x -5 pA, 500 ms hyperpolarising current steps (again from I_{hold} = 0) to neurons first exposed to SR and then to SR+PTX (**Fig.3.5C**). τ_m was calculated by fitting the falling phase of

the average membrane voltage with a mono-exponential decay. The membrane time constant underwent a significant (SR vs SR+PTX, Paired Student's t-test $t_{(4)}$= 6.843 P = 0.001), 7.1%, slowing from SR alone (43.7 ± 3.1 sec) to SR+PTX (46.8 ± 3.1 sec), in line with what would be predicted from the increase in membrane resistance (**Fig.3.5D**). The values for input resistance and membrane time constant recorded in CTRL conditions here are very similar to those previously reported for similar for mature DGGCs in the adult hippocampus (484,526).

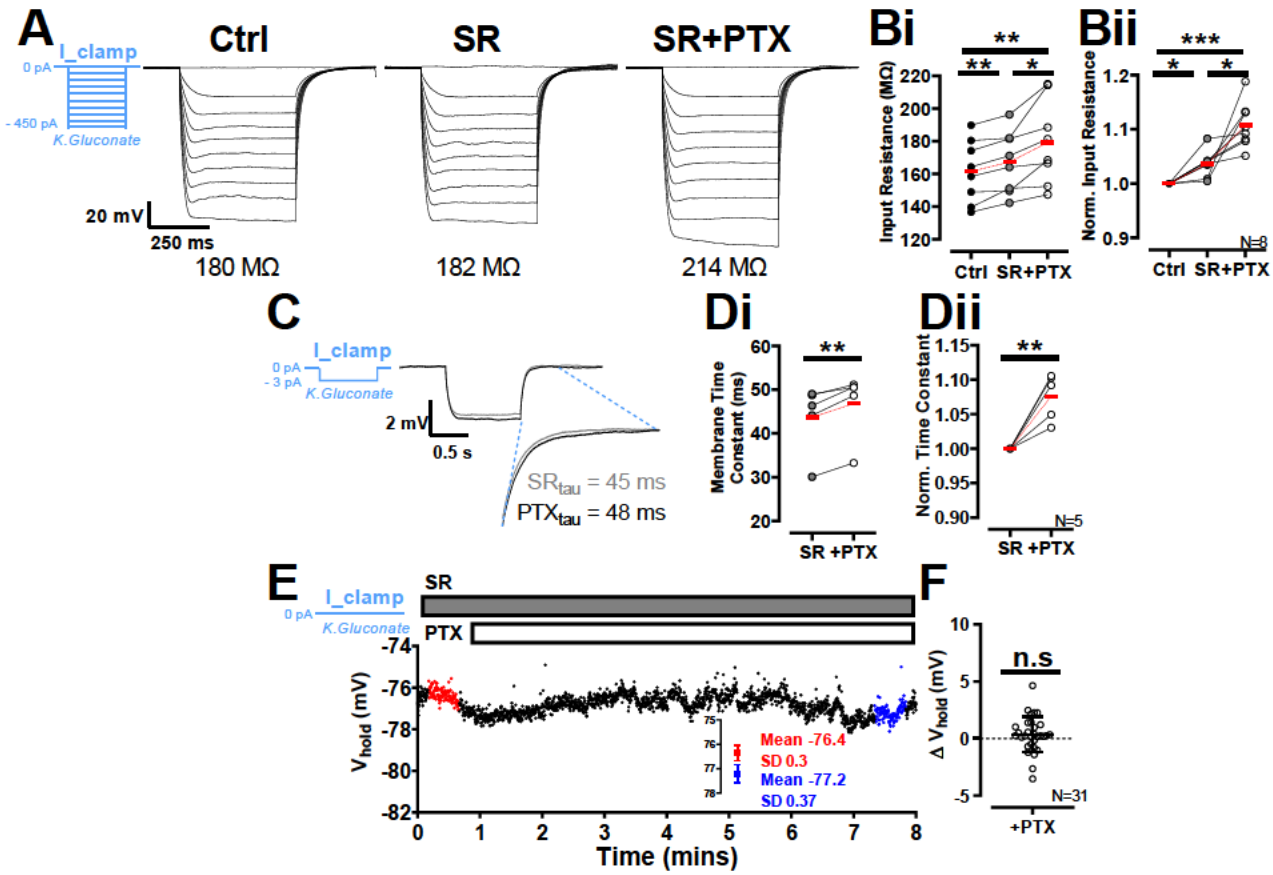

Fig.3.5. Blocking s-GABA$_A$Rs increases input resistance and slows the membrane time constant without affecting RMP.

A) Example WC-current-clamp recordings showing the voltage responses to 9x -50 pA, 500 ms hyperpolarising current steps (K-gluconate; 0 to -450 pA). The protocol was performed in CTRL conditions and then repeated in the same neuron in SR and then SR+PTX; input resistance was calculated from the linear fit regression of the I-V plot. Raw and normalised input resistance values are summarised in **Bi)+Bii)**, respectively: blocking s-GABA$_A$Rs increases input resistance by ~7%, from 167 ± 7 MΩ, to 179 ± 9 MΩ (N=8). Increased resistance was accompanied by a proportionate slowing in the membrane time constant from 43.7 ± 3.1 to 46.8 ± 3.1 ms (τm) **C)+D)**; τm was obtained from the mono-exponential fit of the falling phase of average voltage generated by 30x -5 pA, 500 ms hyperpolarising current steps (N=5). **E)** The change in input resistance was not accompanied by a change in RMP as shown in the voltage-time example trace (Vm sampled over 5 ms epochs at 250 ms intervals). The SR→SR+PTX induced change in Vm from 31 cells is shown in **F)** (= +0.4 ± 0.2 mV). Data points are means throughout (cirles); the average of each plot is shown in red. **F** is mean ± SD. Stats: ANOVA, paired t-test (with Bonferroni correction).

There are two mechanisms by which $GABA_A$Rs inhibit the neuron to reduce excitability: 1) membrane shunting and 2) membrane hyperpolarisation. Membrane shunting (shunting inhibition) is caused by an increase in membrane conductance, which – in accordance with Ohm's law – decreases the voltage change caused by depolarising currents (316–318). Shunting inhibition arises whenever $GABA_A$Rs are active: it is not dependent on the Cl^- driving force. In the DGGC s-$GABA_A$Rs evidently produce a membrane shunt because blocking their activity with PTX causes a significant increase in membrane resistance and slows the τ_m (**Fig.3.5A-D**). Hyperpolarising inhibition, by contrast, is caused by the net influx of anions through $GABA_A$Rs – it, therefore, requires open $GABA_A$Rs *and* an electrochemical gradient that favours the net inward movement of Cl^- and HCO_3^-: E_{GABA}< Vm. Because E_{GABA} and Vm (i.e. RMP) vary quite substantially between different neuron subtypes (and even temporally, *within* the same neuron subtypes), it means that the degree to which GABA is hyperpolarising differs across the brain (218–221). Indeed, in some instances – e.g. in hippocampal interneurons, as reported by Song *et al* in 2011 – tonic $GABA_A$ currents cause *depolarisation* (because E_{GABA} > RMP) (226). At the outset of the present thesis, it was unclear what the function effects of s-$GABA_A$R tonic currents are in DGGCs: are they inhibitory, as hypothesised? Or excitatory, like GABA-dependent tonic currents in hippocampal interneurons (226)? Or are they functionally of *no* consequence?

3.5.4 Blocking s-$GABA_A$Rs does not alter RMP

The effect of s-$GABA_A$Rs on RMP was assessed using a K-gluconate-based (8 mM Cl^-) intracellular solution (I_{hold} =0). In the presence of SR, with s-$GABA_A$R conductance intact, the mean RMP was -72.8 ± 1.3 mV; adding PTX to block s-$GABA_A$Rs had no significant effect on the RMP (SR(before) vs SR+PTX(after), Paired Student's t-test $t_{(30)}$= 1.297 P = 0.204) (**Fig.3.5E**): mean change in Vm was +0.4 ± 0.2 mV; in only nine of the recordings was Vm depolarised by >1 mV, and in only five recordings was Vm hyperpolarised by <-1 mV(**Fig.3.5F**). This is in line with the predicted E_{Cl} -74.3 mV being very close to the RMP. It is also in keeping with the result of performing the same experiment – again with K-gluconate-based intracellular solution (8 mM Cl^-) – but in voltage-clamp mode; when neurons are clamped at -70 mV there was no significant change in holding current following block of s-$GABA_A$Rs: mean ΔI_{hold} = 0.59 ± 2.0 pA (Paired Student's t-test $t_{(3)}$= 0.251 P = 0.818).

3.5.5 s-$GABA_AR$ conductance displays outward rectification

Responses elicited by $GABA_ARs$ – particularly tonic currents (225,288,353,387,388), but also IPSCs (527) and single-channel currents (236,287,528) – frequently exhibit non-Ohmic, outwardly rectifying, I/V plots. This rectification means that even controlling for changes in Cl^- driving force, $GABA_ARs$ can deliver more inhibition at membrane potentials close to/above action potential threshold than they can at RMP. If the s-$GABA_AR$ tonic conductance is outwardly rectifying, this would mean that their impact on cell excitability will likely be greater than predicted from the ~7% membrane shunt they deliver at RMP (**Fig.3.6A-D**).

We characterised the I/V relationship of GABA-gated (evoked IPSCs) and spontaneously opening $GABA_AR$ in voltage-clamp mode using a Cs.methansulfonate-based intracellular solution with physiological [Cl^-] (8 mM); inclusion of Cs^+ and QX-314 allowed us to depolarise the neuron without inducing huge voltage-gated K^+ and Na^+ currents, respectively. Nifedipine was not included for IPSC experiments but was for s-$GABA_AR$ experiments. It is important to note that, as with all other experiments, junction potential was measured and corrected in the bath before patching the neuron and performing the experiment. This worked well for K-gluconate and CsCl-based intracellular solutions – junction potentials were close to predicted values and once corrected the I_{hold} remained stable for minutes in the bath of ACSF. But unfortunately, this was not the case for junction potential associated with the Cs-methanesulfonate-based intracellular solution: the liquid junction potential associated with this solution was extremely difficult to correct for, with the holding current continuing to drift even after 10 minutes in the bath. This resulted in an over-compensation, of +20 mV, to the liquid junction (+34 mV) compared to the calculated value (+14 mV) obtained using the Clampex inbuilt junction potential calculator (Henderson Equation, see (529)). And, so, the holding potential was clamped 20 mV lower than the desired value. Failure to account for this voltage error does not prohibit answering the key question – do *s-$GABA_AR$ currents rectify*? – but, obviously, would affect the recorded E_{GABA}. We did correct the error, post-hoc, for the subsequent analysis and meaning that cells were actually held at -90 mV, not the indicated -70 mV.

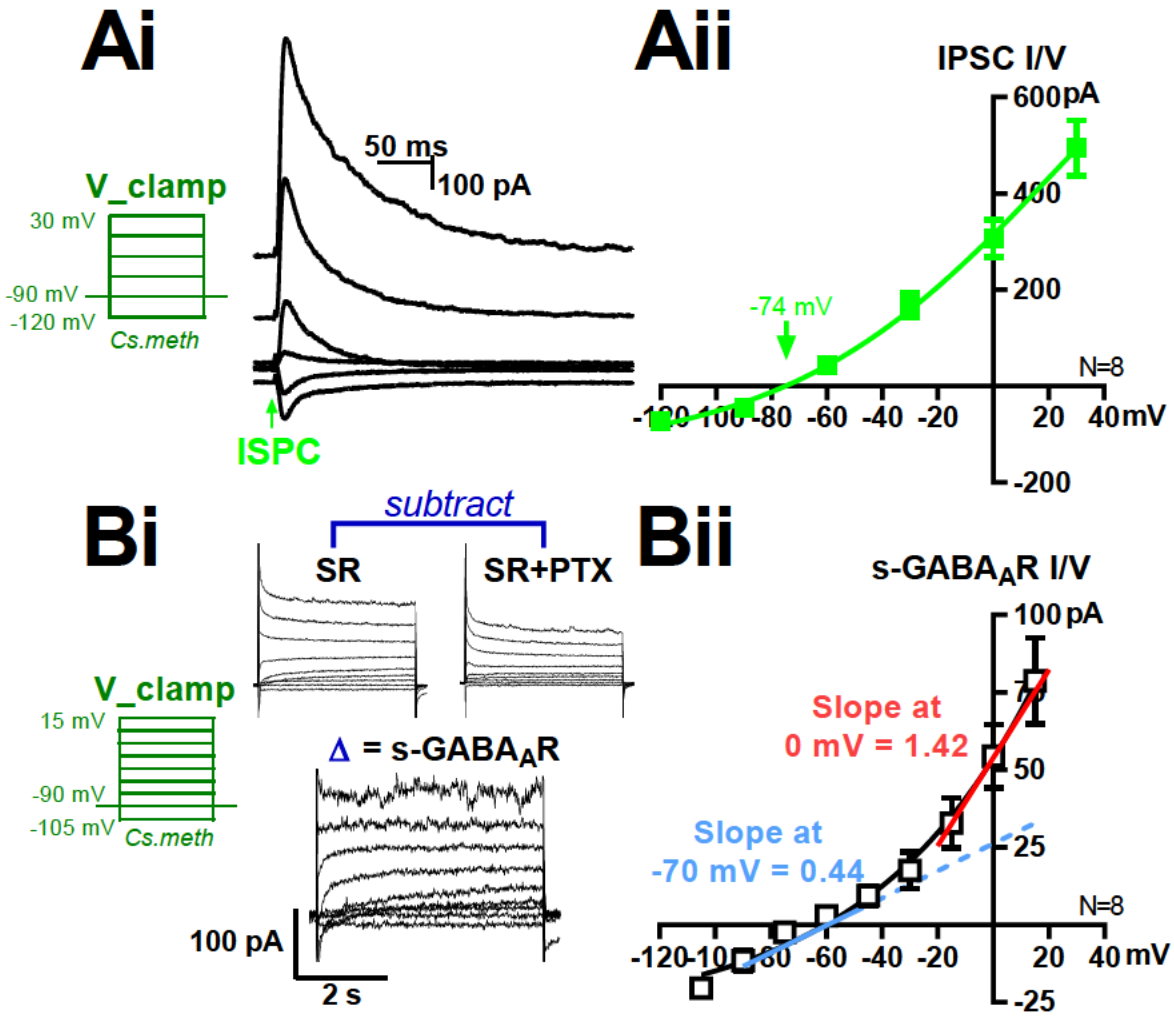

Fig.3.6. s-GABA$_A$R currents, like IPSCs, exhibit outward-rectification.
Ai) A WC-voltage clamp recording of a family of IPSCs generated by repeatedly stimulating the MPP and stepping the holding potential from -120 mV to + 30 mV (Cs.meth, V_{hold}:-90 mV, +30mV increments). **Aii)** An I-V plot, fitted with a Boltzmann function, showing that the average IPSC peak amplitude exhibits outward rectification and reverse at -74 mV. s-GABA$_A$Rs also show outward rectification **Bi+ii).** s-GABA$_A$R I-V plots were generated by stepping the holding voltage from -105 mV to +15 mV (Cs.meth,V_{hold}:-90 mV, +15mV increments) in the presence of SR, and then in the SR+PTX: **Bi)** subtracting the 'SR+PTX'-current from the corresponding 'SR'-current gives rise to the 's-GABA$_A$R'-current. **Bii)** The I-V relationship for s-GABA$_A$Rs is fit with a Boltzmann function; outward rectification is evidenced by the three-fold increase in the slope of the curve at 0 mV (**red tangent**) compared to -70 mV (**blue tangent**). Slope was obtained from the first-order derivative of the Boltzmann function (dI/dV). Data are mean ± SEM. N=8 for both IPSC and s-GABA$_A$R I-V.

To assess IPSC rectification of s-$GABA_A$Rs, neurons were clamped at -90 mV and holding potential was stepped, once every 10 seconds, between -120 to +30 mV using 5 second, 30 mV voltage step. IPSCs (~50% of max) were evoked 4 seconds into the 5 second voltage step, using a bipolar electrode positioned in the medial performant pathway (**Fig.3.6E**; N =8).

The s-$GABA_A$R I/V was measured by recording the whole-cell current response to 15 mV, 5 second voltage steps (again applied once every 10 seconds) from a holding potential of -90 mV, over a range of -105 to +15 mV. Voltage steps were performed in the presence of SR, and then they were repeated in the presence of SR+PTX. Subtracting the two current responses revealed the s-$GABA_A$R I/V (**Fig.3.6B**).

The currents delivered by s-$GABA_A$Rs exhibited an outward rectification (**Fig.3.6B**) that closely matched that of evoked GABA-ergic IPSCs (**Fig.3.6A**). The I/V relationships for IPSC and s-$GABA_A$R currents were well described by Boltzmann functions, as was previously reported by Pavlov *et al,* 2009 (387). Both currents exhibited non-Ohmic, outward rectification at potentials more depolarised than -40 mV. The slope conductance of the s-$GABA_A$R I/V curve was 3.2 times greater at 0 mV than at 70 mV. Slope values were obtained from the first-order derivative of the Boltzmann function (dI/dV). The reversal potential for GABA evoked IPSCs this was -74 mV, and recorded s-$GABA_A$R currents reversed close to this voltage (-75 mV = -2 ± 2 pA; -60 mV = 3 ± 2 pA).

To briefly summarise: it is clear that s-$GABA_A$Rs affect the passive properties of the DGGCs. At RMP, they 'shunt' the membrane without significantly impacting the Vm. Although relatively small (~7%), this increase in membrane conductance affects both the voltage response to a depolarising current and the membrane time constant. Furthermore, the inhibitory effects of s-$GABA_A$Rs are *not* limited to membrane shunt alone. As the I/V curves demonstrate, membrane depolarisation increases the inhibitory effects of s-$GABA_A$Rs in two ways: 1) depolarisation establishes a driving force for the anions HCO_3^- and Cl^- (because Vm>E_{GABA}), which leads to inward hyperpolarising currents; 2) depolarisation also increases the conductance of s-$GABA_A$Rs because they outwardly rectify. We next examined how these factors coalesce to affect the active properties (excitability) of DGGCs.

3.5.6 Blocking s-GABA$_A$Rs increases excitability and F-I curve gain and decreases rheobase

We studied the impact of s-GABA$_A$Rs on neuronal excitability by seeing if we could detect a change in the input-output relationship of the neuron (I-O), as expressed in the firing rate-current (F-I) curve. Changes to a neuron's excitability can affect the F-I curve in two ways (317). The first way is to offset the F-I curve, meaning that the shape of the F-I curve remains the same, but its relative position is offset to the left (more excitable; additive) or right (less excitable; subtractive) (317). The second way is to scale the F-I curve; this means that the shape of the curve, or more specifically its slope, or gain, is increased (multiplicative gain increase) or decreased (divisive gain decrease). To assess how blocking s-GABA$_A$R conductance affects the F-I curve, we used an unpaired experimental design in order to prevent repeat F-I measures being confounded by homeostatic changes to intrinsic excitability that can be triggered by depolarisation/high firing rates e.g. (530,531). This means that experiments were performed in CTRL ACSF, *or* ACSF containing SR, *or* ACSF containing SR+PTX. Neurons were recorded in current-clamp mode, using K-gluconate-based intracellular solution and action potentials were evoked from RMP (I_{hold} = 0 pA), using a family of depolarising current commands (25 pA, 0.5s; 0 to 250 pA) (**Fig.3.7A+B**). Firing number in 0.5 s was not converted to frequency (Hz) because DGGCs exhibit pronounced spike-frequency adaptation when exposed to persistent supra-threshold depolarisation (406,516).

In CTRL conditions (GABA-dependent signalling and –independent signalling intact), depolarisation caused a progressive increase in action potential firing rate; this increase was linear between 50 and 175 pA and plateaued between 200 and 250 pA (n=8) (**Fig.3.7A+B**). Block of GABA-dependent (with SR) and GABA-independent signalling (with SR+PTX) exerted a significant pro-excitatory effect on the F-I curve (Two-way ANOVA: CTRL vs SR vs SR+PTX; $F_{(2,22)} = 7.123$; P= 0.0041) (**Fig.3.7A+B**). There was an explicit pro-excitatory effect of specifically blocking s-GABA$_A$Rs: in the presence SR+PTX, the firing rate was increased at each current step between 50-250 pA, by an average of 41 ± 2%, relative to SR alone. And the area under the F-I curve (0-250 pA) increased by 42%: from 2475 ± 188, to 3518 ± 400 AP.pA (**Fig.3.7C**). And, most importantly and unexpectedly, the slope of the linear part of the curve, measured from 50 pA to 175 pA, which denotes the gain, was significantly increased by approximately

40%, from 0.104 ± 0.015 to 0.146 ± 0.006 AP.pA^{-1} (SR vs SR+PTX, Unpaired Student's t-test, $t_{(7,8)}$= 2.305 P = 0.035) (**Fig.3.7C**).

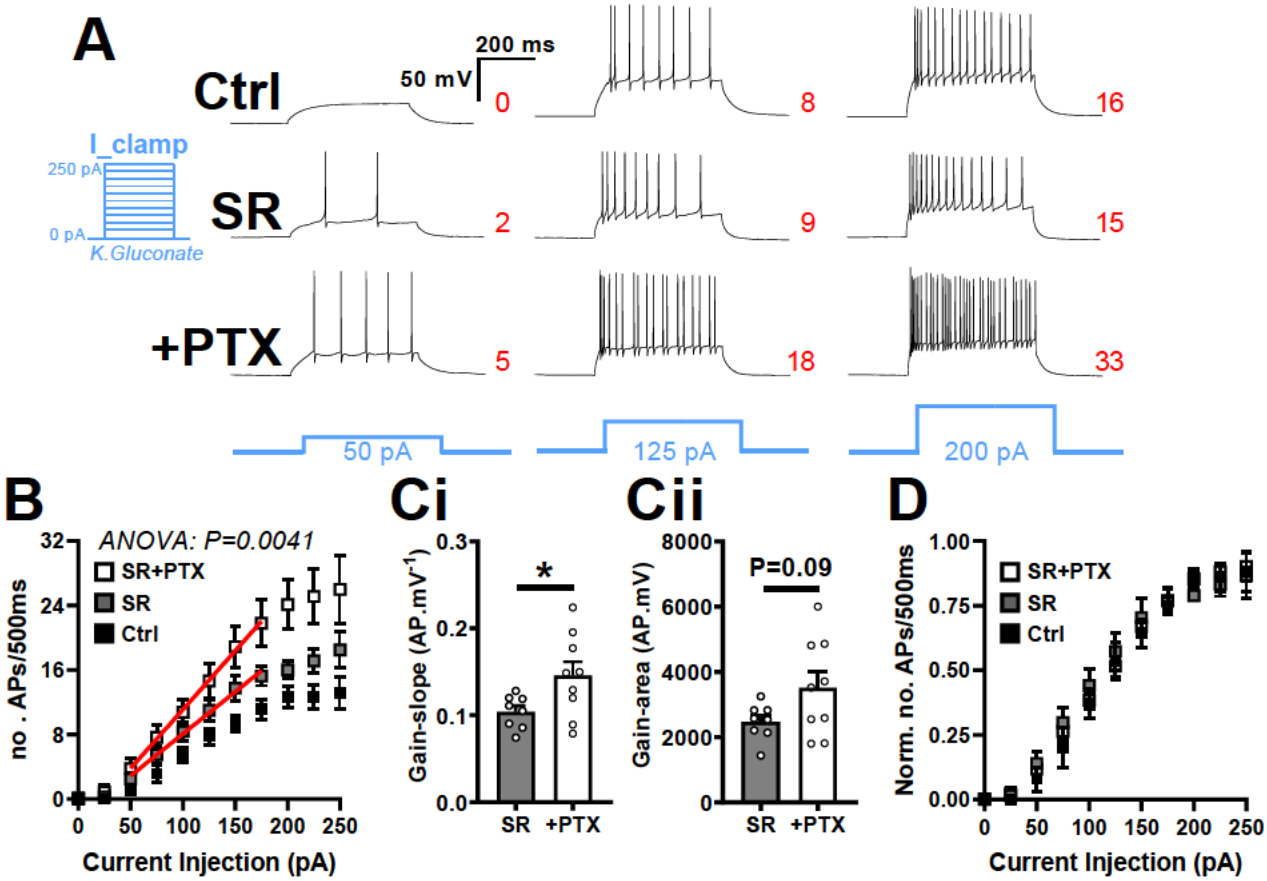

Fig.3.7 Blocking s-GABA$_A$Rs increases neuronal excitability.
A) Examples of WC-current clamp recordings (K-gluconate) from three neurons excited with 50 pA, 125 pA and 200 pA current steps in the presence of CTRL-, SR- or SR+PTX-containing ACSF **B)** Plot of the firing number—current relationship (F-I; 0 to 250 pA; 500 ms, 25 pA steps) shows that block of s-GABA$_A$Rs increases excitability. From 50-250 pA, AP firing number over 0.5s was increased by an average of 41 ± 2% in SR+PTX vs. SR alone. (N= CTRL:8, SR:8, PTX:9) **Ci)** The gain of the F-I relationship, measured as the slope of the linear region of the curve (50 pA to 175 pA), was significantly increased by blocking s-GABA$_A$Rs: SR (0.104 ± 0.015 AP.pA^{-1}), SR-PTX (0.146 ± 0.006 AP.pA^{-1}). **Cii)** The area under the curve (the integral of AP firing rate between 0 pA and 250 pA), is another measure of gain and was also increased by blocking s-GABA$_A$Rs: SR (2475 ± 188 AP.pA), SR-PTX (3518 ± 400 AP.pA). **D)** When the F-I relationship of each cell is normalised to the maximum firing rate in that cell, the shape/gradient of F-I relationship is virtually identical in all three conditions: CTRL, SR, and ST+PTX. This shows that s-GABA$_A$Rs affect the F-I curve by a divisive scaling, not by a subtractive shift. If s-GABA$_A$Rs had a subtractive effect the normalised F-I curve would show a different shape with a steeper gradient. All data is mean ± SEM; stats: F-I curves: ANOVA; slope and area: unpaired t-test.

The increase in F-I gain following the addition of PTX means that s-$GABA_A$R tonic conductances usually exert a *divisive* effect on F-I curves in DGGCs. As further evidence for this, we found that when we plotted the average normalised AP firing number against current for CTRL, SR and SR+PTX, the shape of the curves was virtually identical in all three conditions (**Fig.3.7D**). This means that F-I curves are changed by a common scaling factor (blocking s-$GABA_A$Rs = multiplication); if F-I curves were offset, the shape of the normalised F-I would change. The mechanism by which s-$GABA_A$Rs affect F-I gain is explored later.

The 25 pA depolarising step interval used to generate F-I curves was too large to reliably assess if s-$GABA_A$Rs alter the minimum current required to elicit a single action potential (the rheobase current), with the majority of neurons (19 out of 25) transitioning from a silent state to firing ≥2 APs. The rheobase current is one of the most important, physiologically relevant measures for assessing the functional impact of s-$GABA_A$Rs in DGGCs. DGGCs have been shown to have an unusably high rheobase (> 5 times greater than CA3 and CA1 pyramidal cells *in vivo* (414)); this, coupled with a depolarised voltage threshold, makes DGGCs resistant to excitation and causes them persist in a largely silent state, firing only sparsely (413,467–470). It is the sparse firing across the DGGC population that allows the DG to act as a gatekeeper to aberrant excitation and as a pattern separator. (438,445,451,473). The persistent conductance that s-$GABA_A$Rs produce may be one way that DGGCs' rheobase is kept high and firing is made sparse. To examine this possibility, a new set of experiments was performed using a paired experimental paradigm (serially exposing the neuron to CTRL ACSF, SR and then SR+PTX) and depolarising the neuron with smaller (+5 pA) and longer (0.7s) current steps (**Fig.3.8A**).

In CTRL ACSF neurons required an average of 74.3 ± 10.0 pA to elicit an individual action potential; the mean threshold ($\Delta dV/\Delta t$ = 20 mV/ms) of the action potentials was -36.8 ± 1.3 mV (**Fig.3.8B+C**). Exposing the neuron to SR/SR+PTX significantly affected both the rheobase (One-way, matched ANOVA, $F_{(2,6)} = 17.84$; P=0.0013) and threshold (One-way, matched ANOVA, $F_{(2,6)} = 13.21$; P= 0.0064) (**Fig.3.8B+C**). Post-hoc paired student t-tests with Bonferoni correction revealed that mean rheobase was not significantly altered in the presence of SR (77.9 ± 10.9 pA; Paired Student's t-test $t_{(6)}$= 0.737; P = 0.999), but was significantly reduced by the

subsequent addition PTX, which decreased the rheobase to 53.6 ± 8.8 pA, corresponding to a by 32 ± 4% reduction relative to SR alone (SR vs SR+PTX: Paired Student's t-test $t_{(6)}$= 4.70; P = 0.001); or a 30 ± 4% relative to CTRL (CTRL vs SR+PTX: Paired Student's t-test $t_{(6)}$= 7.488; P = 0.0001) (**Fig.3.8B**). The AP threshold showed a similar pattern of change to the rheobase: threshold was not significantly changed by SR (-38.0 ± 1.3 mV) compared to CTRL (-36.8 ± 1.3 mV) (Paired Student's t-test $t_{(6)}$= 2.426; P = 0.1543), but was significantly hyperpolarised by PTX, by -1.4 mV, to -39.5 ± 1.2 mV, compared to SR alone (Paired Student's t-test $t_{(6)}$= 4.909; P = 0.0081); or -2.7 ± 0.6 mV compared to CTRL (Paired Student's t-test $t_{(6)}$= 3.935; P = 0.0230) (**Fig.3.8C**). The depolarising effect of s-$GABA_A$R tonic conductance on AP threshold may indicate that some of these receptors are localised in the AIS (532) and/or that they are enhancing Na^+ channel inactivation (as a knock on consequence of shunting Na^+ currents) (294,533).

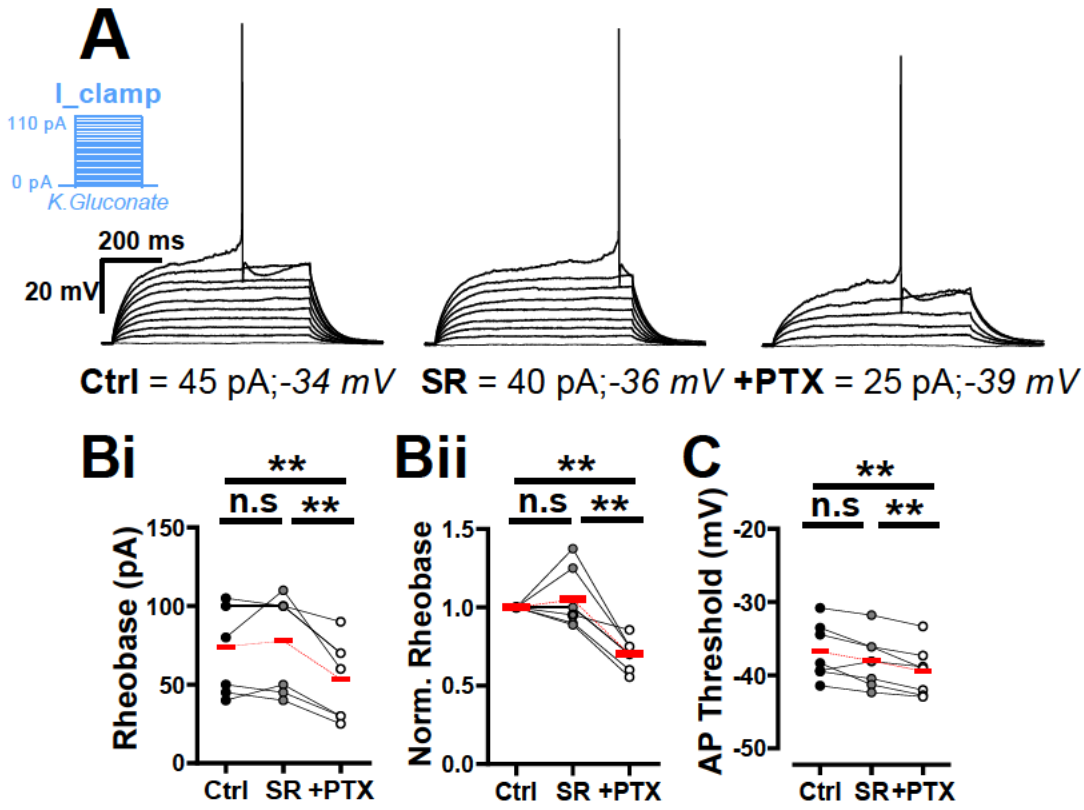

Fig.3.8. Blocking s-$GABA_A$Rs decreases rheobase and hyperpolarises AP threshold.
A) Examples of WC-current clamp recordings (K-gluconate) from a single neuron stimulated to firing with stepwise, +5 pA, 0.7s depolarising currents in the presence of CTRL-, SR- or SR+PTX-containing ACSF. **B)** PTX, not SR, significantly decreases the rheobase from 77.9 ± 10.9 pA in SR to 53.6 ± 8.8 pA in SR+PTX which corresponds to a 32 ± 4% decrease in the minimum current for an action potential as shown in **Bii)**. **C)** The AP threshold voltage, defined as the voltage at which ΔdV/Δt = 20 mV/ms, is hyperpolarised by -1.4 mV in the presence of SR+PTX (-39.5 ± 1.2 mV) vs SR alone (-38.0 ± 1.3 mV). Data points are means throughout (cirles); the average of each plot is shown in red. Stats = ANOVA; and paired t-tests with Bonferroni correction. N=7.

3.5.7 Blocking s-GABA$_A$Rs increases AP firing rate within the theta frequency band

For the next experiment, we wanted to explore further the effect of s-GABA$_A$Rs on AP firing. So far we have measured their impact on F-I curves and on rheobase; here we looked at steady-state firing in the theta rhythm band (4-10 Hz), a rhythm that is thought to be critical for information processing in the entorhinal–hippocampal network (534,535). In current-clamp mode, neurons were depolarised with 0.5s, 10 pA steps until the neuron fired 2-3 APs (mean = 2.6 ± 0.2 APs, or 5.2 ± 0.4 Hz; N=8). The neurons were then exposed to SR, which increased the number of APs fired by ~ 1 AP (mean = +0.8 APs; percentage increase = 33.3%) (**Fig.3.9**). The depolarising stimulus was then reduced by an average of 6.4 ± 2.1 pA, to give an 'SR-adjusted' current that elicited the same number of action potentials as in CTRL conditions. PTX was then added, and the SR-adjusted current was used to repeatedly depolarise the neuron, initially at a 1 minute interval for 5 minutes and then at a 2.5 minute interval for a further 10 minutes. Block of s-GABA$_A$Rs induced a time-dependent increase in average AP frequency (**Fig.3.9C**).

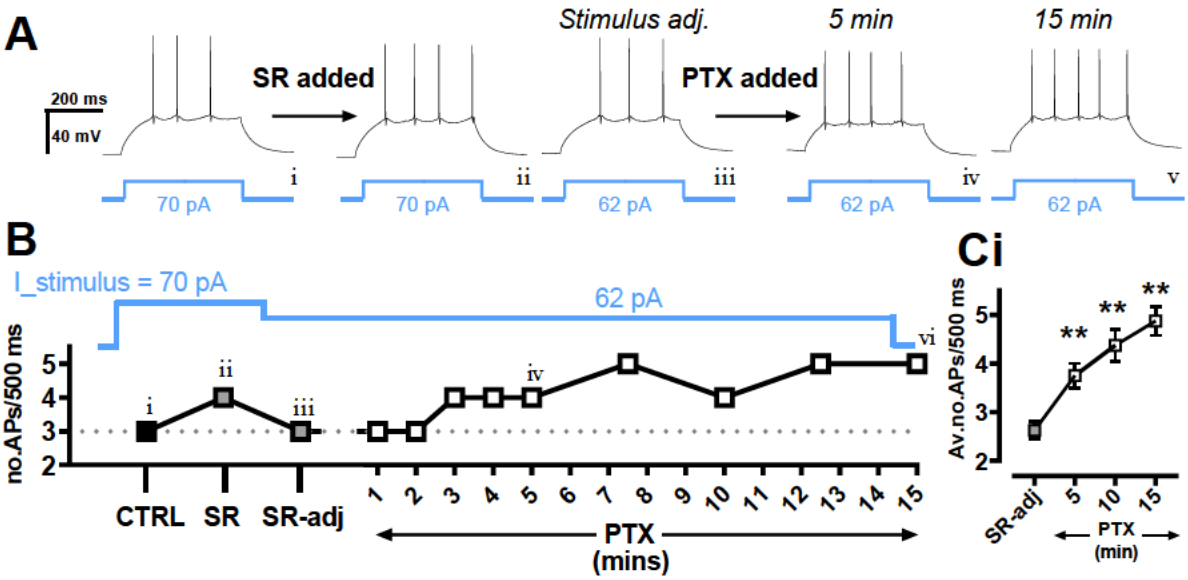

Fig.3.9. Blocking s-GABA$_A$Rs increases firing rate at theta frequency.
A) Examples of WC-current clamp recording (K-gluconate) from a single neuron stimulated with **i)** a 70 pA, 0.5s current step to drive the neuron to fire at the theta frequency in CTRL conditions (4- 10 Hz; 6Hz in the example). The neuron was then exposed to SR **ii)** and stimulated again with 70 pA which increased the frequency to 8 Hz. The stimulus was then adjusted **iii)** to 62 pA to restore firing rate to 6 Hz. The neuron was then exposed to SR+PTX and excited, at 1-to-5 minute intervals (5 and 10 min shown: **iv-vi**), with the 'adjusted' stimulus. **B)** Charts how the AP firing number increased in SR and then again in SR+PTX. **C)** Summarises the results from 8 neurons showing that block of s-GABA$_A$Rs increases the AP number/theta firing rate. Data points in **B)** are raw values from the neuron in **A)**, and in **C)** are means ± SEM. Stats: Paired t-test with Bonferroni correction.

After 5 minutes firing rate was on average increased by more than 1 AP (mean = 1.13 APs; percentage increase = 46 %); by 10 minutes firing rate was increased by nearly 2 APs (mean = 1.75 APs; percentage increase = 71 %); after 15 minutes firing rate close to doubled (mean = 2.25 APs; percentage increase = 93%) (**Fig.3.9C**). The change in AP firing rate was significantly (with Bonferroni correction) increased in SR+PTX relative to SR-adjusted at all three of these time points: 5 minutes (Paired Student's t-test $t_{(7)}$= 4.965; P = 0.0049), 10 minutes (Paired Student's t-test $t_{(7)}$= 5.584; P = 0.0025) and 15 minutes (Paired Student's t-test $t_{(7)}$= 6.148; P = 0.0014) (**Fig.3.9C**).

3.5.8 Exploring the mechanism of neuronal gain control by s-$GABA_A$Rs

For the next part of this section, we wanted to revisit and better understand the increase in gain (F-I slope) that occurs when s-$GABA_A$Rs are blocked (**Data in section 3.6.6; Fig.3.7**). F-I slope gain is important to DGGCs: they have an over four times higher gain than CA1 and CA3 pyramidal neurons (414), and this high gain allows them to transition effectively from a silent state to firing bursts of APs (413,468). Burst firing allows DGGCs to send sparse but powerful excitatory signals, via their mossy fibers, to CA3 pyramidal cells, which is thought to be important for pattern separation (432,445–453). The increase in gain that we reported following the block of s-$GABA_A$Rs was both interesting and unexpected. Although shunting conductance has a divisive effect on sub-threshold voltage transients (Ohm's law: V= I/G) (316–318), most studies have shown that, because of the spiking mechanism, tonic shunting inhibition causes a subtractive effect to the F-I curves, i.e. offsetting them to the right with no effect on the slope/shape (see introduction for a more detailed explanation) (317). That said, there are three scenarios that have so far been identified to allow a shunting conductance, similar to that provided by s-$GABA_A$Rs, to act divisively on the F-I curves and reduce the F-I gain. These are 1) stochastic noise, 2) active dendritic conductances and 3) spike-frequency adaptation (317). We considered it unlikely that there was sufficient stochastic noise to explain the gain change caused by s-$GABA_A$Rs. In support of this, the majority of *in vitro* studies have had to use dynamic clamp to artificially increase stochastic noise to levels observed *in vivo* in order to detect a shunt-induced decrease in gain (292,293). We therefore focussed on the latter two scenarios, and attempted to see if there were any commonalities between those previously

reported findings and our data (**Fig.3.10**). The detailed mechanisms for gain control via stochastic noise, active dendrites and spike-frequency adaptation are presented in the appendix.

Briefly, gain control via active dendrites relies on the shunting conductance acting to decrease the amplitude of the depolarizing afterpotentials that are caused by active dendritic spike backpropagation (295). Depolarising afterpotentials usually act to decrease the AHP amplitude, which, in turn, shortens the interspike interval and increases gain/excitability. By decreasing the amplitude of these depolarising afterpotentials, shunting conductances are able to enhance the AHP amplitude and thereby decrease gain/excitability (295). If s-$GABA_A$Rs are able to modulate gain through this mechanism, the AHP amplitude should be suppressed by blockings-$GABA_A$Rs. However, when we measured the AHP in the presence of SR (-14.3 ± 0.7 mV) vs SR+PTX (-13.523 ± 1.2 mV), we were able to find no significant difference in amplitude (SR vs SR+PTX, Paired Student's t-test $t_{(7)}$= 1.40; P = 0.2039) (**Fig.3.10E**). This likely reflects the relatively low density of voltage-gated Na^+ channels in DGGC dendrites (483); these channels are necessary for the generation of afterpotentials following AP backpropagation (295).

Next, we assessed if s-$GABA_A$Rs were able to modulate gain by altering the spike-frequency adaptation characteristics of the neuron. Spike-frequency adaptation describes the reduction in firing rate that occurs during sustained injections of supra-threshold step currents (294,517,536,537). The indicator for spike-frequency adaptation is that the steady state firing rate (measured towards the end of an excitatory current step) is lower than the initial firing rate (measured at the start of the excitatory step). Previous studies have shown that DGGCs show reasonably pronounced spike-frequency adaptation (480), and we have corroborated this finding in **Fig.3.7** (observe the decrease in firing rate at the end of the current step vs. the start). Spike-frequency adaptation is physiologically important to DGGCs as it allows them to fire in bursts, without runaway, continuous firing (413,468). In 2010, Fernandez *et al* reported that shunting inhibition was able to enhance spike-frequency adaptation in CA1 pyramidal neurons and that the resultant decrease in steady-state firing rate was sufficient to significantly reduce the overall F-I gain (294). The key indicator for this effect was that shunting inhibition had disparate impact on the initial vs. steady-state F-I relationship. Namely, shunting induced a

subtractive offset the initial firing rate, with only a minimal change in gain, but exerted a powerful divisive effect on the gain of the steady-state firing rate (294). We found that blocking s-$GABA_A$Rs exerted similar effects on initial and steady-state curves to what would be predicted from Fernandez *et al*, 2010 (294) (**Fig.3.10A-D**).

Blocking s-$GABA_A$Rs differentially affects the initial vs steady-state F-I curves, and this likely allows s-$GABA_A$Rs to modulate the gain of the overall F-I relationship (**Fig.3.10A-C**). As in Fernandez *et al*, we found that the *initial* F-I relationship was best fit with a linear function (294) (**Fig.3.10Bi**). The authors showed that a shunting conductance causes a subtractive offset the F-I relationship of the initial firing rate (shifting the line to the right), but has a minimal effect on its gain (294). As would be expected from this, we found that blocking the shunting conductance generated by s-$GABA_A$Rs resulted in an additive leftward shift/offset to the initial firing rate F-I relationship. But did not significantly affect its gain (SR vs SR+PTX gain, linear fit 75 to 175 pA: Unpaired Student's t-test, $t_{(6,9)}$=1.367 P = 0.193) (**Fig.3.10Bii**).

Next, we looked at the *steady-state* firing rate. Just like Fernandez *et al*, we found that the steady-state F-I relationship was non-linear (294) and our data were best fit with a second-order polynomial (294) (**Fig.3.10Ci**). In the presence of SR the steady state firing rate reached an approximate plateau of 25.1 ± 5.1 Hz between 175 and 250 pA, which reflects a saturation of the F-I response (**Fig.3.10Ci**). Fernandez *et al*, showed that shunting conductance enhances the degree of saturation and that this leads to a lower maximum sustainable firing rate (294). We found that, as would be expected from Fernandez *et al*'s findings, blocking the s-$GABA_A$R shunt caused a decreases of the degree to which steady-state firing rate is saturated, as indicated by the significant increase in the maximum sustainable firing rate (plateau frequency) from 25.1 ± 5.1 Hz in SR, to 46.7 ± 6.7 Hz in PTX (taken from 175-to-250 pA: SR vs SR+PTX plateau: Unpaired Student's t-test, $t_{(6,9)}$=2.432 P = 0.029) (**Fig.3.10Cii**). As a final step, we compared the gain over the linear portion (75-175 pA) of the steady state-F-I relationship, which Fernandez *et al* showed was decreased by shunting conductance (294). In line with this, we found that when s-$GABA_A$Rs were blocked the gain of the linear portion of the steady state-F-I relationship was significantly increased by ~60% from 0.14 ± 0.02 in SR, to 0.23 ± 0.03 in SR+PTX (taken from 75-to-175 pA: SR vs SR+PTX gain: Unpaired Student's t-test, $t_{(6,9)}$=2.21 P = 0.044) (**Fig.3.10Ciii**).

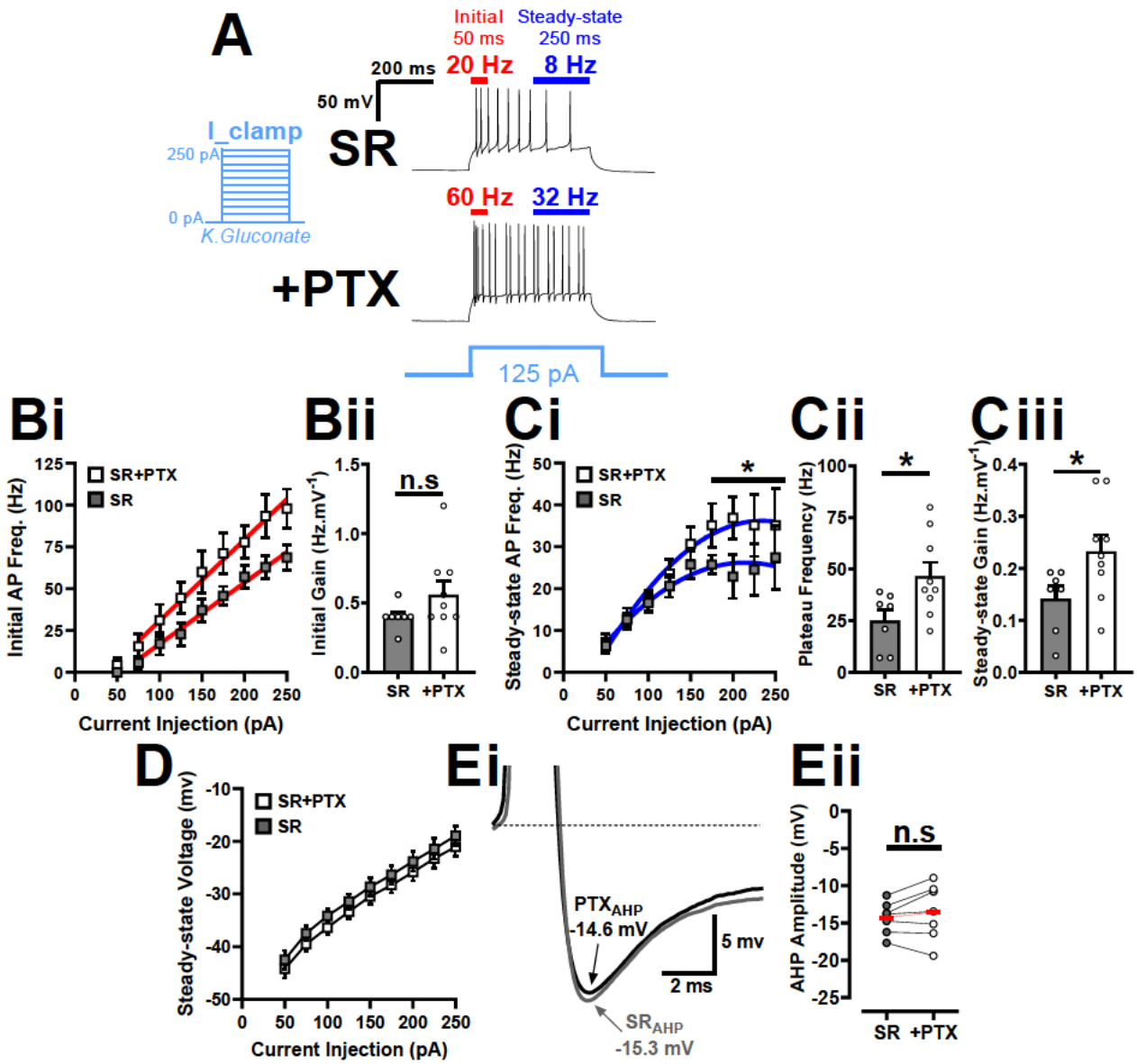

Fig.3.10 s-GABA$_A$Rs differentially affect initial vs. steady state firing rate, but do not alter AHP amplitude.

A) Examples of WC-current clamp recordings (K-gluconate) from two neurons excited with 125 pA current steps in the presence of SR- or SR+PTX-containing ACSF. The initial firing frequency was recorded over the first **50 ms**; the steady-state firing rate was recorded over the last **250 ms.** **Bi)** Plot of the initial firing rate—current relationship (F-I; 50 to 250 pA plotted; 500 ms, 25 pA steps) shows that block of s-GABA$_A$Rs causes an excitatory leftward offset to the F-I curve, **Bii)** with no change in gain (linear fit, 75-to-175 pA). **Ci)** Plot of the steady-state firing rate—current relationship shows that block of s-GABA$_A$Rs increases in the maximum steady-state firing rate **Cii)** (the plateau). **Ciii)** Block of s-GABA$_A$Rs increases the gain of the steady-state firing rate (linear fit, 75-to-175 pA). **D)** The steady-state holding voltage–current graph shows that the steady state potential is consistently more hyperpolarised when s-GABA$_A$Rs are blocked (mean Δ steady state voltage = -1.96 ± 0.05 mV) (N= SR:7, PTX:9). **Ei)** Example WC-current clamp recordings (K-gluconate) showing the AHP amplitude, measured from threshold, in the presence of SR vs. SR+PTX. **Eii)** AHP amplitude is not significantly altered when s-GABA$_A$Rs are blocked. N=7.

Thus our findings very closely match that of Fernandez *et al*, 2010 (294); this indicates that s-$GABA_A$Rs act to increase the amount of spike-frequency adaptation that takes place in DGGCs, and that this, in turn, causes a decrease in F-I gain. But what is the mechanism? In Fernandez *et al's* study, they showed in CA1 neurons that shunting exacerbates the main driver of spike adaptation in these cells: depolarisation-dependent Na^+ channel inactivation (294). Shunting is able to increase Na^+ channel inactivation by attenuating Na^+ currents, which causes both the voltage threshold and the mean firing voltage to be *depolarised* (because neurons have to depolarise further to generate the sufficient amount of Na^+ current to initiate spiking) (294). This persistent increase in depolarisation over the course of AP firing results in a greater amount of Na^+ channel inactivation and, therefore, a more substantial decrease to the steady-state firing rate for a given excitatory current (294). In DGGCs, spike-frequency adaptation is also driven by Na^+ channel inactivation (480); therefore, it seems plausible that s-$GABA_A$Rs in DGGCs, like shunting in CA1 neurons, is enhancing the amount of Na^+ inactivation to exacerbate spike adaptation (294). This view is supported by two pieces of evidence. The first is the effect of s-$GABA_A$Rs on AP threshold that we reported earlier (from the rheobase experiments in **Fig.3.8**): blocking s-$GABA_A$Rs with PTX leads to a significant hyperpolarisation, of -1.4 mV, of the firing threshold, supporting the potential involvement of Na^+ channels (**Fig.3.8C**). The second is that when we compared the mean firing voltage in the presence of SR vs. SR+PTX, we find that with PTX the mean firing voltage is hyperpolarised at every current step by an average of -1.96 ± 0.05 mV (**Fig.3.10D**). This suggests the following mechanism: that when s-$GABA_A$Rs are blocked, the neuron does not have to depolarise as far to generate the Na^+ currents necessary to initiate and sustain firing (because Na^+ currents are no longer being shunted), and that this means there is less depolarisation-dependent Na^+ channel inactivation, less spike-frequency adaptation, and, as a result, a higher excitability/gain.

So far in this chapter we have demonstrated that s-$GABA_A$Rs provide an outwardly rectifying tonic shunting conductance. And that blocking s-$GABA_A$Rs conductance with PTX affects many of the key factors that are critical for the proper signal integration and, in turn, function of DGGCs: namely, input resistance, membrane time constant, AP threshold, F-I gain and rheobase. However, in all of the experiments performed so far, we have utilised only square wave depolarising and hyperpolarising current/voltage steps to examine the functional output of DGGCs. Thus, in the final part of this chapter, we used evoked synaptic potentials to study the impact of s-$GABA_A$Rs on DGGCs in response to more physiologically relevant inputs. Specifically, we assessed the role of s-$GABA_A$Rs in coincidence detection and LTP.

3.5.9 Blocking s-$GABA_A$Rs widens the temporal window for coincidence detection

One of the key properties of DGGCs is the narrow temporal window over which they can summate synaptic inputs; they require a relatively large number of concurrently active excitatory inputs to fire an AP and can, therefore, act as effective coincidence detectors (483–485,487). Underlying this property is 1) the low excitability of DGGCs and 2) the strongly attenuating dendrites (483,485). Concerning to the former, we have demonstrated throughout this chapter that blocking s-$GABA_A$Rs significantly increases the excitability of DGGCs, and thus could affect coincidence detection/temporal precision, as has been reported for $GABA_A$Rs that are activated by GABA (297,298,319). s-$GABA_A$Rs may also be able to affect the strength of dendritic attenuation, in a manner akin to A-type K^+ channel, which are the channels primarily responsible for attenuation in DGGCs (483,485). These voltage-activated channels attenuate EPSPs by providing a shunting conductance; it is likely that s-$GABA_A$Rs are also, to a significant degree, present in dendrites and thus the shunting conductance they provide may also contribute to dendritic attenuation and, in turn, the precision of coincidence detection. In line with this, GABA-activated $GABA_A$Rs have been previously shown to augment dendritic attenuation (295,298). We hypothesised that s-$GABA_A$Rs act to increase the precision of signalling in DGGCs and, therefore, blocking their activity with PTX should widen the temporal window for successful coincidence detection.

We measured the temporal window for coincidence detection by stimulating the two divisions of the perforant path (medial, MPP; lateral, LPP) at varying time intervals, so that MPP was stimulated relative to the LPP from -40 ms to +40 ms, in 10 ms increments (see protocol in **Fig.3.11A**). DGGCs were recorded using whole-cell current-clamp mode in the presence of strychnine and CGP55845, but without excitatory blockers. Stimulation intensity for each path was set so that when they were delivered synchronously, DGGCs fired with a probability of ~50%. Next, the time interval between MPP and LPP stimulations was then varied according to the timing protocol in **Fig.3.11A**; the entire protocol was then repeated a total of three times, which means that for each neuron, at each stimulus interval, there is an accompanying firing probability of either: 0%, 33.3%, 66.6% or 100% **Fig.3.11B**. In control conditions, the average firing probability decreased when time-period between MPP and LPP stimulations was increased, as can be observed from firing probability vs stimulation interval curve in **Fig.3.11C**. Next we repeated the entire stimulation protocol, recording from the same cell with the same stimulus intensity, but in the presence of SR. SR caused a saturation of the coincidence detection response curve (**Fig.3.11C**)**,** which reflects that in the absence of any $GABA_AR$ antagonists evoked potentials are a composite of excitatory and inhibitory signalling. Henceforth, to assess the specific impact of s-$GABA_A$Rs on coincidence detection, we had to first adjust (decrease) the stimulus intensities in the presence of SR to desaturate the response (compare average firing rates with SR: **Fig.3.11C** with SR.adj: **Fig.3.11D**).

The impact of s-$GABA_A$Rs on coincidence detection was assessed by exposing the same neuron to PTX (SR→SR+PTX) and repeating the stimulation protocol using the 'SR-adjusted' stimulus (**Fig.3.11B+D)**. Block of s-$GABA_A$Rs led to a significant widening of the temporal window for coincidence detection, indicating that s-$GABA_A$Rs usually act to increase the precision of signal transmission in DGGCs. This is evidenced from the widening of the average firing probability vs. stimulation interval curve caused by going from SR to SR+PTX (**Fig.3.11D**)**;** comparing the two conditions with a two way ANOVA revealed that the difference was significant curve (Two-way ANOVA: SR vs SR+PTX;$F_{(1,12)}$ = 14.31; P= 0.0026). And comparing the average firing rate at different stimulus intervals (Bonferroni corrected) showed that cells in the presence of SR+PTX (s-$GABA_A$Rs blocked) had a higher probability of firing

than with SR alone (s-GABA$_A$Rs active): MPP 40 ms before LPP (Paired Student's t-test $t_{(6)}$= 6.31; P = 0.0003); MPP 30 ms before LPP (Paired Student's t-test $t_{(6)}$= 4.57; P = 0.0152). MPP 30 ms after LPP (Paired Student's t-test $t_{(6)}$= 3.33; P = 0.0634); MPP 40 ms after LPP (Paired Student's t-test $t_{(6)}$= 4.77; P = 0.0123) (**Fig.3.11B+D**).

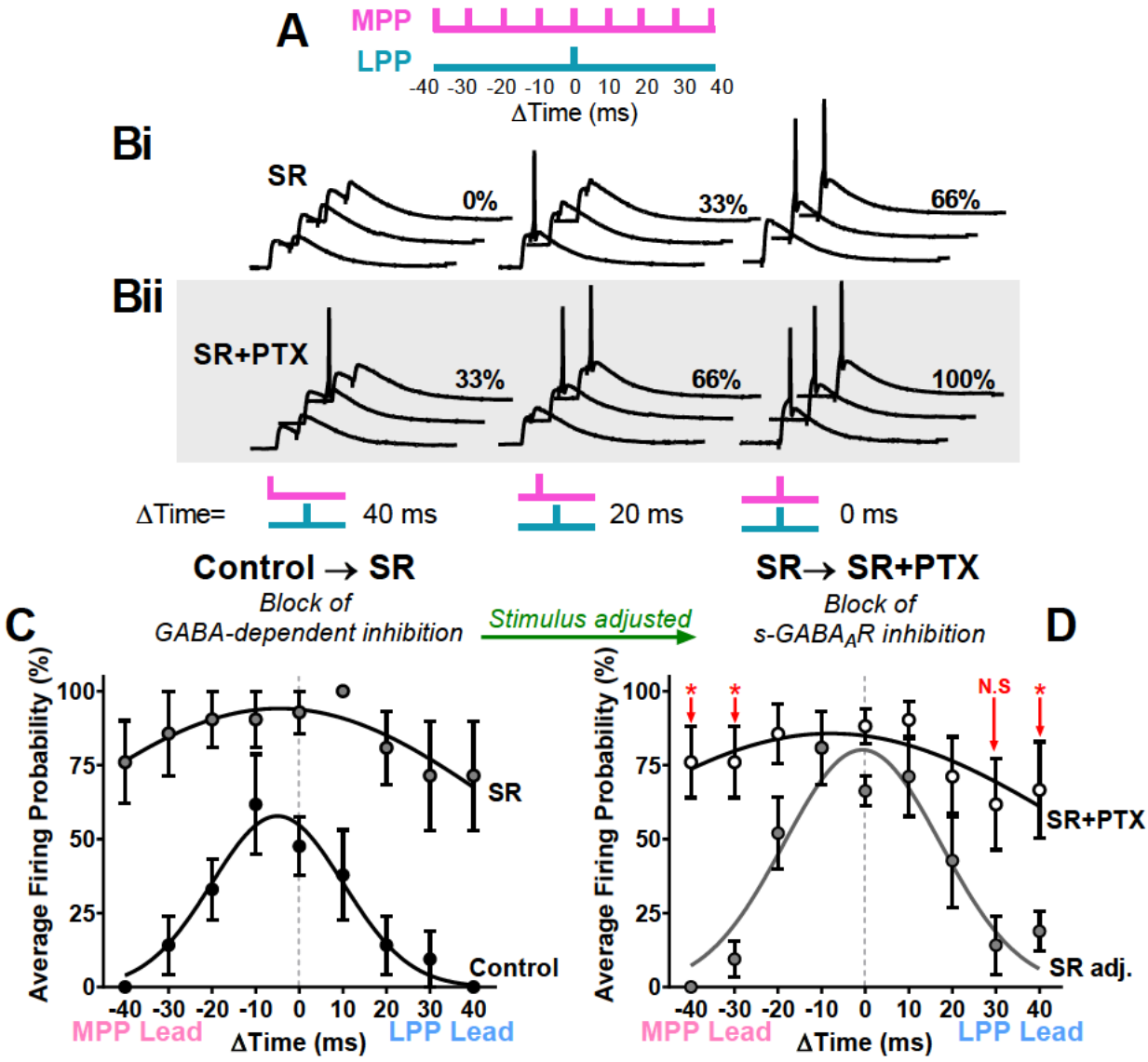

Fig.3.11. Block of s-GABA$_A$Rs widens the window for successful coincidence detection.
EPSPs were evoked by stimulating the MPP (pink) and LPP (cyan) at different time intervals as indicated in the stimulation protocol in **A)** The time interval of stimulation of the MPP was varied relative to the LPP from -40 ms to +40 ms in 10 ms increments. The stimulation protocol was repeated 3 times in each condition, which gives rise to a firing probability of 0, 33.3, 66.6 or 100% for each stimulation interval **Bi)** Example WC-current clamp traces (K-gluconate; 0 pA) from a neuron exposed to SR (s-GABA$_A$Rs intact) and then SR+PTX (s-GABA$_A$Rs blocked) **B)ii**,with MPP EPSPs evoked 40 ms, 20 ms, and 0 ms before the LPP. In both conditions, the probability of spiking increased when time between stimulations decreased; however, the probability of firing was higher for PTX, than SR at all time points displayed (note stimulus intensity was the same in both conditions). **C)** Average firing probability vs stimulation interval, comparing control (black) to SR (grey). Because SR causes saturation of the response, stimulus intensity was decreased (adusted; adj). **D)** Average firing probability vs stimulation interval, comparing SR adj. with SR+PTX shows that blocking s-GABA$_A$Rs widens the temporal window for coincidence detection. N=7; Curves are Gaussian fits; Stats=paired t-test, Bonferroni corrected.

3.5.10 Blocking s-$GABA_A$Rs does not affect the amplitude of LTP at DGGC synapses

For the final experiment in this chapter, we wanted to see if blocking s-$GABA_A$Rs increases the amplitude of LTP that is induced at perforant path-DGGC synapses following theta-burst stimulation (TBS). LTP is a form of synaptic plasticity and has been proposed to be the cellular mechanism for learning and memory in the brain (24,503–511).

In DGGCs, because of their strongly attenuating dendrites, LTP depends on depolarising local dendritic spikes, not back-propagating APs (485). Similar to the proposal made for coincidence detection, it is likely that s-$GABA_A$Rs are present in DGGC dendrites and, thus, they might shunt the dendritic spikes that are necessary for LTP. Henceforth, we hypothesised that by blocking s-$GABA_A$Rs we could increase the amplitude of LTP. This is analogous to the potentiation of dendritic spikes and, in turn, LTP that has been reported observed following block of dendritic A-type K^+ channels, the conductance that is primarily responsible for shunting dendritic spikes (485). Another mechanism by which blocking s-$GABA_A$Rs could possibly increase LTP amplitude owes to the fact that in DGGCs dendritic attenuation is substantial, but not insurmountable: the amplitude of somatic EPSPs decrease to ~30% of their original value by the time they reach distal dendrites (485). The elevation of excitability caused by blocking s-$GABA_A$Rs could increase the amount of depolarisation that back-propagates into the dendrites to the degree that it can facilitate LTP. Indeed, tonic inhibition has previously been shown to attenuate backpropagating APs in hippocampal pyramidal neurons and modulate spike-timing dependent plasticity (538). The proposal that blocking s-$GABA_A$Rs will increase LTP is also supported by previous studies that have shown the detrimental impact increasing GABA-activated tonic currents has on LTP in the DG (299). And that, in general, enhancing $GABA_A$R activity depresses LTP (520), whereas blocking their activity enhances LTP (521).

DGGC population synaptic responses were measured using field EPSP (fEPSP) recordings, and LTP was induced using a theta-burst stimulation protocol (**Fig.3.12**). The impact of s-$GABA_A$Rs on the amplitude of LTP was assessed in an unpaired manner: slices were exposed to *either* SR (N=8) *or* SR+PTX (N=8) throughout the entire experiment; the only other drug included was strychnine, which was present in all recordings in order to prevent a confounding effect of GlyRs.

Recording and bipolar stimulating electrodes were placed in the middle third of the molecular layer and the MPP, respectively. Baseline fPSPs were measured at 30 second intervals using 50 µs in duration voltage pulses, with an intensity set to produce a response (fEPSP slope) that is ~40% of maximum. After a 10 minute stable baseline response was obtained, LTP was induced using a TBS protocol that was repeated a total of 4 times – once every 30 seconds; each TBS consisted of 10 bursts of five pulses at 100 Hz, with each burst separated by 200 ms. We expressly wanted to study the impact of s-$GABA_A$Rs on the amplitude of LTP, not the threshold; and so we used this stimulation protocol because it had been previously shown to induce strong LTP at DGGC-MPP synapses (539). However, we did modify the stimulation protocol to increase its efficacy, first, by repeating four times and, second, by increasing the stimulus duration from 50 µs to 200 µs. Following the 4 episodes of TBS-LTP conditioning, the stimulation duration was returned to 50 µs and fEPSPs were recorded, once every 30 seconds, for 60 minutes (**Fig.3.12**). LTP amplitude was quantified by comparing the average baseline fEPSP slope (10 minutes prior to LTP) to the average fEPSP slope recorded after LTP at three time points: the 5- to 15 minute average, the 25- to 35 minute average and the 50- to 60 minute average.

In the presence of SR alone, with GABA-dependent inhibition blocked but s-$GABA_A$Rs intact, TBS induced an increase in fEPSP slope response that persisted over the 60 minute period, e.g. LTP (**Fig.3.12Ai+B**): the average slope of the fEPSP was increased to 204.0 ± 16.8% of baseline at 5-15 minutes, 185.6 ± 20.77% at 25-35 minutes, and 148.0 ± 20.6% at 50-60 minutes (**Fig.3.12B+C**). To test the impact of s-$GABA_A$Rs, the experiment was repeated in conditions wherein their activity was blocked (SR+PTX) (**Fig.3.12Aii+B**). Although DGGC-MPP synapses were still able to exhibit LTP in the presence of SR+PTX, the amplitude of this potentiation was virtually identical to that observed with SR alone (**Fig.3.12B+C**). The average slope of the fEPSP relative to baseline was not significantly different, even without correcting for multiple comparison, in SR vs SR+PTX at the 5-15 minute time point (205.5 ± 8.9% with PTX; Unpaired Student's t-test, $t_{(7,7)}$=0.08; P = 0.938), or the 25-35 minute time point (179.0 ± 10.0% with PTX; Unpaired Student's t-test, $t_{(7,7)}$=0.288; P = 0.778), or the 50-60 minute time point (133.0 ± 7.6% with PTX; Unpaired Student's t-test, $t_{(7,7)}$=0.684; P = 0.505) (**Fig.3.12B+C**).

Henceforth, it is apparent from this experiment that s-$GABA_A$Rs do not affect the *amplitude* of LTP at DGGC-MPP synapses.

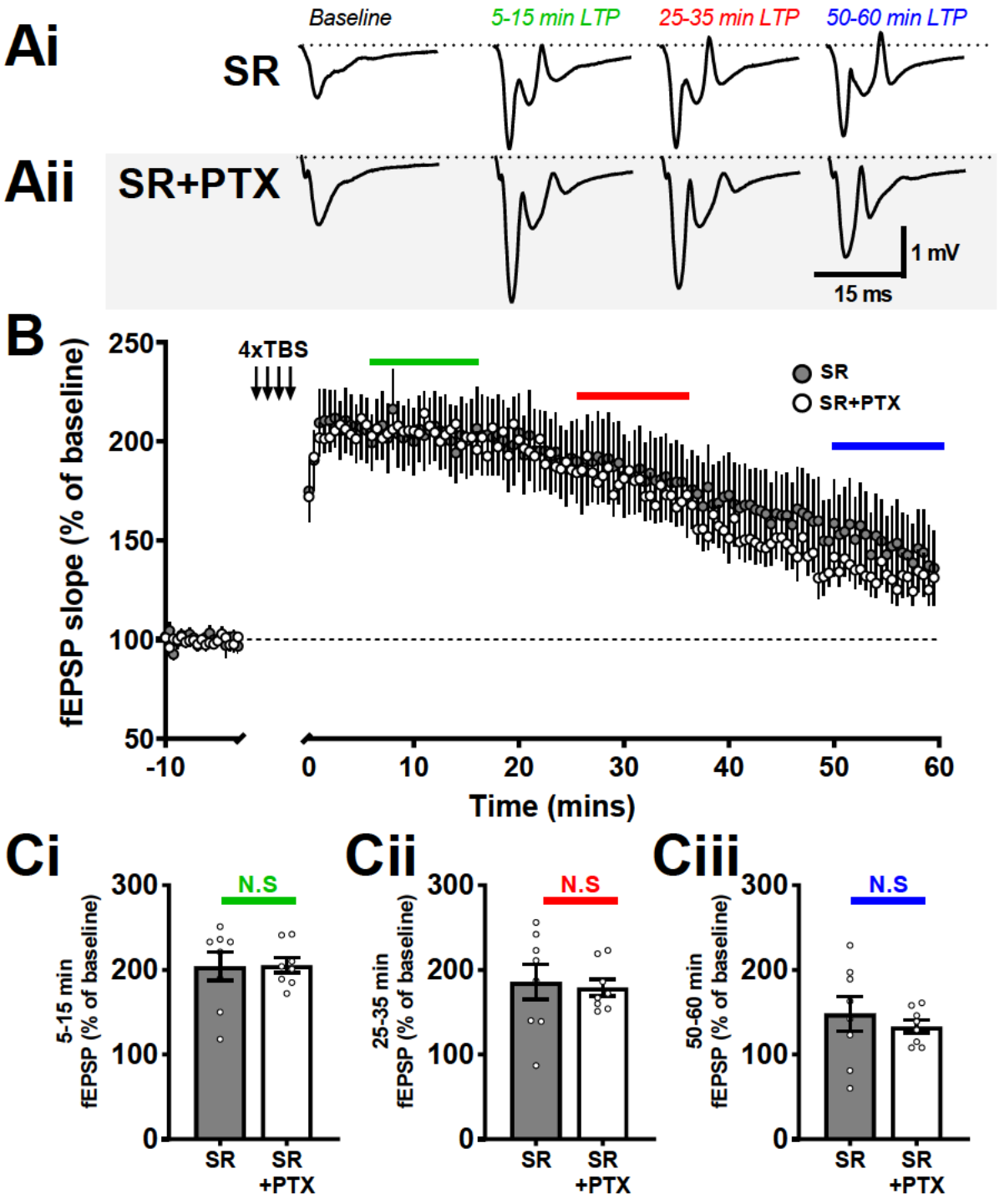

Fig.3.12. Block of s-$GABA_A$Rs does not affect LTP amplitude at DGGC-MPP synapses
Example 10 minute average fEPSP traces recorded in the presence of SR **Ai)** or PTX **Aii)** at DGGC-MPP synapses prior (**black**) to TBS LTP and after LTP, at 5-15 minutes (**green**), 25-35 minutes (**red**) and 50-60 minutes (**blue**). **B)** Percentage change in fEPSP slope relative to baseline vs time shows that the amplitude and time course of TBS LTP was similar between SR (grey; N=8) and SR+PTX (white; N=8). This indicates that the lack of effect of blocking s-$GABA_A$Rs on LTP amplitude, as can also be observed in the average change in baseline fEPSP slope following TBS at **Ci)** 5-15 minutes, **Cii)** 25-35 minutes and **Ciii)** 50-60 minutes Stats=unpaired t-test.

Chapter 4

Modulation of s-$GABA_A$R-mediated Tonic Currents

4.1 Overview

In the previous chapter, we demonstrated that the outwardly rectifying tonic conductance that is delivered by s-$GABA_A$Rs significantly affects DGGC physiological function. However, so far, we have not gained any additional understanding of the pharmacological characteristics of s-$GABA_A$Rs, beyond that previously reported. In this chapter, we explored the mechanisms by which s-$GABA_A$R tonic currents can be modulated. Specifically, we assessed if s-$GABA_A$R tonic currents are modulated by:

1) Ligands acting at extrasynaptic $GABA_A$R isoforms that contain the δ-subunit or α5-subunit (i.e. the receptors that are responsible for generating GABA-dependent tonic currents in DGGCs).

2) Benzodiazepine-site agonists/inverse agonists.

3) Inhibitors and activators of serine/threonine kinases.

Some of the findings presented in this chapter have been published (415,416).

Experimental:

O'Neill N, Sylantyev S. Selective modulation of tonically active $GABA_A$ receptor functional subgroups by G-proteins and protein kinase C. *Experimental Biology and Medicine. 2018;* 243(13), 1046–1055.

Mini-Review:

O'Neill N, and Sylantyev S. The Functional Role of Spontaneously Opening $GABA_A$ Receptors in Neural Transmission. Front. Mol. Neurosci. 2019; 12:72.

4.2 Introduction

We have demonstrated that s-$GABA_AR$-mediated conductance affects DGGC physiology; the question that logically flows from this is whether s-$GABA_AR$ activity can be modulated. Previous studies investigating GABA-dependent tonic currents have shown that the nature and magnitude of this signal can be regulated through a variety of mechanisms, some of which are also relevant for s-$GABA_ARs$. In this chapter, we tested if s-$GABA_AR$ tonic currents can be modulated 1) directly, by a range of compounds that bind to different $GABA_AR$ isoforms to affect their activity and 2) indirectly, by compounds that modulate serine/threonine kinases. At present, our understanding of the pharmacological properties of s-$GABA_ARs$ is limited to the findings reported by McCartney *et al* (in hippocampal pyramidal neurons) (233), Wlodarczyk *et al* (in DGGCs) (74), *and Botta et al* (central amygdala PKCδ positive neurons) (234)*;* **Table 5.1** summarises the pharmacological agents that have been tested at s-$GABA_AR$ tonic currents.

Pharmacological effect:

↓= full block, ↓(-)= partial block, ↑=potentiation, o= no effect, n/a=not tested

	Hippocampal pyramidal	DGGC	PKCδ +ve central amygdala
SR-95531 (0.5-125 μM)	o	o	o
Picrotoxin (100 μM)	↓	↓	↓
Bicuculline (20,10,20 μM)	↓(-)	↓(-)	↓(-)
Zinc (100 μM)	↓(-)	n/a	n/a
Furosemide (600 μM)	o	n/a	n/a
Flunitrazepam (1 μM)	↑	n/a	n/a
Propofol (3-10 μM)	↑	n/a	n/a
Loreclezole (10 μM)	↑	n/a	n/a
Pentylenetetrazol (1.5 mM)	n/a	↓	n/a
TPMPA (50 μM)	n/a	o	n/a
L-655,708 (50 nM–50 μM)	n/a	n/a	↓(-)

PWZ-029 (100 nM–1 μM)	n/a	n/a	↓(-)
3α,5α- THDOC (10–100 nM)	n/a	n/a	o
Zolpidem (20–300 nM)	n/a	n/a	o

Table 5.1. Pharmacology of s-$GABA_AR$ tonic currents.
Zinc an allosteric antagonist of $GABA_ARs$
Furosemide (5-(Aminosulfonyl)-4-chloro-2-([2-furanylmethyl]amino)benzoicacid**):** a non-competitive $GABA_AR$ antagonist.
Flunitrazepam (5-(2-Fluorophenyl)-1,3-dihydro-1-methyl-7-nitro-2H-1,4-benzodiazepin-2-one): BDZ-site agonist
Propofol (6-Bis(1-methylethyl)phenol,2,6-Bis(isopropyl)phenol,2,6-Diisopropylphenol): general anaesthetic, potentiation of GABA-mediated responses and directly activates the $GABA_AR$.
Loreclezole ((Z)-1-[2-Chloro-2-(2,4-dichlorophenyl)ethenyl]-1H-1,2,4-triazole) sedative and an anticonvulsant; positive allosteric modulator of β2 or β3-subunit containing $GABA_ARs$
Pentylenetetrazol (6,7,8,9-Tetrahydro-5H-tetrazolo[1,5-a]azepine): non-competitive $GABA_AR$ antagonist
TPMPA (1,2,5,6-Tetrahydropyridin-4-yl)methylphosphinic acid): GABAA-ρ ($GABA_CR$) antagonist
L-655,708 (11,12,13,13a-Tetrahydro-7-methoxy-9-oxo-9H-imidazo[1,5-a]pyrrolo[2,1-c][1,4]benzodiazepine-1-carboxylic acid, ethyl ester): α5-subunit selective BDZ-site inverse agonist
PWZ-029 (methyl-(8-chloro-5,6-dihydro-5-methyl-6-oxo-4H-imidazo[1,5-α][1,4]benzodiazepin-3-yl)methylether): α5-subunit selective BDZ-site inverse agonist
3α,5α-THDOC: (3α,5α)-3,21-Dihydroxypregnan-20-one): neurosteroid $GABA_AR$ PAM.
Zolpidem (N,N,6-Trimethyl-2-(4-methylphenyl)imidazo[1,2-a]pyridine-3-acetamide): BDZ-site agonist

Table 5.1 shows that s-$GABA_AR$ tonic currents in DGGCs are resistant to SR (a competitive antagonist) and TPMPA (an antagonist at ρ-$GABA_ARs$ [formerly $GABA_CR$]), partially inhibited by bicuculline (an inverse agonist), and completely blocked by PTX and pentylenetetrazol (non-competitive antagonists) (74). Another important takeaway from **Table 5.1** is that most compounds have only been tried in one neuron type and so we do not know how consistent the pharmacological profile of s-$GABA_AR$ currents is across different neurons. Because the pharmacological profile of any $GABA_AR$ is determined by its constituent subunits, this taps into an even more fundamental question, namely: are the same $GABA_AR$ isoforms responsible for generating GABA-independent tonic currents across different neurons? Or are there many possible $GABA_ARs$ isoforms that spontaneously open, with each neuron type expressing a different 'subset' of possible s-$GABA_ARs$ to produce their respective GABA-independent tonic currents? Evidence from McCartney *et al* (233), Wlodarczyk *et al* (74), and *Botta et al* (234) favours the latter proposition: each study posited that a different $GABA_AR$ isoform was

responsible for generating the GABA-independent tonic currents in the neuron under investigation.

4.2.1 $GABA_AR$ isoforms proposed to contribute to GABA-independent tonic currents

s-$GABA_AR$ tonic currents in DGGCs= δ-subunit containing $GABA_ARs$. Wlodarczyk *et al*, demonstrated that knockout mice lacking the δ-subunit (*Gabrd−/−*) have a s-$GABA_AR$ tonic current that is reduced by ~60% compared to wild-type mice (74).

s-$GABA_AR$ tonic currents in PKCδ positive neurons of the central amygdala = α5-subunit containing $GABA_ARs$. *Botta* et al, demonstrated that knockout mice lacking α5-subunit (*Gabra5−/−*) have a reduced s-$GABA_AR$ tonic current. In line with this, α5-subunit selective inverse agonists (L-655,708 and PWZ-029) also decrease s-$GABA_AR$ tonic currents (234).

s-$GABA_AR$ tonic currents in Hippocampal Pyramidal Neurons = α1β1γ2 or α1β3γ2 receptors. McCartney *et al,* demonstrated that the pharmacology of s-$GABA_AR$ tonic currents in hippocampal pyramidal cells most closely matches that of recombinant α1β1γ2 and α1β3γ2 receptor isoforms. Key to this conclusion was the potentiation of s-$GABA_AR$ tonic currents by the benzodiazepine-site agonist, flunitrazepam (233).

In principle, all of the receptor isoforms identified above (and possibly others) could be delivering a portion of the s-$GABA_AR$ tonic current that is found in DGGCs. And, therefore, compounds that are known to modulate the activity of these receptors might also be able to affect s-$GABA_AR$ tonic currents in DGGCs.

The idea that the s-$GABA_AR$ current in DGGCs is the collective endeavour that involves multiple $GABA_AR$ isoforms is supported by the fact that in *Gabrd−/−* mice, which lack the δ-subunit, a significant portion of the s-$GABA_AR$ tonic current, >40%, remains intact (74). Although this may be explained by compensatory increases in other $GABA_AR$ subunits (143,351,540–543), it at least suggests that in WT-DGGCs, other $GABA_AR$ isoforms – perhaps α5βγ and/or α1β1/3γ2 receptors – are also able to open spontaneously to deliver some of the s-$GABA_AR$ current (74). This idea is also supported in the most basic sense by gene and protein expression data: DGGCs express 11 of the 19 total $GABA_AR$ subunit genes (111–116): moderate-to-high levels

of the α1,2,4,5; β1,2,3; γ2 and δ $GABA_AR$ subunits, low/no γ1+3 subunits (111–116); DGGCs may also express α3 (111,112) and ε subunits, although reports of these subunits have been inconsistent (114,115,544). Thus, DGGCs express all the subunits required to assemble α5βγ and α1β1/3γ2 receptors – the other isoforms previously posited to be s-$GABA_ARs$ in other neuron types (233,234). Furthermore, the expression data shows that there are only a few isoforms, such as those containing α6 subunits (111–116), that can be discounted *a priori,* leaving open the possibility that other receptor isoforms contribute to s-$GABA_ARs$ tonic currents. Thus, there are many possible $GABA_AR$ isoforms that could be opening spontaneously to produce the s-$GABA_AR$ current.

We posit that using compounds that affect the activity of extrasynaptic δ-subunit-containing $GABA_AR$ isoforms (δ-$GABA_ARs$) will be a method for modulating s-$GABA_AR$ tonic currents. Compounds that target α5βγ2, which are also extrasynaptic, and α1βγ2 receptor isoforms, as well as those targeting other isoforms that have not been formally identified as s-$GABA_ARs$, may also be able to affect s-$GABA_AR$ tonic currents.

4.2.2 Assessing the modulation of s-$GABA_AR$-mediated tonic currents

There is an important consideration to note before we proceed: in this chapter, we are specifically trying to identify compounds that modulate s-$GABA_AR$ tonic currents by affecting their *spontaneous* activity and *not*, for instance: 1) agonists that bind to the orthosteric site to directly activate s-$GABA_ARs$ (and/or other types of $GABA_ARs$); nor are we aiming to identify 2) compounds that increase the potency for GABA at s-$GABA_ARs$ (and/or other types of $GABA_ARs$) so that they generate GABA-dependent tonic currents. A necessary, albeit not sufficient (see discussion), indication of whether a compound is modulating spontaneous activity is that the effect they produce, for instance, a change in tonic holding current, should persist in the presence of SR, the neutral competitive antagonist that prevents agonists binding to the orthosteric site. If any compounds do produce an SR-resistant effect (e.g. increase or decrease in holding current) then this effect should be blocked PTX to indicate that it is due to s-$GABA_ARs$. Thus, with the aim of this chapter being to modulate the spontaneous activity of s-$GABA_ARs$, it was important to only select compounds that act via non-orthosteric (allosteric)

sites – and ideally compounds that have already been confirmed to affect the constitutive activity of $GABA_A$Rs.

All experiments in this section were whole-cell voltage-clamp recordings using CsCl intracellular solution, which enables $GABA_A$R currents to be recorded at RMP (E_{GABA} ~ 0 mV). In this recording configuration, compounds that potentiate s-$GABA_A$R tonic currents will generate an inward tonic current that is resistant SR *and*, as a result, increase the amplitude of the PTX-induced outward current. Conversely, compounds that inhibit s-$GABA_A$Rs will generate an outward current that is unaffected by SR and, as a result, will lead to a reduction in the amplitude of the subsequent PTX-induced outward current.

4.2.3 Targeting extrasynaptic $GABA_A$Rs to directly modulate s-$GABA_A$R tonic currents

If it is the case that compounds that affect the activity of δ-subunit containing isoforms and/or α5-subunit containing isoforms are able to modulate s-$GABA_A$R tonic currents, it would give further support to the proposition made by Wlodarczyk *et al*. Namely, that in DGGCs, extrasynaptic $GABA_A$R isoforms that can be activated by elevated ambient GABA to produce GABA-dependent tonic currents also exhibit a degree of constitutive activity that allows them, under conditions of low-to-no ambient GABA, to maintain a 'floor' of inhibition because they can open spontaneously (74,224,376).

In DGGCs, δ-subunits (351) primarily assemble with α4-subunits (254) and β2-subunits (352) to form α4β2δ receptors; α4β1δ and α4β3δ receptor isoforms are also likely to be present, but at lower abundances (352,371). The potency of GABA at α4βδ receptor isoforms is high (179,235,372,375), and this allows them, along with α5βγ receptor isoforms, to be persistently activated by low concentrations of GABA to generate relatively small, but long-lived tonic currents (105,179,235,372). α4βδ and α5βγ receptor isoforms can do this despite being located at peri- and extrasynaptic sites (72,179,254,351,352,545,546). The role of α4βδ and α5βγ receptor isoforms in generating the GABA-dependent tonic inhibition was identified by Glykys *et al,* who showed that tonic currents in DGGCs, generated by applying 5 μM GABA to these cells, were virtually absent in double gene-knockout mice that lacked both the δ- and α5-subunits (*Gabra5/Gabrd−/−*) (351). They further showed, using single-knockout mice, that δ-$GABA_A$Rs

contribute >70% of the GABA-dependent tonic current in DGGCs, and that α5-$GABA_A$Rs contribute the remaining ~30% (351). Interestingly the relative proportion of the residual GABA-dependent current that persists following single KO of the δ-subunit (~30%) reported by Glykys *et al* is comparable to the residual s-$GABA_A$R tonic current reported in these mice by Wlodarczyk *et al* (~40%) (74,351). Further supporting evidence for the role of δ-subunit-containing $GABA_A$Rs in generating s-$GABA_A$R tonic currents, is that all three of the α4βδ receptor isoforms have been reported to exhibit constitutive receptor activity and produce leak currents when expressed in recombinant systems: a4β1δ (371,372), a4β2δ (372–375), a4β3δ (371,372,376,377). Indeed, the a4β2δ receptor isoform was recently shown to exhibits an unusually high constitutive open probability (~0.1) (375).

We utilised two compounds that we thought might be able to bi-directionally modulate s-$GABA_A$R tonic currents through their action at α4βδ receptor isoforms: DS2 and DPP-4-PIOL.

The imidazopyridine DS2 (Delta Selective compound 2) is a positive allosteric enhancer modulator at δ-subunit-containing $GABA_A$Rs (selectivity: α4/6βxδ > α1βxδ >> γ2-receptors > α4β3) (377,547). The main effect of DS2 on α4βδ receptor isoforms is to increase the maximal effect (efficacy) of GABA (377,547). Pertinent to the present thesis, DS2 has also been shown to increase the constitutive activity of α4β2δ (374) and α4β3δ (377) receptor isoforms. Because DS2 binds to an allosteric site, we reasoned that DS2 should be able to potentiate the s-$GABA_A$R tonic currents in the presence of SR, and this will be revealed as a larger PTX-sensitive current.

DPP-4-PIOL is a potent, mixed competitive and non-competitive antagonist that has a 3-fold higher potency for α4β3δ vs α1β3γ2 receptor isoforms (548). DPP-4-PIOL has an IC_{50} of 1 nM at α4β3δ receptors expressed in *Xenopus oocytes* and is able to potently suppresses the maximum GABA current due its non-competitive effect (e.g. it exhibits negative efficacy). Using the *in vitro* slice preparation, it was shown that 2.3 nM DPP-4-PIOL can inhibit a portion of GABA-dependent tonic current in DGGCs without affecting IPSCs (268); at higher concentrations (>30 nM) DPP-4-PIOL begins to inhibit IPSCs. We posit that the non-competitive component of DPP-4-PIOL may allow it to suppress constitutive s-$GABA_A$R activity in the

presence of SR, as indicated by an outward current and a decrease in the amplitude of the PTX sensitive current.

α5βγ2 receptor isoforms produce s-$GABA_AR$ tonic currents in PKCδ-positive neurons of the central amygdala (234) and deliver ~30% of the GABA-dependent tonic currents in DGGCs (351). We posit that they might also deliver a portion of the s-$GABA_AR$ tonic current in DGGCs (perhaps corresponding to the residual s-$GABA_AR$ tonic current that remains in *Gabrd−/−* mice) (74). Botta *et al* demonstrated that L-655,708, a partial-inverse agonist that is selective for the benzodiazepine (BDZ)-site of α5βγ2 receptor isoforms (549), can inhibit a portion of s-$GABA_AR$ tonic currents in PKCδ-positive neurons of the central amygdala (234). Thus, L-655,708 might also be able to attenuate s-$GABA_AR$ currents in DGGCs. Importantly, L-655,708 and other BDZ-site ligands, interact with the receptor at an allosteric site (α+/γ- subunit interface), that is distinct from the orthosteric sites (β+/α- subunit interface) (98). This means that they can still affect receptor function when SR is bound to the receptor (74,199,233) and, thus, are a powerful pharmacological mechanism for modulating s-$GABA_ARs$.

4.2.4 Using BDZ-site ligands to directly modulate s-$GABA_AR$ tonic currents

Other BDZ-site ligands might also be able to modulate s-$GABA_ARs$ in DGGCs. This is supported by McCartney *et al,* who showed that s-$GABA_AR$ tonic currents in hippocampal pyramidal neurons are potentiated flunitrazepam (1 μM), a BDZ-site agonist (233), and identified the BDZ-sensitive α1β1γ2 and α1β3γ2 receptor isoforms as potential sources of the s-$GABA_AR$ current (233). When these receptor isoforms (233,369) are expressed in recombinant systems they exhibit constitutive activity to produce s-$GABA_AR$ currents – the same is also true for as well as wild-type α1β2γ2L (198,205) and mutant α1β2γ2L/S receptor isoforms (196,198,199,205,260). And BDZ-site ligands can bidirectionally modulate the constitutive activity of these isoforms (196,198,199,205,233,260,369). Further convincing evidence for s-$GABA_ARs$ being sensitive to BDZ-site ligands comes from studies that, like McCartney *et al*, have shown that BDZ-site ligands can potentiate tonic currents in a manner that is resistant block by SR, but sensitive to bicuculline/PTX (269,270,303,522,550). Although rarely

acknowledged as such, this is an indicator of modulating tonic currents through s-$GABA_AR$ (233).

As a class of drugs, BDZ-site ligands are many and varied. Variation is present both in terms of efficacy: some BDZ-site ligands positively modulate $GABA_ARs$, others negatively; and in terms of subunit selectivity. At the level of the class as a whole, selectivity is conferred by the fact that most BDZ-site ligands are only effective at α1/2/3/5βγ2 receptor isoforms (551,552), whereas α4/6βδ receptor isoforms are generally classed as BDZ-insensitive receptors (553–557). Thus, BDZ-site ligands allow us to test if modulating subunit isoforms that do not contain the δ-subunit can affect s-$GABA_AR$ tonic currents. Selectivity is also present within the class, with different BDZ-site ligands acting at different subunit isoforms, e.g. L-655,708 negatively affects α5β3γ2 receptor responses, but is virtually ineffective at α1β3γ2 receptors. In contrast, the reverse is true for zolpidem: it potentiates α1β3γ2 receptor responses, but does not affect α5β3γ2 receptor responses (549). Thus, BDZ-site ligands provide a way to assess the contribution of specific receptor isoforms to the s-$GABA_AR$ tonic current. For the purposes of clarity, the pharmacology of the BDZ-site ligands used in this section is embedded within the results section.

4.2.5 Targeting PKC and PKA to indirectly modulate s-$GABA_AR$ tonic currents

All of the strategies proposed so far to modulate s-$GABA_AR$ activity involve compounds acting directly on s-$GABA_ARs$ to affect their constitutive activity. However, the activity/expression of $GABA_ARs$ can also be modulated indirectly, through changes to the receptor phosphorylation state that follows from altering the activity of serine/threonine kinases (558). Notably, in DGGCs, Bright *et al* showed that bicuculline-sensitive tonic $GABA_AR$ currents are bidirectionally modulated by PKC: activation of PKC inhibits tonic $GABA_AR$ currents, whereas inhibition of PKC potentiates them (559). They also showed that PKC activation, but not inhibition, had the same effect on GABA-activated currents at recombinant α4β2δ receptor isoforms (559), i.e. extrasynaptic receptors primarily responsible for GABA-dependent tonic currents in DGGCs (254,351,352). Pertinent to the present thesis, Tang *et al* showed that activation of PKA enhances the spontaneous activity of recombinant α4β3δ receptors, both in terms of whole-cell PTX-sensitive currents and increasing single-channel open frequency (376). Interestingly, the

effect of PKA on GABA-activated α4β3δ responses was the opposite to that of constitutive activity, causing inhibition of GABA responses (376), indicating that PKA might be a mechanism to selectively affect s-$GABA_A$Rs. One piece of evidence supporting the modulation of s-$GABA_A$R activity in DGGCs by PKA/PKC (or another cytoplasmic factor) comes from the study by Wlodarczyk *et al:* they failed to detect s-$GABA_A$R single-channel openings using the conventional outside-out recording technique; however, s-$GABA_A$R single-channel openings could be recorded using the nucleated macropatches, in which a larger piece of cell membrane is withdrawn from the cell to include the intact nuclei and cytoplasm (74). This suggests that 1) s-$GABA_A$Rs are expressed at a low density on the cell soma, and/or 2) the activity of s-$GABA_A$Rs depends on, or is augmented by, cytoplasmic factors e.g. PKA/PKC. Potentiation and inhibition of serine/threonine kinases might thus provide an additional mechanism by which to modulate s-$GABA_A$Rs tonic currents.

4.3 Aims

The overall aims of the present chapter (Chapter 4; Results 2) were to, first, characterise the pharmacology of s-$GABA_AR$-mediated tonic currents in DGGCs; and, as an adjunct to this, investigate if the amplitude of these currents is affected by modulating intracellular kinase pathways. Three experimental steps were pursued to achieve this aim:

Step 1) Investigate if ligands targeting extrasynaptic δ-subunit- and α5-subunit-containing $GABA_ARs$, which have been previously shown to modulate GABA-dependent tonic currents, also affect s-$GABA_AR$ tonic current amplitudes.

Step 2) Test if benzodiazepine-site ligands, which have been previously shown to affect constitutive receptor activity, can modulate s-$GABA_AR$ tonic currents.

Step 3) Use intracellular blockers and activators of PKA and PKC-pathways to investigate if – as with GABA-dependent tonic currents – serine/threonine kinase pathways affect the amplitude of s-$GABA_AR$ tonic currents.

4.4 Hypothesis

Previous work using knockout mice indicates that $GABA_A$Rs containing the δ-subunit produce a significant portion of the s-$GABA_A$R tonic current in DGGCs. We, therefore, hypothesise that we will be able to bi-directionally modulate the amplitude of s-$GABA_A$R tonic currents using compounds that target δ-$GABA_A$Rs. Because knockout of the δ-subunit does not completely ablate the s-$GABA_A$R tonic current, we also hypothesise, informed by previous findings in the central amygdala, that α5-subunit $GABA_A$Rs can spontaneously open. If this is the case, then inhibiting α5-$GABA_A$Rs should decrease the amplitude of s-$GABA_A$R currents. As an alternate hypothesis, non-α5/δ-subunit-containing $GABA_A$Rs may make a significant contribution to the s-$GABA_A$R current; we will test this using BDZ-site ligands. The spontaneous activity of $GABA_A$Rs can be altered by serine/threonine kinases and in the DG tonic currents have been shown to be modulated by both PKA and PKC. Therefore, we hypothesise inhibitors and activators of PKA/PKC will be able to modulate s-$GABA_A$Rs tonic currents.

4.5 Results

4.5.1 Zinc partially inhibits s-$GABA_A$R tonic currents

For the first experiment, we performed what essentially amounted to a positive control to ensure that we can detect changes in the s-$GABA_A$R current amplitude. Specifically, we checked if s-$GABA_A$Rs were sensitive to the cation Zinc (Zn^{2+}), an allosteric antagonist of all $GABA_A$Rs (263,560). The potency of Zn^{2+}-mediated antagonism of GABA-gated currents has been shown to vary across different $GABA_A$R subtypes: αβ receptors show high sensitivity to Zn^{2+} inhibition (561–563), αβδ and αβε receptors show intermediate sensitivity (336,350,564), whereas αβγ generally show weak sensitivity (561–563). However, this is not always the case, for instance Brown *et al,* 2002 showed that α4β3δ and α4β3γ2 receptors were equally sensitive to Zn^{2+}(248). Most pertinent to the present thesis, Zn^{2+} can inhibit the spontaneous activity of $GABA_A$Rs (233,336,350). Application of 100 μM Zn^{2+} has been previously shown to partially inhibit native s-$GABA_A$R currents in hippocampal pyramidal cells (233), and the spontaneous activity of recombinant $GABA_A$Rs in HEK293 cells (α1β1γ2 and α1β3γ2) (233) and L929 cells (α1β1ε and α1β3ε) (336,350). Because Zn^{2+} acts via allosteric sites (one at the N-terminal α-β subunit interface and another within the ion channel (561), it means that Zn^{2+} can inhibit the $GABA_A$Rs even when the orthosteric site is occupied by a competitive antagonist (e.g. SR).

To test if Zn^{2+} can block s-$GABA_A$R activity in DGGCs, we exposed neurons (N=6) to 100 μM Zn^{2+} and then to SR→SR+PTX (**Fig.4.1A+B**). In line with the previous report by McCartney *et al* recording from CA1 pyramidal neurons (233), we found that PTX sensitive currents were smaller in the presence of Zn^{2+} (8.5 ± 1.0 pA; "Zn^{2+}+SR"→""+PTX) compared to in CTRL conditions (12.45 ± 0.79 pA; SR→SR+PTX). This represented a significant (Unpaired Student's t-test, $t_{(11,5)}$= 3.04 P = 0.0089), 32% reduction in the amplitude of the s-$GABA_A$R-mediated tonic current (**Fig.4.1**). Thus, Zn^{2+} is able to partially inhibit s-$GABA_A$R activity. This effect was also apparent in the small (3.26 ± 1.15 pA), but significant, outward shift in holding current that supersedes the addition of Zn^{2+} (Paired Student's t-test, $t_{(5)}$= 2.56; P= 0.048). As an aside, Zn^{2+} has been shown to have the opposite effect on GlyRs, in that it positively modulates their currents (233,565). Hence, the inhibitory effect of Zn^{2+} on the SR-resistant PTX-sensitive current further corroborates the report by Wlodarczyk *et al,* that GlyRs are not contributing to

this current. The authors showed that SR-resistant tonic currents are unaltered by strychnine, the GlyR antagonist that blocks spontaneous GlyR openings and is included in the 'blocking cocktail' in this study (566).

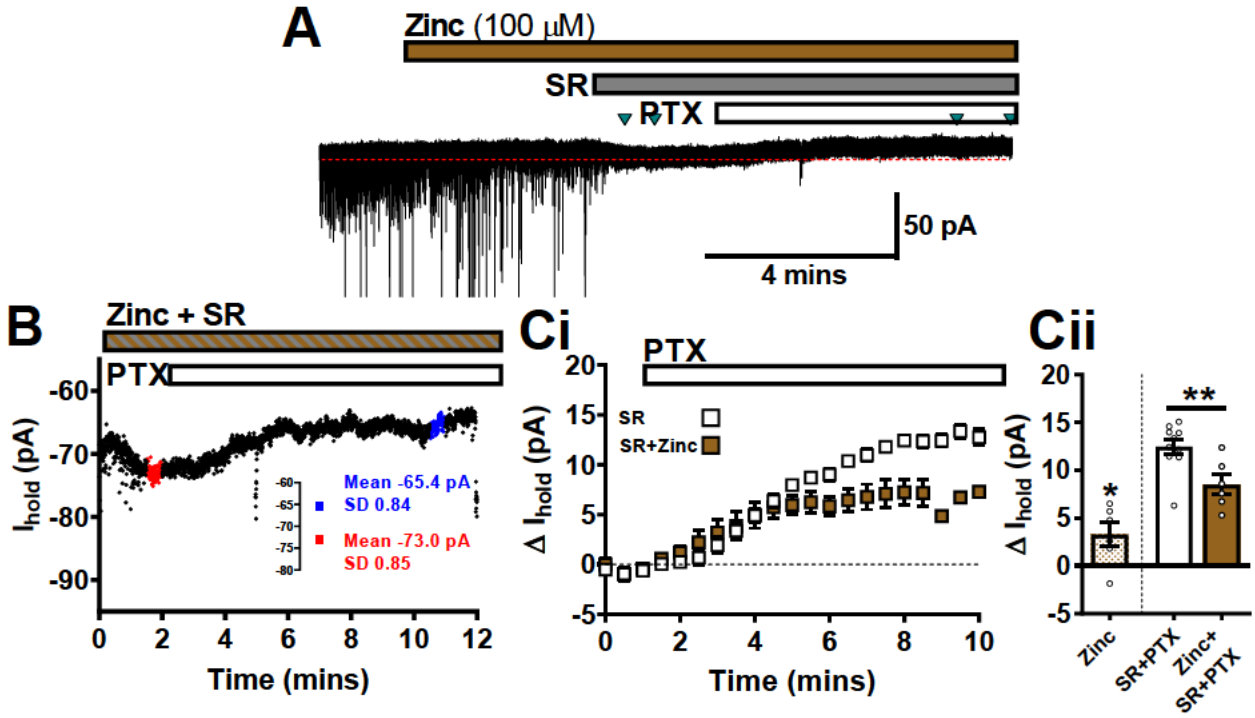

Fig.4.1. s-GABA$_A$R tonic currents in DGGCs are partially inhibited by Zinc.
A) Example WC-voltage clamp trace (-70 mV; CsCl) from a neuron exposed to Zinc (100 µM), and then SR→SR+PTX. The tonic current blocked by PTX in this example was 7.6 pA as shown in the current-time plot in **B)** (sampled at 4 Hz using 5 ms epochs). **Ci)** Average ΔI_{hold}-time plots, taken at 30 seconds epochs, shows that pre-exposure to Zinc (brown squares; N=6) decreases the outward current compared to SR+PTX only (white squares; N=10). **Cii)** Summarises this significant reduction in mean tonic current caused by zinc: SR→PTX (12.45 ± 0.8 pA) and Zinc→SR→PTX (8.5 ± 1.0 pA) and the significant outward current induced by zinc (3.26 ± 1.15 pA). Data are means ± S.E.M. Stats: Paired and Unpaired t-test.

4.5.2 DS2 does not affect the amplitude of s-$GABA_A$R tonic currents

$GABA_A$Rs containing the δ-subunit, primarily the α4β2δ isoform, are responsible for generating the majority of the GABA-dependent tonic currents in DGGCs (179,254,351,352,546). Wlodarczyk *et al* provided evidence, using δ-subunit knockout mice, that these same receptors also generate a significant (~60%) portion of the GABA-independent s-$GABA_A$R tonic current in mouse DGGCs (74); this aligns well with their reported spontaneous openings in certain recombinant expression systems (371–377). The spontaneous activity of δ-subunit-containing receptors is enhanced by DS2 (0.1 – 10 μM), a positive allosteric enhancer that binds at a site distinct from the orthosteric site (374,377). We therefore tested if DS2 could increase GABA-independent tonic currents (**Fig.4.2**). As a first step, we assessed the effect of 3 μM DS2 in the absence of SR (i.e. with GABA-dependent signalling intact) and showed that application of DS2 generates inward tonic current of -7.8 ± 0.43 pA (N=5) (**Fig.4.2A-Ci**), which represents a significant shift in holding current relative to baseline, measured prior to DS2 (CTRL vs DS2 Paired Student's t-test $t_{(4)}$= 18.1; P < 0.0001) and also relative the small inward current induced by SR that was reported in Chapter 3.5.1 (SR vs DS2: Unpaired Student's t-test $t_{(11,4)}$= 4.33; P = 0.0006).

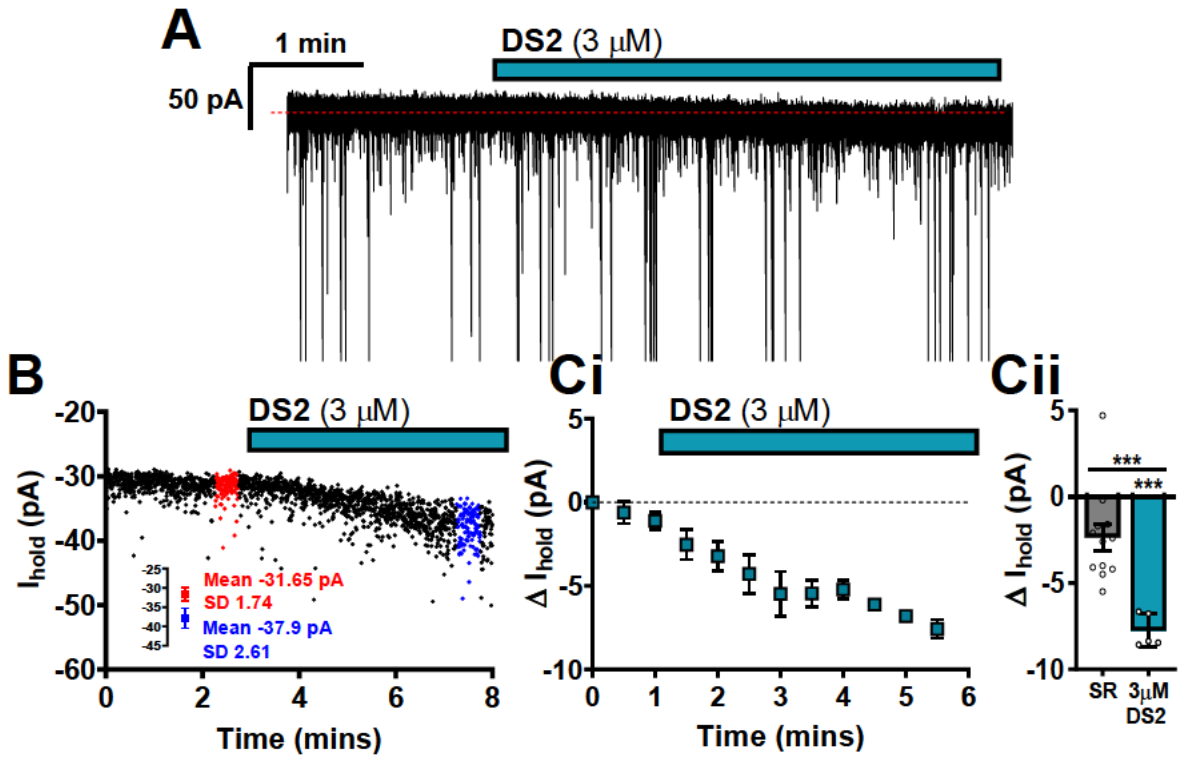

Fig.4.2. DS2 generates inward currents in the absence of SR.
A) Example WC-voltage clamp trace (-70 mV; CsCl) from a neuron exposed to 3 μM DS2. The inward current activated by DS2 in the example trace was -6.25 pA as shown in the current-time plot in **B)** (sampled at 4 Hz using 5 ms epochs). **Ci)** Average ΔI_{hold} -time plots, taken at 30 seconds epochs, shows that 3 μM DS2 (light cyan squares; N=5) produces inward currents. **Cii)** Summarises the amplitude of this current (CTRL→DS2; -7.8 ± 0.43 pA), and compares it to those induced by SR (CTRL→SR;-2.4 ± 0.8 pA), which are significantly smaller. Data are means ± S.E.M. Stats: Unpaired t-test (SR vs DS2) and paired t-test (baseline CTRL vs DS2).

Although DS2 can enhance the spontaneous activity of δ-$GABA_A$Rs (374,377), it also increases the potency (decreased EC_{50}) and the efficacy (maximal response) of GABA at these receptors (377), and has been shown to potentiate GABA-dependent tonic currents induced by 1 µM GABA in DGGCs (567). Thus, the DS2-induced inward current in **Fig.4.2** could be due to 1) potentiation or recruitment of a previously undetectable GABA-activated tonic current carried by δ-$GABA_A$Rs and/or 2) augmentation of their constitutive activity. We tested these possibilities by co-applying 3 µM DS2 with SR to remove any GABA-dependent component **Fig.4.3C**.

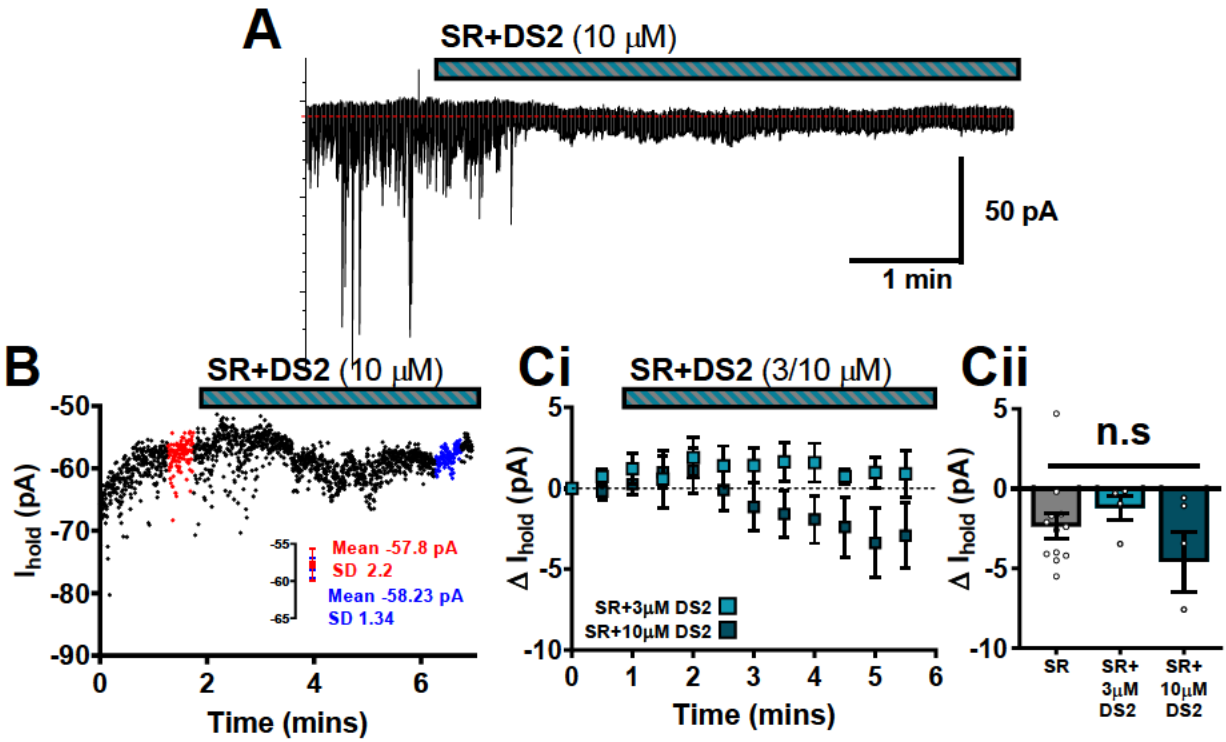

Fig.4.3. Inward currents are not observed when DS2 is co-applied with SR.
A) Example WC-voltage clamp trace (-70 mV; CsCl) from a neuron exposed to 10 µM DS2+SR. No significant inward currents are observed when DS2 is co-applied with SR. The change in holding current in this trace is 0.43 pA ,as shown in the current-time plot in **B)** (sampled at 4 Hz using 5 ms epochs). **Ci)** Average ΔI_{hold}-time plots, taken at 30 seconds epochs, shows that 3 µM DS2+SR (light cyan squares; N=4) and 10 µM DS2+SR (dark cyan squares; N=5) do not generate notable inward currents. **Cii)** Summarises the change in holding current (CTRL→3 µM DS2+SR; -1.21 ± 0.7 pA) and (CTRL→10 µM DS2+SR; -4.5 ± 1.8 pA) and compares it to those induced by SR (CTRL→SR;-2.4 ± 0.8 pA). With SR, neither concentration of DS2 generates significant changes in holding currents relative to baseline or SR. Data are means ± S.E.M. Stats: ANOVA (SR vs 3 µM DS2+SR vs 10 µM DS2+SR) and paired t-test (baseline CTRL vs 3/10 µM DS2+SR).

We found that with SR, DS2 could no longer generate significant inward currents, indicating that the DS2 effect in the absence of SR was GABA-dependent **Fig.4.3A-C**. The average current induced by 3 μM DS2+SR was -1.21 ± 0.7 pA (N=4), which is smaller than with DS2 alone (DS2 vs DS2+SR: Unpaired Student's t-test $t_{(4,3)}$=7.85; P=0.0001) and is not significantly different from the baseline before DS2+SR were added (CTRL vs. 3 μM DS2+SR: Paired Student's t-test $t_{(3)}$= 1.58; P=0.213) **Fig.4.3C.** We also tested if raising the concentration of DS2 could overcome this apparent block by SR **Fig.4.3A-C**. However, we found that even at 10 μM DS2+SR (N=5), the average change in baseline was -4.5 ± 1.8 pA, which is not significant compared to baseline (before adding DS2+SR) (CTRL vs. 10 μM DS2+SR: Paired Student's t-test $t_{(4)}$= 2.44; P=0.0712). That SR can block the inwards currents generated by SR was also demonstrated in the ANOVA of currents induced by SR vs. 3 μM DS2+SR vs. 10 μM DS2+SR (One-way, ANOVA, $F_{(2,18)}$ = 1.60; P= 0.229).

The inability of DS2 (3 or 10 μM) to generate inward currents in the presence of SR suggests that this compound is unable to modulate native s-$GABA_A$Rs in DGGCs, and is instead likely increasing the potency of GABA at δ-$GABA_A$Rs to produce a GABA-dependent tonic conductance. To confirm that DS2 does not modulate s-$GABA_A$Rs we exposed neurons to SR and 3/10 μM DS2 and then, in their continued presence, to PTX. We found that the s-$GABA_A$R current that is blocked by PTX is unchanged by the presence of DS2+SR: 3 μM DS2 (15.24 ± 2.53 pA; N=6) and 10 μM DS2 (10.25 ± 2.02 pA; N=5), relative to SR alone (12.45 ± 0.79 pA; N=10) (One-way, ANOVA, $F_{(2,18)}$ = 1.88; P= 0.181). Despite the ANOVA being >0.05, for the purpose of illustration, we also performed uncorrected t-tests to compare the means of each group with SR→PTX; this again showed that there was no detectable change in the s-$GABA_A$R tonic current with DS2: (3 μM DS2+SR→PTX vs. SR→PTX: Unpaired Student's t-test $t_{(9,5)}$=1.28; P=0.221) and (10 μM DS2+SR→PTX vs. SR→PTX: Unpaired Student's t-test $t_{(9,4)}$=1.22; P=0.241).

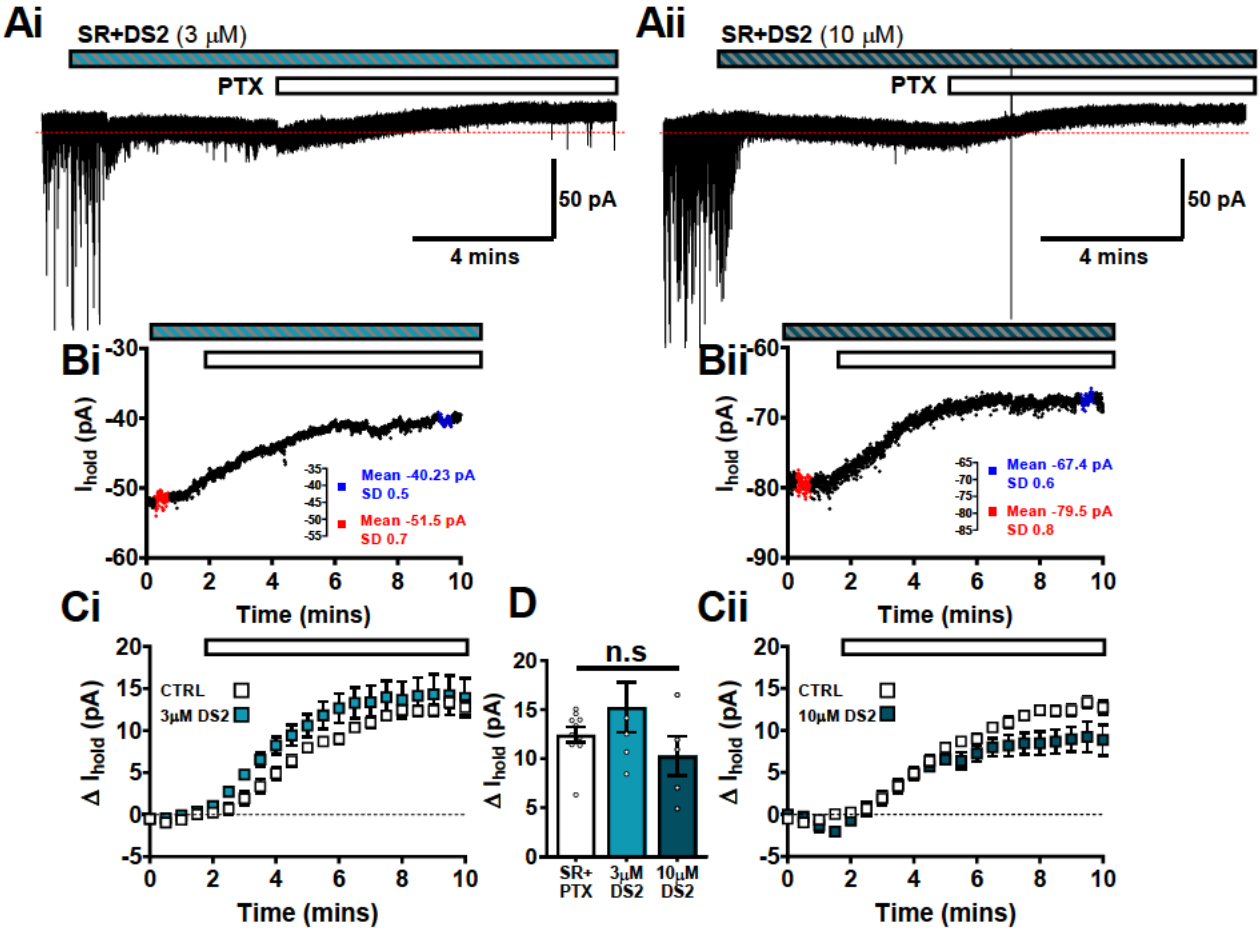

Fig.4.4. DS2 does not potentiate s-GABA$_A$R tonic currents.

Ai+ii) Example WC-voltage clamp traces (-70 mV; CsCl) from two neurons exposed to 3/10 μM DS2+SR, and then to PTX. The change in holding current caused by PTX in trace **Ai)** is 11.27 pA and in **Aii)** is 12.1 pA as shown in the respective current-time plot in **Bi+ii)** (sampled at 4 Hz using 5 ms epochs). Average ΔI_{hold}-time plots, taken at 30 seconds epochs, shows that the PTX sensitive current is similar in the presence of **Ci)** 3 μM DS2+SR (light cyan squares; N=6) and **Cii)** 10 μM DS2+SR (dark cyan squares; N=5), compared to in SR alone (white squares; N=10) **D)** Summarises the change in holding current induced by PTX with 3 μM DS2+SR (15.24 ± 2.53 pA), and 10 μM DS2+SR (10.25 ± 2.02 pA), and SR alone (12.45 ± 0.8 pA). Data are means ± S.E.M. Stats: ANOVA.

4.5.3 DPP-4-PIOL does not block s-GABA$_A$R tonic currents

We next explored if s-GABA$_A$R tonic currents could be fully or partially inhibited by DPP-4-PIOL, a novel mixed competitive and non-competitive antagonist that has a 3-fold higher potency for α4β3δ vs. α1β3γ2 receptor isoforms (548). Although DPP-4-PIOL has not been explicitly shown to block constitutive activity at δ-subunit-containing GABA$_A$Rs, the non-competitive component of its antagonism was shown to decrease the maximum response, by 60%, of α4β3δ receptors to GABA (548), indicating that the compound has a degree of negative efficacy. DPP-4-PIOL has an IC_{50} of 1 nM at α4β3δ expressed in *Xenopus oocytes* and at 2.3 nM was shown to inhibit >70% of the GABA (5 μM) activated tonic currents in DGGCs (IC_{50} for the tonic current was 0.87 nM) (268). If 1) δ-subunit containing GABA$_A$Rs open spontaneously to produce s-GABA$_A$R currents and 2) DPP-4-PIOL can inhibit these openings, then application of DPP-4-PIOL should induce an outward current analogous to those produced by PTX. We tested DPP-4-PIOL on both GABA-dependent and GABA-independent tonic current (**Fig.4.5**). For GABA-dependent tonic currents, neurons were perfused with 5 μM GABA, which activates an inward current of 44.4 ± 8.5 pA (n=4), and then we applied DPP-4-PIOL over a concentration range of 1,3 and 10 nM (N=5); this experiment is analogous to that previously reported (268).

Unfortunately, in contrast to previous reports, we were unable to detect any significant outward currents in the presence of DPP-4-PIOL, reflecting an apparent inability to block GABA-dependent tonic currents in our preparation (**Fig.4.5A-B**). To make sure a persistent leak current was not obscuring a small outward current we measured the change in holding current relative to the previously applied concentration of DPP-4-PIOL (or in the case of 1nM DPP-4-PIOL, relative to GABA baseline), but we were still unable to detect any consistent outward current at any concentration of DPP-4-PIOL (**Fig.4.5C**). Nevertheless, we repeated our experiment in the absence of GABA to test if a portion the s-GABA$_A$R tonic current could be blocked by DPP-4-PIOL over a concentration range of 1, 3, 10 and 30 nM (**Fig.4.5D+E**). However, we were, again, unable to detect any notable outward currents at any of the concentrations (N=8) (**Fig.4.5F**). This indicates that DPP-4-PIOL cannot block the GABA-independent tonic currents that are mediated by s-GABA$_A$Rs.

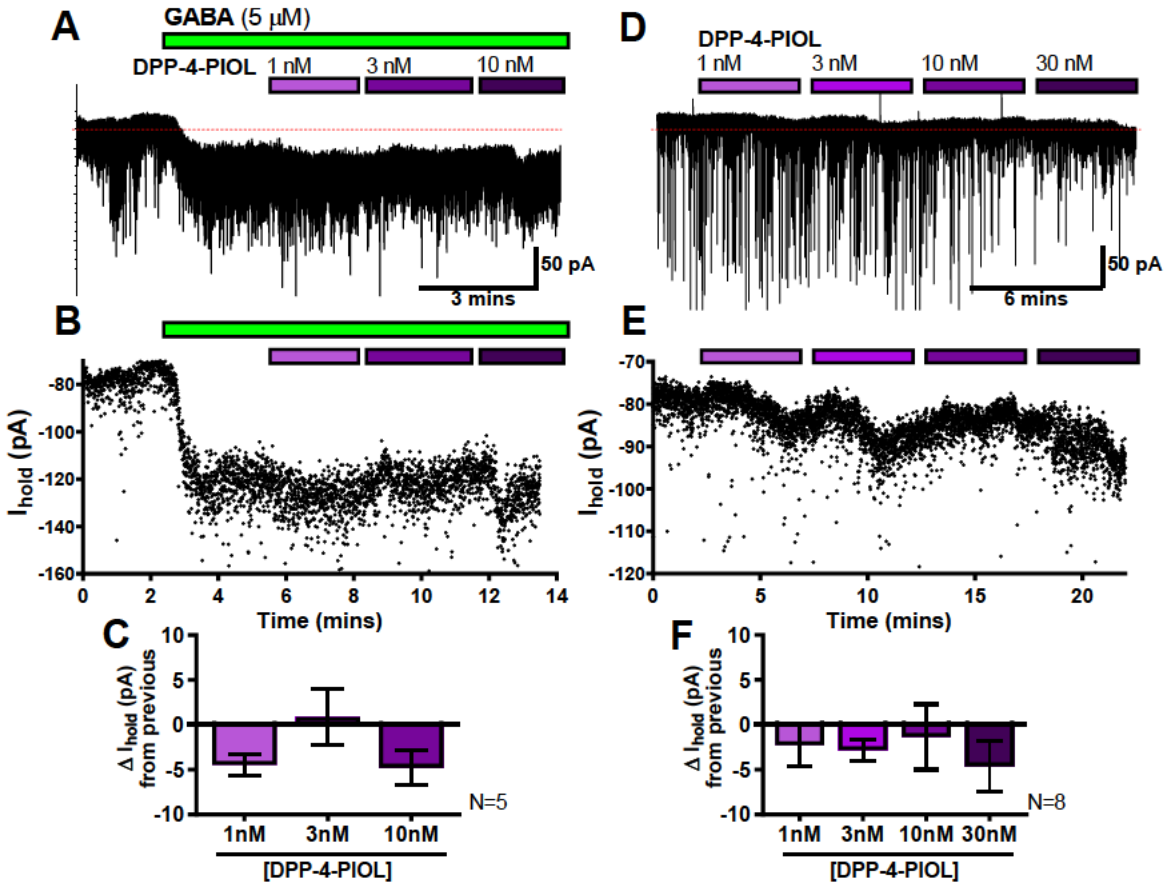

Fig.4.5 DPP-4-PIOL does not block s-GABA$_A$R tonic currents.
Example WC-voltage clamp traces (-70 mV; CsCl) from two neurons, **A)** exposed to 5 µM GABA and then DPP-4-PIOL (1, 3, 10 nM); and **D)** exposed to DPP-4-PIOL only (1, 3, 10, 30 nM). **B)** Current-time plot from the above trace (sampled at 4 Hz using 5 ms epochs) shows that there is no clear block of GABA-dependent tonic currents over the concentration range of DPP-4-PIOL. Similarly the current-time plot in **E)** shows the lack of any notable block of GABA-independent currents. **C+F)** summarise the average change in holding current induced by increasing concentrations of DPP-4-PIOL measured relative to the previously applied concentration of the drug (or in the case of 1nM DPP-4-PIOL, relative to GABA or CTRL).

4.5.4 L-655,708 partially inhibits GABA-dependent tonic currents but not s-$GABA_AR$ currents

Because we found that two ligands that target the δ-$GABA_A$Rs (DS2 and DPP-4-PIOL) were ineffective at modulating the s-$GABA_A$R tonic current, we turned our attention to the α5-$GABA_A$Rs. We hypothesised that $GABA_A$Rs containing the α5-subunit are also spontaneously opening and mediate a portion of the s-$GABA_A$R current (i.e. corresponding to the s-$GABA_A$R current that persists in δ-subunit knockout mice). This is in line with α5-$GABA_A$Rs producing ~30% of the GABA-dependent tonic currents activated by 5 μM GABA (351). Also supporting the involvement of α5-$GABA_A$Rs in generating a portion of the s-$GABA_A$R tonic current is Botta *et al*'s publication. They showed 1) that s-$GABA_A$Rs generate GABA-independent tonic currents in PKCδ positive neurons of the central amygdala, and 2) that these tonic currents could be significantly reduced using α5-subunit selective inverse agonists (L-655,708 and PWZ-029) or by knocking out the α5-subunit (*Gabra5−/−*). We used L-655,708, an imidazo[1,5-α]benzodiazepine that binds to the benzodiazepine (BDZ)-site and functions as a selective, partial inverse agonist at α5-$GABA_A$Rs (568–570); its intrinsic negative efficacy means that it can inhibit ~20% of EC_{20} GABA responses. L-655,708 was used by Botta *et al* to block s-$GABA_A$R currents and has also been shown to block GABA-dependent tonic currents in DGGCs (88,351), CA1 pyramidal cells (351), and a host of other neurons. The concentration we used (20 μM), is within the range of that previously used by Botta *et al* to block s-$GABA_A$R tonic currents: [50 nM, 5 μM, and 50 μM]; and by Scimemi *et al:* [50 μM] (571) and Caraiscos *et al:* [5 – 50 μM] to block GABA-dependent tonic currents (572).

As a first step, and as a positive control, we confirmed that L-655,708 blocks tonic currents activated by 5 µM GABA (**Fig.4.6**). The addition of L-655,708 in the presence of GABA resulted in an outward current of 10.16 ± 2.83 pA (n=5) (**Fig.4.6B+C**), which is significant compared to baseline with GABA only (Paired Student's t-test $t_{(4)}$= 3.59; P=0.0231). The amplitude of this outward current corresponds to 23% of the inward current that is elicited by 5 µM GABA (44.4 ± 8.5 pA; N=4), which is in line with previous reports (351).

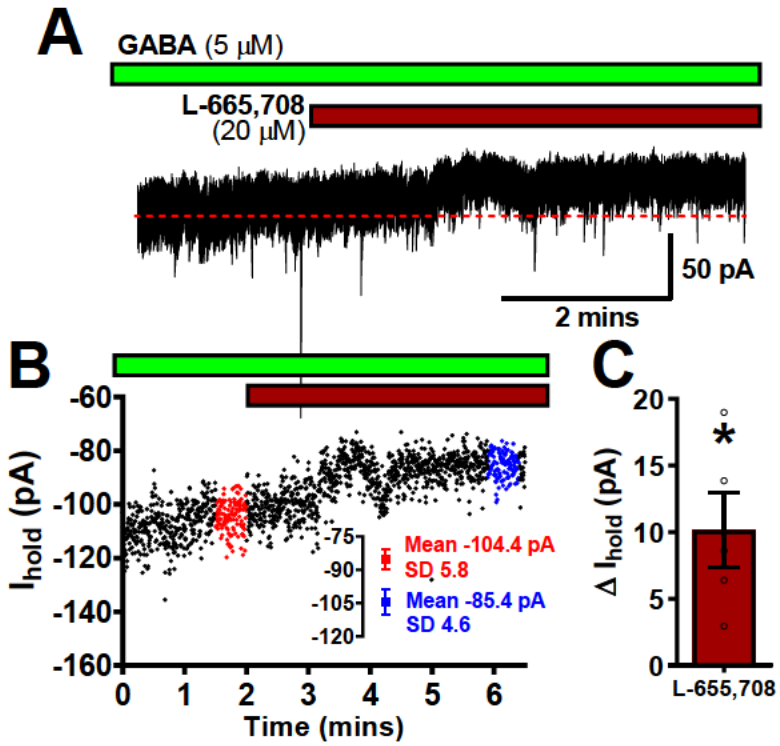

Fig.4.6. L-655,708 partially blocks GABA-dependent tonic currents.
A) Example WC-voltage clamp trace (-70 mV; CsCl) from a neuron with GABA (5 µM)-activated tonic currents exposed to 20 µM L-655,708 **B)** Current-time plot from the above trace (sampled at 4 Hz using 5 ms epochs) shows that L-655,708 causes an 19 pA outward current, reflecting a partial block of GABA-dependent tonic currents. **C)** Summarise the average change in holding current (10.16 ± 2.83 pA) induced by L-655,708 (N=5). Mean± S.E.M. Stats: Paired t-test.

We next assessed if L-655,708 could also block GABA-independent s-$GABA_AR$ tonic currents (**Fig.4.7A+B**). To do this we applied 20 µM L-655,708, and then SR, and then PTX. The s-$GABA_AR$, PTX-sensitive tonic current was 13.42 ± 1.6 pA (N=7), which is not significantly different from the SR→PTX current in the absence of L-655,708 (12.45 ± 0.79 pA; N=10), (L-655,708+SR→PTX vs SR→PTX: Unpaired Student's t-test $t_{(9,6)}$=0.599; P= 0.558) (**Fig.4.7C**). Further supporting the lack of effect of L-655,708 on the s-$GABA_AR$ current is that L-655,708 does not induce significant outward currents relative to baseline before L-655,708 was added (0.29 ± 1.0 pA; N=7) (CTRL→L-655,708: Paired Student's t-test, $t_{(6)}$= 0.29; P= 0.7744 (**Fig.4.7Cii**).

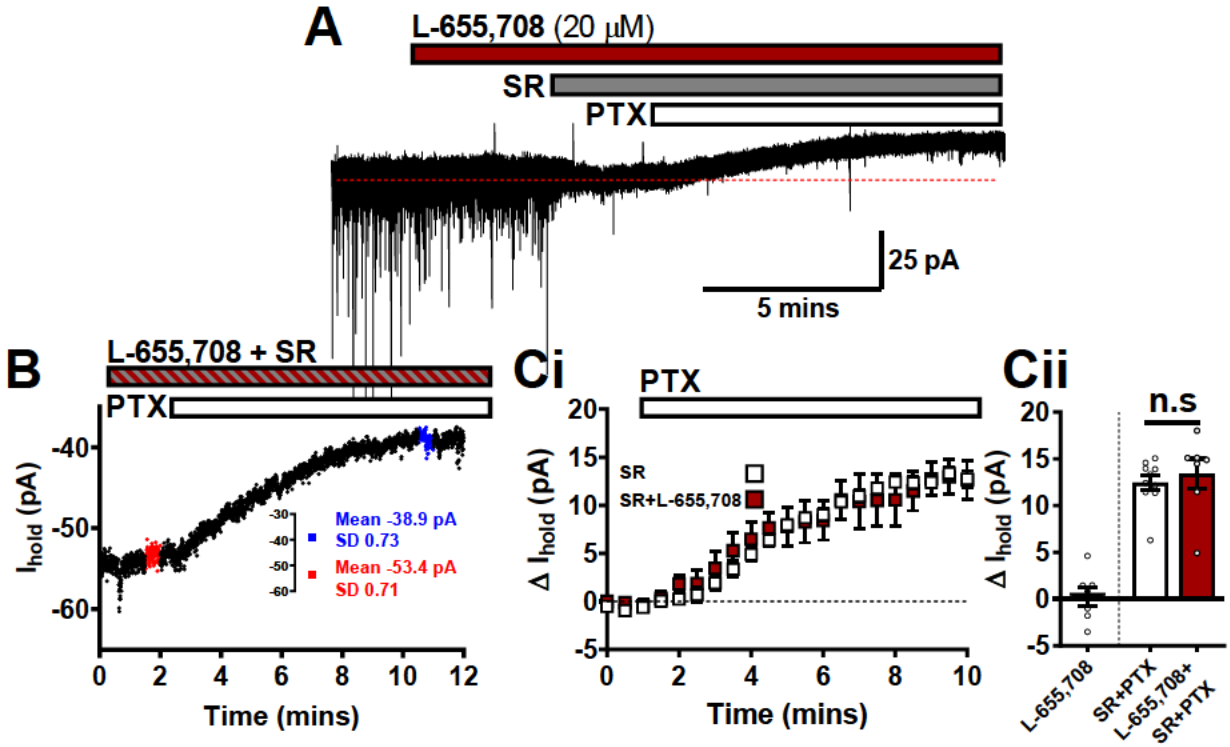

Fig.4.7. L-655,708 does not inhibit s-$GABA_AR$ tonic currents.
A) Example WC-voltage clamp trace (-70 mV; CsCl) from a neuron exposed to L-655,708 (20 µM), and then SR→SR+PTX. The tonic current blocked by PTX in this example was 14.5 pA as shown in the current-time plot in **B)** (sampled at 4 Hz using 5 ms epochs). **Ci)** Average ΔI_{hold}-time plots, taken at 30 seconds epochs, shows that pre-exposure to L-655,708 (red squares; N=7) does not affect the outward current compared to SR+PTX only (white squares; N=10). **Cii)** Summarises the mean tonic current caused by: SR→PTX (12.45 ± 0.8 pA) and L-655,708+SR→PTX (13.42 ± 1.6 pA) and the negligible change in holding current caused by L-655,708 alone (0.29 ± 1.0 pA). Data are means ± S.E.M. Stats: Paired and Unpaired t-test

4.5.5 Benzodiazepine-site ligands modulate s-$GABA_AR$ tonic currents

So far, the only compound that we have found that affects the s-$GABA_AR$ tonic current is Zn^{2+}; modulators acting at δ-$GABA_ARs$ (DS2, DPP-4-PIOL) and α5-$GABA_ARs$ (L-655,708) have proved ineffective. Although L-655,708 interacts with the BDZ-site and has no effect on the s-$GABA_AR$ current, we tested if other BDZ-site ligands, which target other receptor isoforms, could modulate s-$GABA_ARs$.

The canonical high-affinity BDZ-site on the $GABA_AR$ is located within the receptor's extracellular domain, at the α+/γ- subunit interface, in an analogous position to the orthosteric (agonist recognition) sites, which form at the two β+/α- subunit interfaces (98,573). Diazepam and other classical BDZs have the highest affinity and efficacy at receptor isoforms containing α1/2/3/5 subunits in combination with β subunits and the γ2 subunit (BDZ sensitive isoforms), but can also interact, albeit often with a lower affinity/efficacy, with isoforms that incorporate the γ1 or γ3 subunits (551,552). Importantly, α4/6βδ receptor isoforms are generally classed as BDZ-insensitive receptors (553–557). At high concentrations, however, BDZs can also bind and modulate $GABA_ARs$ through lower affinity 'non-canonical' BDZ-sites (98,574–576).

Ligands for the canonical BDZ-site are traditionally (and often exclusively) characterised in reference to their impact on agonist-/partial agonist-evoked responses, be it macroscopic responses (whole-cell current amplitudes), or microscopic responses (frequency of single channel openings), see Sieghart and Savić, 2018 for a comprehensive review (104). Briefly, and with reference to the compounds used in this section, BDZ-site agonists (**diazepam, zolpidem** and **midazolam**) function as $GABA_AR$ positive allosteric modulators: they increase the apparent GABA binding affinity and enhance responses to *non-saturating* concentrations of GABA. This reflects an increase in GABA potency (because the [GABA]-response curve is shifted to the left, i.e. EC_{50} is decreased), but not efficacy (because the maximal response is not increased) (198,203,573,577). BDZ-site agonists are also able to increase the apparent binding affinity and enhance responses to *saturating* concentrations of *partial* agonists (decreasing EC_{50} and increasing the maximal response) (198,203,573). BDZ-site inverse agonists (**DMCM**) function as $GABA_AR$ negative allosteric modulators, reducing the apparent binding affinity and

decreasing electrophysiologic response of the receptor to GABA and partial agonists (198,203,573). BDZ-site competitive antagonists (**flumazenil**) function as null/neutral modulators, meaning that they block the effects of BDZ-site agonists/inverse agonist without affecting the apparent binding affinity or responsiveness of the receptor to GABA and partial agonists (198,203,573).

BDZ-site agonists were originally posited to potentiate GABA responses by increasing the affinity of GABA binding at the orthosteric sites (578,579); however, contemporary research consistently favours an alternative view: that BDZ-site ligands shift the equilibrium between receptor states that link channel shutting and opening (196,198,199,203–205,260,580,581). The exact mechanism for this has not been fully resolved, with some studies inferring that BDZ-site agonists increase the actual efficacy of gating (i.e. shifts the final equilibrium between shut and open states) (196,198,260,580). And other studies convincingly demonstrate that BDZ-site agonists shift the equilibrium between the resting shut states and preactivated (flipped) states – the latter describes the state that immediately precedes channel gating/opening (203–205). Other studies have also posited that intermediate states (581) and/or desensitised states (205) might also be involved in BDZ-site $GABA_AR$ modulation

One of the key experimental findings that evidenced in favour BDZ-site ligands modulating the equilibrium of state transitions was that BDZ-site ligands affect the spontaneous activity of recombinant wild-type α1β2γ2L (198,205) and mutant α1β2γ2L/S receptors (196,198,199,205,260). The same is also true for BDZ-site ligands acting on spontaneously opening recombinant wild-type α1β1γ2L (233) and α1β3γ2L receptors (233,369). *These findings are of direct importance for the present thesis.*

First, they show that the wild-type α1β2γ2 isoform, the most abundant and widespread $GABA_AR$ in the brain, can open spontaneously in the absence of an agonist and, thus, along with α1β1γ2 and α1β3γ2 isoforms, can be considered a potential candidates for producing some or all of the s-$GABA_AR$ current. *Second,* they show that BDZ-site ligands can bi-directionally affect the constitutive activity of spontaneously opening $GABA_ARs$ and thus may be able to affect the s-$GABA_AR$ tonic current in DGGCs.

This results section aimed to test if BDZ-site ligands can modulate s-$GABA_AR$ tonic currents in line with what would be predicted from their effect on recombinant receptors. If this does turn out to be the case, it will evidence that a portion of the GABA-independent tonic inhibition is produced by $GABA_AR$ isoforms that have the canonical BDZ-site. The BDZ-site ligands that we used in this section have all been shown to modulate the spontaneous activity of wildtype and/or mutant α1β2γ2 receptors. The BDZ-site agonists, **diazepam** (196,198,199), **zolpidem** (199,260) and **midazolam** (196), all increase spontaneous receptor activity. The BDZ-site inverse agonist, **DMCM**, decreases spontaneous receptor activity (198,260). **Flumazenil** can be used to antagonise the action of BDZ-site agonists and inverse agonists (196,199) but is actually a very low-efficacy BDZ-site partial agonist (196,199).

To put simply the experimental approach used in this section: if BDZ-site agonists potentiate s-$GABA_AR$ tonic currents in DGGCs, they should generate an inward tonic current that is resistant SR *and*, as a result, increase the amplitude of the PTX-induced outward current. Similarly, if BDZ-site inverse agonists inhibit s-$GABA_AR$ tonic currents, they should cause an outward current that is unaffected by SR and also reduce the amplitude of the PTX-induced outward current. The logic of this approach has been validated experimentally in studies that have demonstrated that the spontaneous currents that are potentiated by BDZ-site agonists are resistant to competitive antagonism by SR (199), but are inhibited by PTX (205). This is also entirely in line with the pharmacology of SR and PTX. SR only exhibits a small amount of negative efficacy and does not compete with ligands binding at the BDZ-site; conversely, PTX acts as an allosteric inverse agonist by binding within the channel and stabilising the receptor in a closed state.

There is already some evidence that suggests that in neurons, BDZ-sensitive $GABA_AR$ isoforms spontaneously open to generate GABA-independent tonic currents. The clearest indication of this was provided by McCartney *et al*, who originally characterised s-$GABA_AR$ tonic currents in pyramidal neurons (233). They showed that in these cells, flunitrazepam (1 μM), a BDZ-site agonist, potentiates s-$GABA_AR$-mediated tonic currents in a manner that is resistant to SR. They went further and also showed that recombinant wild-type α1β1γ2 and α1β3γ2 isoforms, both of which have the canonical BDZ-site, open spontaneously and exhibit a pharmacological

profile that is strikingly similar to the GABA-independent s-$GABA_AR$ tonic currents that were recorded from pyramidal neurons (233). In further support of this, not only have all three of the BDZ-site agonists tested in this section – diazepam (360,582,583), zolpidem (269,303,550), and midazolam (269,270,522) – been shown to potentiate $GABA_AR$ tonic currents, in some instances (269,270,303,522,550) they potentiate tonic currents in a manner that is resistant block by SR, but sensitive to bicuculline/PTX – the pharmacological 'finger-print' of s-$GABA_AR$ tonic currents.

4.5.6 Diazepam does not modulate s-GABA$_A$R tonic currents

We first tested if diazepam, a BDZ-site agonist, could potentiate s-GABA$_A$R-mediated tonic currents (**Fig.4.8**). We used 1 μM diazepam in this set of experiments. At this concentration, diazepam is able to potentiate the spontaneous openings of wildtype and mutant α1β2γ2 (196,198,199) and α1β3γ2 (369) receptor isoforms; it is also able to potentiate the tonic currents (presumed to be GABA-dependent) in sympathetic pre-ganglionic neurons (360), CA3 (582) and CA1 pyramidal neurons (583). When used at 1 μM diazepam has the greatest potentiating effect (highest efficacy) on EC_3 GABA responses generated by α3βγ2 receptors, but also strongly (>3 fold) potentiates α2βγ2, α1βγ2 and α5βγ2 receptor isoforms (549).

First, we exposed neurons (N=4) to 1 μM diazepam and observed a small inward holding current (-5.7 ± 1.0 pA), which was not blocked by the subsequent addition of SR (-8.4 ± 3.1 pA) (**Fig.4.8A-C**); this diazepam+SR current was significantly larger than SR alone (-2.4 ± 0.8 pA) (SR vs SR+diazepam: Unpaired Student's t-test $t_{(11,3)}$= 2.78; P = 0.0146), indicating that this current is to a significant degree GABA-independent (**Fig.4.8A-C**). To confirm this, we then exposed neurons to PTX in the continued presence of diazepam+SR to see if the s-GABA$_A$R tonic currents were enhanced (N=6; 4+ 2 neurons that were already exposed to diazepam just before recording commenced) (**Fig.4.8A+D+E**). The s-GABA$_A$R, PTX-sensitive tonic current in the presence of diazepam was 14.05 ± 1.0 pA, which is not significantly different from the control SR→PTX current (12.45 ± 0.79 pA; N=10), (Diazepam+SR→PTX vs SR→PTX: Unpaired Student's t-test $t_{(9,5)}$=1.243; P= 0.2345) (**Fig.4.8E)**. The lack of effect of diazepam on the PTX-mediated s-GABA$_A$R may reflect a lack of BDZ-sensitive isoforms in the s-GABA$_A$R pool; alternatively, it may be that diazepam is not efficacious enough at increasing spontaneous activity. To test this, we will use zolpidem (199) and midazolam at (196), both of which are more efficacious than diazepam at potentiating spontaneous currents.

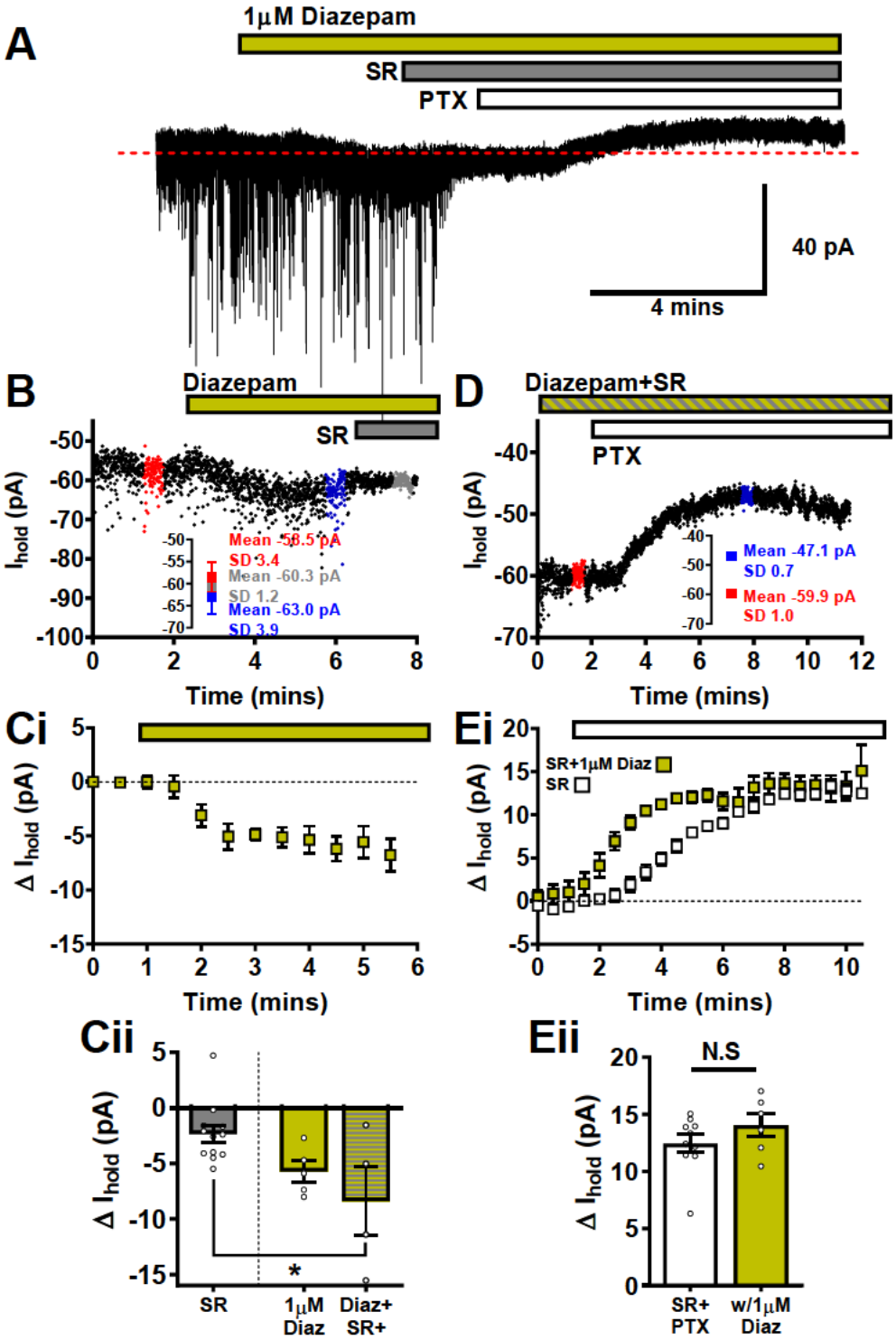

Fig.4.8 Diazepam does not modulate s-GABA$_A$R tonic currents.

A) Example WC-voltage clamp trace (-70 mV; CsCl) from a neuron exposed to diazepam (1 µM), and then SR→SR+PTX. Diazepam activates inward currents; the inward current in this example is -4.5 pA and is only partially blocked by SR as shown in the current-time plot in **B)** (sampled at 4 Hz using 5 ms epochs). **Ci)** Average ΔI_{hold}-time plots, taken at 30 seconds epochs, shows that diazepam (yellow squares; N=4) induces inward currents; the average amplitude is summarised in and **Cii)** (Diaz=-5.7 ± 1.0 pA)(Diaz+SR=-8.4 ± 3.1 pA) compared to in SR alone (-2.4 ± 0.8 pA). Subsequent addition of PTX blocks s-GABA$_A$R currents. The amplitude of this trace in this example was 12.8 pA as shown in the current-time plot in **D). Ei)** Average ΔI_{hold}-time plot shows that pre-exposure diazepam (yellow squares; N=6) does not affect the outward current compared to SR+PTX only (white squares; N=10). **Eii)** Summarises the mean tonic current caused by: SR→PTX (12.45 ± 0.8 pA) and Diaz+SR→PTX (14.05 ± 1.0 pA). Data are means ± S.E.M. Stats: Unpaired t-test.

4.5.7 Zolpidem potentiates s-$GABA_AR$ tonic currents

We next explored if zolpidem could enhance s-$GABA_AR$-mediated tonic currents (**Fig.4.9**). Zolpidem is not chemically a benzodiazepine, it is an imidazopyridine, but it binds to the BDZ-site where it functions as an agonist; importantly, it has been shown to enhance spontaneous α1β2γ2 receptor currents (199,260) and does so with greater efficacy than diazepam (199). Zolpidem has a ten-fold higher apparent affinity and 5-8 times higher potency for α1β3γ2 receptors compared to α2β3γ2 or α3β3γ2 receptors (549). This has led some to characterise zolpidem as an α1-subunit-specific modulator (104); however, zolpidem has a higher efficacy for potentiating α2β3γ2 and α3β3γ2 receptors, than α1β3γ2. As a result, at concentrations >50 nM, zolpidem loses its α1-subunit specificity (549). A notable feature of zolpidem is that it has an ultra-low apparent affinity and efficacy at α5-subunit-containing receptors (549), meaning that any potentiation of the s-$GABA_AR$ tonic current will not be due to α5-$GABA_ARs$, nor the traditional BDZ-insensitive α4- and α6-receptors (549). Zolpidem has been shown to increase tonic currents in layers II/III and V pyramidal somatosensory pyramidal neurons (269), dorsal motor nucleus neurons of the vagus (550) and fast-spiking interneurons in the motor cortex (303). The latter two studies are of specific relevance to the study of s-$GABA_ARs$ (303,550). In neurons in the dorsal motor nucleus of the vagus, zolpidem potentiated tonic currents are partially insensitive to SR – a hallmark of s-$GABA_ARs$ (550). In fast-spiking interneurons in the motor cortex, there is evidence that zolpidem is potentiating tonic currents by altering gating kinetics to stabilise the receptor in a spontaneously open (unbound) receptor state (303). Zolpidem is able to enhance spontaneous openings of recombinant α1β2γ2 receptors when used at a concentration of 1 μM (199,260); in our experiments we opted for 500 nM in order to try and mitigate any off-target effects of zolpidem acting through non-canonical BDZ-sites (584). Based upon the effect of zolpidem on GABA EC_3 responses, 500 nM zolpidem will be potentiating α1βγ2, α2βγ2 and α3βγ2 responses to an equal degree, with no effect on α5, α4, or α6 subunit-containing receptors (549). We assessed the impact of zolpidem on s-$GABA_AR$ tonic currents in an analogous fashion to experiments performed with diazepam: i.e zolpidem→zolpidem+SR→zolpidem+SR+PTX (N=6) (**Fig.4.9A**).

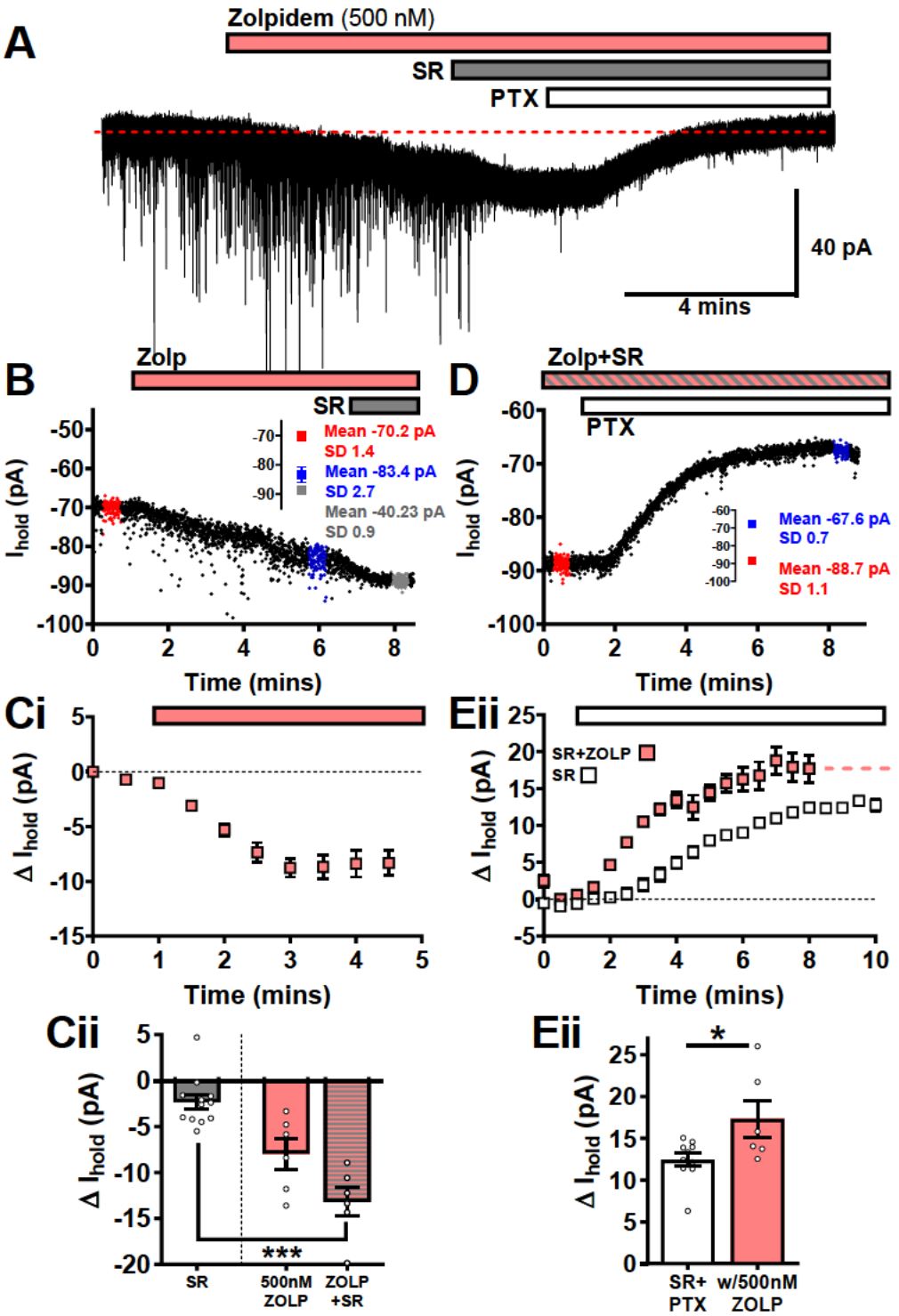

Fig.4.9 Zolpidem potentiates s-GABA$_A$R tonic currents.

A) Example WC-voltage clamp trace (-70 mV; CsCl) from a neuron exposed to zolpidem (500 nM), and then SR→SR+PTX. Zolpidem activates inward currents; the inward current in this example is -13.2 pA and is not blocked by SR, as shown in the current-time plot in **B)** (sampled at 4 Hz using 5 ms epochs). **Ci)** Average ΔI_{hold}-time plots, taken at 30 seconds epochs, shows that zolpidem (pink squares; N=6) induces inward currents; the average amplitude is summarised in and **Cii)** (ZOLP =-7.96 ± 1.66 pA)(ZOLP+SR =-13.22± 1.54 pA) compared to in SR alone (-2.4 ± 0.8 pA). Subsequent addition of PTX blocks s-GABA$_A$R currents. The amplitude of this trace in this example was 21.1 pA as shown in the current-time plot in **D). Ei)** Average ΔI_{hold}-time plot shows that pre-exposure zolpidem (pink squares; N=6) potentiates the outward current compared to SR+PTX only (white squares; N=10). **Eii)** Summarises the mean tonic current caused by: SR→PTX (12.45 ± 0.8 pA) and ZOLP+SR→PTX (17.32 ± 2.19 pA). Data are means ± S.E.M. Stats: Unpaired t-test.

As with diazepam, zolpidem induced inward currents (-7.96 ± 1.66 pA) that persisted in the presence of SR (-13.22 ± 1.54 pA) and were significantly larger than those reported for SR alone (-2.4 ± 0.8 pA) (SR vs SR+zolpidem: Unpaired Student's t-test $t_{(11,5)}$= 7.083; P < 0.0001) (**Fig.4.9A-C**). This increase in SR-resistant current translated into an increase in the PTX-sensitive s-$GABA_A$R tonic current (**Fig.4.9D+E**). The amplitude of outward current induced by PTX in the presence of zolpidem+SR was 17.32 ± 2.19 pA (N=6), which represents a significant, 39%, potentiation compared to control conditions (SR→PTX = 12.45 ± 0.79 pA; N=10). (zolpidem+SR→PTX vs SR→PTX: Unpaired Student's t-test $t_{(9,5)}$=2.492; P= 0.0259) (**Fig.4.9D+E**).

4.5.8 Zolpidem-mediated potentiation of s-GABA$_A$R tonic currents is blocked by flumazenil

Because zolpidem can act via non-canonical BDZ-sites (584), we wanted to ensure that the reported potentiation of s-GABA$_A$R was mediated through the canonical BDZ-site. To do this, we repeated the experiment in the presence of flumazenil, a very low efficacy BDZ-site partial agonist that is able to block the binding of BDZ-site full agonists, such as zolpidem, while exerting minimal effect on the receptor opening (196,199) (**Fig.4.10**). Flumazenil (10 µM) was applied after zolpidem+SR, but before PTX:

i.e. zolpidem→zolpidem+SR →"zolpidem+SR+flumazenil"→""PTX)

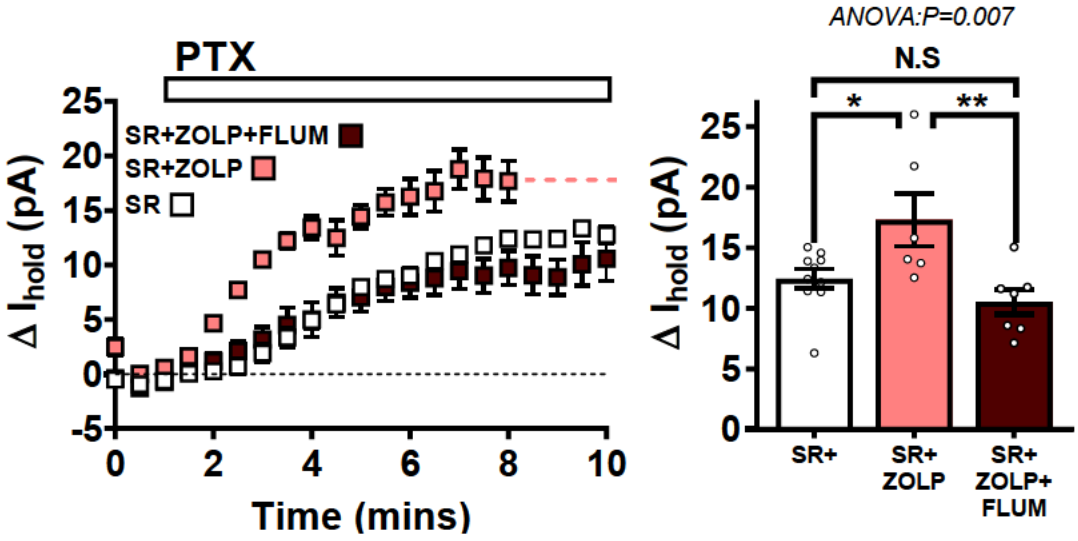

Fig.4.10 Flumazenil blocks the potentiation of s-GABA$_A$R tonic currents by zolpidem.
A) Average ΔI_{hold}-time plots, taken at 30 seconds epochs, shows that flumazenil (10 µM, dark purple squares; N=7) prevents zolpidem induced potentiation of s-GABA$_A$R tonic currents: potentiated tonic currents with ZOLP+SR→PTX (pink squares; N=6) compared to SR+PTX only (white squares; N=10). **B)** Summarises the mean tonic current caused by SR→PTX (12.45 ± 0.8 pA), ZOLP+SR→PTX (17.32 ± 2.19 pA), and FLUM+ZOLP+SR→PTX (10.53 ± 1.02 pA). Data are means ± S.E.M. Stats: ANOVA and Unpaired t-test.

In the presence of flumazenil (with zolpidem and SR) the PTX-induced outward current was 10.53 ± 1.02 pA (N=7) (**Fig.4.10A+B**). This is notably less with the PTX current with zolpidem+SR (17.32 ± 2.191 pA) but on par with that recorded with just SR (12.45 ± 0.79 pA; N=10) (**Fig.4.10A+B**). Performing an ANOVA revealed the effect of the three treatments on the PTX-sensitive current (one-way ANOVA: $F_{(2,20)}$ = 6.432; P=0.007); and Bonferroni corrected post-hoc test revealed that there was a specific effect of flumazenil: the outward current was significantly lower than with SR+zolpidem (Corrected unpaired Student's t-test $t_{(20df)}$=3.49; P= 0.0069), and not significantly different from the control PTX-sensitive current, in the presence of just SR (Corrected unpaired Student's t-test $t_{(20df)}$=1.113; P= 0.8369). In addition, the potentiation of the PTX-sensitive tonic current by zolpidem relative to control conditions (with just SR) was still present, even with the Bonferroni correction (Corrected unpaired Student's t-test $t_{(20df)}$=2.698; P= 0.0415). These findings demonstrate that the zolpidem is acting as a BDZ-site agonist to potentiate the SR-resistant, PTX-sensitive s-$GABA_A$R current.

The apparent potentiation of SR-resistant, PTX-sensitive s-$GABA_A$R tonic currents by zolpidem is an important finding – there are, however, multiple possible explanations. One explanation is that zolpidem is binding to the basal 's-$GABA_A$R pool' of already constitutively active receptors and augmenting their constitutive activity to generate larger GABA-independent currents. Another potential explanation is that zolpidem is recruiting additional $GABA_A$Rs, which are not typically spontaneously active, into the 's-$GABA_A$R pool' of receptors. We wanted to try and tease apart these possibilities. We reasoned that if BDZ-site agonists are potentiating receptors that are already constitutively active at rest, a BDZ-site inverse agonist should inhibit their activity; and that this should be detectable as a decrease in the amplitude of the s-$GABA_A$R tonic currents. Conversely, if s-$GABA_A$R tonic currents are not inhibited by BDZ-site inverse agonists, this would imply that 1) the basal pool of s-$GABA_A$Rs is BDZ-insensitive and 2) BDZ-site agonists potentiate GABA-independent currents by causing additional, otherwise non-constitutively active, receptors to spontaneously open. We used the BDZ-site inverse agonist, DMCM, to assess if we could decrease the constitutive activity of s-$GABA_A$Rs.

4.5.9 DMCM partially inhibits s-$GABA_AR$ tonic currents

The β-carboline DMCM is a BDZ-site full inverse agonist that has been shown to decrease spontaneous receptor activity of wild-type and mutant α1β2γ2 receptors (198,260). DMCM has a high level of negative efficacy in that it blocks 50-70% of EC_{20} GABA currents at α1-5β3γ2 receptors (585) – for comparison L-655,708, a BDZ-site partial inverse agonist, only blocks 20% (570). If DMCM is able to inhibit the tonic currents generated by the basal pool of s-$GABA_AR$s we would expect to see two things. First, DMCM should produce outward currents that are similar but smaller, perhaps 50—70%, to those produced by PTX in control conditions and that these currents should not be affected by the subsequent addition of SR. Second, the partial block of basal tonic currents should translate into a smaller PTX-mediated outward current. The sum of the DMCM and the PTX current with DMCM should be roughly equivalent to the total PTX-sensitive current in control conditions. We opted for 5 μM DMCM, a concentration that has been previously shown to near maximally inhibit $GABA_AR$ currents evoked by 5 μM GABA in histaminergic neurons (586); higher concentrations can lead to a potentiation of the response. The protocol was as follows: DMCM→DMCM+SR→DMCM+SR+PTX (N=9) (**Fig.4.11A**).

The effect of DMCM (5 μM) on holding current was mixed; in 4 of the 9 cells tested, we observed outward currents averaging 2.31 ± 1.30 pA. However, the remaining 5 cells displayed small inward currents averaging -2.53 ± 0.66 pA, meaning that overall there was no overall effect of DMCM on holding current = -0.38 ± 0.96 pA, N=9 (**Fig.4.11B+C**); this change of holding current is not significantly different from baseline before vs after DMCM: (Paired Student's t-test, $t_{(8)}$= 0.396; P= 0.702) or compared to the effect of SR alone (Unaired Student's t-test, $t_{(8,11)}$= 1.618; P= 0.1221). We did note, however, that the percentage of cells displaying outward currents following DMCM (44%), was higher than in cells just exposed to SR (8%; 1/12 cells tested). Based on the subsequent effect of DMCM on the PTX-sensitive s-$GABA_AR$ current, we suggest that a slow leak current, which tends to arise during long recordings, may have been masking a small outward current by DMCM. In support of this, when we applied SR→SR+PTX in the presence of DMCM, we found that the s-$GABA_AR$ current was 8.37 ± 1.65 pA (N=9), which represents a significant, 33%, reduction compared to control conditions (SR→PTX = 12.45 ± 0.79 pA; N=10): (DMCM+SR→PTX vs SR→PTX: Unpaired Student's t-test $t_{(9,8)}$=2.302; P= 0.0342) (**Fig.4.11D+E**).

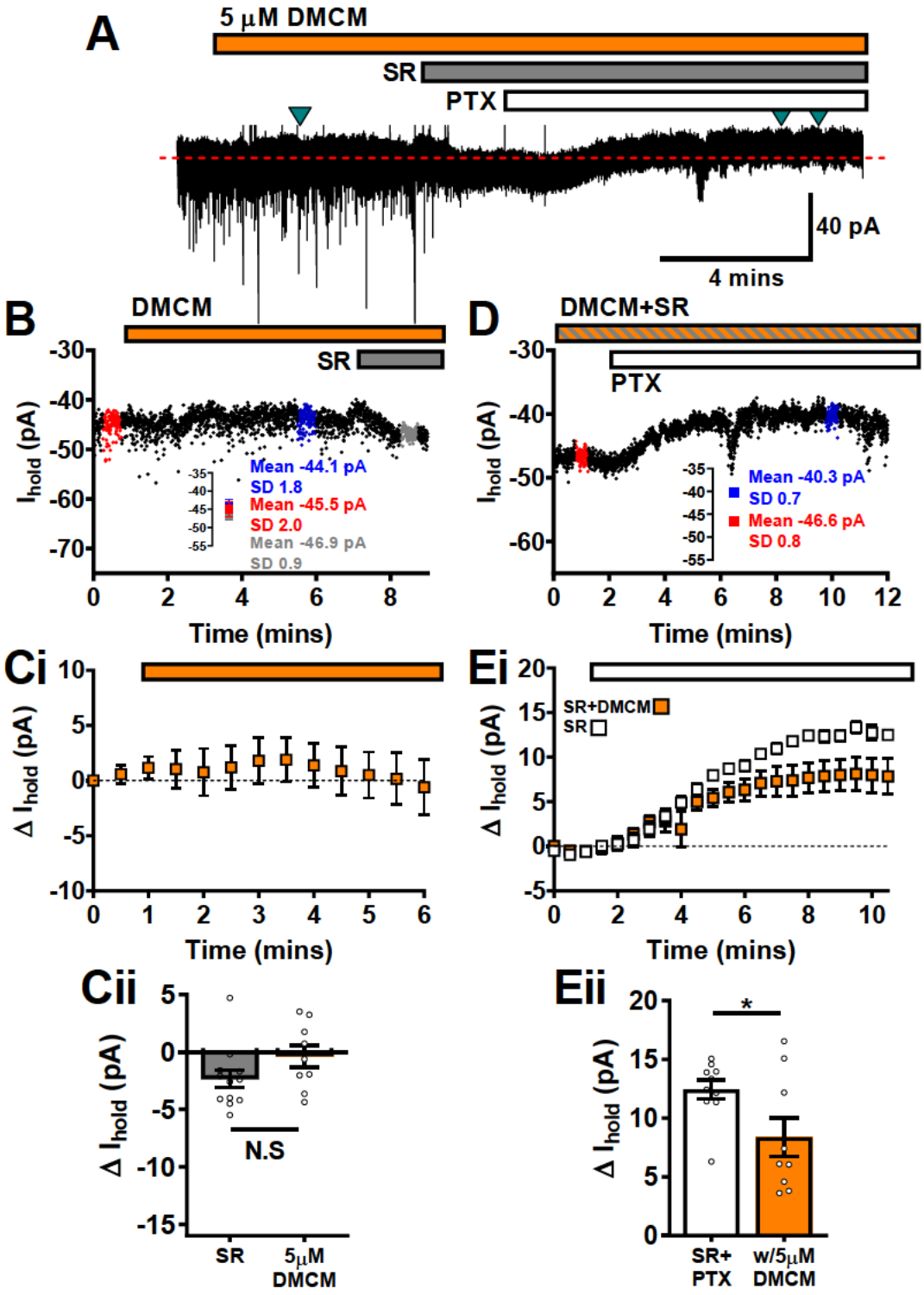

Fig.4.11 DMCM partially inhibits s-GABA$_A$R tonic currents.

A) Example WC-voltage clamp trace (-70 mV; CsCl) from a neuron exposed to DMCM (5 µM), and then SR→SR+PTX. In the example trace DMCM causes a small outward current of 1.4 pA as shown in the current-time plot in **B)** (sampled at 4 Hz using 5 ms epochs). **Ci)** However, as the average ΔI_{hold}-time plots taken at 30 seconds epochs shows, DMCM does not consistently produce outward currents (orange squares; N=9); the average change in holding current caused by DMCM was -0.38 ± 0.96 pA which is not significantly different from SR alone (-2.4 ± 0.8 pA; N=12) Subsequent addition of PTX blocks s-GABA$_A$R currents. The amplitude of this trace in this example was 6.3 pA as shown in the current-time plot in **D). Ei)** Average ΔI_{hold}-time plot shows that pre-exposure to DMCM (orange squares; N=9) decreases the outward s-GABA$_A$R current compared to SR+PTX only (white squares; N=10). **Eii)** Summarises the mean tonic current caused by: SR→PTX (12.45 ± 0.8 pA) and DMCM (8.37 ± 1.65 pA). Data are means ± S.E.M. Stats: Unpaired t-test.

4.5.10 Midazolam potently potentiates s-$GABA_AR$ tonic currents

The result of the DMCM experiment suggests that a portion of the receptors in the basal s-$GABA_AR$ pool contain the canonical BDZ-site, and that BDZ-site agonists are not causing additional $GABA_ARs$ to enter into spontaneously active state. As a final step in examining the modulation of s-$GABA_ARs$ by BDZ-site ligands, we explored the effect of midazolam, another BDZ-site agonist, which we hypothesised would potentiate s-$GABA_ARs$ to a greater degree than zolpidem. We viewed this as an important experiment because the degree of potentiation by zolpidem was quite marginal (39%). The efficacies of zolpidem and midazolam at potentiating spontaneously opening receptors have, to the best of our knowledge, not been directly compared; however, both compounds have been separately compared to diazepam (196,199), and midazolam appears to be the more efficacious (196). Another reason we opted to study midazolam is that it has been reported to potentiate $GABA_AR$ tonic currents in cultured hippocampal neurons (270,522) and in layer V pyramidal neurons (269) in a manner that was insensitive competitive antagonism by SR, but sensitive to bicuculline/PTX (269,270,522). This strongly suggests that midazolam can potentiate s-$GABA_ARs$. We opted to use midazolam at 40 nM and 120 nM; these concentrations have been previously shown to give rise to a partial and maximal potentiation of tonic currents, respectively (270). Modelling of the midazolam effect at recombinant receptors by Rüsch *et al* indicates that 40 nM midazolam increases the spontaneous opening probability by ~75%, whereas 120 nM midazolam increases it by approximately 125% (196). Based upon the effect midazolam at modulating GABA EC_{10} responses, at 40 nM and 120 nM midazolam will be effectively potentiating α3β2γ2 receptors, as well as, to a slightly lesser degree α2β2γ2, α1β2γ2 and α5β2γ2 receptors; conversely, midazolam is ineffective at α4- and α6-subunit-containing receptors (587).

We applied SR, then midazolam at 40 nM (N=8) or 120 nM (N=6) and then, in their continued presence, added PTX (**Fig.4.12A**). As with all BDZ-site agonists tested, midazolam generates inward currents in the presence of SR: 40 nM midazolam+SR = -9.98 ± 0.87 pA; 120 nM midazolam+SR = -9.02 ± 1.39 pA (**Fig.4.12A-C**). Comparing the midazolam+SR induced inward currents with SR alone revealed a significant different between the means (one-way ANOVA: $F_{(2,21)}$ = 21.72; P<0.0001) post-hoc Bonferroni test revealed that both 40 nM midazolam (Corrected unpaired Student's t-test $t_{(23df)}$=5.97; P<0.0001) and 120 nM (Corrected unpaired

Student's t-test $t_{(23df)}$=4.77; P=0.0002) are larger than SR, but not significantly different from each other (Corrected unpaired Student's t-test $t_{(23df)}$=0.637; P>0.999). The increase in SR-resistant current caused by midazolam translated into an increase in the PTX-sensitive tonic current (**Fig.4.12D+E**).

The amplitude of outward current induced by PTX in the presence of 40 nM midazolam+SR was 19.29 ± 2.27 pA (N=8), which represents a 55% potentiation compared to control conditions (SR→PTX = 12.45 ± 0.79 pA; N=10). The amplitude of the PTX-sensitive current was increased still further by 120 nM midazolam+SR to 26.3 ± 2.5 pA (N=6), a 111% increase relative to control, with just SR (**Fig.4.12E**). The degree of potentiation of the s-$GABA_A$R tonic current is in line with predictions made by Rüsch *et al* from midazolam's effect at recombinant receptors (196). An ANOVA indicated that the effect of midazolam was significant (One-way ANOVA: $F_{(2,21)}$ = 14.59; <0.0001); post-hoc Bonferroni test revealed that the increase in tonic current compared to control was significant for both 40 nM midazolam (Corrected unpaired Student's t-test $t_{(23df)}$= 2.87; P=0.0271) and 120 nM (Corrected unpaired Student's t-test $t_{(23df)}$=5.35; P<0.0001). The difference in the tonic current amplitude between 40 nM and 120 nM was at the threshold for significance (Corrected unpaired Student's t-test $t_{(23df)}$= 2.58; P=0.051).

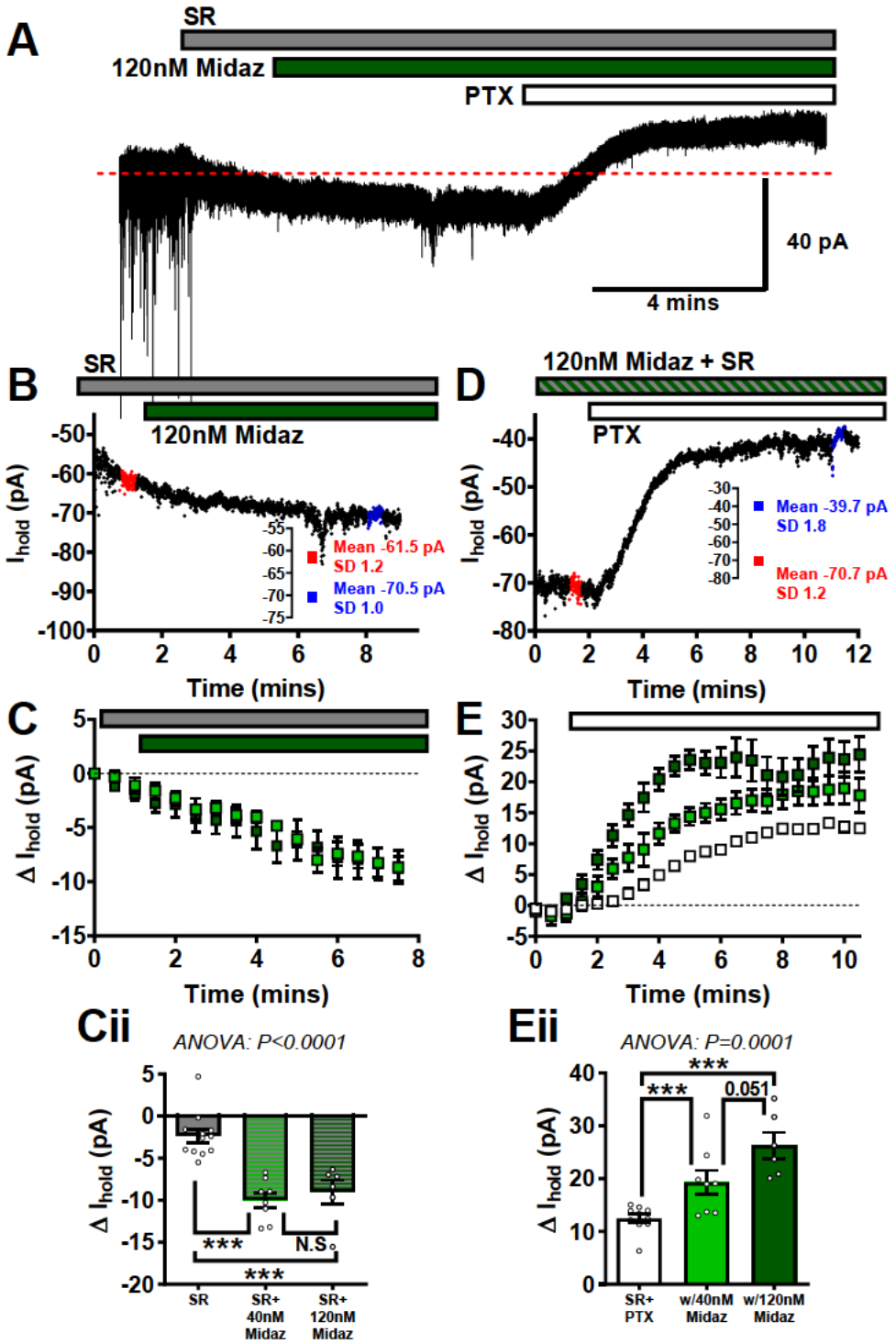

Fig.4.12 Midazolam potentiates s-GABA$_A$R tonic currents.

A) Example WC-voltage clamp trace (-70 mV; CsCl) from a neuron exposed to SR, then midazolam (120 nM), and then PTX. In the example trace Midazolam activates an inward current of -9.0 pA in the presence of SR, as shown in the current-time plot in **B)** (sampled at 4 Hz using 5 ms epochs. **Ci)** Average ΔI_{hold}-time plots, taken at 30 seconds epochs, shows that in the presence of SR, midazolam induces inward currents at 40 nM (-9.98 ± 0.87 pA; light green squares;N=8) and 120 nM (-9.02 ± 1.39 pA; dark green squares; N=6); the average amplitude compared to SR alone (-2.4 ± 0.8 pA) is summarised in and **Cii)**. Subsequent addition of PTX blocks s-GABA$_A$R currents. The amplitude of this trace in this example was 31 pA as shown in the current-time plot in **D). Ei)** Average ΔI_{hold}-time plot shows that pre-exposure to 40 nM midazolam and 120 nM midazolam potentiates the outward current compared to SR+PTX only (white squares; N=10). **Eii)** Summarises the mean tonic current caused by: SR→PTX (12.45 ± 0.8 pA) and 40 nM midaz+SR→PTX (19.29 ± 2.27 pA; N=8) 40 nM midaz+SR→PTX (26.3 ± 2.5 pA; N=6).Data are means ± S.E.M. Stats: ANOVA and Unpaired t-test.

In summary, we have demonstrated that BDZ-site ligands can bi-directionally modulate s-$GABA_AR$ tonic currents. The direction and magnitude of this modulation is consistent with the previously reported actions of these ligands at constitutively active and GABA-activated recombinant receptors. Diazepam, the least efficacious BDZ-site agonist at potentiating spontaneous activity, did not alter the s-$GABA_AR$ current; whereas zolpidem, and the even more efficacious midazolam, both potentiated the s-$GABA_ARs$ current. The different chemical structure of these compounds, together with the sensitivity of the zolpidem-mediated potentiation to flumazenil, suggests that their effects are mediated through the canonical BDZ-site. The sensitivity of the basal s-$GABA_AR$ currents to the BDZ-site inverse agonist, DMCM, evidences that BDZ-site agonists are potentiating the activity of the existing pool of s-$GABA_ARs$, and not simply converting additional receptor isoforms into a spontaneously active state. Henceforth we conclude, like McCartney *et al,* that BDZ-sensitive $GABA_AR$ isoforms can spontaneously open to produce a portion of the s-$GABA_AR$ tonic current.

4.5.11 Targeting PKC and PKA to indirectly modulate s-$GABA_AR$ tonic currents

In the final section of this chapter, we wanted to test if s-$GABA_ARs$ tonic currents could be modulated indirectly, by altering the activity of PKA and PKC. Both of these serine/threonine kinases have been shown previously to modulate tonic currents in DGGCs. Specifically, activation of PKC inhibits tonic $GABA_AR$ currents, whereas inhibition of PKC potentiates them (559). Analogous to this, decreasing in PKA activity by way of activating metabotropic $GABA_BRs$ has been shown to potentiate GABA-dependent tonic currents in DGGCs (588). However, the reverse was true at spontaneously opening recombinant α4β3δ receptors, which are potentiated by PKA (376). To assess the impact of serine/threonine kinase signalling on s-$GARA_AR$ tonic currents, we included blockers of PKA and PKC pathways in the intracellular solution (CsCl) and then performed the standard SR→SR+PTX protocol. Applying drugs to the intracellular solution allowed us to test the impact of serine/threonine kinases specifically on the cell being recorded, without any off-target presynaptic/network effects.

For the first experiment, the intracellular solution contained pertussis toxin (1 µg/mL), which catalyses the ADP ribosylation of the α-subunit of the trimeric G-protein Gi/o (589). This

maintains Gαi/o-proteins in an inactive (GDP bound) state and means that it can no longer inhibit adenylate cyclase (its normal biological function) (589). The manifestation of pertussis toxin is thus higher adenylate cyclase activity, elevated cAMP, and, in turn, enhanced PKA activity (589). In the presence of intracellular pertussis toxin, we found that the s-$GABA_AR$ tonic current was 9.84 ± 0.92 pA (N=7), which represents only a small, ~20%, decrease in tonic current compared to control with just SR+PTX (12.45 ± 0.79 pA; N=10) that was at the threshold for significance (Unpaired Student's t-test $t_{(9,6)}$=2.113; P= 0.0499) (**Fig.4.13**). This, on its own, is a reasonably unconvincing effect, but it does suggest that modulating PKA activity may be able to alter the s-$GABA_AR$ current. Specifically, increasing PKA activity should inhibit s-$GABA_AR$ tonic currents, whereas inhibiting PKA should potentiate these currents.

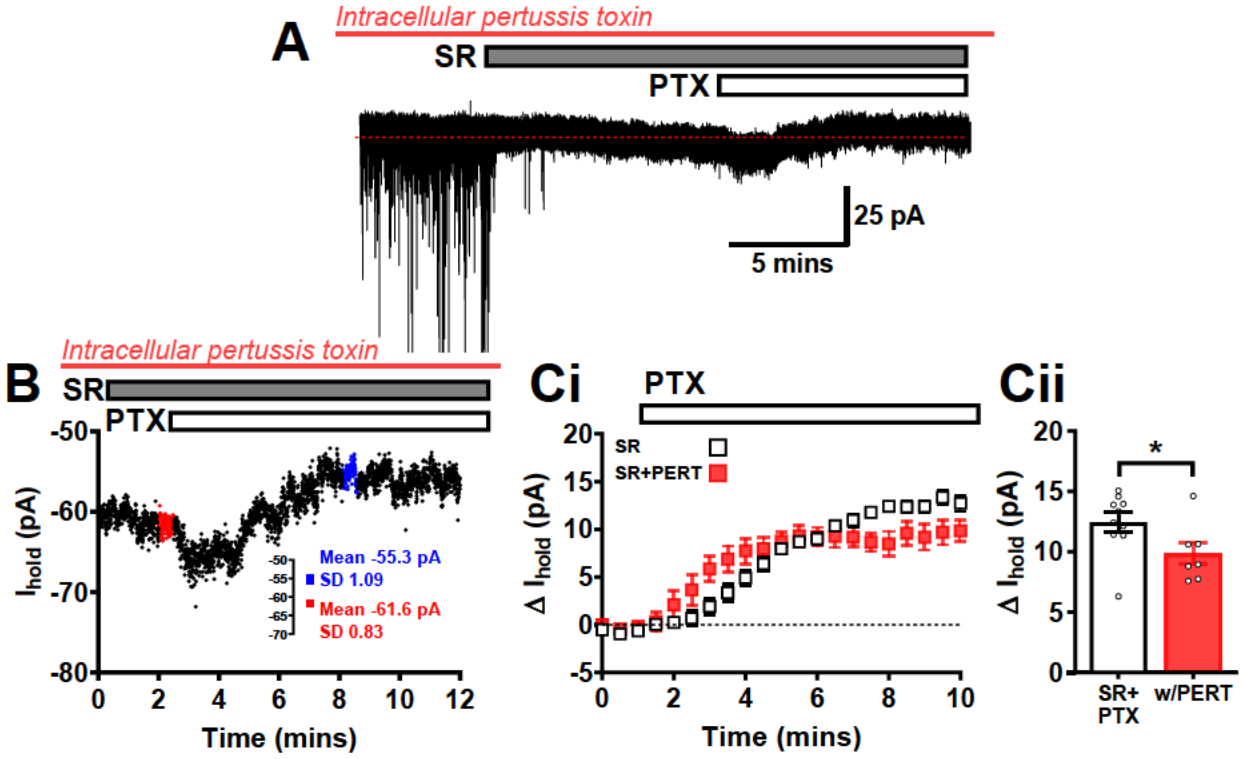

Fig.4.13 Pertussis toxin causes a small decrease in s-$GABA_AR$ tonic currents.
A) Example WC-voltage clamp trace with pertussis toxin (PERT) included in the intracellular solution (-70 mV; CsCl) from a neuron exposed to SR→SR+PTX. The tonic current blocked by PTX in this example was 6.3 pA as shown in the current-time plot in **B)** (sampled at 4 Hz using 5 ms epochs). **Ci)** Average ΔI_{hold}-time plots, taken at 30 seconds epochs, shows that in the presence of PERT (red squares; N=7) s-$GABA_AR$ tonic current is slightly decreased compared to SR+PTX only (white squares; N=10). **Cii)** Summarises the mean tonic current caused by: SR→PTX (12.45 ± 0.8 pA) and PERT+SR→PTX (9.84 ± 0.92 pA; N=7). Data are means ± S.E.M. Stats: Unpaired t-test

However, when the intracellular solution contained the PKA blocker, PKI 5–24 (PKI, 10 μM), or the PKA activator, 8-Br-cAMP (1 mM), we found no notable effect on s-$GABA_A$R tonic currents (**Fig.4.14**). Indeed, although above the significance threshold (even without Bonferroni correction), in the presence of PKI, which according to the small effect of pertussis toxin should increase s-$GABA_A$R tonic currents, actually slightly depressed them (10.77 ± 1.03 pA; N=8) (Unpaired Student's t-test $t_{(9,7)}$= 1.32; P=0.207) (**Fig.4.14A+B**), whereas with 8-Br-cAMP, which we posited would curtail s-$GABA_A$R tonic currents, was indistinguishable from control (11.51 ± 1.51; N=8) (Unpaired Student's t-test $t_{(9,7)}$= 0.58; P=0.571) (**Fig.4.14A+C**). We also tested if PKC, which has been shown to modulate tonic currents in DGGCs (559), could affect s-$GABA_A$R tonic currents by including the PKC-inhibitor, bisindolylmaleimide-II (50 nM), in the pipette solution. However, we reported no significant effect on the s-$GABA_A$R tonic current amplitude (13.53 ± 0.43 pA; N=8) (Unpaired Student's t-test $t_{(9,7)}$= 1.11; P=0.283) (**Fig.4.14A+D**). Of note is that subsequent experiments performed by Dr Sergiy Sylantyev (see Discussion) suggest that the lack of effect of modulating PKA is not an indicator that the pertussis toxin effect is an artefact: its inhibitory effect on s-$GABA_A$Rs persists both at the single-channel level (lower average open time and frequency) and on cell excitability (416).

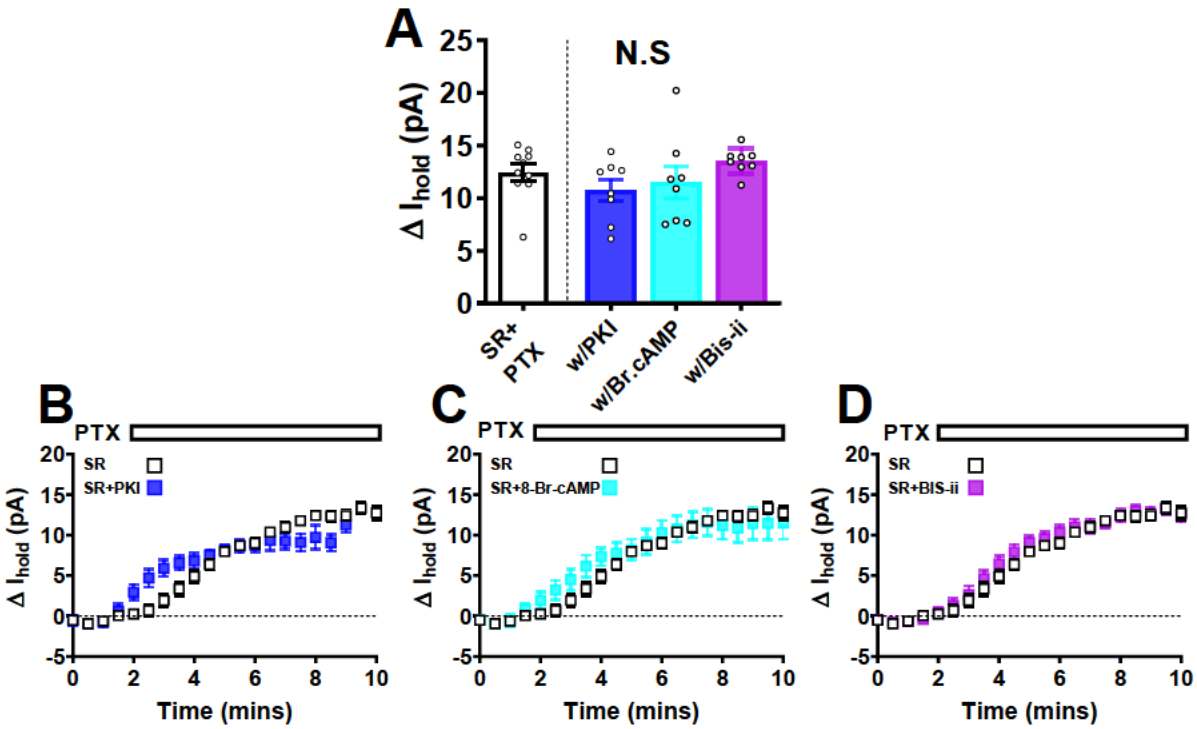

Fig.4.14 Modulating PKA/PKC does not affect the s-$GABA_A$R tonic currents.
A) Summarises the mean s-$GABA_A$R tonic current in each condition and **B-D)** Shows the average ΔI_{hold}-time plots, taken at 30 seconds epochs for: **A-D)** SR→PTX (12.45 ± 0.8 pA) white squares, **B)** PKI+SR→PTX (10.77 ± 1.03 pA; N=8) blue squares, **C)** 8-Br-cAMP+SR→PTX (11.51 ± 1.51 pA; N=8) cyan squares, **D)** Bis-ii+SR→PTX (13.53 ± 0.43 pA; N=8) purple squares, Data are means ± S.E.M. Stats: Unpaired t-test.

Chapter 5

General discussion and future directions

Key findings

In the present thesis, we show that spontaneously opening $GABA_A$Rs, activating independently of GABA, generate a tonic conductance that suppresses DGGC excitability. This is, to our knowledge, the first direct demonstration of the functional role of s-$GABA_A$Rs in hippocampal neurons.

The importance of s-$GABA_A$Rs to DGGCs is demonstrated by their contribution to inhibitory tone: s-$GABA_A$Rs transfer twenty times more inhibitory charge than IPSCs. And blocking s-$GABA_A$Rs shifts DGGCs into a more excitable state, as evidenced by the decrease in the rheobase current and the increase in input-output gain following s-$GABA_A$R block. Thus, without s-$GABA_A$R conductance, neurons require less excitation to fire an AP, and when they are firing, they are able to fire at a higher rate and are more sensitive to changes in excitation. s-$GABA_A$Rs also enhance the precision of excitatory transmission in DGGCs: blocking s-$GABA_A$R conductance widens the temporal window over which two excitatory signals can be successfully summated to fire an action potential.

We also demonstrate that BDZ-site ligands, which affect γ2-subunit-containing $GABA_A$Rs, can bidirectionally modulate the s-$GABA_A$R-meditated tonic conductance. This is in contrast to compounds targeting the prototypical extrasynaptic $GABA_A$R isoforms (containing the δ- or α5-subunit), which did not affect the s-$GABA_A$R-meditated tonic conductance.

The present thesis answers several key unknowns: the s-$GABA_A$R-mediated tonic conductance is *not* a stochastic artefact, and clinically used drugs *do* modulate their activity. The work presented here also opens up many new avenues for future studies into s-$GABA_A$R function and pharmacological modulation.

5.1 The functional impact of s-$GABA_A$Rs in DGGCs

We utilised the different mechanisms of action of the $GABA_A$R antagonists SR (competitive) and PTX (channel-blocker) to characterise the hitherto unknown function of s-$GABA_A$Rs in DGGCs. SR is applied at saturating concentrations to block the action of GABA at $GABA_A$Rs, whilst preserving the constitutive activity of s-$GABA_A$Rs. In the continued presence of SR, PTX is then added to block constitutive s-$GABA_A$R activity. The difference between SR and PTX corresponds to the s-$GABA_A$R signal.

Using this approach, we characterised the nature of the s-$GABA_A$R signal that is inputted to DGGCs. At RMP, the effect of s-$GABA_A$Rs in DGGCs is limited to a small, ~7%, but significant membrane shunt, which decreases the input resistance and quickens the membrane time constant without affecting Vm. Importantly, this experiment represents the first time that hippocampal s-$GABA_A$Rs have been detected using an intracellular solution with a physiological [Cl^-](8 mM); thus spontaneous $GABA_A$R openings are not an artefact of high levels of intracellular Cl^-, which have been previously used to study s-$GABA_A$Rs (74,233).

Membrane shunting is a key mechanism for inhibition in the brain. The contaminant increase in membrane conductance and decrease in membrane time constant means that voltage transients are 1) divisively scaled-down and 2) decay faster. Shunting decreases excitability because more excitatory current is required to reach threshold (the rheobase current) (80,317). Shunting also increases the temporal fidelity of neuronal firing because excitatory inputs need to coincide within a narrower temporal window to successfully summate and cross threshold (coincidence detection) (298). Shunting inhibition also decreases first spike latency and jitter (319).

The inhibitory power of shunting is evidenced by its ability to override the excitatory effect of depolarising tonic $GABA_A$R currents (226,298). Moreover, shunting can further decrease excitability by exacerbating the cumulative depolarisation-dependent inactivation of voltage-gated Na^+ channels (294,298). The decrease in excitability that is caused by shunting is indicated by a multiplicative increase in rheobase and a change to the input-output (I-O; F-I) relationship. Specifically, in the absence of synaptic noise, shunting is generally assumed to cause a subtraction in F-I curves (there are important exceptions to this, as will be detailed

later). As explained in the introduction, the different effect of shunting below (division/multiplication) vs. above (subtraction/addition) threshold is because the spiking mechanism clamps the steady-state potential at (or close to) threshold potential and converts the shunt into source for a hyperpolarising 'leak' current (322,325). In line with this, early investigations into the function of tonic inhibition demonstrated that in cerebellar granule cells, recorded *in vitro* (80) and *in vivo* (590), block of tonic $GABA_AR$ shunt offsets the I-O relationship (F-I curve) to the left without a significant change in gain; i.e. less current is required to achieve a given firing rate. As is explained in the appendix, the presence of synaptic noise can allow a shunting conductance to affect gain (292,293). Noise achieves this by exerting an asymmetric effect on the upper vs lower part of the F-I curve, causing a leftward *offset* (addition) and a *decrease* in the gain (division) (292–294,317,519,591). Because shunting reduces noise amplitude, it provides a route through which shunting can modulate gain (292,293). In the recordings that we performed to characterise the impact of s-$GABA_AR$-mediated shunt on the I-O relationship, excitatory transmission was blocked. Thus, although a degree of noise is present due to intrinsic channel activity (592), gain control through modulation of noise should not feature in our experiments

Based on the small, ~7%, s-$GABA_AR$-mediated shunt at RMP, we expected that inhibiting s-$GABA_ARs$ would cause a similarly small (5-10%) decrease in rheobase current (because rheobase = depolarisation voltage/input resistance). And that block of s-$GABA_ARs$ would lead to a leftward offset in the F-I curve, not a multiplative increase in gain. If this were the case, it would still be an important finding (after all, the functional role of s-$GABA_ARs$ in the hippocampus was unknown prior to this PhD), but it would indicate that s-$GABA_ARs$ are only of minor importance to DGGCs. However, when we characterised the impact of s-$GABA_ARs$ upon excitability, contrary to expectation, we found that block of s-$GABA_AR$ tonic conductance resulted in a substantial *decrease* in rheobase current of ~30%, and an *increase* in F-I gain (slope) of ~40%.

Also relevant here, is that blocking IPSCs with SR did not affect the rheobase current. Moreover, the amount of inhibitory charge that is transferred by s-$GABA_ARs$ exceeds that of IPSCs by a factor of twenty-to-one. The direction and magnitude of this difference is consistent

with previous studies that have compared the charge transferred by GABA-dependent tonic and phasic currents (80,524). It is the *persistence* of tonic currents that enables them to pass such large amounts of inhibitory charge, often in spite of their relatively small amplitudes (80,524). Despite the good alignment with previous findings it is, nevertheless, still impressive – and perhaps counterintuitive – that, in terms of charge transfer and the effect on rheobase, *the* most significant contributor to inhibition in DGGCs is the GABA-*independent* s-$GABA_A$Rs

We demonstrated that s-$GABA_A$Rs suppress excitability to a much greater degree than would be predicted from their small effect at RMP. In the absence of s-$GABA_A$R-mediated tonic conductance, neurons require notably less excitatory current to fire an action potential. And when they are firing, they are much more sensitive to changes in the excitatory current. In short, s-$GABA_A$Rs as a significant break on excitability in DGGCs. We found that both the s-$GABA_A$R signal *and* a number of intrinsic properties of DGGCs act collaboratively to enhance the inhibitory effect of s-$GABA_A$Rs.

The idea that the functional consequences of a tonic $GABA_A$R signal are influenced by the electrophysiological properties of the neuron is supported by many studies (225,226,294,295,317,387,517). Bryson *et al,* in their assessment of the functional impact of tonic inhibition in interneurons, provides a good recent example. They found that in fast-spiking interneurons, tonic inhibition suppresses F-I gain, but in non–fast-spiking interneurons, it increases gain. This disparate effect of tonic inhibition was attributed to 1) whether the tonic conductance was linear or outwardly rectifying and 2) cell-specific differences in a) the magnitude of an “ultraslow” conductance responsible for spike-frequency adaptation and b) repolarising K^+ currents (291). They demonstrated, using modelling, that identical tonic $GABA_A$R input signals can elicit very different output responses in different interneurons, due to variations in the intrinsic spiking dynamics (291).

DGGCs have a variety of intrinsic (active and passive) properties that facilitate their sparse activity pattern. DGGCs have a relatively hyperpolarised membrane potential, typically between -68 mV and -80 mV (404–411,413,414), a depolarised AP threshold of ~ -41 mV (~ 10 mV more depolarised than CA1 pyramidal neurons) (414), a high rheobase current (414), high input-output gain (414), strong dendritic attenuation (483,485), and substantial spike-frequency

adaptation that is caused by depolarisation-dependent Na^+ channel inactivation (480). In the present thesis, we show, for the first time, that s-$GABA_A$R tonic conductance is outwardly rectifying. We provide *direct* evidence that the outward rectification of s-$GABA_A$Rs works together with the depolarised AP threshold to increase the rheobase current. Moreover, we show that s-$GABA_A$Rs actually depolarise the threshold, which will further increase the rheobase current. We also provide *direct* evidence that divisive effect that s-$GABA_A$Rs have on F-I gain is due to an enhancement of spike-frequency adaptation. This increase in adaptation is associated with a depolarised steady-state firing potential. In line with this, we provide *indirect* evidence that the depolarised AP threshold and the enhanced adaptation are due to s-$GABA_A$Rs increasing the depolarisation-dependent Na^+ channel inactivation.

Outward rectification of tonic $GABA_A$R responses has been observed across multiple neuron types, including hippocampal pyramidal neurons (387) and interneurons (225,296), and can be observed in GABA-activated single-channel openings in DGGCs (593). Membrane depolarisation thus enhances the inhibitory effect of s-$GABA_A$Rs in two ways. First, it establishes a driving force on the permeant anions, which leads to inward hyperpolarising currents. And, second, depolarisation increases the s-$GABA_A$R conductance due to outward rectification. As a result, when DGGCs approach threshold, s-$GABA_A$Rs transmit progressively larger hyperpolarising currents *and* are able to shunt excitatory currents to a greater degree than at RMP. Both these factors, directly and indirectly, respectively, suppress DGGC excitability. Importantly, DGGCs have a relatively depolarised AP threshold: -38 mV in our study, which is in line with previous reports (414), and is ~ 10 mV more depolarised than CA1 pyramidal neurons (414). Because of the depolarised AP threshold, DGGCs will experience a greater effect of s-$GABA_A$R outward rectification in the lead up to spiking than neurons with a more hyperpolarised threshold. Indeed, Pavlov *et al* demonstrated that in CA1 neurons, outward rectification only has a minimal impact on sub-threshold voltage noise because, in these neurons, the outward rectification is activated at a potential close to the spiking mechanism (387). However, in DGGCs there is at least a 10 mV window in which outward rectification is the clearly present, but the neuron is not yet at threshold. Added onto this, s-$GABA_A$Rs appear to actually depolarise the AP threshold and thereby enhance the effect of outward rectification still further. Interestingly, the depolarisation of DGGC AP threshold is not unique to s-$GABA_A$Rs:

GABA-activated tonic currents have been shown to depolarise the AP threshold of DGGCs in post-natal day 7 and adult mice (71). It is likely because of the outward rectification of s-$GABA_A$Rs, in conjunction depolarised voltage threshold, that blocking s-$GABA_A$Rs causes a ~30% reduction in rheobase, which is over four times greater than would be predicted from their shunting effect at RMP. As an aside, the reversal at E_{GABA} is further proof the s-$GABA_A$R current blocked by PTX is not due to PTX blocking another channel (e.g. 5-HT_3R, which would cause a depolarised reversal).

One of the most surprising findings was that s-$GABA_A$Rs exert a divisive effect on the F-I curves and decrease neuronal gain. Blocking s-$GABA_A$Rs caused a ~40% increase in the slope and area under the curve of the F-I curves. Thus blocking s-$GABA_A$Rs not only increase the excitability of DGGCs, but also increase their sensitivity to changes in excitation. Of note, is that it has previously been reported that artificially inducing GABA-dependent tonic inhibition in DGGCs, using NO-711, reduces F-I curve gain, indicating that our observation is not an experimental artefact (e.g due to the use of PTX) (313). Gain is an important property of DGGCs because it allows them to transition from a silent state to burst firing, and, therefore, once active to signal to CA3 pyramidal neurons effectively. This is thought to be important for pattern separation (432,445–453). Modulation of gain was evidently not due to shunting of synaptic noise because excitatory transmission was blocked in our experiments (292,293). We also demonstrated that s-$GABA_A$Rs were unlikely to be modulating gain by an effect on active dendritic conductances: the AHP amplitude, an important readout for gain control by active dendrites, was not altered by blocking s-$GABA_A$Rs (295). In line with this, DGGCs dendrites are strongly attenuate back-propagating APs and afterpotentials (483,485), the effective propagation of which is necessary for gain control by active dendrites (295).

Instead, we report that s-$GABA_A$Rs *decrease* gain by *enhancing* spike-frequency adaptation (the decrease in firing rate during prolong suprathreshold depolarisation). DGGCs show profound spike-frequency adaptation; this intrinsic neuron property prevents runaway excitation and supports burst firing (413,468,480). Importantly, spike-frequency adaptation is not just a mechanism for reducing overall excitability: it decreases gain as well, by changing the shape (reducing the slope) of the F-I curve (536). In our study, and others (294), adaptation can be

observed from the decrease in firing rate that occurs during sustained injections of supra-threshold step currents (i.e. the firing rate immediate to depolarisation is higher than at the steady-state firing rate at the end of the depolarising step). Changes to spike adaptation are evidenced by asymmetric changes in the initial firing rate F-I vs the steady-state firing rate F-I (294). In line with s-$GABA_A$Rs controlling gain through the spike-frequency adaptation mechanism, we showed that blocking s-$GABA_A$R conductance differentially affected the initial firing rate F-I vs the steady-state firing rate F-I. Specifically, the initial firing rate F-I, before adaptation occurs, was linear, and the effect of inhibiting s-$GABA_A$Rs was to shift the F-I relationship to the left without a change in gain. Thus, if the depolarising currents used to excite DGGCs were extremely short-lived, adaptation would not be engaged and s-$GABA_A$Rs would not affect gain. In contrast, the steady-state firing rate F-I was non-linear and plateaued (saturated) with high levels of depolarisation; inhibiting s-$GABA_A$Rs caused a substantial, ~60%, increase in gain of the linear portion of the F-I, and increased the plateau frequency. The steady-state F-I relationship was thus multiplicatively scaled by s-$GABA_A$Rs, not offset. Most importantly, when s-$GABA_A$Rs were blocked, the multiplicative increase of the steady-state F-I gain is sufficient to *increase* the gain of the F-I relationship as a whole (i.e. when frequency was recorded over the entire depolarising step). This mechanism of gain control is analogous to that reported by Fernandez and White (294). They showed that shunting inhibition enhances spike-frequency adaptation to decrease the gain of CA1 pyramidal (294).

In both DGGCs (480) and CA1 pyramidal neurons (294), spike-frequency adaptation depends on depolarization-dependent partial inactivation of Na^+ channels. In DGGCs, this inactivation is associated with a spreading of the AIS from the soma (480). The initiation of AP spiking at threshold voltage depends on the availability of Na^+ channel current; thus, inactivation of Na^+ channels decreases excitability (i.e. adapts the firing rate) (594). The level of Na^+ channel inactivation depends on depolarisation: at more depolarised potentials, more of the channels inactivate (594).

In the present thesis, we provide *indirect* evidence that that the s-$GABA_A$R-mediated shunting conductance exacerbates Na^+ channel inactivation; and that it is this that leads to an increase in spike-frequency adaptation and a decrease in gain. The evidence supporting this is that both

the AP threshold voltage and the steady-state firing voltage were hyperpolarised when s-$GABA_A$Rs were blocked. Thus, under normal conditions, the intact s-$GABA_A$R conductance acts to *depolarise* these firing potentials. Although as yet unproven, it is likely that because the neuron is more depolarised during spiking in the presence of s-$GABA_A$Rs, a greater proportion of Na^+ channels will inactivate and that this will decrease the steady-state firing rate (more adaptation).

If this is the case, it would be analogous to the mechanism put forward in Fernandez and White's study (294). They demonstrate that when a neuron is depolarised, a conductance that is shunting at rest produces an outward leak current that opposes the inward Na^+ current that is needed for spiking (594). To initiate spiking in the presence of a tonic shunt, neurons require a greater amount of Na^+ current to overcome the leak current and the increase in conductance (294,533). The only way this can be achieved is by further depolarising the membrane potential (294,533). Thus, the voltage at which spiking is initiated, the threshold, is *depolarised* in the presence of shunting conductance and, as a knock-on effect, so is the mean firing voltage (294). This persistent increase in depolarisation over the course of AP firing results in a greater amount of Na^+ channel inactivation and, therefore, a more substantial decrease to the steady-state firing rate for a given excitatory current (294). Thus the apparent paradox: that in the presence of a shunting conductance, neurons are more depolarised yet fire less frequently, is resolved by more depolarisation leading to more Na^+ channel inactivation (294). The reason why the *initial* firing rate, measured at the stimulus onset, is not diminished is because Na^+ channel inactivation is not instantaneous: the initial APs occur before Na^+ inactivation can take place (294). Interestingly, in Fernandez and White's study, the depolarised spiking threshold also caused the rheobase current to be increased to a larger degree than would be predicted from the conductance alone (294). Thus relief from Na^+ channel inactivation can also explain the hyperpolarisation of AP threshold and substantial decrease in rheobase that occurred following block of s-$GABA_A$Rs.

Although this mechanism is attractive in explaining the observed effects of s-$GABA_A$Rs on DGGC excitability, it currently remains conjecture. To assess if s-$GABA_A$Rs do enhance Na^+ channel inactivation, future studies should measure the rate of rise of the AP upstroke of

individual spikes at steady-state. The rate at which the AP rises is used to quantify the availability of Na^+ current; if s-$GABA_A$Rs do cause Na^+ channel inactivation, then blocking s-$GABA_A$R conductance should increase the rate of AP rise (294). Future studies should also assess the voltage relationship of steady-state inactivation of Na^+ channel inactivation in DGGCs. To effectively clamp Na^+ channel currents, it may be necessary to reduce the Na^+ driving force and to apply low concentrations of TTX (517). Steady-state inactivation of Na^+ channel currents should be apparent at voltages at the reported AP threshold for DGGCs with intact s-$GABA_A$R tonic conductance (517). Furthermore, there should be a detectable decrease in the amount of inactivation at the hyperpolarised AP threshold that is reported for DGGCs with s-$GABA_A$Rs blocked. In addition, the effects of blocking s-$GABA_A$Rs on threshold (hyperpolarised), spike-frequency adaptation (decreased) and gain (increased) should be recapitulated by Na^+ channel activators, e.g. anemone toxin or veratridine (595). And further to this, the effect of blocking s-$GABA_A$Rs should be prevented by partially inactivating Na^+ channels with TTX (294).

Interestingly, activation of $GABA_A$Rs has been previously shown to depolarise the AP threshold of DGGCs, but only when $GABA_A$Rs on the axon were activated; activation of somatic $GABA_A$Rs does not alter threshold (532). Thus, s-$GABA_A$Rs might be enriched at or close to the AIS. Different $GABA_A$R isoforms are known to preferentially cluster in different cell compartments (144,228,229), and the spatial distribution of $GABA_A$Rs is known to affect their functional impact (295,596). It is not currently known where s-$GABA_A$Rs are localised in DGGCs. A way to assess this would be to perform voltage-clamp recordings in the presence of SR and then ‘puff’ on PTX to different cell compartments. If, for instance, s-$GABA_A$Rs are enriched in/restricted to the AIS, then puffs of PTX to this region should result in the block of s-$GABA_A$R-mediated tonic currents, whereas puffs of PTX on the dendrites/soma should not block tonic currents. Likewise, puffing on PTX to the AIS should be sufficient to increase DGGC excitability. One limiting factor here is the relatively slow effect of PTX (it requires open-channels to access its binding site); thus, high concentrations of bicuculline, which partially inhibits s-$GABA_A$Rs, may be more useful. To ensure that the antagonist (PTX or bicuculline) is not diffusing and blocking s-$GABA_A$Rs in other compartments, the antagonist should be applied

to an adjacent cell and should not block tonic currents of the recorded neuron. The incorporation of fluorescent dyes into the antagonist puff solution would also be of utility here.

It is not just $GABA_A$Rs that are compartmentalised in neurons – Cl^- is too. The intracellular [Cl^-] varies across different subcellular compartments, and, with it, so does E_{GABA} (216). The intracellular solution we used to characterise the functional impact of s-$GABA_A$Rs matches that found in mature DGGCs, approximating both the native RMP and E_{GABA}. Nevertheless, by recording in whole-cell mode, directly from the soma, we will have disrupted the internal Cl^- environment. Variations to Cl^- compartmentalisation can affect measures of neural excitability, including the I-O relationship (597). Henceforth, *the most important* future experiment immediate to the present thesis is to record the functional impact of s-$GABA_A$Rs in conditions wherein the native Cl^- environment of DGGCs is unperturbed. The perforated patch-clamp recording technique will be of great utility to this end (296), and when combined with dynamic clamp, could also be used to assess the influence of stochastic noise on s-$GABA_A$R-mediated gain modulation of DGGCs (292,293).

It would also be of interest to record the impact of s-$GABA_A$Rs on the spontaneous firing of DGGCs, without the need for non-physiological depolarising current steps. However, hampering this experiment is that DGGCs are largely quiescent (441): recordings from awake behaving rats or mice have demonstrated that only a small portion (2-5%) of the DGGC population are active during a given cognitive task (467,468), and that the DGGCs that are active have a low overall firing rate (413,468–470), typically < 1 Hz. However, DGGC excitability can be artificially increased by altering the composition of the extracellular fluid: e.g. Rojas *et al* reported that DGGCs could be driven to fire at 2-10 Hz with an extracellular solution with altered levels of $Ca^{2+,}$ Mg^{2+} and K^+ (0.25 mM $CaCl_2$, 0.25 mM $MgCl_2$, and 4 mM K^+) (532). Using this approach, the impact of s-$GABA_A$Rs on spontaneous firing rate could be studied using loose cell-attached patched and puffing on SR and then SR+PTX. The difference in the average spontaneous firing rate in SR vs SR+PTX would reflect the effect of the s-$GABA_A$R tonic conductance. From our experiments, we predict that in conditions with s-$GABA_A$Rs blocked (SR+PTX), DGGCs will spontaneously fire at a higher rate than when their conductance is intact (SR).

DGGCs are regarded as effective coincidence detectors because of the narrow temporal window over which they can summate synaptic inputs to fire an action potential. If synaptic inputs arrive outside of this narrow time window, the probability that DGGC will fire an AP is extremely low. Relatively large amounts of convergent excitation are, therefore, required for DGGCs to send an output (e.g. fire one or a burst of APs) to CA3. By acting as coincidence detectors, DGGCs are able to filter incoming perforant path inputs before they reach the downstream hippocampal circuits. This 'filtering' is thought to be an essential component of the DG acting as a gatekeeper and as a pattern separator. Multiple factors contribute to DGGCs functioning as effective coincidence detectors, both in terms of the DG circuit organisation and the DGGC intrinsic properties that affect excitability and EPSP summation. In the present thesis, we show that s-$GABA_A$Rs appear to be an important conductance for establishing a narrow temporal window for successful coincidence detection. Blocking s-$GABA_A$Rs caused a widening of the time window over which two subthreshold perforant path inputs, activated asynchronously, could summate to effectively trigger an action potential. Inter-stimulus intervals that were previously too far apart to reliably drive DGGCs to spike (e.g. were effectively filtered out) were able, in the absence of s-$GABA_A$R conductance, to drive DGGCs to spike with a high probability. This represents a severe disruption in the capacity of DGGCs to filter input noise; it turns DGGCs from effective coincidence detectors with a high signalling fidelity into integrators with a low signalling fidelity. This finding has since been repeated – and confirmed – by Dr Sergiy Sylantyev, using a greater number of repeat stimulations over a wider time window (415).

Together, these results show that s-$GABA_A$Rs enhance the precision of coincidence detection coding in DGGCs. s-$GABA_A$Rs could be achieving this by 1) depressing DGGC intrinsic excitability (through the mechanisms outlined above) and/or by shunting excitatory inputs in the dendrites (thereby increasing EPSP attenuation and decay). Both intrinsic excitability and EPSP size/duration are negatively correlated with the sharpness of coincidence detection (298). However, because we used a suprathreshold read-out 'signal' to assess coincidence detection in our experiments (i.e. the probability the neuron fired), we are currently not able to assess whether it was a change in excitability and/or a change in EPSP size and decay that was the primary driver of changes in coincidence detection. Clearly, as outlined above, s-$GABA_A$Rs do have a strong effect on intrinsic excitability; it, therefore, seems a virtual certainty that part of the

effect on coincidence detection will be due to a change in rheobase. Nevertheless, because the EPSP duration is short relative to the step currents used to assess excitability, it is possible that synaptic excitation will not engage some of the mechanisms that appear to amplify the inhibitory effect of s-$GABA_A$Rs in DGGCs (e.g. depolarisation of AP threshold that may be driven by Na^+ inactivation). Because s-$GABA_A$Rs increase membrane conductance and decrease the membrane time constant, they also have the ability to improve coincidence detection by suppressing EPSP amplitude and accelerating their decay (298). Moreover, if s-$GABA_A$Rs are enriched within the dendrites, their ability to shunt EPSPs would be amplified (295,538). This would be similar to A-type K^+ channel, which are the channels primarily responsible for attenuation in DGGCs (483,485).

To assess the mechanisms of how s-$GABA_A$Rs modulate suprathreshold coincidence detection, future studies should repeat the coincidence detection experiment using a subthreshold 'read-out' signal. Specifically, future experiments could assess the effect of s-$GABA_A$Rs on the amplitude and decay of EPSPs and EPSP coincidence detection. Relevant to this, is the study by Schmidt-Hieber *et al,* which assessed subthreshold dendritic signal processing and coincidence detection in DGGCs (484). They recorded from the DGGC soma and stimulated evoked EPSPs at proximal and distal dendrites to assess the distance-dependent attenuation of EPSPs. The influence of s-$GABA_A$Rs on this attenuation could be assessed by performing the experiment in the presence of SR and then SR+PTX. To assess subthreshold coincidence detection, Schmidt-Hieber *et al* evoked two synaptic events separated by time intervals. The 'read-out' for subthreshold coincidence detection was the change in EPSP amplitude relative when two synaptic events were evoked relative to a single EPSP. They showed that DGGCs have a very narrow time window (<10 ms), over which EPSPs can be effectively summated to give rise to an EPSP with a larger amplitude than the single EPSP. Blocking s-$GABA_A$Rs may widen this temporal window.

LTP has been proposed to be the cellular mechanism for learning and memory in the brain (24,503–511) and might be involved in pattern separation in the DG (452,491). In DGGCs, because of their strongly attenuating dendrites, LTP depends on depolarising local dendritic spikes, not back-propagating APs (485). As outlined in Chapter 3, we hypothesised that

blocking s-$GABA_A$Rs would be able to increase LTP amplitude at perforant path synapses. Perhaps by decreasing the shunt of dendritic spikes and/or increasing intrinsic excitability so that more depolarisation can back propagates into the dendrites. In line with this, increasing GABA-activated tonic conductance in DGGCs has been previously shown to be detrimental to LTP in the DG (299). However, we found that there was no notable effect of blocking s-$GABA_A$Rs on LTP at perforant path synapses. Importantly, in our study, we were explicitly studying the effect of s-$GABA_A$Rs on LTP *amplitude*; however, it remains unknown if s-$GABA_A$Rs affect the *threshold* for LTP. Studying the threshold for LTP is slightly more complex than amplitude. Future studies will need to perform what essentially amounts to a dose-response analysis on LTP at perforant path synapses, by varying the intensity of the LTP induction protocol and recording the amplitude of potentiation. The intensity of the LTP induction protocol can be altered by changing the frequency of stimulation (598), the number of stimulation trains (599), or the number of pulses within a train (600). The influence of s-$GABA_A$Rs could be assessed by first, designing an LTP induction protocol that is subthreshold in the presence of SR (e.g. does not induce LTP), and then repeating this experiment in the presence of SR+PTX. We predict that s-$GABA_A$Rs raise the threshold for LTP; if this is the case, then an LTP induction protocol that is subthreshold with SR should be able to produce LTP in the presence of SR+PTX (e.g. is suprathreshold). Future studies should also assess the impact of s-$GABA_A$Rs on LTD; this plasticity mechanism is thought to support pattern separation in the DG by removing redundant DGGC representations (452,491).

5.2 The pharmacological modulation of s-$GABA_A$Rs in DGGCs

One of the frustrations that we encountered when examining the functional impact of s-$GABA_A$R mediated tonic conductance in DGGCs was that, at the time, no compounds had been identified to potentiate the GABA-independent activity of s-$GABA_A$Rs in these neurons. Hence, in the present thesis, the most significant finding pertaining to the pharmacology of s-$GABA_A$Rs was that BDZ-site ligands bidirectionally modulate s-$GABA_A$R-mediated tonic currents. Specifically, SR-resistant, PTX-sensitive tonic currents are potentiated by the BDZ-site agonists, zolpidem, and to a greater degree, midazolam; and are partially inhibited by the BDZ-site inverse agonist, DMCM. These findings are important for the s-$GABA_A$R field for three key reasons. First, BDZ-site ligands will be of great utility to future functional studies on s-$GABA_A$Rs (we now have the tools to *potentiate*, as well as inhibit their activity). Second, understanding the pharmacology of any receptor is an important end in and of itself; it also gives us a greater understanding of the mechanisms of action of drugs that are regularly used in the laboratory and clinical settings. Third, it provides a window into the $GABA_A$R subunit isoforms that are delivering the s-$GABA_A$R tonic conductance.

The finding is also relevant to the study of tonic inhibition more generally. One of the difficulties when examining the function of GABA-dependent tonic inhibition has been that ligands that potentiate or activate this mode of tonic inhibition also affect phasic inhibition. Moreover, ligands that block tonic currents rarely preserve phasic inhibition (because both forms of inhibition are GABA-dependent). And because the alterations to GABA-dependent tonic and phasic currents occur simultaneously, it is not always possible to causally link the functional effect of a ligand (e.g increase in rheobase) with the change in tonic inhibition (80,298). However, by modulating s-$GABA_A$Rs using BDZ-site ligands in conjunction with SR, the effect of phasic and tonic inhibition can be teased apart. First, phasic currents are blocked by SR without an impact on tonic inhibition (the effect of phasic inhibition can be quantified). And then, second, a BDZ-site ligand is added to alter the level of tonic inhibition. Any functional changes that occur between SR and SR+BDZ-site ligand can be attributed to changes in tonic inhibition.

Initially, we were surprised to observe that BDZ-site ligands were able to modulate s-$GABA_A$R-mediated tonic currents. This was primarily because the action of BDZ-site ligands is virtually always framed around their effect on GABA-activated $GABA_A$R responses (104). With the

benefit of hindsight, however, it should have been more apparent to us that BDZ-site ligands have the ability to modulate s-$GABA_A$Rs. This is informed by 1) McCartney *et al's* report that s-$GABA_A$R-mediated tonic currents in CA1 pyramidal cells are potentiated by flunitrazepam (233). 2) Birnir *et al's* study showing that diazepam increases the conductance of s-$GABA_A$R single-channel openings in CA1 pyramidal cells (349). And 3) that BDZ-site ligands affect the spontaneous activity of recombinant wild-type α1β2γ2L (198,205), α1β1γ2L (233), and α1β3γ2L receptors (233,369) and mutant α1β2γ2L/S receptors (196,198,199,205,260). Linked to this, is that BDZ-site ligands are thought to modulate $GABA_A$Rs through an effect on gating, not agonist affinity (196,198,199,203–205,260,580,581).

Our results indicate that, under basal conditions in the *ex vivo* slice, BDZ-sensitive $GABA_A$R isoform(s) have a degree of constitutive activity and contribute to the s-$GABA_A$R tonic conductance in DGGCs. As explained in Chapter 4 (Results 2), BDZ-site ligands behave as would be expected from their previously detailed effects on spontaneously opening recombinant $GABA_A$Rs. Midazolam was the most effective BDZ-site agonist at potentiating s-$GABA_A$R-mediated tonic conductance and will be a useful tool for subsequent studies of these receptors. Future studies should confirm that, as with zolpidem, midazolam's potentiating effects can be blocked by the BDZ-site antagonist, flumazenil, to ensure that it is acting through the canonical BDZ-site. To this same end, future studies could utilise the γ2F77I-swap mutant mouse (549). These mice carry a point mutation in their γ2 subunit that disrupts the canonical BDZ-site and eliminates the ability of zolpidem, diazepam, DMCM and flumazenil to modulate EC_3 GABA responses (midazolam has not been tried) (549). s-$GABA_A$R-mediated tonic conductance should not be affected by BDZ-site ligands in these mutant mice.

Probably the most important future experiment pertaining to modulation of s-$GABA_A$Rs by BDZ-site ligands is to record the effect of these ligands on spontaneous single-channel openings. Wlodarczyk *et al* indicated that nucleated patches are needed to record s-$GABA_A$R single-channel openings from DGGCs, not the more conventional outside-out patches (74). However, experiments performed by Dr Sergiy Sylantyev indicate that s-$GABA_A$R openings can be recorded in the outside-out configuration, providing that low-impedance pipettes (~3 MΩ) are used (415). This likely reflects a relatively low density of s-$GABA_A$Rs on the soma, aggravated by the tendency of $GABA_A$Rs to cluster (601).

Characterising the effect of BDZ-site ligands on single-channel s-$GABA_AR$ openings is necessary for two reasons. The first is to ensure that, in our slice recordings, BDZ-site agonists are actually increasing the constitutive activity of s-$GABA_ARs$ and not the potency/apparent affinity of $GABA_ARs$ for GABA, to the degree that they can deliver a GABA-dependent tonic conductance. Although the use of saturating concentrations of SR and the effect of DMCM to inhibit s-$GABA_ARs$ argues against this possibility, it is, nevertheless, an important control. To limit the impact of ambient GABA, outside-out patches should be excised from DGGCs and moved away from the slice to near the top of the bath. Next, a double-barrelled (θ-glass), piezo-driven micropipette should be brought close to the excised patch so that when solutions are ejected, they saturate the patch (602). One pipette channel should be filled with standard ACSF, and the other channel should be filled with ACSF and the BDZ-site agonist of choice e.g. midazolam. Both of these solutions should be analysed with an HPLC assay to ensure there is no contamination with GABA (212). Continuous pressure ejection this GABA-free ACSF onto the patch prevents any contaminating effect of GABA; the piezoelectric element allows for rapid and controlled exchange of ACSF and BDZ-ACSF. If, as we propose, BDZ-site agonists are potentiating the constitutive activity of s-$GABA_ARs$, this should be evidenced in the spontaneous single-channel openings. Specifically, based on previous reports, BDZ-site agonists could be increasing s-$GABA_AR$ single-channel open-times (205) or conductance (349). Based on our work, midazolam should be a more efficacious potentiator of single-channel openings than zolpidem, whereas DMCM should be a partial inhibitor of single-channel openings.

The second reason to perform single-channel analysis of s-$GABA_ARs$ is to ensure that the potentiating effects of BDZ-site agonists are not due to a conversion of SR into a weak partial agonist. Indeed, at mutant β2(Y157S) receptors, both SR and bicuculline can act as weak partial agonists (246). Perhaps BDZ-site ligands could cause an analogous conformational change, turning SR from an antagonist/weak inverse agonist into a partial agonist. Furthermore, Chesnoy-Marchais demonstrated that in hypoglossal motor neurons, SR can actually act as a partial agonist at the atypical ρ-subunit-containing $GABA_ARs$ (previously termed $GABA_CRs$) (140,523). However, ρ-subunit-containing $GABA_ARs$ evidently do not produce tonic currents in DGGCs because these receptor isoforms are insensitive to both bicuculline and PTX (140,523); and Wlodarczyk *et al* demonstrated that TPMPA, an antagonist at ρ-subunit-containing

$GABA_A$Rs, does not block DGGC tonic currents (74). To test the possibility of BDZ-site ligand induced partial agonism of SR, the above single-channel analysis should be repeated but with one pipette chamber containing the GABA free-ACSF and the other chamber containing ACSF+SR. s-$GABA_A$R should be present in the GABA free-ACSF, and, as in Wlodarczyk *et al*, they should not be affected by application of 25 μM SR. Next, the pipette solutions should be exchanged so that one chamber contains ACSF+BDZ-site agonist and the other chamber contains ACSF+BDZ-site agonist+SR. Multiple drug-exchange filaments will be required to achieve solution exchange – for an example, see (602). The ACSF+BDZ-site agonist solution should be first applied to the patch; this should potentiate the constitutive activity of s-$GABA_A$Rs (e.g. increased open time). Then the solution containing the SR+BDZ-site agonist should be applied. If, as expected, SR does not act as a partial agonist, then the single-channel s-$GABA_A$Rs activity in the presence of BDZ-site agonists should be unaffected with SR vs without SR. Indeed, given SR's reported negative efficacy (246), s-$GABA_A$Rs might even be suppressed. Conversely, if BDZ-site agonists do enable SR to act as a partial agonist, then single-channel s-$GABA_A$R activity in the presence of BDZ-site agonists should be increased with SR vs without SR.

The inhibitory effect of DMCM, a BDZ-site inverse agonist, on the SR-resistant, PTX-sensitive tonic s-$GABA_A$R current was an important finding. It indicates that the basal pool of s-$GABA_A$Rs contains BDZ-sensitive $GABA_A$R isoforms. And that BDZ-site agonists are not just recruiting additional $GABA_A$Rs, which are not typically spontaneously opening, into s-$GABA_A$Rs. The classical BDZ-sensitive receptor isoforms are α1βγ2, α2βγ2, α3βγ2, or α5βγ2. BDZ-sensitive receptor isoforms were also evidenced to be s-$GABA_A$Rs by McCartney *et al* (α1β1γ2 and α1β3γ2) (233) and Botta *et al* (α5βγ2) (234). And as indicated in the introduction, many of these isoforms have been shown to spontaneously open when expressed in recombinant systems.

What can the pharmacology of the s-$GABA_A$R-mediated tonic currents tell us about their subunit composition in DGGCs? Zolpidem has an ultra-low apparent affinity and efficacy at α5βγ2 receptor isoforms and has no effect on EC_3 GABA responses at this receptor (549). Hence, the potentiating effect of zolpidem that we observed shows that receptors, in addition to/other than α5βγ2 isoforms, are constitutively active in DGGCs: α1,2,3βγ2. This is in contrast to PKCδ-positive neurons of the central amygdala, where zolpidem is ineffective (234). Based on this, it

is tempting to conclude that the lack of effect of L-655,708 that we observed confirms that α5βγ2 receptor isoforms are not involved in generating the s-$GABA_AR$ tonic current. However, this would be premature: α5-subunits are expressed in DGGCs, and their associated receptors mediate ~30% of the GABA-dependent tonic inhibition (351). L-655,708 is a BDZ-site *partial* inverse agonist selective for α5βγ2; we used L-655,708 because it was demonstrated to inhibit s-$GABA_ARs$ in the central amygdala (234). However, the negative efficacy of L-655,708 is not high: it only inhibits ~20% of EC_{20} GABA responses (568–570). If α5βγ2 receptor isoforms make a small-to-moderate contribution to the s-$GABA_AR$ tonic current, a blocking effect of L-655,708 may fall below the limit of detection in our assay. Related to this, we presumed that the larger potentiation of s-$GABA_AR$ tonic currents by midazolam than zolpidem simply reflected a higher efficacy of the former at s-$GABA_ARs$. However, midazolam, unlike zolpidem, can potentiate α5βγ2 responses (doubling the response of α5β2γ2 receptors to EC_{20} GABA) (587). Thus, the powerful effect of midazolam on s-$GABA_AR$ tonic currents may actually reflect potentiation of α5βγ2 receptor constitutive activity (which zolpidem cannot achieve). To test these possibilities, midazolam should be applied with SR and then, in their continued presence, L-655,708 should be applied. If a significant portion of midazolam's potentiation of s-$GABA_AR$ is due an effect on α5βγ2 receptors, then L-655,708 should partially reverse the SR-resistant increase in tonic current, and decrease the outward current that is caused by PTX. α5IA-II is another allosteric, α5-subunit selective inverse agonist with greater negative efficacy than L-655,708 (585); it could be useful as alternative to L-655,708 (585). PWZ-029 could also be used; this compound was shown to be more effective than L-655,708 at inhibiting s-$GABA_ARs$ currents in the central amygdala (234).

Ultimately, to test which $GABA_AR$ isoforms are potentiated by BDZ-site agonists to increase the s-$GABA_AR$ tonic current requires a genetic approach. Future studies should consider using α_(H1__R) mutant mice (603). This histidine to arginine point-mutation in α1, α2, α3 or α5 subunits disrupts the binding of BDZ-site ligands, thereby turning specific BDZ-sensitive isoforms into BDZ-insensitive isoforms. Using α5 (H105R) mice it would be possible to assess if the differences in the degree of potentiation of s-$GABA_ARs$ tonic currents by zolpidem and midazolam are due to differential effects on α5βγ2 receptors. If, as McCartney indicated (233), α1β1/3γ2 receptors function as s-$GABA_ARs$, then midazolam, zolpidem, and DMCM should be

less effective at modulating s-$GABA_AR$ tonic currents in α1(H101R) mice. Similarly, α2(H101R) and α3(H126R) mice would be of interest because BDZ-sensitivity in α2βγ2 receptors is necessary for various behavioural effects of midazolam (604), and midazolam most effectively potentiates GABA responses at α3βγ2 receptors (587).

Just as it is improper to conclude that α5-$GABA_ARs$ are not involved in producing the s-$GABA_AR$ tonic current based on the lack of effect of L-655,708, it is also wrong to infer that the lack of effect of DS2 and DPP-4-PIOL reflects a lack of contribution from δ-$GABA_ARs$. α4βδ receptor isoforms still represent a key candidate for s-$GABA_ARs$ in DGGCs. This is primarily based on the finding reported in Wlodarczyk *et al* that in δ-subunit null mice, s-$GABA_AR$-mediated tonic conductance is depressed by ~60% relative to WT-mice (74). Even when caveated with the possibility of species differences (a portion of DGGC tonic current in mice is GABA-dependent, but is not in rats (74)), α4βδ receptors do appear to be mediating a portion of s-$GABA_AR$ tonic current. That said, it is not impossible to imagine that the δ-subunit knockout might trigger loss of the s-$GABA_AR$ tonic current *indirectly*. In this scenario, the deficit in s-$GABA_AR$ current arises not as a direct result of lack of δ-$GABA_ARs$, but, instead, results from a compensatory cascade following knockout that leads to an altered expression/subunit composition of the 'actual' s-$GABA_AR$ isoforms, leading to a decrease in their current. For instance, if, as in CA1 pyramidal cells (233), α1βγ2 receptor isoforms are s-$GABA_ARs$ in DGGCs, δ-subunit knockout may lead to an increase in α4βγ2 receptors and a decrease in α1βγ2 receptor (potentially s-$GABA_ARs$) expression. Although this possibility may seem remote, $GABA_AR$ subunit knockouts are known to be plagued by compensatory changes (143,351,540–543). And moreover, in pilocarpine-treated epileptic mice, there is a decrease in δ-subunit expression in DGGCs, which leads to an increase in α4βγ2 receptors, which is consistent with a shift in localisation and subunit incorporation of the γ2 subunit (141,142); similar changes are reported in δ-subunit knockout mice (543). The reverse to this is also possible: that α4βδ receptor isoforms produce virtually all the s-$GABA_AR$ current, and knockout triggers a compensatory increase in the other potential s-$GABA_ARs$ to partially restore the GABA-independent signal. That said, our finding that DGGC s-$GABA_AR$ currents are BDZ-sensitive indicates that, under basal conditions, the BDZ-insensitive α4βδ receptor isoforms are not the sole mediator of the s-$GABA_AR$ current. Our finding that Zn^{2+} partially blocks the s-$GABA_AR$ current could be taken as evidence for a major contribution of

α4βδ to s-$GABA_A$Rs. This is based on recombinant studies showing that Zn^{2+} is a much more potent blocker of α1β1δ receptors than α1β1γ2S receptors (605). However, McCartney *et al* demonstrated that BDZ-sensitive s-$GABA_A$Rs can also be blocked by Zn^{2+} (233), and in our study, Zn^{2+} was primarily investigated to see how consistent the pharmacology of s-$GABA_A$Rs was across different neurons (Zn^{2+} had not been previously trialled against DGGC s-$GABA_A$Rs) (74).

DS2 was expected to potentiate the s-$GABA_A$R current, given that it 1) can increase the spontaneous activity of δ-subunit-containing receptors, and 2) binds at a site distinct from the orthosteric site (374,377). However, our results indicate that it instead potentiates a previously undetectable GABA-dependent tonic conductance (the increase in holding current was sensitive to SR). DPP-4-PIOL is a novel and relatively unexplored compound; it has not previously been shown to modulate spontaneous $GABA_A$R activity, but was trialled against s-$GABA_A$Rs because it was shown to decrease the maximum response, by 60%, of α4β3δ receptors to GABA, inferring a that it has non-competitive effect/negative efficacy (548). Future studies should further explore this interesting compound. Future studies might also consider the use of neuroactive steroids, for which α4βδ receptors are a target, to try and modulate s-$GABA_A$R tonic currents. THDOC (allotetrahydrodeoxycorticosterone), for instance, is a naturally occurring neuroactive steroid that potentiates α4βδ receptor currents activated by GABA and is active in the nanomolar range (248,606). And THDOC potentiates the GABA-dependent tonic current in DGGCs recorded from wild-type mice; knocking out the δ-subunit (*Gabrd−/−*) greatly curtails this potentiation (546). Importantly, although neuroactive steroids are allosteric modulators, binding within the transmembrane domain, they are able to activate the receptor in the absence of GABA. For instance, recombinant α6β2δ receptors exhibit constitutive activity that can be potentiated by 5α-THDOC (259). And, of particular note, GABA-independent allosteric activation by the neuroactive steroid, alphaxalone, is partially resistant to SR in recombinant $GABA_A$Rs (246). Similarly, (3,5)-3-hydroxypregnan-20-one activates $GABA_A$Rs in the absence of GABA in cultured hippocampal neurons; and, as would be expected, this activation is partially resistant to SR (607).

Other compounds that might be of interest to the study of s-$GABA_A$Rs more generally include flurazepam (205) and flunitrazepam (233). Both of these BDZ-site agonists have been shown to

increase the constitutive activity of recombinant $GABA_AR$s, and the latter has been shown to potentiate s-$GABA_AR$ tonic currents in CA1 pyramidal neurons (233). It would also be of interest to test the effect of high-efficacy BDZ-site agonists such as indiplon, which is efficacious at all $GABA_AR$ subtypes investigated. Although to our knowledge, indiplon has not been used at constitutively active $GABA_AR$s, it would be of interest to see if, owing to its high efficacy, it can potentiate s-$GABA_AR$ responses to a greater degree than midazolam. Certain compounds have been shown to enhance tonic $GABA_AR$ responses in a manner that is resistant to SR and are thus also of interest to future studies on s-$GABA_AR$s. These include menthol (363), methyleugenol (365), and propofol (233). Interestingly, we did try to modulate s-$GABA_AR$ tonic currents with propofol in a series of pilot experiments; however, we observed cell-swelling when neurons were exposed to propofol and following the addition of PTX seals rapidly degraded (unpublished observation). This could be due to Cl^- loading and, if so, supports the view laid out by Yelhekar *et al* that s-$GABA_AR$s facilitate recovery from Cl^- loading (which is prevented by PTX) (366). Henceforth, perhaps, in addition to regulating excitability, s-$GABA_AR$s are necessary for proper intracellular Cl^- homeostasis (366).

Many of the pharmacological experiments performed in this thesis circle in on the big unknown concerning s-$GABA_AR$s in DGGCs. Namely, which $GABA_AR$ subunit isoforms, probably in addition to α4βδ receptors, are producing the s-$GABA_AR$ tonic current? An obvious way to address this is with subunit knockout mice. Specifically of interest is the double gene-knockout mice that lack both the δ- and α5-subunits (*Gabra5/Gabrd−/−*) (351). This mouse-line was used by Glykys *et al* to show that δ- and α5-$GABA_AR$s produce virtually all the GABA-dependent tonic current in DGGCs that was activated by adding 5 μM GABA to the perfusate (351). This mouse line could, thus, be used to test that the hypothesis laid out by Wlodarczyk *et al*: that the same high potency $GABA_AR$s that produce GABA-dependent tonic inhibition are also able, in conditions of no-to-low GABA, to activate spontaneously and produce the s-$GABA_AR$ tonic current. If this is the case, then the SR-resistant, PTX-sensitive s-$GABA_AR$ tonic current in DGGCs should be absent in the *Gabra5/Gabrd−/−* mice (74). However, as explained above, $GABA_AR$ subunit knockouts are not without their complications. An alternative approach would be to use a knock-in/chemogenetic approach. Specifically, to use mice with a point mutation in the δ or γ2 subunit that renders them insensitive to PTX (69). This point mutation allows for the

pharmacological separation of $GABA_AR$ isoforms and has been previously used to demonstrate the contribution of δ-$GABA_ARs$ to IPSC kinetics in DGGCs (69). In mutant mice with PTX-resistant δ-$GABA_ARs$, the application of PTX will block all other $GABA_ARs$ but leave the δ-$GABA_ARs$ unscathed. Crucially, this point mutation does not alter the activation kinetics of δ-$GABA_ARs$ or their expression (69). If the amplitude of the PTX sensitive s-$GABA_AR$-mediated tonic currents in DGGCs was suppressed in these mice, it would conclusively demonstrate that δ-$GABA_AR$ are s-$GABA_ARs$ and would allow investigators to assess if the δ-knockout did promote any compensational changes. Unfortunately, in mice with PTX-resistant γ2-$GABA_ARs$ the kinetics of the receptor are changed (IPSC decay and frequency) (69). However, it is not clear if this mutation alters the spontaneous activity of these receptors – recombinant studies would be required to assess this – and, thus, this mutant mice might also prove useful to assess the contribution of BDZ-sensitive $GABA_ARs$ to s-$GABA_AR$ tonic currents.

In this study we also demonstrated that s-$GABA_AR$-mediated tonic currents could be slightly suppressed by the inclusion of pertussis toxin into the intracellular solution; however, we did not find any effect of modulating PKA (the kinase associated with pertussis toxin's effect) or PKC. It is also not clear how pertussis toxin is modulating s-$GABA_ARs$: i.e. the results could be explained by a change in s-$GABA_AR$ activity or expression. However, the effect of pertussis toxin does not appear to be a false-positive in this thesis. In additional published experiments by Dr Sergiy Sylantyev, pertussis toxin was shown to significantly decrease the open-time GABA-activated $GABA_ARs$ and the open-time fraction of s-$GABA_ARs$. Pertussis toxin was also shown to attenuate the increase in DGGC excitability that was caused by block of s-$GABA_ARs$: the ratio of APs recorded in SR vs SR+PTX was lower in the presence of pertussis toxin than in control conditions (416).

Other experiments performed by Dr Sergiy Sylantyev pertaining to s-$GABA_ARs$ show that spontaneous single-channel openings have a lower frequency and shorter average open-time than GABA-activated $GABA_ARs$, but have the same conductance (415). Evidence was also provided that s-$GABA_ARs$ contribute to the decay kinetics of GABA-activated responses evoked from nucleated patches and of native IPSCs (415). And, finally, the role of s-$GABA_ARs$ in narrowing the window for successful coincidence detection was reaffirmed (415). These findings demonstrate that s-$GABA_ARs$ may have a number of roles in neurons in addition to generating

tonic conductance, and further reaffirms the importance of further studies into this unusual signalling mechanism. Based upon our findings on the functional impact of s-$GABA_A$Rs in DGGCs, it is clear that studies into tonic inhibition should incorporate the possibility of a GABA-independent signal into their analysis. As a bare minimum, this requires testing the relative effectiveness of SR and PTX at blocking tonic inhibition. It is also worth noting that, in this thesis, we demonstrate that clinically used drugs (midazolam and zolpidem) modulate s-$GABA_A$R activity. It is, of course, not clear if the clinical efficacy of these drugs is determined or affected by s-$GABA_A$Rs; nevertheless, modulation of s-$GABA_A$Rs may represent an underappreciated route through which $GABA_A$R ligands could be mediating their effect on neural function. Likewise, s-$GABA_A$Rs would be an interesting target for novel experimental compounds and therapeutics. Finally, and related to this, it will be important to assess if known disease-causing mutations in $GABA_A$Rs, such as those that cause temporal lobe epilepsy (312), affect the levels of constitutive activity. If this is the case, then it will provide evidence that, like with GPCRs, constitutive activity is a physiologically important mechanism through which receptors can signal.

5.3 Conclusion

In conclusion, we demonstrate that constitutively active s-$GABA_A$Rs, opening in the absence of GABA, are important regulators of DGGC excitability. Blocking s-$GABA_A$Rs affected many of the intrinsic DGGC properties that are necessary for both sparse firing and proper signal integration. Moreover, our findings demonstrate that there is a reciprocal relationship between the intrinsic properties of DGGCs and s-$GABA_A$Rs. The outward rectification of s-$GABA_A$R currents works with the depolarised AP threshold to amplify the inhibitory effect of s-$GABA_A$Rs in DGGCs. In the absence of s-$GABA_A$R conductance, DGGCs are much more easily excited and are no longer able to properly filter excitatory signals. Henceforth, this atypical and previously underappreciated mode of $GABA_A$R signalling can now be recognised as a key component of DGGC physiology. The interaction between intrinsic neuron properties and the s-$GABA_A$R signal suggests that the function of s-$GABA_A$Rs will vary across different neuron types. Given that there is already some evidence that s-$GABA_A$R signalling is more widespread than previously anticipated, future studies should aim to characterise both the presence and function of s-$GABA_A$R-mediated tonic conductance in other neuron-types. In the present thesis, we identify various pharmacological tools that will aid these investigations. Most notably, we demonstrate that BDZ-site ligands can bidirectionally modulate s-$GABA_A$R activity. This finding suggests that $GABA_A$Rs containing the γ2-subunit are able to open spontaneously to produce a portion of the s-$GABA_A$R tonic conductance in DGGCs.

Chapter 6

Appendix

Mechanisms of controlling gain by a shunting conductance

6.1 The effect of stochastic noise on shunting conductance

In vivo, neurons face a constant barrage of excitatory and inhibitory synaptic inputs that induce high-amounts of stochastic fluctuations in the membrane potential (519). This 'noise' converts a relatively stable membrane potential into a distribution of voltage values (it increases the standard deviation of Vm) (292–294,317,519,591). If the distribution is sufficiently broad, it means that threshold voltage can be crossed, and the spiking mechanism initiated, even when the average voltage value is well below threshold (292–294,317,519,591). Noise thus increases the responsiveness of the neuron; it allows inputs that would usually be subthreshold to make transient excursions beyond threshold to initiate spiking (591). Importantly, this pro-excitatory effect of noise is *not* uniform across the F-I curve (292,591). Noise increases excitability at the lower part of the F-I curve: increasing AP firing rate when excitation currents are small, the mean voltage is approaching or just above threshold, and the neuron is silent/infrequently firing (292,591). But has a much weaker effect on the upper part of the F-I curve: AP number firing rate is not changed when excitation currents are large, the mean voltage is consistently above threshold, and the neuron is firing frequently (292,591). By acting in an asymmetric manner on the low vs high excitation currents/firing rates, noise results in a leftward *offset* (addition) and a *decrease* in the gain (division) of the F-I curves (292–294,317,519,591). And so whilst the responsiveness of a neuron to a small excitatory current is increased by noise, it also decreases its sensitivity to a further change in this current. (292–294,317,519,591).

Although noise is present to a degree in neurons that are recorded *ex vivo* – arising from short-range synaptic inputs and intrinsic channel activity (592) – the overall amount of noise is substantially diminished, primarily due to the sheering of the long range inputs that occurs during the slicing procedure (317). *Ex vivo* levels of noise can be artificially increased to approximate those found *in vivo* using the dynamic clamp technique (317). Dynamic clamp was

used to explore how noise interacts with shunting conductance to affect neuronal activity in the early 2000's by Chance *et al*, recording *ex vivo* from the rat somatosensory cortex (292), and by Mitchell and Silver, recording *ex vivo* from cerebellar granule cells (293). These two studies showed that, given a specific set of externalities, *in vivo*-like levels noise can convert the effect of shunting from subtraction to division (292,293).

Briefly, Chance *et al* delivered balanced excitatory and inhibitory inputs to a neuron, which allowed the authors to add noise and/or shunting conductance without changing its membrane polarisation (292). They found that, as expected, addition of only noise induced a leftward offset *and* a decrease in gain of the F-I curve, whereas addition of only shunting conductance induced a rightward (subtractive) offset in the F-I (292). When noise and shunting conductance were applied in unison, however, their opposing *offsets* cancelled out, meaning that the only net effect was a pure decrease in F-I curve gain (292). Importantly, to observe this purely divisive effect, the amount of noise and shunting conductance introduced had to be properly matched (292).

Mitchell *et al* used a more complex methodology to explore the interaction of shunting conductance and noise (293). Instead of stimulating the neuron with simple excitatory current steps, they used excitatory-rate coded inputs – a form of stimulation found *in vivo* in which excitation current is positively coupled to noise (i.e. larger excitation currents = more noise) (293). In the presence of shunting conductance, because of the subtractive effect on F-I curves outlined earlier (322), a greater amount of excitatory current was required to elicit a given firing rate (293). But because noise is positively coupled to excitatory current in rate-coded inputs, there was also a greater amount of noise for a given firing rate (293). It is this increase in noise, prompted by shunting inhibition and driven by rate-coded inputs, that causes the F-I curve to undergo divisive scaling of gain (293,317).

Although these two studies show that shunting conductance *can* decrease F-I gain in the presence of noise, it must be stressed that in both studies a constrained set of externalities was required to see this divisive effect – be it balanced excitation and inhibition, and appropriately matched noise and conductance (292); or rate-coded inputs (293). As such, it is not possible to generalise these mechanisms of gain reduction across different externalities and/or different

neuron types (317). Keeping with this theme, other studies have failed to find any effect of shunting inhibition paired with noise on F-I gain (608). Moreover, in 2010, Pavlov *et al* presented good evidence that in CA1 pyramidal neurons, in the presence of injected noise, shunting conductance can actually *increase* the gain of the F-I curve (N.B. this finding is in the supplementary Fig.S4 of their publication) (387). This effect was dependent on the shunting conductance exhibiting a linear I-V and decreasing the amplitude of sub-threshold voltage fluctuations (387). If the shunting conductance was outwardly rectifying the effect on gain completely dissipated (because it's effect on sub-threshold voltage fluctuations was greatly attenuated) (387).

6.2 The effect of active dendrites on shunting conductance

A distinct but related factor to stochastic input noise is the transmission and computation of the input signal through dendrites. Whilst some excitatory synapses are present on the cell body and transmit currents directly into the soma, the vast majority are located on the dendritic tree. One of the short-comings of the seminal modelling study of Koch and Holt was viewing dendrites to be passive cables; indeed, they stated that "active dendritic conductances complicate the interaction of synaptic excitation and inhibition" (322). It is now clear that dendrites do not function as passive cables – in most neurons they are 'active' in their own right due to expression of voltage dependent conductances (317). This endows them with the ability to modulate incoming signals in a variety of ways. Active dendrites can amplify excitatory inputs coming from distant parts of the dendritic tree, which would otherwise be diminished by travelling on passive cables (317). They can also prevent saturation of close-together inputs, allowing currents to summate in a supra-linear manner as 'dendritic spikes', rather than divisively shunt each other (317). Furthermore, and perhaps of most relevant to gain control in neurons, voltage-dependent conductances, specifically dendritic voltage-gated Na^+ channels, support the active 'back-propagation' of APs (295,317). This means that the AP waveform does *not* just travel forward, from the AIS to the axon terminals: it also propagates antidromically, back into the dendritic tree. These back-propagating action potentials (b-APs) generate a new source of depolarising current that flows into the dendritic tree *and* also re-invades the soma; the dendro-somatic current flow creates a change in somatic voltages that is termed the "depolarising after potential" (DAP) (295,317). DAPs have been shown to affect neural function

by altering the late phase of the AP waveform in the soma; this has a role in determining the rate at which a neuron can fire and, in turn, the gain of the F-I curve (295,317). Based on these findings it was hypothesised that a shunting conductance could perform gain control in neurons by diminishing the amplitude of the DAP (295,317).

In 2005 Mehaffey *et al* investigated the role of DAPs, and of shunting conductance on DAPs, in electrosensory lateral line lobe pyramidal cells of the *Apteronotus leptorhynchus* (295). They used depolarising square wave currents to excite the neuron and demonstrated that DAPs – generated by b-APs – have a pro-excitatory effect on pyramidal cells: blocking DAPs with a focal application of TTX to the dendritic tree caused neurons to fire less frequently in response to a given current step; this resulted in a divisive reduction to F-I curve gain (295). Henceforth, the inherent effect of DAPs in pyramidal neurons is to facilitate firing and increase (multiply) the gain of the F-I curve (295). The authors showed that DAPs increase gain because they occur simultaneously with – and thus act to decrease the amplitude of – the AHP of the preceding AP (295). Attenuation of AHP allows the next AP to occur more rapidly. Indeed, when DAPs were blocked by TTX applied to the dendrites, a large AHP was revealed that extended the inter-spike interval and decreased the firing rate (295).

The authors subsequently tested if a dendritic shunt – generated by focal application of muscimol, the $GABA_AR$ agonist – could exert a similar effect on neural function as dendritic application of TTX (295). They found that a dendritic shunting conductance accelerated the repolarisation phase of the b-AP, which resulted in a smaller DAP reaching the soma, manifesting itself as an augmented AHP (295). The increase of the AHP amplitude resulted in a divisive scaling of the F-I curve. Thus, b-APs generated by active dendrites can allow shunting conductance to reduce neural gain (295). It is important to note that this mechanism of shunt-induced gain control is not unique to the *Apteronotus leptorhynchus.* Indeed, shunting inhibition has been shown to regulate neuronal gain by affecting the discharge characteristics of active dendrites of CA1 pyramidal cells (*in vitro*) (289), neocortical layer V pyramidal neurons (*in vivo*) (290), and somatostain interneurons (*in vitro* + modelling) (291).

6.3 The effect of spike-frequency adaptation on shunting conductance

Spike-frequency adaptation (sometimes termed spike accommodation) describes the reduction in firing rate that occurs during sustained injections of supra-threshold step currents (294,517,536,537). It is a near-ubiquitous phenomenon across the brain, with most neurons showing a higher firing rate at the onset of the stimulus than near the end, when the neuron is firing at a 'steady-state' frequency (294,517,536,537). Spike-frequency adaptation is not just a mechanism to decrease firing rate, it also controls gain: the slope of the F-I curve is steeper when firing rate is measured at stimulus onset, than if it is measured at steady-state (294). There are three main 'adaptation currents' that dictate the degree to which firing rate decays over time. They are 1) M-type currents (high threshold potassium channels), 2) AHP currents (calcium-activated potassium channels) and 3) currents arising from the inactivation (and recovery from inactivation) of voltage-gated Na^+ channels (533,536). In DGGCs, spike-frequency adaptation depends on depolarization-dependent partial inactivation of anxonal Na^+ channels, which leads to spreading of the AIS away from the soma (480).

Because of the divisive effect of spike-frequency adaptation on gain, Fernandez and White investigated if it could provide a route through which shunting could impact gain (294). That is to say, could shunting conductance affect any (or many) of the 'adaptation currents' in a way that has a knock-on impact on gain? Recording *ex vivo* from CA1 pyramidal neurons and stimulating them with long (4 sec) current steps, Fernandez and White showed that shunting conductance differentially affected the onset firing rate vs the steady state firing rate of the neuron – this asymmetric effect demonstrated that shunting conductance was altering spike-frequency adaptation mechanism (294). Specifically, shunting conductance had little effect on firing rate measured at the *onset* of the stimulus (when the neuron was in a non-adapted state), but had a powerful effect on the steady state firing rate, causing it to be significantly reduced (294). Shunting inhibition was thus *enhancing* the degree to which the neuron adapts to prolonged excitation (294). Most importantly, this enhancement of spike-frequency adaptation, which caused a decrease in steady-state firing rate, was sufficient to cause a *decrease* in gain of the F-I response as a whole (i.e. when frequency was recorded over the entire 4 seconds) (294). In CA1 neurons shunting conductance is thus able to decrease neuronal gain.

Looking further into the mechanism, Fernandez and White used an experimental and theoretical approach to show that the *enhancement* of spike-frequency adaptation that drove the *decrease* in gain, likely occurred because shunting conductance exacerbated Na^+ channel inactivation (294). The initiation of AP spiking at threshold voltage depends on the availability of Na^+ channel current (594). Na^+ channels require depolarisation to activate, but they do not remain open indefinitely: in the presence of sustained depolarisation they undergo progressive inactivation; and at more depolarised potentials, more of them inactivate (594). This 'slow' form of inactivation, which takes place on the millisecond time-scale, is the main driver of spike adaptation in CA1 pyramidal neurons (294). Fernandez and White, supported by previous work (533), showed, firstly, that expression of a shunting conductance causes larger amounts of outward leak currents to be transferred when the neuron is depolarised and, secondly, that this outward leak current works against the inward Na^+ current that is needed for spiking (594). To counteract the leak current and initiate spiking, the neuron therefore requires a greater amount of Na^+ current (294,533). The only way this can be achieved is by further depolarising the membrane potential (294,533). Thus, the voltage at which spiking is initiated, the threshold, is *depolarised* in the presence of shunting conductance and, as a knock on effect, so is the mean firing voltage (294). This persistent increase in depolarisation over the course of AP firing results in a greater amount of Na^+ channel inactivation and, therefore, a more substantial decrease to the steady-state firing rate for a given excitatory current (294). Thus the apparent paradox: that in the presence of a shunting conductance neurons are more depolarised yet fire less frequently, is resolved by more depolarisation leading to more Na^+ channel inactivation (294). The reason why the initial firing rate, measured at the stimulus onset, is not diminished is because Na^+ channel inactivation is not instantaneous: the initial APs occur before Na^+ inactivation can take place (294). Interestingly, the depolarised spiking threshold also causes the rheobase current to be increased to a larger degree than would be predicted from the conductance alone; this is because the input current not only has to overcome the divisive effect of a leakier cell (V=I/G), but also has to take the cell to a more depolarised membrane potential to initiate spiking (294).

Bibliography

1. Naumann RK, Anjum F, Roth-Alpermann C, Brecht M. Cytoarchitecture, areas, and neuron numbers of the Etruscan Shrew cortex. J Comp Neurol. 2012;520(11):2512–30.

2. Herculano-Houzel S, Mota B, Lent R. Cellular scaling rules for rodent brains. Proc Natl Acad Sci U S A [Internet]. 2006;103(32):12138–43. Available from: http://www.pnas.org/cgi/doi/10.1073/pnas.0604911103

3. Bandeira F, Lent R, Herculano-Houzel S. Changing numbers of neuronal and non-neuronal cells underlie postnatal brain growth in the rat. Proc Natl Acad Sci U S A. 2009;106(33):14108–13.

4. Herculano-Houzel S. The human brain in numbers: a linearly scaled-up primate brain. Front Hum Neurosci. 2009;3:31.

5. DeFelipe J, Alonso-Nanclares L, Arellano JI. Microstructure of the neocortex: Comparative aspects. J Neurocytol [Internet]. 2002;31(3):299–316. Available from: https://doi.org/10.1023/A:1024130211265

6. Bayés À, van de Lagemaat LN, Collins MO, Croning MDR, Whittle IR, Choudhary JS, et al. Characterization of the proteome, diseases and evolution of the human postsynaptic density. Nat Neurosci [Internet]. 2011;14(1):19–21. Available from: https://doi.org/10.1038/nn.2719

7. Park H-J, Friston K. Structural and Functional Brain Networks: From Connections to Cognition. Science (80-) [Internet]. 2013 Nov 1;342(6158):1238411. Available from: http://science.sciencemag.org/content/342/6158/1238411.abstract

8. Zhu F, Cizeron M, Qiu Z, Benavides-Piccione R, Kopanitsa M V., Skene NG, et al. Architecture of the Mouse Brain Synaptome. Neuron [Internet]. 2018;99(4):781-799.e10. Available from: https://linkinghub.elsevier.com/retrieve/pii/S0896627318305816

9. Dombeck DA, Khabbaz AN, Collman F, Adelman TL, Tank DW. Imaging Large-Scale Neural Activity with Cellular Resolution in Awake, Mobile Mice. Neuron [Internet]. 2007;56(1):43–57. Available from: http://www.sciencedirect.com/science/article/pii/S0896627307006149

10. Sofroniew NJ, Flickinger D, King J, Svoboda K. A large field of view two-photon mesoscope with subcellular resolution for in vivo imaging. Elife [Internet]. 2016 Jun 14;5:e14472. Available from: https://pubmed.ncbi.nlm.nih.gov/27300105

11. Jun JJ, Steinmetz NA, Siegle JH, Denman DJ, Bauza M, Barbarits B, et al. Fully integrated silicon probes for high-density recording of neural activity. Nature [Internet]. 2017 Nov 8;551(7679):232–6. Available from: https://pubmed.ncbi.nlm.nih.gov/29120427

12. Dobzhansky T. Nothing in Biology Makes Sense except in the Light of Evolution. Am Biol Teach [Internet]. 1973 Mar 1;35(3):125 LP – 129. Available from: http://abt.ucpress.edu/content/35/3/125.abstract

13. Ryan TJ, Grant SGNN. The origin and evolution of synapses. Nat Rev Neurosci. 2009;10(11):701–12.

14. Mitchell KJ. The genetics of brain wiring: from molecule to mind. PLoS Biol [Internet]. 2007 Apr;5(4):e113–e113. Available from: https://pubmed.ncbi.nlm.nih.gov/17439300

15. Mitchell KJ. Innate: How the wiring of our brains shapes who we are. Princeton University Press; 2020.

16. Rakic P. Evolution of the neocortex: a perspective from developmental biology. Nat Rev Neurosci [Internet]. 2009;10(10):724–35. Available from: https://doi.org/10.1038/nrn2719

17. Kohl J, Babayan BM, Rubinstein ND, Autry AE, Marin-Rodriguez B, Kapoor V, et al. Functional circuit architecture underlying parental behaviour. Nature [Internet]. 2018;556(7701):326–31. Available from: https://doi.org/10.1038/s41586-018-0027-0

18. Root CM, Denny CA, Hen R, Axel R. The participation of cortical amygdala in innate, odour-driven behaviour. Nature. 2014;515(7526):269–73.

19. Isosaka T, Matsuo T, Yamaguchi T, Funabiki K, Nakanishi S, Kobayakawa R, et al. Htr2a-expressing cells in the central amygdala control the hierarchy between innate and learned fear. Cell. 2015;163(5):1153–64.

20. Lendvai B, Stern EA, Chen B, Svoboda K. Experience-dependent plasticity of dendritic spines in the developing rat barrel cortex in vivo. Nature [Internet]. 2000;404(6780):876–81. Available from: https://doi.org/10.1038/35009107

21. Trachtenberg JT, Chen BE, Knott GW, Feng G, Sanes JR, Welker E, et al. Long-term in vivo imaging of experience-dependent synaptic plasticity in adult cortex. Nature [Internet]. 2002;420(6917):788–94. Available from: https://doi.org/10.1038/nature01273

22. Holtmaat A, Svoboda K. Experience-dependent structural synaptic plasticity in the mammalian brain. Nat Rev Neurosci [Internet]. 2009;10(9):647–58. Available from: https://doi.org/10.1038/nrn2699

23. Takeuchi T, Duszkiewicz AJ, Morris RGM. The synaptic plasticity and memory hypothesis: encoding, storage and persistence. Philos Trans R Soc B Biol Sci. 2014;369(1633):20130288.

24. Pignatelli M, Ryan TJ, Roy DS, Lovett C, Smith LM, Muralidhar S, et al. Engram Cell Excitability State Determines the Efficacy of Memory Retrieval. Neuron [Internet]. 2019;101(2):274-284.e5. Available from: https://linkinghub.elsevier.com/retrieve/pii/S0896627318310389

25. Hawrylycz MJ, Lein ES, Guillozet-Bongaarts AL, Shen EH, Ng L, Miller JA, et al. An anatomically comprehensive atlas of the adult human brain transcriptome. Nature [Internet]. 2012;489(7416):391–9. Available from: https://doi.org/10.1038/nature11405

26. Zhang Y, Chen K, Sloan SA, Bennett ML, Scholze AR, O'Keeffe S, et al. An RNA-sequencing transcriptome and splicing database of glia, neurons, and vascular cells of the cerebral cortex. J Neurosci [Internet]. 2014 Sep 3;34(36):11929–47. Available from: https://pubmed.ncbi.nlm.nih.gov/25186741

27. Bakken TE, Miller JA, Ding S-L, Sunkin SM, Smith KA, Ng L, et al. A comprehensive transcriptional map of primate brain development. Nature [Internet]. 2016;535(7612):367–75. Available from: https://doi.org/10.1038/nature18637

28. Tasic B, Yao Z, Graybuck LT, Smith KA, Nguyen TN, Bertagnolli D, et al. Shared and distinct transcriptomic cell types across neocortical areas. Nature [Internet]. 2018;563(7729):72–8. Available from: https://doi.org/10.1038/s41586-018-0654-5

29. Hodge RD, Bakken TE, Miller JA, Smith KA, Barkan ER, Graybuck LT, et al. Conserved cell types with divergent features in human versus mouse cortex. Nature [Internet]. 2019;573(7772):61–8. Available from: https://doi.org/10.1038/s41586-019-1506-7

30. Sohal VS, Rubenstein JLR. Excitation-inhibition balance as a framework for investigating mechanisms in neuropsychiatric disorders. Mol Psychiatry [Internet]. 2019;24(9):1248–57. Available from: https://doi.org/10.1038/s41380-019-0426-0

31. Roberts E, Frankel S. Gamma-aminobutyric acid in brain. In: Federation Proceedings. FEDERATION AMER SOC EXP BIOL 9650 ROCKVILLE PIKE, BETHESDA, MD 20814-3998; 1950. p. 219.

32. Roberts E, Frankel S. γ-aminobutyric acid in brain: its formation from glutamic acid. J Biol Chem. 1950;187:55–63.

33. Awapara J, Landua AJ, Fuerst R, Seale B. Free γ-aminobutyric acid in brain. J Biol Chem. 1950;187:35–9.

34. Bazemore A, Elliott KAC, Florey E. Factor I and γ-Aminobutyric Acid. Nature [Internet]. 1956;178(4541):1052–3. Available from: https://doi.org/10.1038/1781052a0

35. Bazemore AW, Elliott KAC, Florey E. Isolation of Factor I. J Neurochem [Internet]. 1957 Aug 1;1(4):334–9. Available from: https://doi.org/10.1111/j.1471-4159.1957.tb12090.x

36. Florey E. An inhibitory and an excitatory factor of mammalian central nervous system, and their action on a single sensory neuron. Arch Int Physiol. 1954;62(1):33–53.

37. Otsuka M, Iversen LL, Hall ZW, Kravitz EA. Release of gamma-aminobutyric acid from inh bitory nerves of lobster. Proc Natl Acad Sci U S A [Internet]. 1966 Oct;56(4):1110–5. Available from: https://pubmed.ncbi.nlm.nih.gov/5230136

38. Krnjević K, Schwartz S. The action of γ-Aminobutyric acid on cortical neurones. Exp Brain Res [Internet]. 1967;3(4):320–36. Available from: https://doi.org/10.1007/BF00237558

39. Dreifuss JJ, Kelly JS, Krnjević K. Cortical inhibition and γ-aminobutyric acid. Exp Brain Res [Internet]. 1969;9(2):137–54. Available from: https://doi.org/10.1007/BF00238327

40. Curtis DR, Duggan AW, Felix D, Johnston GAR. GABA, Bicuculline and Central Inhibition. Nature [Internet]. 1970;226(5252):1222–4. Available from: https://doi.org/10.1038/2261222a0

41. Johnston GAR. Advantages of an antagonist: bicuculline and other GABA antagonists. Br J Pharmacol [Internet]. 2013 May 1;169(2):328–36. Available from: https://doi.org/10.1111/bph.12127

42. Beaumont K, Chilton WS, Yamamura HI, Enna SJ. Muscimol binding in rat brain: Association with synaptic GABA receptors. Brain Res [Internet]. 1978;148(1):153–62. Available from: http://www.sciencedirect.com/science/article/pii/0006899378903852

43. Chan-Palay V. Autoradiographic localization of gamma-aminobutyric acid receptors in the rat central nervous system by using [3H]muscimol. Proc Natl Acad Sci U S A [Internet]. 1978 Feb;75(2):1024–8. Available from: https://pubmed.ncbi.nlm.nih.gov/273213

44. Bowery NG, Hudson AL, Price GW. GABAA and GABAB receptor site distribution in the rat central nervous system. Neuroscience [Internet]. 1987;20(2):365–83. Available from: http://www.sciencedirect.com/science/article/pii/0306452287900984

45. Schofield PR, Darlison MG, Fujita N, Burt DR, Stephenson FA, Rodriguez H, et al. Sequence and functional expression of the GABAA receptor shows a ligand-gated receptor super-family. Nature [Internet]. 1987;328(6127):221–7. Available from: https://doi.org/10.1038/328221a0

46. Kaupmann K, Huggel K, Heid J, Flor PJ, Bischoff S, Mickel SJ, et al. Expression cloning of GABAB receptors uncovers similarity to metabotropic glutamate receptors. Nature [Internet]. 1997;386(6622):239–46. Available from: https://doi.org/10.1038/386239a0

47. Houamed KM, Bi be G, Smart TG, Constanti A, Brown DA, Barnard EA, et al. Expression of functional GABA, glycine and glutamate receptors in Xenopus oocytes injected with rat brain mRNA. Nature [Internet]. 1984;310(5975):318–21. Available from: https://doi.org/10.1038/310318a0

48. Olsen RW, Li G-D. Chapter 18 - GABA. In: Brady ST, Siegel GJ, A bers RW, Price DLBT-BN (Eighth E, editors. New York: Academic Press; 2012. p. 367–76. Available from: http://www.sciencedirect.com/science/article/pii/B9780123749475000183

49. Walls AB, Nilsen LH, Eyjolfsson EM, Vestergaard HT, Hansen SL, Schousboe A, et al. GAD65 is essential for synthesis of GABA destined for tonic inhibition regulating epileptiform activity. J Neurochem. 2010;115(6):1398–408.

50. Kaufman DL, Houser CR, Tobin AJ. Two Forms of the γ-Aminobutyric Acid Synthetic Enzyme Glutamate Decarboxylase Have Distinct Intraneuronal Distributions and Cofactor Interactions. J Neurochem. 1991;56(2):720–3.

51. Asada H, Kawamura Y, Maruyama K, Kume H, Ding RG, Kanbara N, et al. Cleft palate and decreased brain γ-aminobutyric acid in mice lacking the 67-kDa isoform of glutamic acid decarboxylase. Proc Natl Acad Sci U S A. 1997;94(12):6496–9.

52. She kh SN, Martin SB, Martin DL. Regional distr bution and relative amounts of glutamate decarboxylase isoforms in rat and mouse brain. Neurochem Int. 1999;35(1):73–80.

53. Kass I, Hoke DE, Costa MGS, Reboul CF, Porebski BT, Cowieson NP, et al. Cofactor-dependent conformational heterogeneity of GAD65 and its role in autoimmunity and neurotransmitter homeostasis. Proc Natl Acad Sci U S A. 2014;111(25).

54. Patel AB, De Graaf RA, Martin DL, Battaglioli G, Behar KL. Evidence that GAD65 mediates increased GABA synthesis during intense neuronal activity in vivo. J Neurochem. 2006;97(2):385–96.

55. Tian N, Petersen C, Kash S, Baekkeskov S, Copenhagen D, Nicoll R. The role of the synthetic enzyme GAD65 in the control of neuronal γ-aminobutyric acid release. Proc Natl Acad Sci U S A. 1999;96(22):12911–6.

56. Battaglioli G, Liu H, Martin DL. Kinetic differences between the isoforms of glutamate decarboxylase: Implications for the regulation of GABA synthesis. J Neurochem. 2003;86(4):879–87.

57. Waagepetersen HS, Schousboe ABT-RM in BS. Glial GABA and Glutamate Metabolism. In: Encyclopedia of Neuroscience [Internet]. Elsevier; 2009. p. 789–92. Available from: http://www.sciencedirect.com/science/article/pii/B9780128012383046183

58. Armijo JA, Arteaga R, Valiente R, Herranz JL. Platelet GABA-aminotransferase in epileptic patients. Int J Clin Pharmacol Res [Internet]. 1989;9(4):283–5. Available from: http://europepmc.org/abstract/MED/2777429

59. Bright D, Houston C, Brickley S. Sources of GABA That Activate Extrasynaptic GABAA Receptors. In: Errington AC, Di Giovanni G, Crunelli V, editors. Extrasynaptic GABAA Receptors [Internet]. New York, NY: Springer New York; 2014. p. 85–124. Available from: https://doi.org/10.1007/978-1-4939-1426-5_6

60. Edwards RH, Jorgensen EM, McIntire SL, Reimer RJ, Schuske K, Edwards RH, et al. Identification and characterization of the vesicular GABA transporter. Nature [Internet]. 1997;389(6653):870–6. Available from: http://www.nature.com/doifinder/10.1038/39908%5Cnpapers3://publication/doi/10.1038/39908

61. Farrant M, Nusser Z. Variations on an inh bitory theme: phasic and tonic activation of GABA(A) receptors. Nat Rev Neurosci. 2005;6(3):215–29.

62. Barberis A, Petrini EM, Cherubini E. Presynaptic source of quantal size variability at GABAergic synapses in rat hippocampal neurons in culture. Eur J Neurosci [Internet]. 2004 Oct 1;20(7):1803–10. Available from: https://doi.org/10.1111/j.1460-9568.2004.03624.x

63. Mozrzymas JW, Zarnowska ED, Pytel M, Mercik K. Modulation of GABA(A) receptors by hydrogen ions reveals synaptic GABA transient and a crucial role of the desensitization process. J Neurosci [Internet]. 2003 Sep 3;23(22):7981–92. Available from: https://pubmed.ncbi.nlm.nih.gov/12954859

64. Hájos N, Nusser Z, Rancz EA, Freund TF, Mody I. Cell type- and synapse-specific variability in synaptic GABAA receptor occupancy. Eur J Neurosci [Internet]. 2000 Mar 1;12(3):810–8. Available from: https://doi.org/10.1046/j.1460-9568.2000.00964.x

65. Scanziani M. GABA Spillover Activates Postsynaptic $GABA_B$ Receptors to Control Rhythmic Hippocampal Activity. Neuron [Internet]. 2000 Mar 1;25(3):673–81. Available from: https://doi.org/10.1016/S0896-6273(00)81069-7

66. Zarnowska ED, Keist R, Rudolph U, Pearce RA. GABAA receptor α5 subunits contr bute to GABAA, slow synaptic inhibition in mouse hippocampus. J Neurophysiol [Internet]. 2008/12/10. 2009 Mar;101(3):1179–91. Available from: https://pubmed.ncbi.nlm.nih.gov/19073796

67. Vargas-Caballero M, Martin LJ, Salter MW, Orser BA, Paulsen O. alpha5 Subunit-containing GABA(A) receptors mediate a slowly decaying inh bitory synaptic current in CA1 pyramidal neurons following Schaffer collateral activation. Neuropharmacology [Internet]. 2009/11/23. 2010 Mar;58(3):668–75. Available from: https://pubmed.ncbi.nlm.nih.gov/19941877

68. Jarvis S, Nikolic K, Schultz SR. Neuronal gain modulability is determined by dendritic morphology : A computational optogenetic study. 2018;(319818):1–21.

69. Sun M-Y, Shu H-J, Benz A, Bracamontes J, Akk G, Zorumski CF, et al. Chemogenetic isolation reveals synaptic contr bution of δ GABAA receptors in mouse dentate granule neurons. J Neurosci [Internet]. 2018;(314):0799–18. Available from: http://www.jneurosci.org/lookup/doi/10.1523/JNEUROSCI.0799-18.2018%0Ahttp://www.ncbi.nlm.nih.gov/pubmed/30076210

70. Glykys J, Mody I. The main source of ambient GABA responsible for tonic inhibition in the mouse hippocampus. J Physiol [Internet]. 2007;582(Pt 3):1163–78. Available from: http://www.ncbi.nlm.nih.gov/pmc/articles/PMC2075237/

71. Holter NI, Zylla MM, Zuber N, Bruehl C, Draguhn A. Tonic GABAergic control of mouse dentate granule cells during postnatal development. Eur J Neurosci [Internet]. 2010 Oct 1;32(8):1300–9. Available from: https://doi.org/10.1111/j.1460-9568.2010.07331.x

72. Wei W, Zhang N, Peng Z, Houser CR, Mody I. Perisynaptic localization of delta subunit-containing GABA(A) receptors and their activation by GABA spillover in the mouse dentate gyrus. J Neurosci [Internet]. 2003;23(33):10650–61. Available from: http://www.jneurosci.org/cgi/content/full/23/33/10650%5Cnpapers3://publication/uuid/FAF82695-B488-4E3E-833C-CBFED05B0B8B

73. Tossman U, Jonsson G, Ungerstedt U. Regional distribution and extracellular levels of amino acids in rat central nervous system. Acta Physiol Scand [Internet]. 1986 Aug 1;127(4):533–45. Available from: https://doi.org/10.1111/j.1748-1716.1986.tb07938.x

74. Wlodarczyk AI, Sylantyev S, Herd MB, Kersante F, Lambert JJ, Rusakov DA, et al. GABA-Independent GABAA Receptor Openings Maintain Tonic Currents. J Neurosci [Internet]. 2013;33(9):3905–14. Available from: http://www.jneurosci.org/cgi/doi/10.1523/JNEUROSCI.4193-12.2013

75. Bianchi L, Ballini C, Colivicchi MA, Della Corte L, Giovannini MG, Pepeu G. Investigation on acetylcholine, aspartate, glutamate and GABA extracellular levels from ventral hippocampus during repeated exploratory activity in the rat. Neurochem Res. 2003;28(3–4):565–73.

76. Zieminska E, Toczylowska B, Diamandakis D, Hilgier W, Filipkowski RK, Polowy R, et al. Glutamate, Glutamine and GABA Levels in Rat Brain Measured Using MRS, HPLC and NMR Methods in Study of Two Models of Autism. Front Mol Neurosci [Internet]. 2018 Nov 16;11:418. Available from: https://pubmed.ncbi.nlm.nih.gov/30505268

77. Rea K, Cremers TIFH, Westerink BHC. HPLC conditions are critical for the detection of GABA by microdialysis. J Neurochem [Internet]. 2005 Aug 1;94(3):672–9. Available from: https://doi.org/10.1111/j.1471-4159.2005.03218.x

78. van der Zeyden M, Oldenziel WH, Rea K, Cremers TI, Westerink BH. Microdialysis of GABA and glutamate: Analysis, interpretation and comparison with microsensors. Pharmacol Biochem Behav [Internet]. 2008;90(2):135–47. Available from: http://www.sciencedirect.com/science/article/pii/S0091305707002791

79. Kaneda M, Farrant M, Cull-Candy SG. Whole-cell and single-channel currents activated by GABA and glycine in granule cells of the rat cerebellum. J Physiol [Internet]. 1995 Jun 1;485 (Pt 2(Pt 2):419–35. Available from: https://pubmed.ncbi.nlm.nih.gov/7545231

80. Brickley SG, Cull-Candy SG, Farrant M. Development of a tonic form of synaptic inh bition in rat cerebellar granule cells resulting from persistent activation of GABAA receptors. J Physiol. 1996;497(3):753–9.

81. Song I, Volynski K, Brenner T, Ushkaryov Y, Walker M, Semyanov A. Different transporter systems regulate extracellular GABA from vesicular and non-vesicular sources. Front Cell Neurosci [Internet]. 2013 Mar 13;7(March):23. Available from: https://pubmed.ncbi.nlm.nih.gov/23494150

82. Scimemi A. Structure, function, and plasticity of GABA transporters. Front Cell Neurosci [Internet]. 2014 Jun 17;8:161. Available from: https://pubmed.ncbi.nlm.nih.gov/24987330

83. Nusser Z, Mody I. Selective modulation of tonic and phasic inhibitions in dentate gyrus granule cells. J Neurophysiol. 2002;87(5):2624–8.

84. Rossi DJ, Hamann M, Attwell D. Multiple modes of GABAergic inhibition of rat cerebellar granule cells. J Physiol [Internet]. 2003/02/14. 2003 Apr 1;548(Pt 1):97–110. Available from: https://pubmed.ncbi.nlm.nih.gov/12588900

85. Wu Y, Wang W, Díez-Sampedro A, Richerson GB. Nonvesicular inhibitory neurotransmission via reversal of the GABA transporter GAT-1. Neuron [Internet]. 2007 Dec 6;56(5):851–65. Available from: https://pubmed.ncbi.nlm.nih.gov/18054861

86. Ribak CE, Tong WMY, Brecha NC. GABA plasma membrane transporters, GAT-1 and GAT-3, display different distr butions in the rat hippocampus. J Comp Neurol [Internet]. 1996 Apr 15;367(4):595–606. Available from: https://doi.org/10.1002/(SICI)1096-9861(19960415)367:4%3C595::AID-CNE9%3E3.0.CO

87. Keros S, Hablitz JJ. Subtype-specific GABA transporter antagonists synergistically modulate phasic and tonic GABAA conductances in rat neocortex. J Neurophysiol. 2005;94(3):2073–85.

88. Pandit S, Lee GS, Park JB. Developmental changes in GABA(A) tonic inhibition are compromised by multiple mechanisms in preadolescent dentate gyrus granule cells. Korean J Physiol Pharmacol [Internet]. 2017/10/30. 2017 Nov;21(6):695–702. Available from: https://pubmed.ncbi.nlm.nih.gov/29200913

89. Da by NO. GABA-level increasing and anticonvulsant effects of three different GABA uptake inhibitors. Neuropharmacology [Internet]. 2000;39(12):2399–407. Available from: http://www.sciencedirect.com/science/article/pii/S0028390800000757

90. Savtchenko L, Megalogeni M, Rusakov DA, Walker MC, Pavlov I. Synaptic GABA release prevents GABA transporter type-1 reversal during excessive network activity. Nat Commun [Internet]. 2015;6(1):6597. Available from: https://doi.org/10.1038/ncomms7597

91. Le Meur K, Mendizabal-Zubiaga J, Grandes P, Audinat E. GABA release by hippocampal astrocytes. Front Comput Neurosci [Internet]. 2012;6:59. Available from: https://www.frontiersin.org/article/10.3389/fncom.2012.00059

92. Héja L, Nyitrai G, Kékesi O, Dobolyi A, Szabó P, Fiáth R, et al. Astrocytes convert network excitation to tonic inhibition of neurons. BMC Biol [Internet]. 2012 Mar 15;10:26. Available from: https://pubmed.ncbi.nlm.nih.gov/22420899

93. Héja L, Barabás P, Nyitrai G, Kékesi KA, Lasztóczi B, Toke O, et al. Glutamate uptake triggers transporter-mediated GABA release from astrocytes. PLoS One [Internet]. 2009 Sep 24;4(9):e7153–e7153. Available from: https://pubmed.ncbi.nlm.nih.gov/19777062

94. Lee S, Yoon B-E, Berglund K, Oh S-J, Park H, Shin H-S, et al. Channel-Mediated Tonic GABA Release from Glia. Science (80-) [Internet]. 2010 Nov 5;330(6005):790 LP – 796. Available from: http://science.sciencemag.org/content/330/6005/790.abstract

95. Benarroch EE. GABAB receptors. Neurology [Internet]. 2012 Feb 21;78(8):578 LP – 584. Available from: http://n.neurology.org/content/78/8/578.abstract

96. Mott DD, Lewis D V. Facilitation of the induction of long-term potentiation by GABAB receptors. Science (80-) [Internet]. 1991 Jun 21;252(5013):1718 LP – 1720. Available from: http://science.sciencemag.org/content/252/5013/1718.abstract

97. Hübner CA, Holthoff K. Anion transport and GABA signaling. Front Cell Neurosci. 2013;7(OCT):1–12.

98. Masiulis S, Desai R, Uchański T, Serna Martin I, Laverty D, Karia D, et al. GABA A receptor signalling mechanisms revealed by structural pharmacology. Nature [Internet]. 2019;565(7740):454–9. Available from: http://www.nature.com/articles/s41586-018-0832-5

99. Miller PS, Aricescu AR. Crystal structure of a human GABAA receptor. Nature. 2014;512(7514):270–5.

100. Miller PS, Smart TG. Binding , activation and modulation of Cys-loop receptors. Trends Pharmacol Sci [Internet]. 2010;31(4):161–74. Available from: http://dx.doi.org/10.1016/j.tips.2009.12.005

101. Changeux JP. The nicotinic acetylcholine receptor: A typical 'allosteric machine.' Philos Trans R Soc B Biol Sci. 2018;373(1749).

102. Steinbach JH, Akk G. Applying the Monod-Wyman-Changeux allosteric activation model to pseudo–steady-state responses from GABAA receptors. Mol Pharmacol [Internet]. 2019;95(1):106–19. Available from: http://molpharm.aspetjournals.org/lookup/doi/10.1124/mol.118.113787

103. Laverty D, Desai R, Uchański T, Masiulis S, Stec WJ, Malinauskas T, et al. Cryo-EM structure of the human α1β3γ2 GABAA receptor in a lipid bilayer. Nature. 2019;565(7740):516–20.

104. Sieghart W, Savic MM. International union of basic and clinical pharmacology. CVI: GABAA receptor subtype- and function-selective ligands: Key issues in translation to humans. Pharmacol Rev [Internet]. 2018;70(4):836–78. Available from: http://www.ncbi.nlm.nih.gov/pubmed/30275042

105. Olsen RW, Sieghart W. International Union of Pharmacology. LXX. Subtypes of γ-Aminobutyric Acid(A) Receptors: Classification on the Basis of Subunit Composition, Pharmacology, and Function. Update. Pharmacol Rev [Internet]. 2008 Sep 1;60(3):243 LP – 260. Available from: http://pharmrev.aspetjournals.org/content/60/3/243.abstract

106. Olsen RW, Sieghart W. GABAA receptors: Subtypes provide diversity of function and pharmacology. Neuropharmacology [Internet]. 2009;56(1):141–8. Available from: http://dx.doi.org/10.1016/j.neuropharm.2008.07.045

107. Smart TG, Stephenson FA. A half century of γ-aminobutyric acid. Brain Neurosci Adv [Internet]. 2019 Jan 1;3:2398212819858249. Available from: https://doi.org/10.1177/2398212819858249

108. Bateson AN, Lasham A, Darlison MG. γ-Aminobutyric acidA receptor heterogeneity is increased by alternative splicing of a novel β-subunit gene transcript. J Neurochem. 1991;56(4):1437–40.

109. Levin ML, Chatterjee A, Pragliola A, Worley KC, Wehnert M, Zhuchenko O, et al. A comparative transcription map of the murine bare patches (Bpa) and striated (Str) critical regions and human Xq28. Genome Res. 1996;6(6):465–77.

110. Mehta AK, Ticku MK. An update on GABAA receptors. Brain Res Rev. 1999;29(2–3):196–217.

111. Hörtnagl H, Tasan RO, Wieselthaler A, Kirchmair E, Sieghart W, Sperk G. Patterns of mRNA and protein expression for 12 GABAA receptor subunits in the mouse brain. Neuroscience [Internet]. 2013;236:345–72. Available from: http://dx.doi.org/10.1016/j.neuroscience.2013.01.008

112. Pirker S, Schwarzer C, Wieselthaler A, Sieghart W, Sperk G. GABAA receptors: immunocytochemical distr bution of 13 subunits in the adult rat brain. Neuroscience [Internet]. 2000;101(4):815–50. Available from: http://www.sciencedirect.com/science/article/pii/S0306452200004425

113. Sperk G, Schwarzer C, Tsunashima K, Fuchs K, Sieghart W. GABA(A) receptor subunits in the rat hippocampus I: Immunocytochemical distribution of 13 subunits. Neuroscience. 1997;80(4):987–1000.

114. Cembrowski MS, Wang L, Sugino K, Shields BC, Spruston N. Hipposeq: A comprehensive RNA-seq database of gene expression in hippocampal principal neurons. Elife. 2016;5(APRIL2016):1–22.

115. Nakamura NH, Akiyama K, Naito T. Quantitative gene-expression analysis of the ligand-receptor system for classical neurotransmitters and neuropeptides in hippocampal CA1, CA3, and dentate gyrus. Hippocampus. 2011;21(11):1228–39.

116. Wisden W, Laurie DJ, Monyer H, Seeburg PH. The distribution of 13 GABAA receptor subunit mRNAs in the rat brain. I. Telencephalon, diencephalon, mesencephalon. J Neurosci [Internet]. 1992 Mar;12(3):1040–62. Available from: https://pubmed.ncbi.nlm.nih.gov/1312131

117. Sarto-Jackson I, Sieghart W. Assembly of GABAA receptors (Review). Mol Membr Biol [Internet]. 2008 Jan

1;25(4):302–10. Available from: https://doi.org/10.1080/09687680801914516

118. Taylor PM, Connolly CN, Kittler JT, Gorrie GH, Hosie A, Smart TG, et al. Identification of Residues within GABAA Receptor α Subunits That Mediate Specific Assembly with Receptor β Subunits. J Neurosci [Internet]. 2000 Feb 15;20(4):1297 LP – 1306. Available from: http://www.jneurosci.org/content/20/4/1297.abstract

119. Hannan S, Smart TG. Cell surface expression of homomeric GABAA receptors depends on single residues in subunit transmembrane domains. J Biol Chem. 2018;293(35):13427–39.

120. Klausberger T, Sarto I, Ehya N, Fuchs K, Furtmüller R, Mayer B, et al. Alternate Use of Distinct Intersubunit Contacts Controls GABAA Receptor Assembly and Stoichiometry. J Neurosci [Internet]. 2001 Dec 1;21(23):9124 LP – 9133. Available from: http://www.jneurosci.org/content/21/23/9124.abstract

121. Taylor PM, Thomas P, Gorrie GH, Connolly CN, Smart TG, Moss SJ. Identification of amino acid residues within GABA(A) receptor beta subunits that mediate both homomeric and heteromeric receptor expression. J Neurosci [Internet]. 1999 Aug 1;19(15):6360–71. Available from: https://pubmed.ncbi.nlm.nih.gov/10414965

122. Klausberger T, Fuchs K, Mayer B, Ehya N, Sieghart W. GABAA Receptor Assembly Identification and structure of γ2 sequences forming the intersubunit contacts with α1 and β3 subunits. J Biol Chem. 2000;275(12):8921–8.

123. Wooltorton JRA, Moss SJ, Smart TG. Pharmacological and Physiological Characterization of Murine Homomeric p3 GABAA Receptors. 1997;9:2225–35.

124. Saras A, Gisselmann G, Vogt-Eisele AK, Erlkamp KS, Kletke O, Pusch H, et al. Histamine action on vertebrate GABAA receptors: Direct channel gating and potentiation of GABA responses. J Biol Chem. 2008;283(16):10470–5.

125. Cestari IN, Uchida I, Li L, Burt D, Yang J. The agonistic action of pentobarbital on GABAA β-subunit homomeric receptors. Neuroreport [Internet]. 1996;7(4). Available from: https://journals.lww.com/neuroreport/Fulltext/1996/03220/The_agonistic_action_of_pentobarbital_on_GABAA.23.aspx

126. Belelli D, Hales TG, Lambert JJ, Luscher B, Olsen R, Peters JA. GABA A receptors (version 2019 . 4) in the IUPHAR / BPS Guide to Pharmacology Database. 2019;1–23.

127. Mortensen M, Smart TG. Extrasynaptic alpha beta subunit GABAA receptors on rat hippocampal pyramidal neurons. J Physiol [Internet]. 2006;577(3):841–56. Available from: http://www.pubmedcentral.nih.gov/articlerender.fcgi?artid=1890388&tool=pmcentrez&rendertype=abstract

128. Baumann SW, Baur R, Sigel E. Forced Subunit Assembly in α1β2γ2 GABAA Receptors. Insight Into The Absolute Arrangement. J Biol Chem. 2002;277(48):46020–5.

129. Tretter V, Ehya N, Fuchs K, Sieghart W. Stoichiometry and assembly of a recombinant GABAA receptor subtype. J Neurosci. 1997;17(8):2728–37.

130. Patel B, Mortensen M, Smart TG. Stoichiometry of δ subunit containing GABAA receptors. Br J Pharmacol. 2014;171(4):985–94.

131. Pollard S, Thompson CL, Stephenson FA. Quantitative characterization of α6 and α1α6 subunit-containing native γ-aminobutyric acidA receptors of adult rat cerebellum demonstrates two α subunits per receptor oligomer. J Biol Chem. 1995;270(36):21285–90.

132. Duggan MJ, Pollard S, Stephenson FA. Immunoaffinity purification of GABAA receptor alpha-subunit iso-oligomers. Demonstration of receptor populations containing alpha 1 alpha 2, alpha 1 alpha 3, and alpha 2 alpha 3 subunit pairs. J Biol Chem. 1991;266(36):24778–84.

133. Thomas P, Mortensen M, Hosie AM, Smart TG. Dynamic mobility of functional GABA A receptors at inhibitory synapses. Nat Neurosci. 2005;8(7):889–97.

134. Triller A, Choquet D. Surface trafficking of receptors between synaptic and extrasynaptic membranes: and yet they do move! Trends Neurosci. 2005;28(3):133–9.

135. Bogdanov Y, Michels G, Armstrong-Gold C, Haydon PG, Lindstrom J, Pangalos M, et al. Synaptic GABAA receptors are directly recruited from their extrasynaptic counterparts. EMBO J. 2006;25(18):4381–9.

136. Kasugai Y, Swinny JD, Roberts JDB, Dalezios Y, Fukazawa Y, Sieghart W, et al. Quantitative localisation of synaptic and extrasynaptic GABAA receptor subunits on hippocampal pyramidal cells by freeze-fracture replica immunolabelling. Eur J Neurosci. 2010;32(11):1868–88.

137. Li P, Akk G. Synaptic-type α1β2γ2L GABAa receptors produce large persistent currents in the presence of ambient GABA and anesthetic drugs. Mol Pharmacol. 2015;87(5):776–81.

138. Brickley SG, Mody I. Extrasynaptic GABA A Receptors: Their Function in the CNS and Implications for Disease. Neuron [Internet]. 2012;73(1):23–34. Available from: http://dx.doi.org/10.1016/j.neuron.2011.12.012

139. Brickley SG, Cull-Candy SG, Farrant M. Single-channel properties of synaptic and extrasynaptic GABAA receptors suggest differential targeting of receptor subtypes. J Neurosci [Internet]. 1999 Apr 15;19(8):2960–73. Available from: https://pubmed.ncbi.nlm.nih.gov/10191314

140. Chesnoy-Marchais D. Bicuculline- and neurosteroid-sensitive tonic chloride current in rat hypoglossal motoneurons and atypical dual effect of SR95531. Eur J Neurosci. 2013;37(3):366–79.

141. Peng Z. Altered Expression of the δ Subunit of the GABAA Receptor in a Mouse Model of Temporal Lobe Epilepsy. J Neurosci [Internet]. 2004;24(39):8629–39. Available from: http://www.jneurosci.org/cgi/doi/10.1523/JNEUROSCI.2877-04.2004

142. Zhang N, Wei W, Mody I, Houser CR. Altered localization of GABA(A) receptor subunits on dentate granule cell dendrites influences tonic and phasic inhibition in a mouse model of epilepsy. J Neurosci. 2007;27(28):7520–31.

143. Tretter V, Hauer B, Nusser Z, Mihalek RM, Höger H, Homanics GE, et al. Targeted Disruption of the GABAA Receptor δ Subunit Gene Leads to an Up-regulation of γ2 Subunit-containing Receptors in Cerebellar Granule Cells. J Biol Chem. 2001;276(13):10532–8.

144. Wongsamitkul N, Baur R, Sigel E. Toward Understanding Functional Properties and Subunit Arrangement of α4β2δ γ-Aminobutyric Acid, Type A (GABAA) Receptors. J Biol Chem [Internet]. 2016/07/05. 2016 Aug 26;291(35):18474–83. Available from: https://pubmed.ncbi.nlm.nih.gov/27382064

145. Brisson A, Unwin PN. Tubular crystals of acetylcholine receptor. J Cell Biol [Internet]. 1984 Oct 1;99(4):1202–11. Available from: https://doi.org/10.1083/jcb.99.4.1202

146. Brisson A, Unwin PNT. Quaternary structure of the acetylcholine receptor. Nature [Internet]. 1985;315(6019):474–7. Available from: https://doi.org/10.1038/315474a0

147. Kubalek E, Ralston S, Lindstrom J, Unwin N. Location of subunits within the acetylcholine receptor by electron image analysis of tubular crystals from Torpedo marmorata. J Cell Biol [Internet]. 1987 Jul 1;105(1):9–18. Available from: https://doi.org/10.1083/jcb.105.1.9

148. Unwin N, Toyoshima C, Kubalek E. Arrangement of the acetylcholine receptor subunits in the resting and desensitized states, determined by cryoelectron microscopy of crystallized Torpedo postsynaptic membranes. J Cell Biol [Internet]. 1988 Sep 1;107(3):1123–38. Available from: https://doi.org/10.1083/jcb.107.3.1123

149. Toyoshima C, Unwin N. Three-dimensional structure of the acetylcholine receptor by cryoelectron microscopy and helical image reconstruction. J Cell Biol [Internet]. 1990 Dec 1;111(6):2623–35. Available from: https://doi.org/10.1083/jcb.111.6.2623

150. Unwin N. Nicotinic Acetylcholine Receptor at 9 Å Resolution. J Mol Biol. 1993;229:1101.

151. Unwin N. Acetylcholine receptor channel imaged in the open state. Nature [Internet]. 1995;373(6509):37–43. Available from: https://doi.org/10.1038/373037a0

152. Unwin N. Projection Structure of the Nicotinic Acetylcholine Receptor: Distinct Conformations of the α Subunits. J Mol Biol [Internet]. 1996;257(3):586–96. Available from: http://www.sciencedirect.com/science/article/pii/S0022283696901874

153. Beroukhim R, Unwin N. Distortion correction of tubular crystals: improvements in the acetylcholine receptor structure. Ultramicroscopy [Internet]. 1997;70(1):57–81. Available from: http://www.sciencedirect.com/science/article/pii/S0304399197000703

154. Miyazawa A, Fujiyoshi Y, Stowell M, Unwin N. Nicotinic acetylcholine receptor at 5 Å resolution. In: Final Program & The Book of Abstracts of the Third Congress of the Asian-Pacific Organization for Cell Biology. 1998.

155. Miyazawa A, Fujiyoshi Y, Unwin N. Structure and gating mechanism of the acetylcholine receptor pore. Nature [Internet]. 2003;423(6943):949–55. Available from: https://doi.org/10.1038/nature01748

156. Unwin N. Refined structure of the nicotinic acetylcholine receptor at 4 Å resolution. J Mol Biol. 2005;346(4):967–89.

157. Nayeem N, Green TP, Martin IL, Barnard EA. Quaternary structure of the native GABAA receptor determined by electron microscopic image analysis. J Neurochem. 1994;62(2):815–8.

158. Puthenkalam R, Hieckel M, Simeone X, Suwattanasophon C, Feldbauer R V, Ecker GF, et al. Structural Studies of GABAA Receptor Binding Sites: Which Experimental Structure Tells us What? . Front Mol Neurosci [Internet]. 2016;9(June):44. Available from: https://www.frontiersin.org/article/10.3389/fnmol.2016.00044

159. O'Mara M, Cromer B, Parker M, Chung S-HH. Homology Model of the GABAA Receptor Examined Using Brownian Dynamics. Biophys J [Internet]. 2005;88(5):3286–99. Available from: http://www.pubmedcentral.nih.gov/articlerender.fcgi?artid=1305477&tool=pmcentrez&rendertype=abstract%5Cnhttp://www.biophysj.org/cgi/content/abstract/88/5/3286

160. Michałowski MA, Kraszewski S, Mozrzymas JW. Binding site opening by loop C shift and chloride ion-pore interaction in the GABAA receptor model. Phys Chem Chem Phys [Internet]. 2017; Available from: http://xlink.rsc.org/?DOI=C7CP00582B

161. Cromer BA, Morton CJ, Parker MW. Anxiety over $GABA_A$ receptor structure relieved by AChBP. Trends Biochem Sci [Internet]. 2002 Jun 1;27(6):280–7. Available from: https://doi.org/10.1016/S0968-0004(02)02092-3

162. Hibbs RE, Gouaux E. Principles of activation and permeation in an anion-selective Cys-loop receptor. Nature [Internet]. 2011;474(7349):54–60. Available from: http://dx.doi.org/10.1038/nature10139

163. Amundarain MJ, R beiro RP, Costabel MD, Giorgetti A. GABAA receptor family: overview on structural characterization. Future Med Chem [Internet]. 2019 Feb 1;11(3):229–45. Available from: https://doi.org/10.4155/fmc-2018-0336

164. Phulera S, Zhu H, Yu J, Claxton DP, Yoder N, Yoshioka C, et al. Cryo-EM structure of the benzodiazepine-sensitive α1β1γ2S tri-heteromeric GABAA receptor in complex with GABA. Swartz KJ, Aldrich R, editors. Elife [Internet]. 2018;7:e39383. Available from: https://doi.org/10.7554/eLife.39383

165. Liu S, Xu L, Guan F, Liu YT, Cui Y, Zhang Q, et al. Cryo-EM structure of the human α5β3 GABAA receptor. Cell Res [Internet]. 2018;28(9):958–61. Available from: http://www.nature.com/articles/s41422-018-0077-8

166. Laverty D, Thomas P, Field M, Andersen OJ, Gold MG, Biggin PC, et al. Crystal structures of a GABAA-receptor chimera reveal new endogenous neurosteroid-binding sites. Nat Struct Mol Biol [Internet]. 2017;24(11):977–85. Available from: https://doi.org/10.1038/nsmb.3477

167. Chen Q, Wells MM, Arjunan P, Tillman TS, Cohen AE, Xu Y, et al. Structural basis of neurosteroid anesthetic action on GABA A receptors. Nat Commun. 2018;9(1):1–10.

168. Zhu S, Noviello CM, Teng J, Walsh RM, Kim JJ, Hibbs RE. Structure of a human synaptic GABAA receptor. Nature [Internet]. 2018;559(7712):67–72. Available from: http://www.nature.com/articles/s41586-018-0255-3

169. Jensen ML, Timmermann DB, Johansen TH, Schousboe A, Varming T, Ahring PK. The β subunit determines the ion selectivity of the GABA A receptor. J Biol Chem. 2002;277(44):41438–47.

170. Hansen SB, Wang HL, Taylor P, Sine SM. An ion selectivity filter in the extracellular domain of Cys-loop receptors reveals determinants for ion conductance. J Biol Chem. 2008;283(52):36066–70.

171. Wotring VE, Miller TS, Weiss DS. Mutations at the GABA receptor selectivity filter: A possible role for effective charges. J Physiol. 2003;548(2):527–40.

172. Wotring VE, Weiss DS. Charge scan reveals an extended region at the intracellular end of the GABA receptor pore that can influence ion selectivity. J Gen Physiol. 2008;131(1):87–97.

173. Keramidas A, Moorhouse AJ, Schofield PR, Barry PH. Ligand-gated ion channels: Mechanisms underlying ion selectivity. Vol. 86, Progress in Biophysics and Molecular Biology. 2004. 161–204 p.

174. Gielen M, Corringer PJ. The dual-gate model for pentameric ligand-gated ion channels activation and desensitization. J Physiol. 2018;596(10):1873–902.

175. O'Toole KK, Jenkins A. Discrete M3-M4 intracellular loop subdomains control specific aspects of γ-aminobutyric acid type A receptor function. J Biol Chem. 2011;286(44):37990–9.

176. Brandon NJ, Bedford FK, Connolly CN, Couve A, Kittler JT, Hanley JG, et al. Synaptic targeting and regulation of GABAA receptors. Portland Press Ltd.; 1999.

177. Vien TN, Moss SJ, Davies PA. Regulating the Efficacy of Inhibition Through Trafficking of γ-Aminobutyric Acid Type A Receptors. Anesth Analg [Internet]. 2016 Nov;123(5):1220–7. Available from:

https://pubmed.ncbi.nlm.nih.gov/27285004

178. Jurd R, Tretter V, Walker J, Brandon NJ, Moss SJ. Fyn kinase contributes to tyrosine phosphorylation of the GABAA receptor γ2 subunit. Mol Cell Neurosci [Internet]. 2010;44(2):129–34. Available from: http://www.sciencedirect.com/science/article/pii/S1044743110000461

179. Mortensen M, Patel B, Smart TG. GABA Potency at GABAA Receptors Found in Synaptic and Extrasynaptic Zones. Front Cell Neurosci [Internet]. 2012;6(January):1. Available from: http://www.pubmedcentral.nih.gov/articlerender.fcgi?artid=3262152&tool=pmcentrez&rendertype=abstract

180. Weir CJ. Ion channels, receptors, agonists and antagonists. Anaesth Intensive Care Med [Internet]. 2010;11(9):377–83. Available from: http://www.sciencedirect.com/science/article/pii/S1472029910001505

181. Colquhoun D, Farrant M. The binding issue. Nature. 1993;366(6455):510–1.

182. Colquhoun D. Binding, gating, affinity and efficacy: The interpretation of structure-activity relationships for agonists and of the effects of mutating receptors. Br J Pharmacol [Internet]. 1998 Nov 1;125(5):923–47. Available from: https://doi.org/10.1038/sj.bjp.0702164

183. Bianchi MT, Haas KF, Macdonald RL. Structural determinants of fast desensitization and desensitization-deactivation coupling in GABAa receptors. J Neurosci. 2001;21(4):1127–36.

184. Jones M V., Westbrook GL. Desensitized states prolong GABAAchannel responses to brief agonist pulses. Neuron. 1995;15(1):181–91.

185. Del Castillo J, Katz B. Interaction at end-plate receptors between different choline derivatives. Proc R Soc Lond B Biol Sci. 1957;146(924):369–81.

186. Colquhoun D, Lape R. Perspectives on: conformational coupling in ion channels: allosteric coupling in ligand-gated ion channels. J Gen Physiol [Internet]. 2012 Dec;140(6):599–612. Available from: https://pubmed.ncbi.nlm.nih.gov/23183696

187. Mortensen M, Kristiansen U, Ebert B, Frølund B, Krogsgaard-Larsen P, Smart TG. Activation of single heteromeric GABA(A) receptor ion channels by full and partial agonists. J Physiol [Internet]. 2004/02/27. 2004 Jun 1;557(Pt 2):389–413. Available from: http://www.pubmedcentral.nih.gov/articlerender.fcgi?artid=1665090&tool=pmcentrez&rendertype=abstract

188. Jones M V, Westbrook GL. Desensitized states prolong GABAA channel responses to brief agonist pulses. Neuron. 1995;15(1):181–91.

189. Petrini EM, Nieus T, Ravasenga T, Succol F, Guazzi S, Benfenati F, et al. Influence of GABAAR monoliganded states on GABAergic responses. J Neurosci [Internet]. 2011 Feb 2;31(5):1752–61. Available from: https://pubmed.ncbi.nlm.nih.gov/21289185

190. Mortensen M, Ebert B, Wafford K, Smart TG. Distinct activities of GABA agonists at synaptic- and extrasynaptic-type GABAA receptors. J Physiol. 2010;588(Pt 8):1251–68.

191. Haas KF, Macdonald RL. GABAA receptor subunit γ2 and δ subtypes confer unique kinetic properties on recombinant GABAA receptor currents in mouse f broblasts. J Physiol [Internet]. 1999 Jan 1;514 (Pt 1(Pt 1):27–45. Available from: https://pubmed.ncbi.nlm.nih.gov/9831714

192. Chang Y, Weiss DS. Allosteric activation mechanism of the α1β2γ2 γ-aminobutyric acid type A receptor revealed by mutation of the conserved M2 leucine. Biophys J. 1999;77(5):2542–51.

193. Monod J, Wyman J, Changeux J-P. On the nature of allosteric transitions: A plausible model. J Mol Biol [Internet]. 1965;12(1):88–118. Available from: http://www.sciencedirect.com/science/article/pii/S0022283665802856

194. Changeux J-P. Allostery and the Monod-Wyman-Changeux Model After 50 Years. Annu Rev Biophys. 2012;41(1):103–33.

195. Rüsch D, Zhong H, Forman SA. Gating allosterism at a single class of etomidate sites on α 1β2γ2L GABAA receptors accounts for both direct activation and acronist modulation. J Biol Chem. 2004;279(20):20982–92.

196. Rüsch D, Forman SA. Classic benzodiazepines modulate the open-close equilibrium in alpha1beta2gamma2L gamma-aminobutyric acid type A receptors. Anesthesiology [Internet]. 2005;102(4):783–92. Available from: http://www.ncbi.nlm.nih.gov/pubmed/15791108

197. Szabo A, Nourmahnad A, Halpin E, Forman SA. Monod-Wyman-Changeux allosteric shift analysis in mutant α1β3γ2L GABAA receptors indicates selectivity and crossta k among intersubunit transmembrane anesthetic

sites. Mol Pharmacol. 2019;95(4):408–17.

198. Campo-Soria C, Chang Y, Weiss DS. Mechanism of action of benzodiazepines on GABA A receptors. Br J Pharmacol. 2006;148(7):984–90.

199. Downing SS, Lee YT, Farb DH, Gibbs TT. Benzodiazepine modulation of partial agonist efficacy and spontaneously active GABA A receptors supports an allosteric model of modulation. Br J Pharmacol. 2005;145(7):894–906.

200. Auerbach A. Thinking in cycles: MWC is a good model for acetylcholine receptor-channels. J Physiol [Internet]. 2012;590(1):93–8. Available from: http://www.pubmedcentral.nih.gov/articlerender.fcgi?artid=3300048&tool=pmcentrez&rendertype=abstract

201. Sivilotti L, Colquhoun D. In praise of single channel kinetics. J Gen Physiol [Internet]. 2016;148(2):79–88. Available from: http://www.jgp.org/lookup/doi/10.1085/jgp.201611649

202. Colquhoun D, Lape R. Allosteric coupling in ligand-gated ion channels. J Gen Physiol [Internet]. 2012;140(6):599–612. Available from: http://www.jgp.org/lookup/doi/10.1085/jgp.201210844

203. Gielen M, Lumb M, Smart T. Benzodiazepines Modulate GABAA Receptors by Regulating the Preactivation Step after GABA Binding. J Neurosci [Internet]. 2012;32(17):5707–15. Available from: http://discovery.ucl.ac.uk/1344170/

204. Goldschen-Ohm MP, Haroldson A, Jones M V., Pearce RA. A nonequil brium binary elements-based kinetic model for benzodiazepine regulation of GABAA receptors. J Gen Physiol [Internet]. 2014;144(1):27–39. Available from: http://www.jgp.org/lookup/doi/10.1085/jgp.201411183

205. Jatczak-Śliwa M, Terejko K, Brodzki M, Michałowski MA, Czyzewska MM, Nowicka JM, et al. Distinct modulation of spontaneous and GABA-evoked gating by flurazepam shapes cross-talk between agonist-free and liganded gabaa receptor activity. Front Cell Neurosci [Internet]. 2018;12(August):1–18. Available from: https://www.frontiersin.org/article/10.3389/fncel.2018.00237/full

206. Steinbach JH, Akk G. Modulation of GABAA receptor channel gating by pentobarbital. J Physiol [Internet]. 2001 Dec 1;537(3):715–33. Available from: https://doi.org/10.1111/j.1469-7793.2001.00715.x

207. Twyman RE, Rogers CJ, Macdonald RL. Intraburst kinetic properties of the GABAA receptor main conductance state of mouse spinal cord neurones in culture. J Physiol. 1990;423(1):193–220.

208. Maconochie DJ, Zempel JM, Steinbach JH. How quickly can GABAA receptors open? Neuron [Internet]. 1994;12(1):61–71. Available from: http://www.sciencedirect.com/science/article/pii/089662739490152X

209. Weiss DS, Magleby KL. Gating scheme for single GABA-activated Cl-channels determined from stability plots, dwell-time distributions, and adjacent-interval durations. J Neurosci. 1989;9(4):1314–24.

210. Kisiel M, Jatczak M, Brodzki M, Mozrzymas JW. Spontaneous activity, singly bound states and the impact of alpha1Phe64 mutation on GABAAR gating in the novel kinetic model based on the single-channel recordings. Neuropharmacology [Internet]. 2018;131(November):453–74. Available from: https://doi.org/10.1016/j.neuropharm.2017.11.030

211. Szczot M, Kisiel M, Czyzewska MM, Mozrzymas JW. α1F64 residue at GABAA receptor binding site is involved in gating by influencing the receptor flipping transitions. J Neurosci [Internet]. 2014;34(9):3193–209. Available from: http://www.jneurosci.org/cgi/doi/10.1523/JNEUROSCI.2533-13.2014

212. Lape R, Colquhoun D, Sivilotti LG. On the nature of partial agonism in the nicotinic receptor superfamily. Nature. 2008;454(7205):722–7.

213. Burzomato V. Single-Channel Behavior of Heteromeric α1β Glycine Receptors: An Attempt to Detect a Conformational Change before the Channel Opens. J Neurosci [Internet]. 2004;24(48):10924–40. Available from: http://www.jneurosci.org/cgi/doi/10.1523/JNEUROSCI.3424-04.2004

214. Scott S, Aricescu AR. A structural perspective on GABAA receptor pharmacology. Curr Opin Struct Biol. 2019;54:189–97.

215. Mukhtasimova N, Lee WY, Wang H-LL, Sine SM. Detection and trapping of intermediate states priming nicotinic receptor channel opening. Nature [Internet]. 2009/04/01. 2009 May 21;459(7245):451–4. Available from: https://pubmed.ncbi.nlm.nih.gov/19339970

216. Doyon N, Vinay L, Prescott SA, De Koninck Y. Chloride Regulation: A Dynamic Equilibrium Crucial for Synaptic Inh bition. Neuron [Internet]. 2016;89(6):1157–72. Available from: http://linkinghub.elsevier.com/retrieve/pii/S0896627316001471

217. Kaila K, Price TJ, Payne JA, Puskarjov M, Voipio J. Cation-chloride cotransporters in neuronal development, plasticity and disease. Nat Rev Neurosci [Internet]. 2014;15(10):637–54. Available from: https://doi.org/10.1038/nrn3819

218. Berglund K, Wen L, Dunbar RL, Feng G, Augustine GJ. Optogenetic visualization of presynaptic tonic inhibition of cerebellar parallel fibers. J Neurosci. 2016;36(21):5709–23.

219. Berglund K, Schleich W, Krieger P, Loo LS, Wang D, Cant NB, et al. Imaging synaptic inhibition in transgenic mice expressing the chloride indicator, Clomeleon. Brain Cell Biol [Internet]. 2008/04/05. 2006 Dec;35(4–6):207–28. Available from: https://pubmed.ncbi.nlm.nih.gov/18398684

220. Kuner T, Augustine GJ. A genetically encoded ratiometric indicator for chloride: Capturing chloride transients in cultured hippocampal neurons. Neuron. 2000;27(3):447–59.

221. Hara M, Inoue M, Yasukura T, Ohnishi S, M kami Y, Inagaki C. Uneven distr bution of intracellular Cl- in rat hippocampal neurons. Neurosci Lett. 1992;143(1–2):135–8.

222. Payne JA, Stevenson TJ, Donaldson LF. Molecular characterization of a putative K-Cl cotransporter in rat brain A neuronal-specific isoform. J Biol Chem. 1996;271(27):16245–52.

223. Sipilä ST, Huttu K, Soltesz I, Voipio J, Kaila K. Depolarizing GABA acts on intrinsically bursting pyramidal neurons to drive giant depolarizing potentials in the immature hippocampus. J Neurosci. 2005;25(22):5280–9.

224. Lee V, Maguire J. The impact of tonic GABAA receptor-mediated inhibition on neuronal excitability varies across brain region and cell type. Front Neural Circuits [Internet]. 2014;8(February):3. Available from: http://journal.frontiersin.org/article/10.3389/fncir.2014.00003/abstract

225. Pavlov I, Savtchenko LP, Song I, Koo J, Pimashkin A, Rusakov DA, et al. Tonic GABA bidirectionally controls interneuron firing pattern and synchronization in the CA3 hippocampal network. 2014;2–7.

226. Song I, Savtchenko L, Semyanov A. Tonic excitation or inhibition is set by GABA(A) conductance in hippocampal interneurons. Nat Commun [Internet]. 2011;2:376. Available from: http://eutils.ncbi.nlm.nih.gov/entrez/eutils/elink.fcgi?dbfrom=pubmed&id=21730957&retmode=ref&cmd=prlinks%5Cnpapers3://publication/doi/10.1038/ncomms1377

227. Chen K, Aradi I, Thon N, Eghbal-Ahmadi M, Baram TZ, Soltesz I. Persistently modified h-channels after complex febrile seizures convert the seizure-induced enhancement of inh bition to hyperexcitability. Nat Med. 2001;7(3):331–7.

228. Tretter V, Jacob TC, Mukherjee J, Fritschy J-M, Pangalos MN, Moss SJ. The clustering of GABA(A) receptor subtypes at inh bitory synapses is facilitated via the direct binding of receptor α2 subunits to Gephyrin. J Neurosci [Internet]. 2008 Feb 6;28(6):1356–65. Available from: https://pubmed.ncbi.nlm.nih.gov/18256255

229. Kowalczyk S, Winkelmann A, Smolinsky B, Förstera B, Neundorf I, Schwarz G, et al. Direct binding of GABAA receptor β2 and β3 subunits to gephyrin. Eur J Neurosci [Internet]. 2013 Feb 1;37(4):544–54. Available from: https://doi.org/10.1111/ejn.12078

230. Bright DP, Smart TG. Methods for recording and measuring tonic GABAA receptor-mediated inhibition. Front Neural Circuits [Internet]. 2013;7(December):193. Available from: http://www.pubmedcentral.nih.gov/articlerender.fcgi?artid=3852068&tool=pmcentrez&rendertype=abstract

231. Glykys J, Mody I. Activation of GABAA Receptors: Views from Outside the Synaptic Cleft. Neuron. 2007;56(5):763–70.

232. Mody I, Pearce RA. Diversity of inhibitory neurotransmission through GABA A receptors. 2004;27(9).

233. McCartney MR, Deeb TZ, Henderson TN, Hales TG. Tonically Active GABAA Receptors in Hippocampal Pyramidal Neurons Exhibit Constitutive GABA-Independent Gating. Mol Pharmacol. 2007;71(2):539–48.

234. Botta P, Demmou L, Kasugai Y, Markovic M, Xu C, Fadok JP, et al. Regulating anxiety with extrasynaptic inhibition. Nat Neurosci [Internet]. 2015;18(10):1493–500. Available from: http://0-www.nature.com.jabega.uma.es/neuro/journal/v18/n10/full/nn.4102.html

235. Karim N, Wellendorph P, Hanrahan JR, Cheb b M. Potency of GABA at human recombinant GABA A receptors expressed in Xenopus oocytes : a mini review. 2013;1139–49.

236. Birnir B, Everitt AB, Lim MSF, Gage PW. Spontaneously Opening GABA A Channels in CA1 Pyramidal Neurones of Rat Hippocampus. J Membr Biol [Internet]. 2000;174(1):21–9. Available from: http://www.springerlink.com/openurl.asp?genre=article&id=doi:10.1007/s002320001028

237. Lindquist CEL, Birnir B. Graded response to GABA by native extrasynaptic GABAA receptors. J Neurochem. 2006;97(5):1349–56.

238. Hamann M, Desarmenien M, Desaulles E, Bader MF, Feltz P. Quantitative evaluation of the properties of a pyridazinyl GABA derivative (SR 95531) as a GABAA competitive antaginist. An electrophysiological approach. Brain Res. 1988;442(2):287–96.

239. Heaulme M, Chambon J, I RL, Molimard J, Wermuth CG, I KB. Biochemical Characterization of the Interaction of Three Pyridazinyl-GABA Derivatives with the GABA A Receptor Site. 1986;384:224–31.

240. Wermuth CG, Bourguignon JJ, Schlewer G, Gies JP, Schoenfelder A, Melikian A, et al. Synthesis and structure-activity relationships of a series of aminopyridazine derivatives of γ-aminobutyric acid acting as selective GABA-A antagonists. J Med Chem. 1987;30(2):239–49.

241. Michaud JC, Mienville JM, Chambon JP, Bizière K. Interactions between three pyridazinyl-GABA derivatives and central GABA and glycine receptors in the rat, an in vivo microiontophoretic study. Neuropharmacology. 1986;25(11):1197–203.

242. Heaulme M, Chambon JP, Leyris R, Wermuth CG, Biziere K. Specific binding of a phenyl-pyridazinium derivative endowed with GABA A receptor antagonist activity to rat brain. Neuropharmacology. 1986;25(11):1279–83.

243. Melikian A, Schlewer G, Chambon JP, Wermuth CG. Condensation of muscimol or thiomuscimol with aminopyridazines yields GABA-A antagonists. J Med Chem [Internet]. 1992 Oct 1;35(22):4092–7. Available from: https://doi.org/10.1021/jm00100a015

244. Frølund B, Jørgensen AT, Tagmose L, Stensbøl TB, Vestergaard HT, Engblom C, et al. Novel class of potent 4-arylalkyl substituted 3-isoxazolol GABAA antagonists: Synthesis, pharmacology, and molecular modeling. J Med Chem. 2002;45(12):2454–68.

245. Mortensen M, Iqbal F, Pandurangan AP, Hannan S, Huckvale R, Topf M, et al. Photo-antagonism of the GABA A receptor. Nat Commun. 2014;5.

246. Ueno S, Bracamontes J, Zorumski C, Weiss DS, Steinbach JH. Bicuculline and gabazine are allosteric inhibitors of channel opening of the GABAA receptor. J Neurosci. 1997;17(2):625–34.

247. Zhang J, Xue F, Chang Y. Structural Determinants for Antagonist Pharmacology That Distinguish the ρ1 GABAC Receptor from GABAA Receptors. Mol Pharmacol [Internet]. 2008 Oct 1;74(4):941 LP – 951. Available from: http://molpharm.aspetjournals.org/content/74/4/941.abstract

248. Brown N, Kerby J, Bonnert TP, Whiting PJ, Wafford KA. Pharmacological characterization of a novel cell line expressing human α4β3δ GABAA receptors. Br J Pharmacol. 2002;136(7):965–74.

249. Iqbal F, Ellwood R, Mortensen M, Smart TG, Baker JR. Synthesis and evaluation of highly potent GABA(A) receptor antagonists based on gabazine (SR-95531). Bioorg Med Chem Lett [Internet]. 2011;21(14):4252–4. Available from: http://www.ncbi.nlm.nih.gov/pubmed/21664131

250. Kloda JH, Czajkowski C. Agonist-, Antagonist-, and Benzodiazepine-Induced Structural Changes in the alpha 1 Met 113 -Leu 132 Region of the GABA A Receptor. Mol Pharmacol. 2007;71(2):483–93.

251. Wagner DA, Czajkowski C. Structure and dynamics of the GABA binding pocket: A narrowing cleft that constricts during activation. J Neurosci. 2001;21(1):67–74.

252. Ebert B, Mortensen M, Thompson SA, Kehler J, Wafford KA, Krogsgaard-Larsen P. Bioisosteric determinants for subtype selectivity of ligands for heteromeric GABAA receptors. Bioorganic Med Chem Lett. 2001;11(12):1573–7.

253. Lindquist CEL, Laver DR, Birnir B. The mechanism of SR95531 inh bition at GABAA receptors examined in human α1β1 and α1β1γ2S receptors. J Neurochem. 2005;94(2):491–501.

254. You H, Dunn SMJ. Identification of a domain in the δ subunit (S238-V264) of the α4β3δ GABAA receptor that confers high agonist sensitivity. J Neurochem. 2007;103(3):1092–101.

255. Newell JG. Mutation of Glutamate 155 of the GABAA Receptor β2 Subunit Produces a Spontaneously Open Channel: A Trigger for Channel Activation. J Neurosci [Internet]. 2004;24(50):11226–35. Available from: http://www.jneurosci.org/cgi/doi/10.1523/JNEUROSCI.3746-04.2004

256. Uchida I, Cestari IN, Yang J. The differential antagonism by bicuculline and SR95531 of pentobarbitone-induced currents in cultured hippocampal neurons. Eur J Pharmacol [Internet]. 1996;307(1):89–96. Available from: http://www.sciencedirect.com/science/article/pii/0014299996001562

257. Mortensen M, Wafford KA, Wingrove P, Ebert B. Pharmacology of GABAA receptors exh biting different levels of spontaneous activity. Eur J Pharmacol. 2003;476(1–2):17–24.

258. Eisenman LN, Kress G, Zorumski CF, Mennerick S. A spontaneous tonic chloride conductance in solitary glutamatergic hippocampal neurons. Brain Res. 2006;1118(1):66–74.

259. Hadley SH, Amin J. Rat α6β2δ GABAA receptors exhibit two distinct and separable agonist affinities. J Physiol. 2007;581(Pt 3):1001–18.

260. Thompson S, Smith MZ, Wingrove PB, Whiting PJ, Wa KA. Mutation at the putative GABA A ion-channel gate reveals changes in allosteric modulation. 1999;1349–58.

261. Jones M V, Sahara Y, Dzubay J a, Westbrook GL. Defining affinity with the GABAA receptor. J Neurosci. 1998;18(21):8590–604.

262. Jones M V., Westbrook GL. Shaping of IPSCs by endogenous calcineurin activity. J Neurosci. 1997;17(20):7626–33.

263. Carver CM, Chuang S-H, Reddy DS. Zinc Selectively Blocks Neurosteroid-Sensitive Extrasynaptic δGABAA Receptors in the Hippocampus. J Neurosci [Internet]. 2016;36(31):8070–7. Available from: http://www.jneurosci.org/cgi/doi/10.1523/JNEUROSCI.3393-15.2016

264. Massey SC, Linn DM, Kittila CA, Mirza W. Contributions of GABA(A) receptors and GABA(C) receptors to acetylcholine release and directional selectivity in the rabbit retina. Vis Neurosci. 1997;14(5):939–48.

265. Ge YX, Liu Y, Tang HY, Liu XG, Wang X. ClC-2 contr butes to tonic inh bition mediated by α5 subunit-containing GABAA receptor in experimental temporal lobe epilepsy. Neuroscience. 2011;186:120–7.

266. Zhang N, Peng Z, Tong X, Lindemeyer AK, Cetina Y, Huang CS, et al. Decreased surface expression of the δ subunit of the GABAA receptor contributes to reduced tonic inhibition in dentate granule cells in a mouse model of fragile X syndrome. Exp Neurol. 2017;

267. Stell BM, Mody I. Receptors with different affinities mediate phasic and tonic GABA(A) conductances in hippocampal neurons. J Neurosci [Internet]. 2002;22(10):RC223. Available from: http://www.ncbi.nlm.nih.gov/pubmed/12006605

268. Boddum K, Frølund B, Kristiansen U. The GABAA antagonist DPP-4-PIOL selectively antagonises tonic over phasic GABAergic currents in dentate gyrus granule cells. Neurochem Res. 2014;39(11):2078–84.

269. Yamada J, Furukawa T, Ueno S, Yamamoto S, Fukuda A. Molecular basis for the GABAA receptor-mediated tonic inh bition in rat somatosensory cortex. Cereb Cortex [Internet]. 2007;17(8):1782–7. Available from: https://academic.oup.com/cercor/article-lookup/doi/10.1093/cercor/bhl087

270. Bai D, Zhu G, Pennefather P, Jackson MF, MacDonald JF, Orser BA. Distinct functional and pharmacological properties of tonic and quantal inh bitory postsynaptic currents mediated by γ-aminobutyric acid(A) receptors in hippocampal neurons. Mol Pharmacol [Internet]. 2001;59(4):814–24. Available from: http://molpharm.aspetjournals.org/lookup/doi/10.1124/mol.59.4.814

271. Nicoll RA, Wojtowicz JM. The effects of pentobarbital and related compounds on frog motoneurons. Brain Res [Internet]. 1980;191(1):225–37. Available from: http://www.sciencedirect.com/science/article/pii/000689938090325X

272. Barker JL, Harrison NL, Lange GD, Owen DG. Potentiation of gamma-aminobutyric-acid-activated chloride conductance by a steroid anaesthetic in cultured rat spinal neurones. J Physiol [Internet]. 1987 May;386:485–501. Available from: https://pubmed.ncbi.nlm.nih.gov/2445967

273. Peters JA, Kirkness EF, Callachan H, Lambert JJ, Turner AJ. Modulation of the GABAA receptor by depressant barbiturates and pregnane steroids. Br J Pharmacol [Internet]. 1988 Aug;94(4):1257–69. Available from: https://pubmed.ncbi.nlm.nih.gov/2850060

274. Rho JM, Donevan SD, Rogawski MA. Direct activation of GABAA receptors by barbiturates in cultured rat hippocampal neurons. J Physiol [Internet]. 1996 Dec 1;497 (Pt 2(Pt 2):509–22. Available from: https://pubmed.ncbi.nlm.nih.gov/8961191

275. James OT, Livesey MR, Qiu J, Dando O, Bilican B, Haghi G, et al. Ionotropic GABA and glycine receptor subunit composition in human pluripotent stem cell-derived excitatory cortical neurones. J Physiol [Internet]. 2014;592(Pt 19):4353–63. Available from: http://www.pubmedcentral.nih.gov/articlerender.fcgi?artid=4215781&tool=pmcentrez&rendertype=abstract

276. Sedelnikova A, Erkkila BE, Harris H, Zakharkin SO, Weiss DS. Stoichiometry of a pore mutation that abolishes

picrotoxin-mediated antagonism of the GABAA receptor. J Physiol. 2006;577(2):569–77.

277. Mitchell SJ, Silver RA. GABA spillover from single inh bitory axons suppresses low-frequency excitatory transmission at the cerebellar glomerulus. J Neurosci [Internet]. 2000 Dec 1;20(23):8651–8. Available from: https://pubmed.ncbi.nlm.nih.gov/11102470

278. Calero CI, Vickers E, Moraga Cid G, Aguayo LG, von Gersdorff H, Calvo DJ. Allosteric modulation of retinal GABA receptors by ascorbic acid. J Neurosci [Internet]. 2011 Jun 29;31(26):9672–82. Available from: https://pubmed.ncbi.nlm.nih.gov/21715633

279. Bowery NG, Brown DA, Collins GGS, Galvan M, Marsh S, Yamini G. Indirect effects of amino-acids on sympathetic ganglion cells mediated through the release of γ-aminobutyric acid from glial cells. Br J Pharmacol [Internet]. 1976 May 1;57(1):73–91. Available from: https://doi.org/10.1111/j.1476-5381.1976.tb07658.x

280. Brown DA. Extrasynaptic GABA systems. Trends Neurosci [Internet]. 1979;2:271–3. Available from: http://www.sciencedirect.com/science/article/pii/0166223679901073

281. Otis TS, Staley KJ, Mody I. Perpetual inhibitory activity in mammalian brain slices generated by spontaneous GABA release. Brain Res [Internet]. 1991;545(1):142–50. Available from: http://www.sciencedirect.com/science/article/pii/000689939191280E

282. Valeyev AY, Cruciani RA, Lange GD, Smallwood VS, Barker JL. Cl− channels are randomly activated by continuous GABA secretion in cultured embryonic rat hippocampal neurons. Neurosci Lett [Internet]. 1993;155(2):199–203. Available from: http://www.sciencedirect.com/science/article/pii/030439409390707R

283. Ben-Ari Y, Tseeb V, Raggozzino D, Khazipov R, Gaiarsa JL. γ-Aminobutyric acid (GABA): a fast excitatory transmitter which may regulate the development of hippocampal neurones in early postnatal life. In: Van Pelt J, Corner MA, Uylings HBM, Lopes Da Silva FHBT-P in BR, editors. The Self-Organizing Brain: From Growth Cones to Functional Networks [Internet]. Elsevier; 1994. p. 261–73. Available from: http://www.sciencedirect.com/science/article/pii/S0079612308605452

284. Salin PA, Prince DA. Spontaneous GABAA receptor-mediated inhibitory currents in adult rat somatosensory cortex. J Neurophysiol [Internet]. 1996;75(4):1573–88. Available from: http://jn.physiology.org/content/75/4/1573.full-text.pdf+html

285. Wall MJ, Usowicz MM. Postnatal development of spontaneous GABAergic transmission at the Golgi cell-granule cell synapse of rat cerebellum. J Physiol. 1996;494:P83–4.

286. Tia S, Wang JF, Kotchabhakdi N, Vicini S. Developmental changes of inh bitory synaptic currents in cerebellar granule neurons: role of GABA(A) receptor alpha 6 subunit. J Neurosci [Internet]. 1996 Jun 1;16(11):3630–40. Available from: https://pubmed.ncbi.nlm.nih.gov/8642407

287. Jin Z, Jin Y, Kumar-mendu S, Degerman E, Groop L, Birnir B. Insulin reduces neuronal excitability by turning on GABAA channels that generate tonic current. PLoS One. 2011;6(1):1–8.

288. Bonin RP, Martin LJ, Macdonald JF, Orser BA. α5GABAA Receptors Regulate the Intrinsic Excitability of Mouse Hippocampal Pyramidal Neurons. J Neurophysiol. 2007;98:2244–54.

289. Lovett-barron M, Turi GF, Kaifosh P, Lee PH, Bolze F, Sun X, et al. Regulation of neuronal input transformations by tunable dendritic inhibition. Nat Publ Gr. 2012;15(3).

290. Nevian T, Bock T, Senn W, Larkum ME, Murayama M, Pe E. Dendritic encoding of sensory stimuli controlled by deep cortical interneurons. 2009;457(February).

291. Bryson A, Hatch RJ, Zandt B-J, Rossert C, Berkovic SF, Reid CA, et al. GABA-mediated tonic inhibition differentially modulates gain in functional subtypes of cortical interneurons. Proc Natl Acad Sci [Internet]. 2020 Feb 11;117(6):3192 LP – 3202. Available from: http://www.pnas.org/content/117/6/3192.abstract

292. Chance FS, Abbott LF, Reyes AD. Gain modulation from background synaptic input. Neuron. 2002;35(4):773–82.

293. Mitchell SJ, Silver RA. Shunting inh bition modulates neuronal gain during synaptic excitation. Neuron. 2003;

294. Fernandez FR, White JA. Gain Control in CA1 Pyramidal Cells Using Changes in Somatic Conductance. 2010;30(1):230–41.

295. Mehaffey WH, Doiron B, Maler L, Turner RW. Deterministic multiplicative gain control with active dendrites. J Neurosci. 2005;25(43):9968–77.

296. Song I, Savtchenko L, Semyanov A. Tonic excitation or inh bition is set by GABAA conductance in

hippocampal interneurons. Nat Commun. 2011;

297. Duguid I, Branco T, London M, Chadderton P, Hausser M. Tonic Inhibition Enhances Fidelity of Sensory Information Transmission in the Cerebellar Cortex. J Neurosci [Internet]. 2012;32(32):11132–43. Available from: http://www.jneurosci.org/cgi/doi/10.1523/JNEUROSCI.0460-12.2012

298. Tang Z-QQ, Dinh EH, Shi W, Lu Y. Ambient GABA-activated tonic inhibition sharpens auditory coincidence detection via a depolarizing shunting mechanism. J Neurosci [Internet]. 2011;31(16):6121–31. Available from: http://www.ncbi.nlm.nih.gov/entrez/query.fcgi?cmd=Retrieve&db=PubMed&dopt=Citation&list_uids=21508237

299. Wu Z, Guo Z, Gearing M, Chen G. Tonic inhibition in dentate gyrus impairs long-term potentiation and memory in an Alzheimer's [corrected] disease model. Nat Commun [Internet]. 2014;5(May):4159. Available from: http://www.pubmedcentral.nih.gov/articlerender.fcgi?artid=4159602&tool=pmcentrez&rendertype=abstract

300. Etherington LA, Mihalik B, Pálvölgyi A, Ling I, Pallagi K, Kertész S, et al. Selective inhibition of extra-synaptic α5-GABAA receptors by S44819, a new therapeutic agent. Neuropharmacology. 2017;125:353–64.

301. Mann EO, Mody I. Control of hippocampal gamma oscillation frequency by tonic inhibition and excitation of interneurons. Nat Neurosci [Internet]. 2010;13(2):205–12. Available from: http://www.pubmedcentral.nih.gov/articlerender.fcgi?artid=2843436&tool=pmcentrez&rendertype=abstract

302. Ferando I, Mody I. Altered gamma oscillations during pregnancy through loss of δ subunit-containing GABA(A) receptors on parvalbumin interneurons. Front Neural Circuits [Internet]. 2013;7(September):144. Available from: http://www.pubmedcentral.nih.gov/articlerender.fcgi?artid=3775147&tool=pmcentrez&rendertype=abstract

303. Prokic EJ, Weston C, Yamawaki N, Hall SD, Jones RSG, Stanford IM, et al. Cortical oscillatory dynamics and benzodiazepine-site modulation of tonic inhibition in fast spiking interneurons. Neuropharmacology [Internet]. 2015;95:192–205. Available from: http://www.sciencedirect.com/science/article/pii/S0028390815000982

304. Sun Y, Wu Z, Kong S, Jiang D, Pitre A, Wang Y, et al. Regulation of epileptiform activity by two distinct subtypes of extrasynaptic GABA A receptors. 2013;1–13.

305. Chuang SH, Reddy DS. Zinc reduces antiseizure activity of neurosteroids by selective blockade of extrasynaptic GABA-A receptor-mediated tonic inhibition in the hippocampus. Neuropharmacology [Internet]. 2019;148:244–56. Available from: https://linkinghub.elsevier.com/retrieve/pii/S0028390818308633

306. Maguire JL, Stell BM, Rafizadeh M, Mody I. Ovarian cycle–linked changes in GABAA receptors mediating tonic inhibition alter seizure suscept bility and anxiety. Nat Neurosci [Internet]. 2005;8(6):797–804. Available from: https://doi.org/10.1038/nn1469

307. Lee V, Mackenzie G, Hooper A, Maguire J. Reduced tonic inhibition in the dentate gyrus contr butes to chronic stress-induced impairments in learning and memory. Hippocampus. 2016;26(10):1276–90.

308. Engin E, Zarnowska ED, Benke D, Tsvetkov E, Sigal M, Keist R, et al. Tonic Inhibitory Control of Dentate Gyrus Granule Cells by α5-Containing GABAA Receptors Reduces Memory Interference. J Neurosci [Internet]. 2015;35(40):13698–712. Available from: http://www.jneurosci.org/content/35/40/13698.full

309. Diaz MR, Morton RA. Ethanol untangles the amygdala-anxiety circuit through tonic GABA inhibition. Alcohol Clin Exp Res. 2014;38(3):619–23.

310. Houston CM, McGee TP, MacKenzie G, Troyano-Cuturi K, Rodriguez PM, Kutsarova E, et al. Are Extrasynaptic GABAA Receptors Important Targets for Sedative/Hypnotic Drugs? J Neurosci. 2012;32(11):3887–97.

311. Jia F, Pignataro L, Schofield CM, Yue M, Harrison NL, Goldstein PA. An Extrasynaptic GABA A Receptor Mediates Tonic Inhibition in Thalamic VB Neurons. J Neuro-physiol. 2005;94:4491–501.

312. Schipper S, Aalbers MW, Rijkers K, Sw jsen A, Rigo JM, Hoogland G, et al. Tonic GABAA Receptors as Potential Target for the Treatment of Temporal Lobe Epilepsy. Mol Neurobiol [Internet]. 2016;53(8):5252–65. Available from: http://link.springer.com/10.1007/s12035-015-9423-8

313. Zhan R-Z, Nadler JV. Enhanced tonic GABA current in normotopic and hilar ectopic dentate granule cells after pilocarpine-induced status epilepticus. J Neurophysiol [Internet]. 2009;102(2):670–81. Available from: http://jn.physiology.org/cgi/doi/10.1152/jn.00147.2009%5Cnpapers3://publication/doi/10.1152/jn.00147.2009

314. Modgil A, Vien TN, Ackley MA, Doherty JJ, Moss SJ, Davies PA. Neuroactive steroids reverse tonic inhibitory deficits in fragile X syndrome mouse model. Front Mol Neurosci [Internet]. 2019;12(February):1–11. Available from: https://www.frontiersin.org/article/10.3389/fnmol.2019.00015/full

315. Clarkson AN, Huang BS, Macisaac SE, Mody I, Carmichael ST. Reducing excessive GABA-mediated tonic inhibition promotes functional recovery after stroke. Nature [Internet]. 2010;468(7321):305–9. Available from: http://dx.doi.org/10.1038/nature09511

316. Koch C. Chapter 12 Multiplying with Synapses and Neurons. 1992. 315–345 p.

317. Silver RA. Neuronal arithmetic. Nat Rev Neurosci. 2010;11(7):474–89.

318. Rose D. On the arithmetical operation performed by inhibitory synapses onto the neuronal soma. Exp Brain Res. 1977;28(3–4):221–3.

319. Wlodarczyk AI, Xu C, Song I, Doronin M, Wu Y-W, Walker MC, et al. Tonic GABAA conductance decreases membrane time constant and increases EPSP-sp ke precision in hippocampal pyramidal neurons. Front Neural Circuits [Internet]. 2013;7(December):205. Available from: http://www.pubmedcentral.nih.gov/articlerender.fcgi?artid=3872325&tool=pmcentrez&rendertype=abstract

320. Carandini M, Heeger DJ. Summation and division by neurons in primate visual cortex. Science (80-) [Internet]. 1994 May 27;264(5163):1333 LP – 1336. Available from: http://science.sciencemag.org/content/264/5163/1333.abstract

321. Nelson ME. A Mechanism for Neuronal Gain Control by Descending Pathways. Neural Comput [Internet]. 1994 Mar 1;6(2):242–54. Available from: https://doi.org/10.1162/neco.1994.6.2.242

322. Holt GR, Koch C. Shunting Inh bition Does Not Have a Divisive Effect on Firing Rates. Neural Comput. 1997;9(5):1001–13.

323. Katz B. Depolarization of sensory terminals and the initiation of impulses in the muscle spindle. J Physiol [Internet]. 1950 Oct 16;111(3–4):261–82. Available from: https://pubmed.ncbi.nlm.nih.gov/14795439

324. Granit R. Sensory mechanisms of the retina. Sensory mechanisms of the retina. New York, NY, US: Oxford University Press; 1947. 412 p.

325. Holt GR. PhD Thesis: A Critical Reexamination of Some Assumptions and Implications of Cable Theory in Neurobiology. 1998;1998.

326. Sah P, Faber ESL. Channels underlying neuronal calcium-activated potassium currents. Prog Neurobiol. 2002 Apr;66(5):345–53.

327. Cope DW, Hughes SW, Crunelli V. GABAA Receptor-Mediated Tonic Inhibition in Thalamic Neurons. J Neurosci [Internet]. 2005;25(50):11553–63. Available from: http://www.jneurosci.org/content/25/50/11553%5Cnhttp://www.jneurosci.org/content/25/50/11553.full%5Cnhttp://www.jneurosci.org/content/25/50/11553.full.pdf%5Cnhttp://www.ncbi.nlm.nih.gov/pubmed/16354913

328. Chen X, Keramidas A, Lynch JW. Physiological and pharmacological properties of inhibitory postsynaptic currents mediated by α5β1γ2, α5β2γ2 and α5β3γ2 GABA A receptors. Neuropharmacology. 2017;

329. Huck S, Lux HD. Patch-clamp study of ion channels activated by GABA and glycine in cultured cerebellar neurons of the mouse. Neurosci Lett. 1987;79(1–2):103–7.

330. Weiss DS, Barnes EM, Hablitz JJ. Whole-cell and single-channel recordings of GABA-gated currents in cultured chick cerebral neurons. J Neurophysiol [Internet]. 1988;59(2):495–513. Available from: http://www.ncbi.nlm.nih.gov/pubmed/2450972

331. Porter NM, Twyman RE, Uhler MD, Macdonald RL. Cyclic AMP-dependent protein kinase decreases $GABA_A$ receptor current in mouse spinal neurons. Neuron [Internet]. 1990 Dec 1;5(6):789–96. Available from: https://doi.org/10.1016/0896-6273(90)90338-G

332. Hamill OP, Bormann J, Sakmann B. Activation of multiple-conductance state chloride channels in spinal neurones by glycine and GABA. Nature. 1983;305(5937):805–8.

333. Mathers DA. Spontaneous and GABA-induced single channel currents in cultured murine spinal cord neurons. Can J Physiol Pharmacol. 1985;63(10):1228–33.

334. Macdonald RL, Rogers CJ, Twyman RE. Kinetic properties of the GABAA receptor main conductance state of mouse spinal cord neurones in culture. J Physiol [Internet]. 1989;410:479–99. Available from: http://www.pubmedcentral.nih.gov/articlerender.fcgi?artid=1190491&tool=pmcentrez&rendertype=abstract

335. Blair LA, Levitan ES, Marshall J, Dionne VE, Barnard EA. Single subunits of the GABAA receptor form ion channels with properties of the native receptor. Science (80-) [Internet]. 1988 Oct 28;242(4878):577 LP – 579. Available from: http://science.sciencemag.org/content/242/4878/577.abstract

336. Neelands TR, Fisher JL, Bianchi M, Macdonald RL. Spontaneous and gamma-aminobutyric acid (GABA)-activated GABA(A) receptor channels formed by epsilon subunit-containing isoforms. MolPharmacol. 1999;55(1):168–78.

337. Neher E, Sakmann B. Noise analysis of drug induced voltage clamp currents in denervated frog muscle f bres. J Physiol [Internet]. 1976 Jul;258(3):705–29. Available from: https://pubmed.ncbi.nlm.nih.gov/1086359

338. Neher E, Sakmann B. Single-channel currents recorded from membrane of denervated frog muscle f bres. Nature [Internet]. 1976;260(5554):799–802. Available from: https://doi.org/10.1038/260799a0

339. Neher E, Sakmann B, Steinbach JH. The extracellular patch clamp: A method for resolving currents through individual open channels in biological membranes. Pflügers Arch [Internet]. 1978;375(2):219–28. Available from: https://doi.org/10.1007/BF00584247

340. Sigworth FJ, Neher E. Single Na+ channel currents observed in cultured rat muscle cells. Nature [Internet]. 1980;287(5781):447–9. Available from: https://doi.org/10.1038/287447a0

341. Hamill OP, Marty A, Neher E, Sakmann B, Sigworth FJ. Improved patch-clamp techniques for high-resolution current recording from cells and cell-free membrane patches. Pflügers Arch [Internet]. 1981;391(2):85–100. Available from: https://doi.org/10.1007/BF00656997

342. Colquhoun D, Sakmann B. Fluctuations in the microsecond time range of the current through single acetylcholine receptor ion channels. Nature [Internet]. 1981;294(5840):464–6. Available from: https://doi.org/10.1038/294464a0

343. Sakmann B, Hamill OP, Bormann J. Patch-Clamp Measurements of Elementary Chloride Currents Activated by the Putative Inhibitory Transmitters GABA and Glycine in Mammalian Spinal Neurons. In: Goldstein M, Jellinger K, Riederer P, editors. Basic Aspects of Receptor Biochemistry. Vienna: Springer Vienna; 1983. p. 83–95.

344. Khrestchatisky M, MacLennan AJ, Chiang M-Y, Xu W, Jackson MB, Brecha N, et al. A novel α subunit in rat brain GABAA receptors. Neuron [Internet]. 1989 Dec 1;3(6):745–53. Available from: https://doi.org/10.1016/0896-6273(89)90243-2

345. Sigel E, Baur R, Malherbe P, Möhler H. The rat β1-subunit of the GABAA receptor forms a picrotoxin-sensitive anion channel open in the absence of GABA. FEBS Lett. 1989;257(2):377–9.

346. Sanna E, Garau F, Harris RA. Novel properties of homomeric β1 gamma-aminobutyric acid type A receptors: Actions of the anesthetics propofol and pentobarbital. MolPharmacol. 1995;47:213–7.

347. Krishek BJ, Moss SJ, Smart TG. Homomeric β1 γ-aminobutyric acid A receptor-ion channels: evaluation of pharmacological and physiological properties. Mol Pharmacol. 1996;49(3):494–504.

348. Knoflach F, Benke D, Wang Y, Scheurer L, Luddens H, Hamilton, Beverly J, et al. Pharmacological Modulation Recombinant of the Diazepam-Insensitive Acid A Receptors and α6β2γ2. Mol Pharmacol. 1996;50:1253–61.

349. Birnir B, Eghbali M, Everitt AB, Gage PW. Bicuculline, pentobarbital and diazepam modulate spontaneous GABA(A) channels in rat hippocampal neurons. Br J Pharmacol [Internet]. 2000;131(4):695–704. Available from: http://www.pubmedcentral.nih.gov/articlerender.fcgi?artid=1572380&tool=pmcentrez&rendertype=abstract

350. Maksay G, Thompson SA, Wafford KA. The pharmacology of spontaneously open α1β3ε GABAA receptor-ionophores. Neuropharmacology. 2003;44(8):994–1002.

351. Glykys J, Mann EO, Mody I. Which GABAA Receptor Subunits Are Necessary for Tonic Inhibition in the Hippocampus? J Neurosci [Internet]. 2008;28(6):1421–6. Available from: http://www.jneurosci.org/cgi/doi/10.1523/JNEUROSCI.4751-07.2008

352. Herd MB, Haythornthwaite AR, Rosahl TW, Wafford KA, Homanics GE, Lambert JJ, et al. The expression of GABAA β subunit isoforms in synaptic and extrasynaptic receptor populations of mouse dentate gyrus granule cells. J Physiol. 2008;586(4):989–1004.

353. Semyanov A, Walker MC, Kullmann DM. GABA uptake regulates cortical excitability via cell type-specific tonic inhibition. Nat Neurosci. 2003;6(5):484–90.

354. Bieda MC, MacIver M. Major Role For Tonic GABAA Conductances in Anesthetic Suppression of Intrinsic Neuronal Excitability. J Neurophysiol [Internet]. 2004;92(3):1658–67. Available from: http://jn.physiology.org/cgi/doi/10.1152/jn.00223.2004

355. Bouairi E, Kamendi H, Wang X, Gorini C, Mendelowitz D. Multiple Types of GABAA Receptors Mediate

Inh bition in Brain Stem Parasympathetic Cardiac Neurons In the Nucleus Ambiguus. J Neurophysiol. 2006;

356. Overstreet LS, Westbrook GL. Paradoxical reduction of synaptic inh bition by vigabatrin. J Neurophysiol. 2001;86(2):596–603.

357. Jin BP, Skalska S, Stern JE. Characterization of a novel tonic γ-aminobutyric acidAreceptor-mediated inhibition in magnocellular neurosecretory neurons and its modulation by glia. Endocrinology. 2006;147(8):3746–60.

358. Park JB, Skalska S, Son S, Stern JE. Dual GABAA receptor-mediated inh bition in rat presympathetic paraventricular nucleus neurons. J Physiol [Internet]. 2007/05/10. 2007 Jul 15;582(Pt 2):539–51. Available from: https://pubmed.ncbi.nlm.nih.gov/17495040

359. McDougall SJ, Bailey TW, Mendelowitz D, Andresen MC. Propofol enhances both tonic and phasic inhibitory currents in second-order neurons of the solitary tract nucleus (NTS). Neuropharmacology [Internet]. 2007/11/07. 2008 Mar;54(3):552–63. Available from: https://pubmed.ncbi.nlm.nih.gov/18082229

360. Wang L, Spary E, Deuchars J, Deuchars SA. Tonic GABAergic Inhibition of Sympathetic Preganglionic Neurons : A Novel Substrate for Sympathetic Control. 2008;28(47):12445–52.

361. Gao H, Smith BN. Tonic GABAA receptor-mediated inhibition in the rat dorsal motor nucleus of the vagus. J Neurophysiol [Internet]. 2009/12/16. 2010 Feb;103(2):904–14. Available from: https://pubmed.ncbi.nlm.nih.gov/20018836

362. Maeda A, Katafuchi T, Shiokawa H, Yoshimura M. Enhancement of GABAergic Tonic Currents by Midazolam and Noradrenaline in Rat Substantia. 2016;(2):429–37.

363. Lau BK, Karim S, Goodchild AK, Vaughan CW, Drew GM. Menthol enhances phasic and tonic GABAA receptor-mediated currents in midbrain periaqueductal grey neurons. Br J Pharmacol [Internet]. 2014 Jun 1;171(11):2803–13. Available from: https://doi.org/10.1111/bph.12602

364. Bhattarai JP, Park SA, Park JB, Lee SY, Herbison AE, Ryu PD, et al. Tonic Extrasynaptic GABAA Receptor Currents Control Gonadotropin-Releasing Hormone Neuron Excitability in the Mouse. Endocrinology [Internet]. 2011 Apr 1;152(4):1551–61. Available from: https://doi.org/10.1210/en.2010-1191

365. Liu YM, Fan HR, Deng S, Zhu T, Yan Y, Ge WH, et al. Methyleugenol potentiates central amygdala GABaergic inhibition and reduces anxiety. J Pharmacol Exp Ther [Internet]. 2019;368(1):1–10. Available from: http://jpet.aspetjournals.org/lookup/doi/10.1124/jpet.118.250779

366. Yelhekar TD, Druzin M, Johansson S. Contribution of Resting Conductance, GABAA-Receptor Mediated Miniature Synaptic Currents and Neurosteroid to Chloride Homeostasis in Central Neurons. Eneuro [Internet]. 2017;4(April):ENEURO.0019-17.2017. Available from: http://eneuro.sfn.org/lookup/doi/10.1523/ENEURO.0019-17.2017

367. Lindquist CEL, Dalziel JE, Cromer BA, Birnir B. Penicillin blocks human α1β1 and α1β1γ2S GABAA channels that open spontaneously. Eur J Pharmacol [Internet]. 2004;496(1–3):23–32. Available from: http://www.ncbi.nlm.nih.gov/pubmed/15288571

368. Othman NA, Gallacher M, Deeb TZ, Baptista-Hon DT, Perry DC, Hales TG. Influences on blockade by t-butylbicyclo-phosphoro-thionate of GABA(A) receptor spontaneous gating, agonist activation and desensitization. J Physiol [Internet]. 2012;590(Pt 1):163–78. Available from: http://www.pubmedcentral.nih.gov/articlerender.fcgi?artid=3300054&tool=pmcentrez&rendertype=abstract

369. Bianchi MT, Macdonald RL. Agonist Trapping by GABAA Receptor Channels. J Neurosci. 2001;21(23):9083–91.

370. Baker C, Sturt BL, Bamber BA. Multiple roles for the first transmembrane domain of GABAA receptor subunits in neurosteroid modulation and spontaneous channel activity. Neurosci Lett [Internet]. 2010;473(3):242–7. Available from: http://dx.doi.org/10.1016/j.neulet.2010.02.058

371. Hoestgaard-Jensen K, Da by NO, Krall J, Hammer H, Krogsgaard-Larsen P, Frølund B, et al. Probing α4βδ GABAA receptor heterogeneity: differential regional effects of a functionally selective α4β1δ/α4β3δ receptor agonist on tonic and phasic inhibition in rat brain. J Neurosci [Internet]. 2014;34(49):16256–72. Available from: http://www.jneurosci.org/content/34/49/16256.long

372. Karim N, Wellendorph P, Absalom N, Bang LH, Jensen ML, Hansen MM, et al. Low nanomolar GABA effects at extrasynaptic α4β1/β3δ GABAA receptor subtypes indicate a different binding mode for GABA at these receptors. Biochem Pharmacol [Internet]. 2012;84(4):549–57. Available from: http://dx.doi.org/10.1016/j.bcp.2012.05.017

373. Eaton MM, Bracamontes J, Shu H-J, Li P, Mennerick S, Steinbach JH, et al. γ-aminobutyric acid type A α4, β2,

and δ subunits assemble to produce more than one functionally distinct receptor type. Mol Pharmacol [Internet]. 2014;86(6):647–56. Available from: http://www.ncbi.nlm.nih.gov/pubmed/25238745%5Cnhttp://www.pubmedcentral.nih.gov/articlerender.fcgi?artid=PMC4244592

374. Hartiadi LY, Ahring PK, Cheb b M, Absalom NL. High and low GABA sensitivity α4β2δ GABAA receptors are expressed in Xenopus laevis oocytes with divergent stoichiometries. Biochem Pharmacol [Internet]. 2016;103:98–108. Available from: http://dx.doi.org/10.1016/j.bcp.2015.12.021

375. Pierce SR, Senneff TC, Germann AL, Akk G. Steady-state activation of the high-affinity isoform of the α4β2δ GABAA receptor. Sci Rep [Internet]. 2019;9(1):15997. Available from: https://doi.org/10.1038/s41598-019-52573-z

376. Tang X, Hernandez CC, Macdonald RL. Modulation of spontaneous and GABA-evoked tonic α4β3δ and α4β3γ2L GABAA receptor currents by protein kinase A. J Neurophysiol [Internet]. 2010;103(2):1007–19. Available from: http://jn.physiology.org/cgi/doi/10.1152/jn.00801.2009%5Cnpapers3://publication/doi/10.1152/jn.00801.2009

377. Jensen ML, Wafford KA, Brown AR, Belelli D, Lambert JJ, Mirza NR. A study of subunit selectivity, mechanism and site of action of the delta selective compound 2 (DS2) at human recombinant and rodent native GABA A receptors. Br J Pharmacol. 2013;168(5):1118–32.

378. Taly A, Corringer P-J, Grutter T, de Carvalho LP, Karplus M, Changeux J-P. Implications of the quaternary twist allosteric model for the physiology and pathology of nicotinic acetylcholine receptors. Proc Natl Acad Sci [Internet]. 2006 Nov 7;103(45):16965 LP – 16970. Available from: http://www.pnas.org/content/103/45/16965.abstract

379. Bhattacharya A, Dang H, Zhu Q-M, Schnegelsberg B, Rozengurt N, Cain G, et al. Uropathic Observations in Mice Expressing a Constitutively Active Point Mutation in the 5-HT3A Receptor Subunit. J Neurosci [Internet]. 2004 Jun 16;24(24):5537 LP – 5548. Available from: http://www.jneurosci.org/content/24/24/5537.abstract

380. Tao Y-X. Constitutive activation of G protein-coupled receptors and diseases: Insights into mechanisms of activation and therapeutics. Pharmacol Ther [Internet]. 2008;120(2):129–48. Available from: http://www.sciencedirect.com/science/article/pii/S0163725808001277

381. Cerione RA, Codina J, Benovic JL, Lefkowitz RJ, Birnbaumer L, Caron MG. Mammalian β2-adrenergic receptor: reconstitution of functional interactions between pure receptor and pure stimulatory nucleotide binding protein of the adenylate cyclase system. Biochemistry [Internet]. 1984 Sep 25;23(20):4519–25. Available from: https://doi.org/10.1021/bi00315a003

382. Costa T, Herz A. Antagonists with negative intrinsic activity at delta opioid receptors coupled to GTP-binding proteins. Proc Natl Acad Sci U S A [Internet]. 1989 Oct;86(19):7321–5. Available from: https://pubmed.ncbi.nlm.nih.gov/2552439

383. Fan W, Boston BA, Kesterson RA, Hruby VJ, Cone RD. Role of melanocortinergic neurons in feeding and the agouti obesity syndrome. Nature. 1997;385:165–8.

384. Fan W, Voss-Andreae A, Cao WH, Morrison SF. Regulation of thermogenesis by the central melanocortin system. Peptides. 2005;26:1800–13.

385. Adan RAH, Kas MJH. Inverse agonism gains weight. Trends Pharmacol Sci [Internet]. 2003;24(6):315–21. Available from: http://europepmc.org/abstract/MED/12823958

386. Srinivasan S, Lubrano-Berthelier C, Govaerts C, Picard F, Santiago P, Conklin BR, et al. Constitutive activity of the melanocortin-4 receptor is maintained by its N-terminal domain and plays a role in energy homeostasis in humans. J Clin Invest [Internet]. 2004 Oct;114(8):1158–64. Available from: https://pubmed.ncbi.nlm.nih.gov/15489963

387. Pavlov I, Savtchenko LP, Kullmann DM, Semyanov A, Wa ker MC. Outwardly rectifying tonically active GABAA receptors in pyramidal cells modulate neuronal offset, not gain. J Neurosci. 2009;29(48):15341–50.

388. Szemes M, Davies RL, Garden CLP, Usowicz MM. Weaker control of the electrical properties of cerebellar granule cells by tonically active GABA A receptors in the Ts65Dn mouse model of Down ' s syndrome. 2013;1–23.

389. Teyler TJ. Brain slice preparation: Hippocampus. Brain Res Bull [Internet]. 1980;5(4):391–403. Available from: http://dx.doi.org/10.1016/S0361-9230(80)80009-8

390. Bischofberger J, Engel D, Li L, Geiger JRP, Jonas P. Patch-clamp recording from mossy f ber terminals in hippocampal slices. Nat Protoc. 2006;1(4):2075–81.

391. Pastoll H, White M, Nolan M. Preparation of parasagittal slices for the investigation of dorsal-ventral organization of the rodent medial entorhinal cortex. J Vis Exp. 2012;(61):1–9.

392. Ting JT, Lee BR, Chong P, Soler-Llavina G, Cobbs C, Koch C, et al. Preparation of Acute Brain Slices Using an Optimized N-Methyl-D-glucamine Protective Recovery Method. J Vis Exp. 2018;(132):1–13.

393. Xu-Friedman MA. Preparing brain slices to study basic synaptic properties. Cold Spring Harb Protoc. 2017;2017(1):26–32.

394. Thomas Papouin and Philip G. Haydon. Obtaining Acute Brain Slices Thomas. 2015;91(2):165–71.

395. Tanaka Y, Tanaka Y, Furuta T, Yanagawa Y, Kaneko T. The effects of cutting solutions on the viability of GABAergic interneurons in cerebral cortical slices of adult mice. J Neurosci Methods. 2008;

396. Ye JH, Zhang J, Xiao C, Kong JQ. Patch-clamp studies in the CNS illustrate a simple new method for obtaining viable neurons in rat brain slices: Glycerol replacement of NaCl protects CNS neurons. J Neurosci Methods. 2006;158(2):251–9.

397. Richerson GB, Messer C. Effect of composition of experimental solutions on neuronal survival during rat brain slicing. Exp Neurol. 1995;131(1):133–43.

398. Aitken PG, Breese GR, Dudek FF, Edwards F, Espanol MT, Larkman PM, et al. Preparative methods for brain slices: a discussion. J Neurosci Methods. 1995;59(1):139–49.

399. Moyer JR, Brown TH. Methods for whole-cell recording from visually preselected neurons of perirhinal cortex in brain slices from young and aging rats. J Neurosci Methods. 1998;86(1):35–54.

400. Booker SA, Song J, Vida I. Whole-cell patch-clamp recordings from morphologically- and neurochemically-identified hippocampal interneurons. J Vis Exp [Internet]. 2014;(91):e51706. Available from: http://www.jove.com/video/51706/whole-cell-patch-clamp-recordings-from-morphologically

401. Pathak HR, Weissinger F, Terunuma M, Carlson GC, Hsu F, Moss SJ, et al. Disrupted Dentate Granule Cell Chloride Regulation Enhances Synaptic Excitability during Development of Temporal Lobe Epilepsy. 2007;27(51):14012–22.

402. Elgueta C, Bartos M. Dendritic inhibition differentially regulates excitability of dentate gyrus parvalbumin-expressing interneurons and granule cells. Nat Commun [Internet]. (2019). Available from: http://dx.doi.org/10.1038/s41467-019-13533-3

403. Silayeva L, Deeb TZ, Hines RM, Kelley MR, Munoz MB, Lee HHC. KCC2 activity is critical in limiting the onset and severity of status epilepticus. 2015;112(11):3523–8.

404. Dietrich D, Podlogar M, Ortmanns G, Clusmann H, Kral T. Calbindin-D 28k content and firing pattern of hippocampal granule cells in amygdala-kindled rats : a perforated patch-clamp study. 2005;1032:123–30.

405. Yarishkin O, Lee DY, Kim E, Cho C, Choi JH, Lee CJ, et al. TWIK-1 contributes to the intrinsic excitability of dentate granule cells in mouse hippocampus. 2014;1–11.

406. Staley KJ, Otis TS, Mody I. Membrane properties of dentate gyrus granule cells: Comparison of sharp microelectrode and whole-cell recordings. J Neurophysiol. 1992;67(5):1346–58.

407. Patel LS, Ju H, Schwartzkroin PA. Physiological and Morphological Characterization of Dentate Granule Cells in the p35 Knock-Out Mouse Hippocampus : Evidence for an Epileptic Circuit. 2004;24(41):9005–14.

408. Kobayashi M, Buckmaster PS. Reduced Inhibition of Dentate Granule Cells in a Model of Temporal Lobe Epilepsy. 2003;23(6):2440–52.

409. Kirchheim F, Tinnes S, Haas CA, Stegen M, Wolfart J. Regulation of action potential delays via voltage-gated potassium Kv1.1 channels in dentate granule cells during hippocampal epilepsy. Front Cell Neurosci [Internet]. 2013;7(December):1–14. Available from: http://journal.frontiersin.org/article/10.3389/fncel.2013.00248/abstract

410. Lübke J, Frotscher M, Spruston N. Specialized electrophysiological properties of anatomically identified neurons in the hilar region of the rat fascia dentata. J Neurophysiol. 1998;79(3):1518–34.

411. Spruston N, Johnston D. Perforated patch-clamp analysis of the passive membrane properties of three classes of hippocampal neurons. J Neurophysiol. 1992;67(3):508–29.

412. Mishra P, Narayanan R. Heterogeneities in intrinsic excitability and frequency-dependent response properties of granule cells across the blades of the rat dentate gyrus. J Neurophysiol. 2020;123(2):755–72.

413. Pernía-Andrade AJ, Jonas P. Theta-Gamma-Modulated Synaptic Currents in Hippocampal Granule Cells InVivo Define a Mechanism for Network Oscillations. Neuron. 2014;81(1):140–52.

414. Kowalski J, Gan J, Jonas P, Pern AJ. Intrinsic Membrane Properties Determine Hippocampal Differential Firing Pattern In Vivo in Anesthetized Rats. 2016;682(November 2015):668–82.

415. O'Neill N, Sylantyev S. Spontaneously opening GABAA receptors play a significant role in neuronal signal filtering and integration. Cell Death Dis. 2018;9(8).

416. O'Neill N, Sylantyev S. Feature Article: Selective modulation of tonically active GABAA receptor functional subgroups by G-proteins and protein kinase C. Exp Biol Med. 2018;243(13):1046–55.

417. O'Neill N, Sylantyev S. The Functional Role of Spontaneously Opening GABAA Receptors in Neural Transmission. 2019;12(March):1–7.

418. Krishek BJ, Moss SJ, Smart TG. A functional comparison of the antagonist bicuculline and picrotoxin at recombinant GABA(A) receptors. Neuropharmacology. 1996;35(9–10):1289–98.

419. Ebert B, Thompson SA, Saounatsou K, Mckernan R, Krogsgaard-Larsen P, Wafford KA. Differences in agonist/antagonist binding affinity and receptor transduction using recombinant human γ-aminobutyric acid type A receptors. Mol Pharmacol. 1997;52(6):1150–6.

420. Luddens H, Korpi ER. GABA antagonists differentiate between recombinant GABA(A)/benzodiazepine receptor subtypes. J Neurosci. 1995;15(10):6957–62.

421. Smart TG, Constanti A. Differential effect of zinc on the vertebrate GABA(A)-receptor complex. Br J Pharmacol. 1990;99(4):643–54.

422. Kumamoto E, Murata Y. Characterization of GABA current in rat septal cholinergic neurons in culture and its modulation by metal cations. J Neurophysiol. 1995;74(5):2012–27.

423. Marques F, Souza S De, Antunes G, Guo T, Tsai D, Morley JW. How cesium dialysis affects the passive properties of pyramidal neurons: implications for voltage clamp studies of persistent sodium current. 2008;

424. Andersen P, Bliss TVP, Skrede KK. Lamellar organization of hippocampal excitatory pathways. Exp Brain Res. 1971;13(2):222–38.

425. Amaral DG, Scharfman HE, Lavenex P. The dentate gyrus: fundamental neuroanatomical organization (dentate gyrus for dummies). Prog Brain Res. 2007;163:3–22.

426. Burgess N, Maguire EA, Keefe JO. The Human Hippocampus and Spatial and Episodic Memory. 2002;35:625–41.

427. Bird CM, Burgess N. The hippocampus and memory : insights from spatial processing. 2008;9(February).

428. Hainmueller T. of episodic memories. Nat Rev Neurosci [Internet]. Available from: http://dx.doi.org/10.1038/s41583-019-0260-z

429. West MJ, Slomianka L, Gundersen HJG. Unbiased stereological estimation of the total number of neurons in the subdivisions of the rat hippocampus using the optical fractionator. Anat Rec. 1991;231(4):482–97.

430. Hunsaker MR, Mooy GG, Swift JS, Kesner RP. Dissociations of the Medial and Lateral Perforant Path Projections Into Dorsal DG , CA3 , and CA1 for Spatial and Nonspatial (Visual Object) Information Processing. 2007;121(4):742–50.

431. Neunuebel JP, Yoganarasimha D, Rao G, Knierim JJ. Conflicts between local and global spatial frameworks dissociate neural representations of the lateral and medial entorhinal cortex. J Neurosci. 2013;33(22):9246–58.

432. Rolls ET. A computational theory of episodic memory formation in the hippocampus. Behav Brain Res [Internet]. 2010;215(2):180–96. Available from: http://dx.doi.org/10.1016/j.bbr.2010.03.027

433. Yanagawa Y, Obata K, Vida I, Hosp JA, Str M, Jonas P, et al. Morpho-physiological Criteria Divide Dentate Gyrus Interneurons into Classes. 2014;203(October 2013):189–203.

434. Booker SA, Vida I. Morphological diversity and connectivity of hippocampal interneurons. Cell Tissue Res. 2018;373(3):619–41.

435. Jinde S, Zsiros V, Jiang Z, Nakao K, Pickel J, Kohno K, et al. Hilar Mossy Cell Degeneration Causes Transient Dentate Granule Cell Hyperexcitability and Impaired Pattern Separation. Neuron [Internet]. 2012;76(6):1189–

200. Available from: http://dx.doi.org/10.1016/j.neuron.2012.10.036

436. Coulter DA, Carlson GC. Functional regulation of the dentate gyrus by GABA-mediated inhibition. Prog Brain Res. 2007;163(07):235–44.

437. Krook-magnuson E, Armstrong C, Bui A, Lew S, Oijala M, Soltesz I. In vivo evaluation of the dentate gate theory in epilepsy. 2015;10:2379–88.

438. Behr J, Lyson KJ, Mody I. Enhanced propagation of epileptiform activity through the kindled dentate gyrus. J Neurophysiol. 1998;79(4):1726–32.

439. Lothman EW, Stringer JL, Bertram EH. The dentate gyrus as a control point for seizures in the hippocampus and beyond. Epilepsy Res Suppl [Internet]. 1992;7:301—313. Available from: http://europepmc.org/abstract/MED/1334669

440. Knierim JJ, Neunuebel JP. Neurobiology of Learning and Memory Tracking the flow of hippocampal computation : Pattern separation , pattern completion , and attractor dynamics. Neurobiol Learn Mem [Internet]. 2015; Available from: http://dx.doi.org/10.1016/j.nlm.2015.10.008

441. Amari S. Characteristics of sparsely encoded associative memory. Neural Networks [Internet]. 1989;2(6):451–7. Available from: http://www.sciencedirect.com/science/article/pii/0893608089900439

442. Marr D. A theory of cerebellar cortex. J Physiol [Internet]. 1969 Jun;202(2):437–70. Available from: https://pubmed.ncbi.nlm.nih.gov/5784296

443. Marr D. A Theory for Cerebral Neocortex. Proc R Soc London Ser B, Biol Sci [Internet]. 1970 Feb 22;176(1043):161–234. Available from: http://www.jstor.org/stable/76043

444. Marr D. Simple Memory: A Theory for Archicortex. Philos Trans R Soc Lond B Biol Sci [Internet]. 1971 Feb 22;262(841):23–81. Available from: http://www.jstor.org/stable/2417171

445. McNaughton BL, Morris RGM. Hippocampal synaptic enhancement and information storage within a distr buted memory system. Trends Neurosci. 1987;10(10):408–15.

446. McNaughton BL, Nadel L. Hebb-Marr networks and the neurobiological representation of action in space. In: Neuroscience and connectionist theory. Hillsdale, NJ, US: Lawrence Er baum Associates, Inc; 1990. p. 1–63. (Developments in connectionist theory.).

447. Rolls ET. Information Representation, Processin, and Storage in the Brain: Analysis at the Single Neuron Level. Neural Mol Bases Learn. 1987;503–39.

448. Rolls ET. Functions of neuronal networks in the hippocampus and neocortex in memory. In: Neural models of plasticity: Experimental and theoretical approaches. San Diego, CA, US: Academic Press; 1989. p. 240–65.

449. Treves A, Rolls ET. Computational Constraints Suggest the Need for Two Input Systems to the Hippocampal CA3 Network. Hippocampus. 1992;2(2):189–200.

450. Rolls ET, Treves A, Robertson RG, Georges-François P, Panzeri S. Information about spatial view in an ensemble of primate hippocampal cells. J Neurophysiol. 1998;79(4):1797–813.

451. Rolls ET, Kesner RP. A computational theory of hippocampal function, and empirical tests of the theory. Prog Neurobiol. 2006;79(1):1–48.

452. O'Reilly RC, McClelland JL. Hippocampal conjunctive encoding, storage, and recall: Avoiding a trade-off. Hippocampus. 1994;4(6):661–82.

453. O'Reilly RC, Norman KA. Hippocampal and neocortical contributions to memory: Advances in the complementary learning systems framework. Trends Cogn Sci. 2002;6(12):505–10.

454. Hunsaker MR, Kesner RP. The operation of pattern separation and pattern completion processes associated with different attributes or domains of memory. Neurosci Biobehav Rev [Internet]. 2013;37(1):36–58. Available from: http://dx.doi.org/10.1016/j.neubiorev.2012.09.014

455. Yassa MA, Stark CEL. Pattern separation in the hippocampus. Trends Neurosci [Internet]. 2011/07/23. 2011 Oct;34(10):515–25. Available from: https://pubmed.ncbi.nlm.nih.gov/21788086

456. Gilbert PE, Kesner RP, Lee I. Dissociating hippocampal subregions: A double dissociation between dentate gyrus and CA1. Hippocampus. 2001;11(6):626–36.

457. Lee I, Hunsaker MR, Kesner RP. The role of hippocampal subregions in detecting spatial novelty. Behav Neurosci. 2005;119(1):145–53.

458. McHugh TJ, Jones MW, Quinn JJ, Balthasar N, Coppari R, Elmquist JK, et al. Dentate gyrus NMDA receptors mediate rapid pattern separation in the hippocampal network. Science (80-). 2007;317(5834):94–9.

459. Zhuo JM, Tseng HA, Desai M, Bucklin ME, Mohammed AI, Robinson NT, et al. Young adult born neurons enhance hippocampal dependent performance via influences on bilateral networks. Elife. 2016;5:25.

460. Bernier BE, Lacagnina AF, Ayoub A, Shue F, Zemelman B V., Krasne FB, et al. Dentate gyrus contr butes to retrieval as well as encoding: Evidence from context fear conditioning, recall, and extinction. J Neurosci. 2017;37(26):6359–71.

461. Kheirbek MA, Drew LJ, Burghardt NS, Costantini DO, Tannenholz L, Ahmari SE, et al. Differential control of learning and anxiety along the dorsoventral axis of the dentate gyrus. Neuron. 2013;77(5):955–68.

462. Bakker A, Kirwan CB, Miller M, Stark CEL. Pattern separation in the human hippocampal CA3 and dentate gyrus. Science (80-). 2008;319(5870):1640–2.

463. Koolschijn RS, Emir UE, Pantelides AC, Nili H, Behrens TEJ, Barron HC. The Hippocampus and Neocortical Inh bitory Engrams Protect against Memory Interference. Neuron. 2019;101(3):528-541.e6.

464. Leutgeb JK, Leutgeb S, Moser MB, Moser EI. Pattern separation in the dentate gyrus and CA3 of the hippocampus. Science (80-). 2007;315(5814):961–6.

465. van Dijk MT, Fenton AA. On How the Dentate Gyrus Contributes to Memory Discrimination. Neuron. 2018;98(4):832-845.e5.

466. Neunuebel JP, Knierim JJ. CA3 retrieves coherent representations from degraded input: Direct evidence for CA3 pattern completion and dentate gyrus pattern separation. Neuron [Internet]. 2014;81(2):416–27. Available from: http://dx.doi.org/10.1016/j.neuron.2013.11.017

467. Hainmueller T, Bartos M. Parallel emergence of stable and dynamic memory engrams in the hippocampus. Nature. 2018;558(7709):292–6.

468. Jung MW, McNaughton BL. Spatial selectivity of unit activity in the hippocampal granular layer. Hippocampus. 1993;3(2):165–82.

469. Mistry R, Dennis S, Frerking M, Mellor JR. Dentate Gyrus Granule Cell Firing Patterns Can Induce Mossy Fiber Long-Term Potentiation In Vitro. 2011;1168:1157–68.

470. Diamantaki M, Frey M, Berens P, Preston-ferrer P, Burgalossi A. Sparse activity of identified dentate granule cells during spatial exploration. 2016;1–17.

471. Okazaki MM, Evenson DA, Nadler JV. Hippocampal Mossy Fiber Sprouting and Synapse Formation After Status Epilepticus in Rats : Visualization After Retrograde Transport of Biocytin. 1995;352515434.

472. Hendricks WD, Westbrook GL, Schnell E. Early detonation by sprouted mossy fibers enables aberrant dentate network activity. 2019;116(22):1–6.

473. Yim MY, Hanuschkin A, Wolfart J. Intrinsic rescaling of granule cells restores pattern separation ability of a dentate gyrus network model during epileptic hyperexcitability. Hippocampus. 2015;(25):297–308.

474. De Almeida L, Idiart M, Lisman JE. A second function of gamma frequency oscillations: An E%-max winner-take-all mechanism selects which cells fire. J Neurosci. 2009;29(23):7497–503.

475. Braganza O, Müller-Komorowska D, Kelly T, Beck H. Quantitative properties of a feedback circuit predict frequency-dependent pattern separation. bioRxiv [Internet]. 2019;813188. Available from: https://www.biorxiv.org/content/10.1101/813188v1

476. Espinoza C, Guzman SJ, Zhang X, Jonas P. Parvalbumin + interneurons obey unique connectivity rules and establish a powerful lateral-inhibition microcircuit in dentate gyrus. Nat Commun [Internet]. 2018;9(1):1–10. Available from: https://www.nature.com/articles/s41467-018-06899-3?utm_source=researcher_app&utm_medium=referral&utm_campaign=MKEF_USG_Researcher_inbound

477. Guzman SJ, Schlögl A, Espinoza C, Zhang X, Suter B, Jonas P. Fast signaling and focal connectivity of PV+ interneurons ensure efficient pattern separation by lateral inhibition in a full-scale dentate gyrus network model. bioRxiv [Internet]. 2019 Jan 1;647800. Available from: http://biorxiv.org/content/early/2019/05/25/647800.abstract

478. Yuan M, Meyer T, Benkowitz C, Savanthrapadian S, Ansel-Bollepalli L, Foggetti A, et al. Somatostatin-positive interneurons in the dentate gyrus of mice provide local- and long-range septal synaptic inhibition. Elife. 2017;6:1–25.

479. Stefanelli T, Bertollini C, Lüscher C, Muller D, Mendez P. Hippocampal Somatostatin Interneurons Control the Size of Neuronal Memory Ensembles. Neuron. 2016;89(5):1074–85.

480. Scott RS, Henneberger C, Padmashri R, Anders S, Jensen TP, Rusakov DA. Neuronal adaptation involves rapid expansion of the action potential initiation site. Nat Commun [Internet]. 2014;5(May):1–12. Available from: http://dx.doi.org/10.1038/ncomms4817

481. Lawrence JJ, Grinspan ZM, McBain CJ. Quantal transmission at mossy fibre targets in the CA3 region of the rat hippocampus. J Physiol [Internet]. 2004 Jan 1;554(Pt 1):175–93. Available from: https://pubmed.ncbi.nlm.nih.gov/14678500

482. Henze DA, Wittner L, Buzsáki G. Single granule cells reliably discharge targets in the hippocampal CA3 network in vivo. Nat Neurosci. 2002;5(8):790–5.

483. Krueppel R, Remy S, Beck H. Dendritic integration in hippocampal dentate granule cells. Neuron [Internet]. 2011;71(3):512–28. Available from: http://dx.doi.org/10.1016/j.neuron.2011.05.043

484. Schmidt-Hieber C, Jonas P, Bischofberger J. Subthreshold dendritic signal processing and coincidence detection in dentate gyrus granule cells. J Neurosci. 2007;27(31):8430–41.

485. Kim S, Kim Y, Lee SH, Ho WK. Dendritic spikes in hippocampal granule cells are necessary for long-term potentiation at the perforant path synapse. Elife. 2018;7(1973):1–21.

486. McNaughton BL, Barnes CA, Andersen P. Synaptic efficacy and EPSP summation in granule cells of rat fascia dentata studied in vitro. J Neurophysiol [Internet]. 1981 Nov 1;46(5):952–66. Available from: https://doi.org/10.1152/jn.1981.46.5.952

487. Kamijo TC, Hayakawa H, Fukushima Y, Kubota Y, Isomura Y, Tsukada M, et al. Input integration around the dendritic branches in hippocampal dentate granule cells. Cogn Neurodyn. 2014;8(4):267–76.

488. Golding NL, Staff NP, Spruston N. Dendritic sp kes as a mechanism for cooperative long-term potentiation. Nature. 2002;418(6895):326–31.

489. Wang Z, Song D, Berger TW. Contribution of NMDA receptor channels to the expression of LTP in the hippocampal dentate gyrus. Hippocampus [Internet]. 2002 Jan 1;12(5):680–8. Available from: https://doi.org/10.1002/hipo.10104

490. Herron CE, Lester RAJ, Coan EJ, Collingridge GL. Frequency-dependent involvement of NMDA receptors in the hippocampus: a novel synaptic mechanism. Nature [Internet]. 1986;322(6076):265–8. Available from: https://doi.org/10.1038/322265a0

491. Hanson JE, Madison D V. Imbalanced pattern completion vs. separation in cognitive disease: network simulations of synaptic pathologies predict a personalized therapeutics strategy. BMC Neurosci [Internet]. 2010;11(1):96. Available from: https://doi.org/10.1186/1471-2202-11-96

492. Lomo T. Frequency potentiation of excitatory synaptic activity in dentate area of hippocampal formation. In: Acta Physiologica Scandinavica. 1966. p. 128.

493. Bliss T V, Lomo T. Long-lasting potentiation of synaptic transmission in the dentate area of the anaesthetized rabbit following stimulation of the perforant path. J Physiol [Internet]. 1973 Jul;232(2):331–56. Available from: https://pubmed.ncbi.nlm.nih.gov/4727084

494. Bliss T V, Gardner-Medwin AR. Long-lasting potentiation of synaptic transmission in the dentate area of the unanaestetized rabbit following stimulation of the perforant path. J Physiol [Internet]. 1973 Jul;232(2):357–74. Available from: https://pubmed.ncbi.nlm.nih.gov/4727085

495. Ramon y Cajal S. The Croonian lecture.—La fine structure des centres nerveux. Proc R Soc London [Internet]. 1894 Jan 1;55(331–335):444–68. Available from: https://doi.org/10.1098/rspl.1894.0063

496. Cajal SR. Histologie du syste me nerveux de l'Homme et des verte be s. Maloine (Paris). 1911;2:891–942.

497. Konorski J. Conditioned reflexes and neuron organization. 1948;

498. Hebb DO. The organization of behavior. na; 1949.

499. Stevens CF. A Million Dollar Question: Does LTP = Memory? Neuron [Internet]. 1998 Jan 1;20(1):1–2. Available from: https://doi.org/10.1016/S0896-6273(00)80426-2

500. Abraham WC, Logan B, Greenwood JM, Dragunow M. Induction and experience-dependent consolidation of stable long-term potentiation lasting months in the hippocampus. J Neurosci. 2002;22(21):9626–34.

501. McNaughton BL, Douglas RM, Goddard G V. Synaptic enhancement in fascia dentata: Cooperativity among coactive afferents. Brain Res [Internet]. 1978;157(2):277–93. Available from: http://www.sciencedirect.com/science/article/pii/0006899378900306

502. Barrionuevo G, Brown TH. Associative long-term potentiation in hippocampal slices. Proc Natl Acad Sci U S A [Internet]. 1983 Dec;80(23):7347–51. Available from: https://pubmed.ncbi.nlm.nih.gov/6316360

503. Baez MV, Oberholzer MV, Cercato MC, Snitcofsky M, Aguirre AI, Jerusalinsky DA. NMDA receptor subunits in the adult rat hippocampus undergo similar changes after 5 minutes in an open field and after LTP induction. PLoS One. 2013;8(2).

504. Bliss TVP, Collingridge GL, Morris RGM, Reymann KG. Long-term potentiation in the hippocampus: Discovery, mechanisms and function. Neuroforum. 2018;24(3):A103–20.

505. Bliss TVP, Collingridge GL. A synaptic model of memory: long-term potentiation in the hippocampus. Nature. 1993;361(6407):31–9.

506. Martin SJ, Morris RGM. New life in an old idea: the synaptic plasticity and memory hypothesis revisited. Hippocampus. 2002;12(5):609–36.

507. Malenka RC, Bear MF. LTP and LTD: an embarrassment of riches. Neuron. 2004;44(1):5–21.

508. Tim B, Graham C, Richard M. Synaptic Plasticity in the Hippocampus. In: The Hippocampus Book [Internet]. New York: Oxford University Press; 2006. Available from: https://www.oxfordscholarship.com/10.1093/acprof:oso/9780195100273.001.0001/acprof-9780195100273-chapter-10

509. Queenan BN, Ryan TJ, Gazzaniga MS, Gallistel CR. On the research of time past: the hunt for the substrate of memory. Ann N Y Acad Sci. 2017;1396(1):108–25.

510. Tonegawa S, Pignatelli M, Roy DS, Ryan TJ. Memory engram storage and retrieval. Curr Opin Neurobiol [Internet]. 2015;35(August):101–9. Available from: http://dx.doi.org/10.1016/j.conb.2015.07.009

511. Poo M-M, Pignatelli M, Ryan TJ, Tonegawa S, Bonhoeffer T, Martin KC, et al. What is memory? The present state of the engram. BMC Biol [Internet]. 2016;14(1):40. Available from: http://www.pubmedcentral.nih.gov/articlerender.fcgi?artid=4874022&tool=pmcentrez&rendertype=abstract

512. Nabavi S, Fox R, Proulx CD, Lin JY, Tsien RY, Malinow R. Engineering a memory with LTD and LTP. Nature. 2014;511(7509):348–52.

513. Grant SGN. Synapse molecular complexity and the plasticity behaviour problem. Brain Neurosci Adv [Internet]. 2018;2:239821281881068. Available from: http://journals.sagepub.com/doi/10.1177/2398212818810685

514. Gallistel CR, Matzel LD. The Neuroscience of Learning: Beyond the Hebbian Synapse. Annu Rev Psychol. 2013;64(1):169–200.

515. Shors TJ, Matzel LD. Long-term potentiation: What's learning got to do with it? Behav Brain Sci. 1997;20(4):597–655.

516. Fricke RA, Prince DA. Electrophysiology of dentate gyrus granule cells. J Neurophysiol. 1984;51(2):195–209.

517. Fernandez FR, Broicher T, Truong A, White JA. Membrane voltage fluctuations reduce sp ke frequency adaptation and preserve output gain in CA1 pyramidal neurons in a high-conductance state. J Neurosci. 2011;31(10):3880–93.

518. Staley KJ, Mody I. Shunting of excitatory input to dentate gyrus granule cells by a depolarizing GABAA receptor-mediated postsynaptic conductance. J Neurophysiol [Internet]. 1992 Jul 1;68(1):197–212. Available from: https://doi.org/10.1152/jn.1992.68.1.197

519. Puggioni P, Jelitai M, Duguid I, van Rossum MCW. Extraction of Synaptic Input Properties in Vivo. Neural Comput [Internet]. 2017 May 31;29(7):1745–68. Available from: https://doi.org/10.1162/NECO_a_00975

520. Arima-yoshida F, Watabe AM, Manabe T. The mechanisms of the strong inhibitory modulation of long-term

potentiation in the rat dentate gyrus. 2011;33:1637–46.

521. Wigström H, Gustafsson B. Facilitation of hippocampal long-lasting potentiation by GABA antagonists. Acta Physiol Scand [Internet]. 1985 Sep 1;125(1):159–72. Available from: https://doi.org/10.1111/j.1748-1716.1985.tb07703.x

522. Yeung JYTT, Canning KJ, Zhu G, Pennefather P, MacDonald JF, Orser BA, et al. Tonically activated GABAA receptors in hippocampal neurons are high-affinity, low-conductance sensors for extracellular GABA. Mol Pharmacol [Internet]. 2003;63(1):2–8. Available from: http://www.ncbi.nlm.nih.gov/pubmed/12488530

523. Chesnoy-Marchais D. Persistent GABAA/C responses to gabazine, taurine and beta-alanine in rat hypoglossal motoneurons. Neuroscience [Internet]. 2016;330:191–204. Available from: http://dx.doi.org/10.1016/j.neuroscience.2016.05.048

524. Hamann M, Rossi DJ, Attwell D. Tonic and spillover inh bition of granule cells control information flow through cerebellar cortex. Neuron. 2002;33:625–633.

525. Houston CM, Bright DP, Sivilotti LG, Beato M, Smart TG. Intracellular chloride ions regulate the time course of GABA-mediated inhibitory synaptic transmission. J Neurosci [Internet]. 2009;29(33):10416–23. Available from: http://www.jneurosci.org/cgi/doi/10.1523/JNEUROSCI.1670-09.2009

526. Schmidt-Hieber C, Jones P, Bischofberger J, Jonas P, Bischofberger J. Enhanced synaptic plasticity in newly generated granule cells of the adult hippocampus. Nature. 2004;429(6988):184–7.

527. Barker JL, Harrison NL. Outward rectification of inhibitory postsynaptic currents in cultured rat hippocampal neurones. JPhysiol(Lond). 1988;403:41–55.

528. Curmi JP, Premkumar L, Birnir B, Gage PW. The Influence of Membrane Potential on Chloride Channels Activated by GABA in Rat Cultured Hippocampal Neurons. J Membr Biol. 1993;136:273–80.

529. Barry PH. JPCalc, a software package for calculating liquid junction potential corrections in patch-clamp, intracellular, epithelial and bilayer measurements and for correcting junction potential measurements. J Neurosci Methods [Internet]. 1994;51(1):107–16. Available from: http://www.sciencedirect.com/science/article/pii/0165027094900310

530. Paz JT, Mahon S, Tiret P, Genet S, Delord B, Charpier S. Multiple forms of activity-dependent intrinsic plasticity in layer V cortical neurones in vivo. J Physiol. 2009;587(13):3189–205.

531. O'Leary T, van Rossum MCW, Wyllie DJA. Homeostasis of intrinsic excitability in hippocampal neurones: Dynamics and mechanism of the response to chronic depolarization. J Physiol. 2010;588(1):157–70.

532. Rojas P, Akrouh A, Eisenman LN, Mennerick S. Differential effects of axon initial segment and somatodendritic GABA A receptors on excitability measures in rat dentate granule neurons. J Neurophysiol [Internet]. 2011;105(1):366–79. Available from: http://jn.physiology.org/cgi/doi/10.1152/jn.00165.2010

533. Prescott SA, Ratté S, De Koninck Y, Sejnowski TJ. Nonlinear interaction between shunting and adaptation controls a switch between integration and coincidence detection in pyramidal neurons. J Neurosci [Internet]. 2006;26(36):9084–97. Available from: http://www.jneurosci.org/cgi/doi/10.1523/JNEUROSCI.1388-06.2006

534. Colgin LL. Rhythms of the hippocampal network. Nat Rev Neurosci [Internet]. 2016; Available from: http://www.nature.com/doifinder/10.1038/nrn.2016.21

535. Colgin LL. Theta–gamma coupling in the entorhinal–hippocampal system. Curr Opin Neurobiol [Internet]. 2015;31:45–50. Available from: http://www.sciencedirect.com/science/article/pii/S0959438814001639

536. Benda J, Herz AVM. A Universal Model for Spike-Frequency Adaptation. Neural Comput [Internet]. 2003 Nov 1;15(11):2523–64. Available from: https://doi.org/10.1162/089976603322385063

537. Peron SP, Gabbiani F. Role of sp ke-frequency adaptation in shaping neuronal response to dynamic stimuli. Biol Cybern. 2009;100(6):505–20.

538. Groen MR, Paulsen O, Pérez-Garci E, Nevian T, Wortel J, Dekker MP, et al. Development of dendritic tonic GABAergic inhibition regulates excitability and plasticity in CA1 pyramidal neurons. J Neurophysiol [Internet]. 2014;112(2):287–99. Available from: http://jn.physiology.org/cgi/doi/10.1152/jn.00066.2014

539. Yang H, Zhang J, Breyer RM, Chen C. Altered hippocampal long-term synaptic plasticity in mice deficient in the PGE2 EP2 receptor. J Neurochem [Internet]. 2008/11/21. 2009 Jan;108(1):295–304. Available from: https://pubmed.ncbi.nlm.nih.gov/19012750

540. Suryanarayanan A, Liang J, Meyer EM, Lindemeyer AK, Chandra D, Homanics GE, et al. Subunit

Compensation and Plasticity of Synaptic GABA(A) Receptors Induced by Ethanol in α4 Subunit Knockout Mice. Front Neurosci [Internet]. 2011 Sep 23;5:110. Available from: https://pubmed.ncbi.nlm.nih.gov/21977012

541. Liang J, Suryanarayanan A, Chandra D, Homanics GE, Olsen RW, Spigelman I. Functional Consequences of GABAA Receptor α4 Subunit Deletion on Synaptic and Extrasynaptic Currents in Mouse Dentate Granule Cells. Alcohol Clin Exp Res [Internet]. 2008 Jan 1;32(1):19–26. Available from: https://doi.org/10.1111/j.1530-0277.2007.00564.x

542. Brickley SG, Revilla V, Cull-Candy SG, Wisden W, Farrant M. Adaptive regulation of neuronal excitability by a voltage-independent potassium conductance. Nature. 2001;409(6816):88–92.

543. Peng Z, Hauer B, Mihalek RM, Homanics GE, Sieghart W, Olsen RW, et al. GABAA receptor changes in δ subunit-deficient mice: Altered expression of α4 and γ2 subunits in the forebrain. J Comp Neurol [Internet]. 2002 Apr 29;446(2):179–97. Available from: https://doi.org/10.1002/cne.10210

544. Sinkkonen ST, Hanna MC, Kirkness EF, Korpi ER. GABA(A) receptor epsilon and theta subunits display unusual structural variation between species and are enriched in the rat locus ceruleus. J Neurosci [Internet]. 2000;20(10):3588–95. Available from: http://www.ncbi.nlm.nih.gov/pubmed/10804200

545. Sun C, Sieghart W, Kapur J. Distribution of α1, α4, γ2, and δ subunits of GABAA receptors in hippocampal granule cells. Brain Res. 2004;1029(2):207–16.

546. Stell BM, Brickley SG, Tang CY, Farrant M, Mody I. Neuroactive steroids reduce neuronal excitability by selectively enhancing tonic inh bition mediated by delta subunit-containing GABAA receptors. Proc Natl Acad Sci U S A. 2003;100(24):14439–44.

547. Wafford KA, van Niel MB, Ma QP, Horridge E, Herd MB, Peden DR, et al. Novel compounds selectively enhance δ subunit containing GABAA receptors and increase tonic currents in thalamus. Neuropharmacology [Internet]. 2009;56(1):182–9. Available from: http://dx.doi.org/10.1016/j.neuropharm.2008.08.004

548. Krehan D, Storustovu SÍ, Liljefors T, Ebert B, Nielsen B, Krogsgaard-Larsen P, et al. Potent 4-arylalkyl-substituted 3-isothiazolol GABAA competitive/noncompetitive antagonists: Synthesis and pharmacology. J Med Chem. 2006;49(4):1388–96.

549. Ramerstorfer J, Furtmüller R, Vogel E, Huck S, Sieghart W. The point mutation γ2F77I changes the potency and efficacy of benzodiazepine site ligands in different GABAA receptor subtypes. Eur J Pharmacol [Internet]. 2010;636(1–3):18–27. Available from: http://dx.doi.org/10.1016/j.ejphar.2010.03.015

550. Gao H, Smith BN. Zolpidem modulation of phasic and tonic GABA currents in the rat dorsal motor nucleus of the vagus. Neuropharmacology. 2010;58(8):1220–7.

551. Wafford KA, Bain CJ, Whiting PJ, Kemp JA. Functional comparison of the role of γ subunits in recombinant human γ- aminobutyric acid(A)/benzodiazepine receptors. Mol Pharmacol [Internet]. 1993 Aug 1;44(2):437–42. Available from: http://molpharm.aspetjournals.org/content/44/2/437.abstract

552. Dixon C, Sah P, Lynch JW, Keramidas A. GABAa receptor α and γ subunits shape synaptic currents via different mechanisms. J Biol Chem. 2014;289(9):5399–411.

553. Saxena NC, Macdonald RL. Assembly of GABA, Receptor Subunits: Role of the δ Subunit. J Neurosci. 1994;14(11):7077–88.

554. Yang W, Drewe JA, Lan NC. Cloning and characterization of the human GABAA receptor α4 subunit: identification of a unique diazepam-insensitive binding site. Eur J Pharmacol Mol Pharmacol. 1995;291(3):319–25.

555. Korpi ER, Seeburg PH. Natural mutation of GABAA receptor α6 subunit alters benzodiazepine affinity but not allosteric GABA effects. Eur J Pharmacol Mol Pharmacol. 1993;247(1):23–7.

556. Meera P, Olsen RW, Otis TS, Wallner M. Alcohol- and alcohol antagonist-sensitive human GABAA receptors: tracking δ subunit incorporation into functional receptors. Mol Pharmacol [Internet]. 2010/08/10. 2010 Nov;78(5):918–24. Available from: https://pubmed.ncbi.nlm.nih.gov/20699325

557. Rudolph U, Möhler H. GABA A Receptor Subtypes: Therapeutic Potential in Down Syndrome, Affective Disorders, Schizophrenia, and Autism . Annu Rev Pharmacol Toxicol [Internet]. 2014;54(1):483–507. Available from: http://www.annualreviews.org/doi/10.1146/annurev-pharmtox-011613-135947

558. Connelly WM, Errington AC, Di Giovanni G, Crunelli V. Metabotropic regulation of extrasynaptic $GABA_A$ receptors. Front Neural Circuits [Internet]. 2013;7(October):171. Available from: http://www.pubmedcentral.nih.gov/articlerender.fcgi?artid=3829460&tool=pmcentrez&rendertype=abstract

559. Bright DP, Smart TG. Protein kinase C regulates tonic GABAA receptor-mediated inhibition in the hippocampus and thalamus. Eur J Neurosci. 2013;38(10):3408–23.

560. Hosie AM, Dunne EL, Harvey RJ, Smart TG. Zinc-mediated inhibition of GABAA receptors: discrete binding sites underlie subtype specificity. Nat Neurosci [Internet]. 2003;6(4):362–9. Available from: http://www.nature.com/doifinder/10.1038/nn1030

561. Smart TG, Hosie AM, Miller PS. Zn2+ ions: Modulators of excitatory and inhibitory synaptic activity. Neuroscientist. 2004;10(5):432–42.

562. Smart TG, Moss SJ, Xie X, Huganir RL. GABAA receptors are differentially sensitive to zinc: dependence on subunit composition. Br J Pharmacol. 1991;103(4):1837–9.

563. Draguhn A, Verdorn TA, Ewert M, Seeburg PH, Sakmann B. Functional and molecular distinction between recombinant rat GABAA receptor subtypes by Zn2+. Neuron. 1990;5(6):781–8.

564. Saxena NC, Macdonald RL. Properties of putative cerebellar γ-aminobutyric acidA receptor isoforms. Mol Pharmacol. 1996;49(3):567–79.

565. Thio LL, Zhang HX. Modulation of inhibitory glycine receptors in cultured embryonic mouse hippocampal neurons by zinc, thiol containing redox agents and carnosine. Neuroscience. 2006;139(4):1315–27.

566. Beckstead MJ, Phelan R, Trudell JR, Bianchini MJ, Mihic SJ. Anesthetic and ethanol effects on spontaneously opening glycine receptor channels. J Neurochem. 2002;82(6):1343–51.

567. Carver CM, Reddy DS. Neurosteroid Structure-Activity Relationships for Functional Activation of Extrasynaptic δ-GABAA Receptors. J Pharmacol Exp Ther [Internet]. 2016;(April):188–204. Available from: http://www.ncbi.nlm.nih.gov/pubmed/26857959

568. Quirk K, Blurton P, Fletcher S, Leeson P, Tang F, Mellilo D, et al. [3 H]L-655,708, a novel ligand selective for the benzodiazepine site of GABA(A) receptors which contain the α5 subunit. Neuropharmacology. 1996;35(9–10):1331–5.

569. Casula MA, Bromidge FA, Pillai G V, Wingrove PB, Martin K, Maubach K, et al. Identification of amino acid residues responsible for the α5 subunit binding selectivity of L-655,708, a benzodiazepine binding site ligand at the GABAA receptor. J Neurochem. 2001;77:445–51.

570. Atack JR, Bayley PJ, Seabrook GR, Wafford KA, Mckernan RM, Dawson GR. L-655,708 enhances cognition in rats but is not proconvulsant at a dose selective for α5-containing GABAA receptors. Neuropharmacology. 2006;51:1023–9.

571. Scimemi A, Semyanov A, Sperk G, Kullmann DM, Walker MC. Multiple and Plastic Receptors Mediate Tonic GABAA Receptor Currents in the Hippocampus. J Neurosci [Internet]. 2005;25(43):10016–24. Available from: http://www.jneurosci.org/cgi/doi/10.1523/JNEUROSCI.2520-05.2005

572. Caraiscos VB, Elliott EM, You-Ten KE, Cheng VY, Belelli D, Newell JG, et al. Tonic inhibition in mouse hippocampal CA1 pyramidal neurons is mediated by α5 subunit-containing γ-aminobutyric acid type A receptors. Proc Natl Acad Sci U S A. 2004;101(10):3662–7.

573. Sigel E, Ernst M. The Benzodiazepine Binding Sites of GABAA Receptors. Vol. 39, Trends in Pharmacological Sciences. 2018. p. 659–71.

574. Forman SA, Miller KW. Anesthetic sites and allosteric mechanisms of action on Cys-loop ligand-gated ion channels. Vol. 58, Canadian Journal of Anesthesia. 2011. p. 191–205.

575. Wongsamitkul N, Maldifassi MC, Simeone X, Baur R, Ernst M, Sigel E. α subunits in GABA A receptors are dispensable for GABA and diazepam action. Sci Rep. 2017;7:15498.

576. Olsen RW. GABAAreceptor: Positive and negative allosteric modulators. Neuropharmacology [Internet]. 2018;136:10–22. Available from: https://doi.org/10.1016/j.neuropharm.2018.01.036

577. Hammer H, Bader BM, Ehnert C, Bundgaard C, Bunch L, Hoestgaard-Jensen K, et al. A Multifaceted GABAA Receptor Modulator: Functional Properties and Mechanism of Action of the Sedative-Hypnotic and Recreational Drug Methaqualone (Quaalude). Mol Pharmacol [Internet]. 2015;88(2):401–20. Available from: http://www.ncbi.nlm.nih.gov/pubmed/26056160

578. Twyman RE, Rogers CJ, Macdonald RL. Differential regulation of γ-aminobutyric acid receptor channels by diazepam and phenobarbital. Ann Neurol. 1989;25(3):213–20.

579. Rogers CJ, Twyman RE, Macdonald RL. Benzodiazepine and β-carboline regulation of single GABAA receptor

channels of mouse spinal neurones in culture. J Physiol. 1994;475(1):69–82.

580. Li P, Eaton MM, Steinbach JH, Akk G. The benzodiazepine diazepam potentiates responses of α1β2γ2 γ-aminobutyric acid type A receptors activated by either γ-aminobutyric acid or allosteric agonists. Anesthediology. 2013;118(6):1–20.

581. Dixon CL, Harrison NL, Lynch JW, Keramidas A. Zolpidem and eszopiclone prime α1β2γ2 GABAA receptors for longer duration of activity. Br J Pharmacol. 2015;172(14):3522–36.

582. Korol S V, Jin Z, Birnir B. The GLP-1 receptor agonist exendin-4 and diazepam differentially regulate GABAA receptor-mediated tonic currents in rat hippocampal CA3 pyramidal neurons. PLoS One [Internet]. 2015;10(4):e0124765. Available from: http://dx.plos.org/10.1371/journal.pone.0124765

583. Prenosil GA, Gasser EMS, Rudolph U, Keist R, Fritschy J, Vogt KE, et al. Specific Subtypes of GABA A Receptors Mediate Phasic and Tonic Forms of Inhibition in Hippocampal Pyramidal Neurons. 2020;846–57.

584. Che Has AT, Absalom N, Van Nieuwenhuijzen PS, Clarkson AN, Ahring PK, Chebib M. Zolpidem is a potent stoichiometry-selective modulator of α1β3 GABA A receptors: Evidence of a novel benzodiazepine site in the α1-α1 interface. Sci Rep [Internet]. 2016;6(June):1–12. Available from: http://dx.doi.org/10.1038/srep28674

585. Dawson GR, Maubach KA, Collinson N, Cobain M, Everitt BJ, Macleod AM, et al. An Inverse Agonist Selective for α5 Subunit-Containing GABAA Receptors Enhances Cognition. 2006;316(3):1335–45.

586. May AC, Fleischer W, Kletke O, Haas HL, Sergeeva OA. Benzodiazepine-site pharmacology on GABAA receptors in histaminergic neurons. Br J Pharmacol. 2013;170(1):222–32.

587. Moody OA, Jenkins A. The role of loops B and C in determining the potentiation of GABA A receptors by midazolam. Pharmacol Res Perspect [Internet]. 2018;6(6):e00433. Available from: http://doi.wiley.com/10.1002/prp2.433

588. Connelly WM, Fyson SJ, Errington AC, McCafferty CP, Cope DW, Di Giovanni G, et al. GABAB Receptors Regulate Extrasynaptic GABAA Receptors. J Neurosci [Internet]. 2013;33(9):3780–5. Available from: http://www.jneurosci.org/cgi/doi/10.1523/JNEUROSCI.4989-12.2013

589. Mangmool S, Kurose H. G(i/o) protein-dependent and -independent actions of Pertussis Toxin (PTX). Toxins (Basel) [Internet]. 2011/07/15. 2011 Jul;3(7):884–99. Available from: https://pubmed.ncbi.nlm.nih.gov/22069745

590. Chadderton P, Margrie TW, Häusser M. Integration of quanta in cerebellar granule cells during sensory processing. Nature [Internet]. 2004;428(6985):856–60. Available from: https://doi.org/10.1038/nature02442

591. Ho N, Destexhe A. Synaptic Background Activity Enhances the Responsiveness of Neocortical Pyramidal Neurons. J Neurophysiol. 2000;84(3):1488–96.

592. Donnell CO, Rossum MCW Van. Systematic analysis of the contributions of stochastic voltage gated channels to neuronal noise. 2014;8(September):1–14.

593. Birnir B, Everitt a B, Gage PW. Characteristics of GABAA channels in rat dentate gyrus. J Membr Biol. 1994;142:93–102.

594. Platkiewicz J, Brette R. A Threshold Equation for Action Potential Initiation. PLoS Comput Biol. 2010;6(7):e1000850.

595. Mantegazza M, Franceschetti S, Avanzini G. Anemone toxin (ATX II)-induced increase in persistent sodium current: effects on the firing properties of rat neocortical pyramidal neurones. J Physiol [Internet]. 1998 Feb 15;507 (Pt 1(Pt 1):105–16. Available from: https://pubmed.ncbi.nlm.nih.gov/9490824

596. Gulledge AT, Stuart GJ. Excitatory Actions of GABA in the Cortex. Neuron [Internet]. 2003 Jan 23;37(2):299–309. Available from: https://doi.org/10.1016/S0896-6273(02)01146-7

597. Currin CB, Trevelyan AJ, Akerman CJ, Raimondo J V. Chloride dynamics alter the input-output properties of neurons. bioRxiv [Internet]. 2019 Jan 1;710277. Available from: http://biorxiv.org/content/early/2019/07/22/710277.abstract

598. Martin LJ, Zurek AA, MacDonald JF, Roder JC, Jackson MF, Orser BA. α5GABAA Receptor Activity Sets the Threshold for Long-Term Potentiation and Constrains Hippocampus-Dependent Memory. J Neurosci [Internet]. 2010;30(15):5269–82. Available from: http://www.jneurosci.org/cgi/doi/10.1523/JNEUROSCI.4209-09.2010

599. zur Nedden S, Hawley S, Pentland N, Hardie DG, Doney AS, Frenguelli BG. Intracellular ATP influences synaptic plasticity in area CA1 of rat hippocampus via metabolism to adenosine and activity-dependent

activation of adenosine A1 receptors. J Neurosci [Internet]. 2011 Apr 20;31(16):6221–34. Available from: https://pubmed.ncbi.nlm.nih.gov/21508245

600. Roggenhofer E, Fidzinski P, Bartsch J, Kurz F, Shor O, Behr J. Activation of dopamine D1/D5 receptors facilitates the induction of presynaptic long-term potentiation at hippocampal output synapses. Eur J Neurosci [Internet]. 2010 Aug 1;32(4):598–605. Available from: https://doi.org/10.1111/j.1460-9568.2010.07312.x

601. Essrich C, Lorez M, Benson JA, Fritschy J-M, Lüscher B. Postsynaptic clustering of major GABAA receptor subtypes requires the γ2 subunit and gephyrin. Nat Neurosci [Internet]. 1998;1(7):563–71. Available from: https://doi.org/10.1038/2798

602. Sylantyev S, Rusakov DA. Sub-millisecond ligand probing of cell receptors with multiple solution exchange. Nat Protoc [Internet]. 2013/06/06. 2013;8(7):1299–306. Available from: http://www.scopus.com/inward/record.url?eid=2-s2.0-84879326593&partnerID=tZOtx3y1

603. Rudolph U, Knoflach F. Beyond classical benzodiazepines: Novel therapeutic potential of GABA A receptor subtypes. Nat Rev Drug Discov [Internet]. 2011 Jul 29;10(9):685–97. Available from: https://pubmed.ncbi.nlm.nih.gov/21799515

604. Newman EL, Smith KS, Takahashi A, Chu A, Hwa LS, Chen Y, et al. α2-containing GABA(A) receptors: a requirement for midazolam-escalated aggression and social approach in mice. Psychopharmacology (Berl) [Internet]. 2015/09/17. 2015 Dec;232(23):4359–69. Available from: https://pubmed.ncbi.nlm.nih.gov/26381154

605. Krishek BJ, Moss SJ, Smart TG. Interaction of H+ and Zn2+ on recombinant and native rat neuronal GABAA receptors. J Physiol [Internet]. 1998 Mar 15;507:639–52. Available from: https://pubmed.ncbi.nlm.nih.gov/9508826

606. Ahring PK, Bang LH, Jensen ML, Strøbæk D, Hartiadi LY, Chebib M, et al. A pharmacological assessment of agonists and modulators at α4β2γ2 and α4β2δ GABAA receptors: The challenge in comparing apples with oranges. Pharmacol Res [Internet]. 2016; Available from: http://linkinghub.elsevier.com/retrieve/pii/S1043661816301499

607. Shu HJ, Eisenman LN, Jinadasa D, Covey DF, Zorumski CF, Mennerick S. Slow actions of neuroactive steroids at GABAA receptors. J Neurosci [Internet]. 2004;24(30):6667–75. Available from: http://www.jneurosci.org/cgi/doi/10.1523/JNEUROSCI.1399-04.2004

608. Ayaz A, Chance FS. Gain modulation of neuronal responses by subtractive and divisive mechanisms of inhibition. J Neurophysiol. 2009;101(2):958–68.